I. ELECTRON SPIN RELAXATION STUDIES OF MANGANESE(II) COMPLEXES IN ACETONITRILE

II. NUCLEAR SPIN RELAXATION STUDIES OF BROMINE IN TETRABROMOMANGANESE(II) IN ACETONITRILE

Thesis by

Lahmer Lynds

In Partial Fulfillment of the Requirements

For the Degree of

Doctor of Philosophy

California Institute of Technology

Pasadena, California

1970

(Submitted January 26, 1970)

To my lovely wife Rebecca
and our children Jeffrey
and Janice

To the memory of my
Mother and Father

ACKNOWLEDGMENTS

It is a great pleasure to acknowledge my advisor Professor Sunney I. Chan for his continued guidance and encouragement during my graduate career at the Institute.

I am greatly indebted to my colleague Jane E. Crawford for her many valuable contributions which are strongly reflected throughout the work described in this Thesis. I have enjoyed and benefited from many theoretical discussions with Dr. Joe Woong Lee. In fact, I am indebted to all the members of our group for their eager cooperation and free advice. In particular, I want to thank Dr. Tom Burke, Jim Prestegard, Dr. Dale Clutter, Dr. Fred Tsay, Paul Morrison and Joe Karnicky who have contributed immensely to my education and, somehow, have patiently withstood my withering commentary on technical matters over the years. I would also like to mention the tremendous help received from the supporting shop groups (the people who really do the work) which are second to none.

Financial support came from several agencies and they are gratefully acknowledged as follows: the California Institute of Technology, N.A.S.A., the ARCS Foundation and TRW Systems Inc.

I wish to thank Edi Bierce and Joyce Lunstedt for their very professional typing, art work and cooperation in bringing the manuscript together under considerable pressure.

Finally, and most important of all, I thank my wife for her infinite patience and devotion. She has made everything possible and worthwhile.

ABSTRACT

Magnetic resonance techniques have given us a powerful means for investigating dynamical processes in gases, liquids and solids. Dynamical effects manifest themselves in both resonance line shifts and linewidths, and, accordingly, require detailed analyses to extract desired information. The success of a magnetic resonance experiment depends critically on relaxation mechanisms to maintain thermal equilibrium between spin states. Consequently, there must be an interaction between the excited spin states and their immediate molecular environment which promote changes in spin orientation while excess magnetic energy is coupled into other degrees of freedom by non-radiative processes. This is well known as spin-lattice relaxation. Certain dynamical processes cause fluctuations in the spin state energy levels leading to spin-spin relaxation and, here again, the environment at the molecular level plays a significant role in the magnitude of interaction. Relatively few electron spin relaxation studies of solutions have been conducted and the present work is addressed toward the extension of our knowledge in this area and the retrival of dynamical information from line shape analyses on a time scale comparable to diffusion controlled phenomena.

Specifically, the electron spin relaxation of three Mn^{+2} $3d^5$ complexes, $Mn(CH_3CN)_6^{+2}$, $MnCl_4^{-2}$, and $MnBr_4^{-2}$ in acetonitrile has been studied in considerable detail. The effective spin Hamiltonian constants were carefully evaluated under a wide range of experimental

conditions. Resonance widths of these Mn^{+2} complexes were studied in the presence of various excess ligand ions and as a function of concentration, viscosity, temperature and frequency (X-band, ~9.5 Å Hz and K-band, ~35 Å Hz).

A number of interesting conclusions were drawn from these studies. For the Et_4NCl-$MnCl_4^{-2}$ system several relaxation mechanisms leading to resonance broadening were observed. One source appears to arise through spin-orbit interactions caused by modulation of the ligand field resulting from transient distortions of the complex imparted by solvent fluctuations in the immediate surroundings of the paramagnetic ion. An additional spin relaxation was assigned to the formation of ion pairs $[Et_4N^+ \cdots MnCl_4^{-2}]$ and it was possible to estimate the dissociation constant for this specie in acetonitrile.

The Bu_4NBr-$MnBr_4^{-2}$ study was considerably more interesting. As in the former case, solvent fluctuations and ion-pairing of the paramagnetic complex $[Bu_4N^+ \cdots MnBr_4^{-2}]$ provide significant relaxation for the electronic spin system. Most interesting, without doubt, is the onset of a new relaxation mechanism leading to resonance broadening which is best interpreted as chemical exchange. Thus, assuming that resonance widths were simply governed by electron spin state lifetimes, we were able to extract dynamical information from an interaction in which the initial and final states are the same

$$MnBr_4^{-2} + Br^- \rightleftharpoons MnBr_4^{-2} + Br^-.$$

The bimolecular rate constants were obtained at six different temperatures and their magnitudes suggested that the exchange is probably diffusion controlled with essentially a zero energy of activation. The most important source of spin relaxation in this system stems directly from dipolar interactions between the manganese $3d^5$ electrons. Moreover, the dipolar broadening is strongly frequency dependent indicating a deviation between the transverse and longitudinal relaxation times. We are led to the conclusion that the $3d^5$ spin states of ion-paired $MnBr_4^{-2}$ are significantly correlated so that dynamical processes are also entering the picture. It was possible to estimate the correlation time, τ_d, characterizing this dynamical process.

In Part II we study nuclear magnetic relaxation of bromine ions in the $MnBr_4^{-2}$-Bu_4NBr-acetonitrile system. Essentially we monitor the ^{79}Br and ^{81}Br linewidths in response to the $[MnBr_4^{-2}]/[Br^-]$ ratio with the express purpose of supporting our contention that exchange is occurring between "free" bromine ions in the solvent and bromine in the first coordination sphere of the paramagnetic anion. The complexity of the system elicited a two-part study: (1) the linewidth behavior of Bu_4NBr in anhydrous CH_3CN in the absence of $MnBr_4^{-2}$ and (2) in the presence of $MnBr_4^{-2}$. It was concluded in study (1) that dynamical association, $Bu_4NBr \underset{}{\overset{k_1}{\rightleftharpoons}} Bu_4N^+ + Br^-$, was modulating field-gradient interactions at frequencies high enough to provide an estimation of the unimolecular rate constant, k_1. A comparison of the two isotopic bromine linewidth-mole fraction results led to the conclusion that quadrupole interactions provided the dominant

relaxation mechanism. In study (2) the "residual" bromine linewidths for both ^{79}Br and ^{81}Br are clearly controlled by quadrupole interactions which appear to be modulated by very rapid dynamical processes other than molecular reorientation. We conclude that the "residual" linewidth has its origin in chemical exchange and that bromine nuclei exchange rapidly between a "free" solvated ion and the paramagnetic complex, $MnBr_4^{-2}$.

TABLE OF CONTENTS

PART I

TABLE OF CONTENTS

PART II

I. GENERAL INTRODUCTION

The application of magnetic resonance to widely diverse problems in chemistry and physics has been well established. A nuclear or electronic system with a resultant magnetic moment serves as a probe that samples local magnetic effects within a molecular or atomic framework. Factors that determine the local field involve the interplay of nuclear and electron magnetic moments governed by short-range, and to a lesser extent, the long-range chemical environment. From a chemist's view point magnetic resonance has provided an indispensable method for the determination of structure and molecular conformation in solids, liquids and gases. Nuclear magnetic resonance and relaxation studies in the liquid state provide a rich source of dynamical information such as chemical exchange, internal rotations, inversions and relative intermolecular motions for processes that are relatively slow compared to the molecular rotational and collisional time scale. In many cases resonance techniques provide information that cannot be attained by any other method. In contrast, relatively few electron spin relaxation studies of solutions have been conducted and the present work is addressed toward the extension of our knowledge in this area and the retrival of dynamical information on a time scale comparable to diffusion controlled phenomena.

The major differences between nuclear and electron magnetic resonance are time-scale of observations, magnitude of magnetic moment and the physical deployment of the spin states. Nuclear

properties such as spin, magnetic moment and quadrupole moment are more or less insulated from their environment by shielding electrons. In contrast, electronic systems are usually peripheral to the molecular or atomic framework resulting in much larger orbital volumes and the relatively smaller energy to excited states renders the system highly coupled to the outside world. As an example, a paramagnetic ion typically has drastically different magnetic moments, angular momentum and quadrupole interactions depending on the medium that surrounds it. Indeed the hyperfine interactions, zero-field splittings and g-values can change drastically from one crystalline site or solvent to another.

Historically, the question of paramagnetic relaxation arose among low-temperature physicists who were concerned with energy transfer in adiabatic demagnetization experiments. The answer to this problem required an understanding about the nature of thermal contact between an ensemble of electronic magnetic moments and the vibrational degrees of freedom in the crystalline lattice. The time required in attaining equilibrium was called the spin-lattice or longitudinal relaxation time (T_1). A second mechanism involves the rate required for the magnetic assembly to reach internal equilibrium at a temperature independent of the lattice temperature. This has been called the spin-spin or transverse relaxation time (T_2). Electron spin resonance experiments can provide much information about these relaxation mechanisms. Although the relaxation nomenclature was invented with solids clearly in mind, the concepts suffer little when

applied to other phases.

As mentioned above, relaxation of unpaired electron spins in solution is strongly influenced by molecular environment and the widths of electron spin resonance lines are strongly dependent upon the fluctuation of the energy manifold and life-time of the spin-states. Any interaction which causes transitions between two spin-states and has rich Fourier components at the resonance frequency produces strong spin-lattice (T_1) relaxation and line broadening. Other random forces which modulate the spin energy levels at low frequencies without causing transitions between them contribute to a transverse spin-spin (T_2) relaxation but not to T_1. Transitions between electron spin-states are often on the time scale of interesting dynamical phenomena observed in the liquid state such as rapid exchange processes and Brownian motion. Hence a quantitative analysis of line shapes can lead to valuable information concerning relaxation mechanisms which in turn may be related to dynamical processes and even structure on the molecular level.

Relaxation theory of free radicals and transition metal ions in solution has been under steady development for a number of years (1-32). Here we are concerned mainly with paramagnetic transition-metal complex ions since they are usually stable and are present in many chemically and biologically important systems. At present most of the significant relaxation studies have centered around the vanadyl (VO^{+2}) and manganous (Mn^{+2}) ions incorporated in various types of complexes. This is due to the sharpness and observability

of the hyperfine components which is not possible in most other transition-metal complexes. Of these two transition-metal ions, Mn^{+2} is probably the most important because of its role in biological systems. A number of significant electron spin relaxation studies involving these two ions in the liquid state have been conducted and several that are particularly germane to our work will be discussed at greater length.

An illustration of tumbling correlation effects was shown by the electron spin resonance spectrum of VO^{+2} in aqueous solution (33). Linewidths of the individual hyperfine components depend on the nuclear spin orientation, M_I, according to

$$\frac{1}{T_2} \approx \tau_c (\Delta g \beta H_0 + b M_I)^2 / \hbar^2$$

where T_2 is the transverse relaxation time, H_0 is the external field, $\Delta g \equiv g_{||} - g_{\perp}$ and $b \equiv A_{||} - A_{\perp}$ which define the anisotropies in the g and nuclear hyperfine constant tensors, and τ_c is the correlation time for reorientation of the molecular framework and must have the proper magnitude to promote a relaxation mechanism. The results verified the mechanism proposed by H. M. McConnell (2a) involving a "microcrystal" disposed about the axially symmetric VO^{+2} ion which gives rise to anisotropies in both the g and hyperfine tensors. By comparing linewidth measurements obtained at X-band (9.25 GHz) and K-band (24.3 GHz) with the theoretical calculations made by Kivelson (4), the validity of the microcrystallite model was supported.

This provides a beautiful example of the relevance of relaxation studies to structure in solution.

Dynamics and structure of ion-pairing have been the subject of many relaxation studies (34-46). Pearson and Buch (47) investigated ion-pairing by the interaction between paramagnetic cations and paramagnetic anions in aqueous solutions. From the line broadening of one paramagnetic component they were able to measure the rates of ion-pair formation in cases where the interaction was strong. They were able to conclude a basic structure for the pair in which the components were insulated from one another by a layer of solvent. Typical bimolecular rate constants were on the order of 10^{10} sec^{-1} $mole^{-1}$ and agreed closely to those derived from the theory of diffusion controlled reactions between ions in solution (48, 49).

Solvent fluctuation has been established as an important relaxation mechanism and source of line broadening in manganese(II) complexes. Tinkham, Weinstein and Kip (50) were the first to observe an electron spin resonance spectrum of manganese(II) in aqueous solutions and noted that the six hyperfine components had different linewidths. A second order theory accurately predicted the line positions but only partially accounted for differences in linewidths. The precise mechanism leading to this effect and the anomalous linewidth decrease with increasing temperature has been the subject of several studies. Bloembergen and Morgan (51) proposed that electron spin relaxation in $Mn(H_2O)_6^{+2}$ ions at low solution concentrations is induced by fluctuations in the solvent shell about the

complex which causes transient distortions of the complex. These distortions introduce perturbations in the spin-orbit coupling which mixes the spin-states and promotes transitions between levels that are otherwise unallowed. Clearly, electron spin relaxation is correlated with relative solvent motions. Later this was verified by the important work of Garrett and Morgan (52) who extended the density matrix calculations (51) to obtain expressions for the relaxation times associated with various transitions. Electron resonance linewidths for manganese(II) in several high dielectric constant organic solvents and in aqueous solution were studied experimentally. Variation of line shapes with solvent and temperature was obtained and interpreted at low temperatures in terms of a model in which solvent fluctuations about the solvated ion modulate the ligand field and relax the electron spin through spin-orbit coupling to the local environment. This clearly refutes the results of McLachlan (25) and Carrington and Luckhurst (26) who treated the relaxation of electron spin in transition-metal complexes by rotational modulation of zero-field splitting of the spin multiplet. This treatment leads to a single relaxation time for all spin-states in the limit of extreme narrowing and implies equal linewidth for all the hyperfine components in the electron spin resonance spectrum. Garrett and Morgan demonstrated convincingly that this was not the case for manganese(II) in all of the solutions investigated and laid to rest other earlier proposals offered by Bloembergen and Morgan (51) and by McGarvey (1b). High temperature broadening was observed for manganese(II) solvated in DMF,

DEF and DMSO suggesting the onset of a new relaxation mechanism due possibly to ligand-solvent exchange or to internal motion within the complex ion. This effect was not observed in aqueous manganese(II) solutions. Presence of ligand exchange as a relaxation mechanism was not thoroughly established.

Exchange broadening mechanisms have been considered but few definitive experiments have been performed partially due to the uncertainty about species participating in the exchange. The first such observation was made by Avvakumov et al. (53) who studied the effect of a diamagnetic anion on the relaxation of manganese(II). They studied line broadening of $MnCl_2$ solutions between room temperature and 200°C but apparently misinterpreted the results as intrinsic to manganese(II) rather than to the diamagnetic chloride ion present in solution. In contrast, Hayes and Meyers (54) demonstrated that $[Cl^-]$ and $[SO_4^=]$ imposed a strong influence on the hyperfine ($M_I = +\frac{1}{2}$) linewidth and suggested that complex formation was the source of excess linewidth. Three paramagnetic components were considered:
(1) Mn^{+2} with no anion in the first or second coordination sphere;
(2) $Mn^{+2}H_2OX^{n-}$, manganous ions with an ion in the second coordination sphere; (3) $Mn^{+2}X^{n-}$, manganous ion with an ion in the first coordination sphere. The chloride ion contributes little broadening at 0.1 M below 80°C but considerable broadening is obtained above this temperature. They suggest that the linewidth is determined by a first coordination sphere complex. From the chloride data in the presence of so many uncertainties they were not able to evaluate the

rate constant of formation and the activation energy of the process with any accuracy. The sulfate results were more complicated because broadening was observed at all temperatures and was presumably due to an admixture of contributions from both the inner- and outer-sphere complexes. Relaxation times and reaction rate constants could only be estimated indirectly.

Although many stable manganese complexes are known, very few exhibit an electron spin resonance spectrum. Many are low spin complexes and, consequently may be drastically broadened by Jahn-Teller distortions. In fact, any distortion leading to deviations from cubic symmetry can provide strong relaxation mechanisms through spin-orbit interactions and give broad, featureless and sometimes unobservable lines. Recently the electron spin resonance spectra of $Mn(CH_3CN)_6^{+2}$, $MnBr_4^{-2}$ were reported (55). The solvated octahedral complex $Mn(CH_3CN)_6^{+2}$ and the tetrahedral complex $MnCl_4^{-2}$ have well resolved hyperfine components with linewidths on the order of 8 to 10 gauss. In contrast, the ^{55}Mn nuclear hyperfine components of the tetrahedral complex $MnBr_4^{-2}$ were found to be unusually broad and it was observed that line broadening was strongly dependent upon excess bromide ion concentration provided by tetrabutylammonium bromide. It was suggested that the bromide concentration dependent broadening may be attributable to ligand exchange and provided the driving force and central theme for the work described in this thesis. There are several unique features that should provide more definitive dynamical information than previous investigations. First of all,

tetrahedral complexes are in general known to be more facile than octahedral complexes thus improving our chances of being able to see an effect on the electron spin resonance time scale. Secondly, complex stoichiometry can be pretty well guaranteed under proper adjustment of bromide concentration so that exchange effects can be studied between well defined states. Finally we note that the initial and final states are the same:

$$MnBr_4^{-2} + Br^- \rightleftharpoons MnBr_4^{-2} + Br^- .$$

Presumably then, a strong perturbation of the electronic system takes place during bromine exchange so that the lifetimes of the spin-states and hence both the longitudinal and transverse relaxation times are limited to the chemical lifetime of the complex. We set forth evidence to confirm this interpretation and investigate other dynamical processes leading to electron spin relaxation.

II. THEORY

1. Manganese(II) Complexes

Numerous manganese(II) complexes are known to exist in both low and high spin states. Octahedral complexes are the most common and are usually stable in aqueous systems. In contrast, the tetrahedral manganese(II) complexes are unstable in donor solvents such as water but can exist in crystalline environments or certain solvents such as CH_3CN. The high spin $3d^5$ complexes command a unique position among the iron group paramagnetic ions because the unpaired electrons have zero resultant angular momentum. Under these circumstances, the resulting sextet ground state, $^6S_{5/2}$, is expected to behave as an ideal paramagnet rather well insulated from its environment since spin-orbit coupling is small. Consequently, spins can interact with a crystalline field only through higher order quartic terms (56). As a result, the spectroscopic splitting factor, $\langle g \rangle$, should be isotropic and have a value close to 2. In addition, the zero-field splitting is expected to be small.

1.1 Ligand Field Splitting

Electronic spectra of octahedrally coordinated manganese(II) ions such as $Mn(H_2O)_6^{+2}$ and, recently, tetrahedral complexes are fairly well understood and are consistent with the high spin case. The ground state for $^6S_{5/2}$ ions in a cubic field is split into a twofold degenerate level (Γ_7) and a fourfold degenerate level (Γ_8) with a separation of 3a where a is the zero-field splitting parameter.

Ligands affect the $3d^5$ electrons in two separate ways: electrostatic interactions imposed by negative ligand charges and overlap of ligand orbitals to form covalent bonds. To be sure, hybrid situations may also contribute to the picture depending on relative electronegativities, ionic dimensions and so on. Although distinctly different these effects alter the electronic energy levels in the same fashion. To illustrate the effect imposed by ligands on the electronic levels, an energy level scheme is depicted in Fig. 1 for two cubic field cases: (1) octahedral and (2) tetrahedral. In the cases cited here, the ligand field splitting, Δ, is much smaller than coulomb and exchange energies so that the complexes are both high spin cases. It has been demonstrated that all excited states evolve by promotion of an electron from e to t_2 or t_{2g} to e_g levels and, hence, spin-orbit interactions and zero-field splittings will both be small. These spin degeneracies are further removed even in an undistorted complex thus allowing higher order spin-orbit interactions and direct electron dipolar couplings to contribute a new term to the overall effective spin Hamiltonian which is represented by (57)

$$\hat{\mathcal{H}} = \frac{1}{6}a\left[\hat{S}_x^4 + \hat{S}_y^4 + \hat{S}_z^4 - \frac{1}{5}S(S+1)(3S^2 + 3S - 1)\right] \qquad (1)$$

where $\hat{S}_x$, $\hat{S}_y$, $\hat{S}_z$ are the effective spin operators, a is the zero-field splitting constant and S is the total electron spin. Dynamical distortions of the complex lead to additional D and E terms in the Hamiltonian. As a result, the six-fold degeneracy is further removed

FIGURE 1

a) Angular distribution of d orbitals.

b) Relative energy levels of d orbitals split by tetrahedral and octahedral ligand fields. Δ is the ligand field splitting parameter. In the octahedral field for $Mn(H_2O)_6^{+2}$, Δ has a value of 8600 cm^{-1}.

(a)

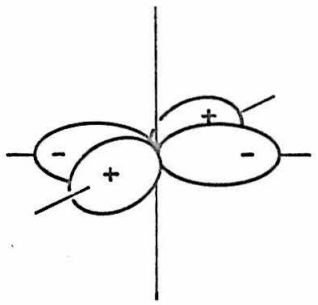

$d_{x^2-y^2}$

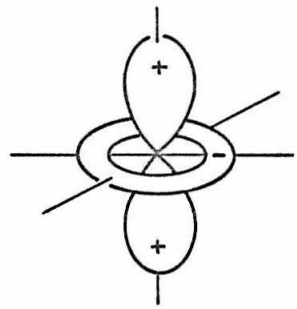

d_{z^2}

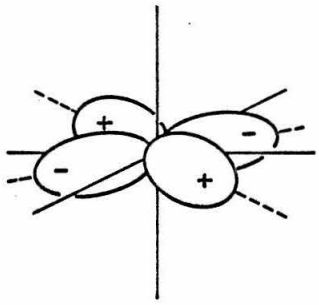

d_{xy}

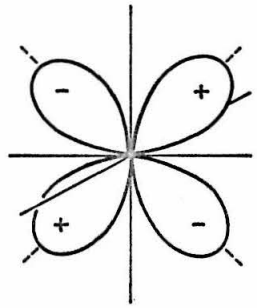

d_{yz}

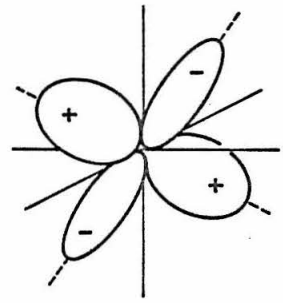

d_{zx}

(b)

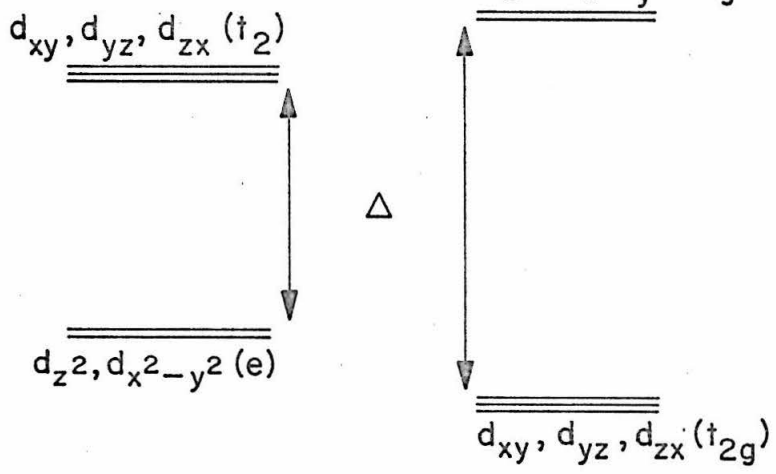

TETRAHEDRAL OCTAHEDRAL

and provides the three Kramers' doublets shown in Fig. 2. The splitting parameters in hexa-aqueous manganese(II) are very small: $a = 10^{-4} \rightarrow 10^{-2}$ cm^{-1} and $D \approx 10^{-2}$ cm^{-1}.

2. The Effective Spin Hamiltonian

2.1 Zero-Field Splitting

In transition-metal ions with $L > 0$ spin-orbit coupling is usually responsible for the zero-field splitting and in many cases the splitting is large enough to prevent the observation of electron spin resonance altogether. This zero-field interaction may be represented by an effective zero-field Hamiltonian

$$\mathcal{H} = \hat{S} \cdot \underset{\sim}{D} \cdot \hat{S} \tag{2}$$

where $\hat{S}$ is the fictitious spin operator and $\underset{\sim}{D}$ is a second rank coupling tensor with components

$$D_{ij} = -\xi^2 \sum_{n} \frac{\langle \psi_0 | L_i | \psi_n \rangle \langle \psi_n | L_j | \psi_0 \rangle}{E_n - E_0} \tag{3}$$

$$i, j = x, y, z$$

where ξ is the spin-orbit coupling constant; ψ_0 and ψ_n are the wavefunctions for the ground (0) and excited (n) states with the corresponding energies E_0 and E_n; L represents the orbital angular momentum. However, for Mn^{+2} complexes with cubic symmetry and a ^6S ground state, we have $\langle L \cdot S \rangle \approx 0$. Consequently, the zero-field Hamiltonian is negligible for the complexes discussed in this work.

FIGURE 2

Schematic energy level diagram showing splitting of the three Kramers' doublets from zero to strong magnetic fields. Additional splittings promoted by nuclear hyperfine interactions are shown together with several allowed transitions.

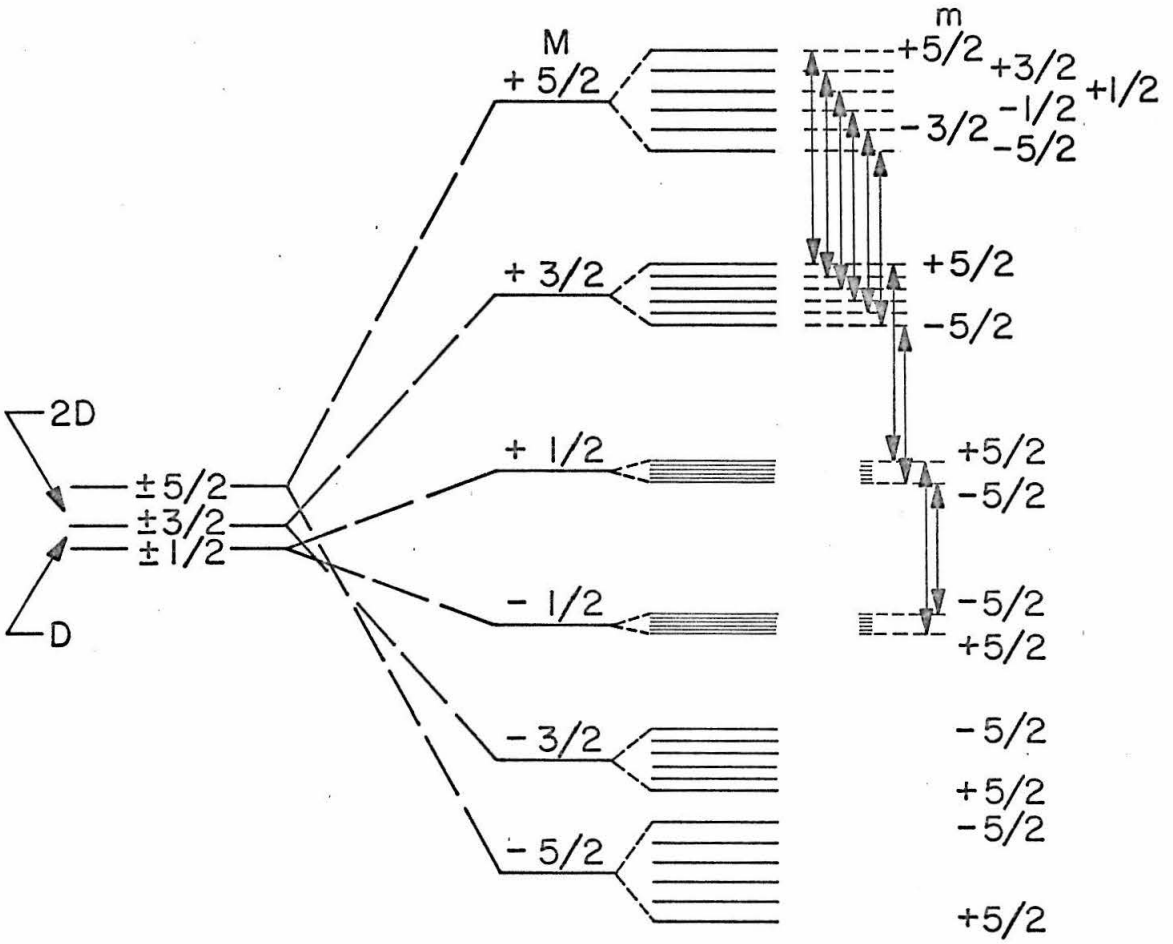
M
m
2D
D
±5/2
±3/2
±1/2
+5/2
+3/2
+1/2
-1/2
-3/2
-5/2
ZERO-FIELD ENERGY LEVELS
HIGH-FIELD LEVELS
NUCLEAR SPLITTING

2.2 The Zeeman Interaction

Application of a strong external magnetic field lifts the zero-field degeneracies and the dominating effect on the spin system is due to the Zeeman interaction. The corresponding Hamiltonian is given by the relation

$$\mathcal{H} = \beta \vec{H} \cdot \underset{\sim}{g} \cdot S - \beta_N \vec{H} \cdot \underset{\sim}{g_N} \cdot I \tag{4}$$

where β is the Bohr magneton, $\vec{H}$ is the applied field, $\underset{\sim}{g}$ is the second-rank g tensor and S is the spin operator. The second term on the right, i.e., the nuclear Zeeman interaction, is negligible. If spin-orbit coupling is operative, i.e., $\underset{\sim}{g}$ tensor is anisotropic, we expect the interaction to mix ground and excited states whose resultant eigenstates are no longer eigenstates of the unperturbed Hamiltonian given above in Eq. (4). The perturbed Hamiltonian becomes

$$\mathcal{H} = \beta \vec{H} \cdot \vec{L} + g_e \beta \vec{H} \cdot \vec{S} \tag{5}$$

under the influence of the interaction between H and orbital angular momentum. g_e is the free electron value (2.0023). This can be represented by an <u>effective</u> spin Hamiltonian

$$\mathcal{H} = \beta \vec{H} \cdot \underset{\sim}{g} \cdot \hat{S} \tag{6}$$

where $\hat{S}$ is a fictitious spin which commutes with the Hamiltonian. On the other hand, if the g tensor is isotropic, the Hamiltonian representing the electronic Zeeman interaction is written

$$\mathcal{H} = \langle g \rangle \beta \vec{H} \cdot \vec{S} \qquad (7)$$

and this is the assumption we apply to the manganese(II) complexes.

2.3 The Hyperfine Interaction

A number of 3d transition state metal ions have a nuclear spin I that can assume 2I + 1 orientations along the direction of an applied external magnetic field. In some cases the nuclear and electron spins couple to exhibit an observable hyperfine spectrum. Since the 3d orbitals theoretically possess nodes at the metal nuclei, the origin of the hyperfine interaction is not immediately obvious and is still currently open to question. In the early days of electron spin resonance it was discovered that manganous(II) solutions displayed a well defined hyperfine spectrum composed of six components. It was proposed by Abragam (58) that a configurational interaction admixing $3s^3 3d^5$ with $3s\,3d^5\,4s$ electrons was responsible for the large anomalous hyperfine coupling. Attempts to explain the magnitude of the coupling have been the subject of many studies. One of the better explanations involves an electrostatic interaction between the $3d^5$ and s-state electrons. Abragam, Horowitz and Pryce (59) proposed core polarization of the inner filled s orbitals imposed by $3d^5$ electrons as a mechanism leading to hyperfine splitting. Their calculations for the configurational interaction model were unsuccessful. Perhaps the best results were obtained through an unrestricted Hartree-Fock procedure (60) which demonstrated that both 2s and 3s orbitals are significantly polarized by the d^5 field. Matamura and Title (61)

observed a correlation between hyperfine coupling and the electronegativity differences in the anion and cation of the host lattice. It has been shown experimentally that the geometry of the complex has the greatest influence on the hyperfine interaction and that the effect of the ligand is clearly secondary. This provides a particularly powerful method in determining the symmetry of manganese(II) environment in both solids and liquids. A typical set of coupling constants are given for two cases: a) octahedral, $\langle A \rangle = -95$ gauss; b) tetrahedral, $\langle A \rangle = -78$ gauss.

In the present case we are concerned only with the isotropic hyperfine interaction and the Hamiltonian is simply

$$\mathcal{H}_{hyp} = \langle A \rangle \vec{I} \cdot \vec{S} \tag{8}$$

where $\vec{I}$ and $\vec{S}$ are the usual nuclear and electron spin operators and $\langle A \rangle$ is the scalar hyperfine coupling constant characterizing the interaction.

2.4 Total Effective Spin Hamiltonian

For manganese(II) complexes having nearly cubic symmetry in solution, the total effective spin Hamiltonian may be represented by

$$\mathcal{H} = \mathcal{H}_{Zeeman} + \mathcal{H}_{Hyperfine}. \tag{9}$$

The total effective spin Hamiltonian may be written in molecular coordinates to include axial components caused by possible dynamical and structural distortions (62)

$$\mathcal{H} = \beta[g_{||} H_r S_r + g_{\perp}(H_p S_p + H_q S_q)]$$

$$+ A_{||} I_r S_r + A_{\perp}(I_p S_p + I_q S_q) + D S_r^2$$

$$p, q, r = \text{molecular coordinates.}$$

To examine the effects of molecular tumbling on the electron spin resonance spectrum, the Hamiltonian is conveniently separated into time dependent and independent parts. A transformation converts the operator into laboratory coordinates and the time dependent or angular terms are collected in the form of spherical harmonics according to Pake (62)

$$\mathcal{H} = g\beta H_0 S_Z + a\,\mathbf{I}\cdot\mathbf{S} + (\frac{D}{2})(3\cos^2\theta - 1) S_Z^2$$

$$+ (\frac{D}{2}) \sin\theta \cos\theta [(S_Z S_+ + S_+ S_Z)e^{-i\phi} + (S_Z S_+ + S_- S_Z)e^{i\phi}]$$

$$+ (\frac{1}{3})(\Delta g\beta H_0 + b I_Z)(3\cos^2\theta - 1) S_Z$$

$$+ (\frac{b}{2}) \sin\theta \cos\theta (I_+ e^{-i\phi} + I_- e^{i\phi}) S_Z$$

$$+ \tfrac{1}{2}(\Delta g\beta H_0 + b I_Z) \sin\theta \cos\theta (S_+ e^{-i\phi} + S_- e^{i\phi})$$

$$+ (\frac{b}{4}) \sin^2\theta (I_+ S_+ e^{-2i\phi} + I_- S_- e^{2i\phi})$$

$$- (\frac{b}{12})(3\cos^2\theta - 1)(I_+ S_- + I_- S_+) \qquad (11)$$

where: $g = \frac{1}{3} g_{||} + \frac{2}{3} g_{\perp}$

$$\Delta g = g_{||} - g_{\perp}$$

$$a = \tfrac{1}{3}A_{\parallel} + \tfrac{2}{3}A_{\perp}$$

$$b = A_{\parallel} - A_{\perp} .$$

Other symbols bear their usual meanings and are defined by Pake (62). The first two terms in Eq. (11) are time independent and are not affected by random motion as the complex tumbles. On the other hand, the remaining terms gain time dependency through the angular dependency. For isotropic complexes, in the limit when motional frequencies far exceed interaction energies, spherical harmonics approach zero and the total effective spin Hamiltonian reduces to simply

$$\mathcal{H} = \langle g \rangle \beta H_0 S_Z + \langle a \rangle \vec{I} \cdot \vec{S} \qquad (12)$$

which adequately predicts the line positions. The eigenvalues for this Hamiltonian to second order are (50)

$$\frac{\hbar\omega}{\langle g \rangle \beta} = H_0 + \langle A \rangle m_I + \frac{\langle A \rangle^2}{2 H_0} \left[I(I+1) - m_I^2 + m_I(2 m_S + 1) \right] . \qquad (13)$$

Selection rules are $\Delta m_I = 0$ and $\Delta m_S = \pm 1$; an energy level diagram was illustrated in Fig. 2. In manganese(II) complexes, the anomalously large hyperfine constant $\langle A \rangle$ leads to a sizeable second order effect. As a result there are 30 allowed non-degenerate transitions contained in six main hyperfine components ($\Delta m_I = 0$) each consisting of five electronic Zeeman transitions ($\Delta m_S = \pm 1$). Clearly, the second order effect is much smaller at K-band frequencies requiring

four times the field, H_0, as in X-band spectroscopy. In practice, however, the spherical harmonics in the spin Hamiltonian are not averaged completely to zero by random motions and, hence, dynamical processes can contribute to linewidth. Although the non-degenerate lines provide a skeleton for the observed linewidths, a much deeper inspection into time dependent phenomena and relaxation theory is required for extraction of dynamical and structural information from a line shape analysis.

3. Theory of Relaxation. The Bloch Equations

A very brief account of relaxation theory will be presented to expose the empirical framework from which we define the often quoted longitudinal and transverse relaxation times. The phenomenological approach of Bloch (63) forms the central theme of the discussion and has been extremely useful in extracting dynamical information at the atomic and molecular level from both nuclear and paramagnetic resonance line shapes. By and large, application of the theory to liquid state problems has enjoyed far more quantitative success than seems possible from the lack of quantum mechanical rigor.

According to Bloch, the equation of motion for nuclear magnetization of an ensemble of uncoupled nuclear spins is simply

$$\frac{d\vec{M}}{dt} = \gamma(\vec{M} \times \vec{H}). \tag{14}$$

The symbols have their usual significance and clearly a similar expression applies to an ensemble of uncoupled electron spins in a homogeneous field. In cases to follow the relationships will, likewise, apply to both nuclear and electron spin. Naturally, the appropriate gyromagnetic ratio must be used. If we now consider the ensemble of spins in a static field defined in the z-direction, the total magnetization at thermal equilibrium is

$$M_z = M_0 = \chi_0 H_0 \tag{15}$$

where the magnetic susceptibility, χ_0, is defined for all N spins

$$\chi_0 = \frac{N\gamma^2\hbar^2 I(I+1)}{3kT} \tag{16}$$

and H_0 is the applied static field. Bloch then proposes a simple linear rate law for the magnetization, M_z, returning to its equilibrium value M_0 defined above

$$\frac{d\vec{M}_z}{dt} = -\frac{(\vec{M}_z - \vec{M}_0)}{T_1}. \tag{17}$$

The time scale, T_1, characterizing the relaxation is known as the longitudinal or spin-lattice relaxation time. In the presence of a radio frequency field (H_1) applied at right angles to the static magnetic field, the magnetic moment will also have precessing components in the X and Y directions. As suggested by Bloch the spin ensemble is, in fact, coupled and one gets a new set of relations

$$\frac{dM_x}{dt} = -\frac{M_x}{T_2} \quad \text{and} \quad \frac{dM_y}{dt} = -\frac{M_y}{T_2} \tag{18}$$

which tells us that the magnetization in the X and Y directions attenuates in a length of time characterized by T_2, the transverse or spin-spin relaxation time. Finally, the Bloch equations can be combined to describe the time rate of change for the total magnetization

$$\frac{d\vec{M}}{dt} = \gamma \vec{M} \times (\vec{H}_0 + \vec{H}_1) - \frac{(\vec{M}_x \vec{i} + \vec{M}_y \vec{j})}{T_2} - \frac{(\vec{M}_z - \vec{M}_0)\vec{k}}{T_1} \tag{19}$$

where, as usual, $\vec{i}$, $\vec{j}$, $\vec{k}$ define a laboratory coordinate system and the last two terms on the right hand side may be considered as "damping" factors. In the rotating frame representation where H_1 and the ijk coordinate system rotate together at the Larmor frequency, ω, we obtain the usual expression

$$\frac{d\vec{M}'}{dt} = \gamma \vec{M} \times (\vec{H}_0 + \frac{\omega}{\gamma}) + \gamma(\vec{M}' \times \vec{H}_1') - \frac{(u\vec{i} + v\vec{j})}{T_2} - \frac{(M_z - M_0)\vec{k}'}{T_1}. \tag{20}$$

As usual, u and v are the transverse components in the rotating frame of reference. Components of the magnetization, $\vec{M}'$, in the rotating frame are

$$\frac{du}{dt} = (\omega_0 - \omega)v - \frac{u}{T_2} \tag{21}$$

$$\frac{dv}{dt} = -(\omega_0 - \omega)u + \gamma H_1 M_z - \frac{v}{T_2}$$

$$\frac{dM_z}{dt} = -\gamma H_1 v - \frac{(M_z - M_0)}{T_1}.$$

Steady state solution of these equations leads to the familiar Lorentzian line shape attainable from the v component and is applicable to the present work on chemical exchange broadened resonance widths.

$$v = M_0 \frac{\gamma H_1 T_2}{1 + T_2^2(\omega_0 - \omega)^2 + \gamma H_1^2 T_1 T_2}. \tag{22}$$

If we accept the concept of spin temperature then it can be shown that in thermal equilibrium the steady state population of spins are governed by Boltzman statistics and the rate of spin exchange between allowed levels can be described by the so-called "Master equation" defined by Slichter (64)

$$\frac{d\rho_n}{dt} = \sum_m (p_m W_{mn} - p_n W_{nm}) \tag{23}$$

where ρ_n is the fractional occupation of state n and W_{mn} is the probability per second that the lattice induces a spin transition from m to n if the system is in state m. Without belaboring the point further and bearing in mind that the linear nature of the above rate equation is an assumption, it follows that the spin-lattice relaxation times are directly related to transition probabilities in the general form developed by Gorter (65)

$$\frac{1}{T_1} = \frac{1}{2} \frac{\sum_{m,n} W_{mn} (E_m - E_n)^2}{\sum_n E_n^2} \tag{24}$$

The transition probabilities, W_{mn}, can be calculated from the density matrix and Redfield (12) approach which apply even when the concept of spin temperature breaks down.

Bloembergen, Purcell and Pound (66) presented a beautiful physical picture explaining line broadening that arises from dynamical sources. Any magnetic interaction resulting from dynamical sources such as dipolar or solvent fluctuations, and so on, that produce fluctuations with a rich Fourier spectrum at the Larmor frequency can promote strong spin-lattice relaxation. For a time-dependent interaction giving rise to transitions between nuclear or electronic levels, time-dependent perturbation theory provides the well-known result for the transition probability

$$W_{mn} = \left| \langle m | \hbar^{-1} \mathcal{H}(t) | n \rangle \right|^2 \cdot \rho(E_f) \tag{25}$$

where $\hbar \mathcal{H}(t)$ is the time-dependent Hamiltonian operator for the particular interaction and $\rho(E_f)$ represents the density of final states. Comparison of Eqs. (24) and (25) reveals that magnetic resonance linewidths in liquid systems for the case of extreme narrowing ($\omega_0 \tau_c \ll 1$) have a very general form

$$\frac{1}{T_1} \propto \left| \langle m | \hbar^{-1} \mathcal{H}(t) | n \rangle \right|^2 \cdot \tau_c . \tag{26}$$

In some cases, $T_1^{-1} = T_2^{-1}$, but in this study we also observe $T_1 \neq T_2$ as reflected by large linewidth dependencies on frequency as we shall see later. A correlation time, τ_c, has been introduced to describe the frequency spectrum of the mean squared energy matrix element and will be discussed at greater length in the following section. It should be realized that in most cases neither $|\langle m|\hbar^{-1}\mathcal{H}(t)|n\rangle|^2$, the mean squared interaction energy matrix element, nor τ_c, the correlation time characterizing the interaction are amenable to measurement. This, of course, is one reason that magnetic resonance linewidths are difficult to interpret. Usually, at best, questionable assumptions must be invoked for τ_c before dynamical information can be extracted from line shapes. They will be discussed and amplified in the following two sections.

3.1 Motional Correlations

In stochastic processes correlation time is defined as the interval of time required so that change of a particular time dependent function is negligible. Another way of saying this is that a correlation time is the length of time required for a fluctuation to die away. At the present time it is impossible to calculate how rapidly spherical harmonics vanish while undergoing completely random motion in a rigorous fashion but fluctuation theory provides a framework to attack the problem on a statistical basis. Obviously such concepts as correlation times are nebulous but once it is specified there is a precisely defined parameter that enters the problem and characterizes the time scale.

Nevertheless fluctuation theory has provided useful relationships for the analysis of nuclear magnetic resonance spectra and, in fact, has given far more quantitative agreement than deserved from the crudeness of the treatment. However, on the electron spin resonance time scale we must examine the assumptions and rationalizations used in the statistical treatment a bit more carefully since the interaction and Larmor frequencies approach one another and raise serious questions about the correlation function and the convergence of spectral density integrals. We shall briefly probe some of the weaknesses in this theory and how they may influence our interpretation. Furthermore we will be able to experimentally examine a case within the "twilight-zone" of the theory in which the observed linewidths depend strongly on the Larmor frequency.

3.2 Rotational Correlation

The simple diffusion model proposed by Debye is one in which a rigid sphere of radius a moves randomly in a medium of macroscopic viscosity, η. Rotation of the spin system can then be treated by a simple diffusion equation

$$\frac{1}{D'}\frac{\partial p}{\partial t} = \nabla^2 P \tag{27}$$

where ∇ is the Laplacian operator over the surface of a sphere, P is the probability of the spin system reaching a certain new location after an elapsed period of time, and D' is the rotational diffusion constant. D' is related to η through the Stokes-Einstein relation

$$D' = \frac{kT}{8\pi a^3 \eta} \tag{28}$$

Equation (27) has well-known solutions in terms of an expansion in normalized, orthogonal spherical harmonics, $Y_{\ell m}(\theta, \phi)$

$$p = \sum_{\ell, m} C_\ell^m(t)\, Y_\ell^m(\theta, \phi)\, e^{-D'\ell(\ell+1)t} \tag{29}$$

where C_ℓ^m are coefficients defined from initial conditions and ℓ is the order of the spherical harmonics. It can be shown for the case of Brownian motion that

$$D'\ell(\ell + 1) = \frac{1}{\tau_c} \tag{30}$$

and from Eqs. (28) and (30) we obtain

$$\tau_c = \frac{8\pi a^3 \eta}{\ell(\ell + 1)kT} \tag{31}$$

where τ_c is the correlation time associated with rotational motions, a is the radius of the rotating component under observation and η is the macroscopic viscosity. The other symbols have their usual meaning. Since magnetic resonance experiments involve second rank interaction tensors ($\ell = 2$), Eq. (31) above assumes its often quoted form

$$\tau_c = \frac{4\pi a^3 \eta}{3kT} \tag{32}$$

and is therefore a natural consequence of the diffusion equation. It should be remembered that this follows from highly idealized hydrodynamic arguments and discretion must be employed when applying the result to quantum mechanical problems.

An exponential correlation function also follows from the statistical approach given by Slichter (64). The correlation function may be determined for a field that jumps between two field values $\pm h_0$ representing states 1 and 2. It is then possible to calculate the correlation function $G(\tau)$

$$G(\tau) = \langle H(t)\, H(t+\tau) \rangle \tag{33}$$

where the brackets designate an ensemble average. If it is assumed that the ensemble averages p_1 and p_2 as a function of τ are related to the transition probabilities by

$$\frac{dp_1}{d\tau} = W(p_2 - p_1)$$

and

$$\frac{dp_2}{d\tau} = W(p_1 - p_2) \tag{34}$$

then the correlation time representing the final ensemble average over the initial fields is simply

$$G(\tau) = \langle \overline{H(0)\, H(\tau)} \rangle = h_0^2\, e^{-2W\tau} \tag{35}$$

where $2W \approx 1/\tau_c$.

3.3 Field Dependent Relaxation Times

To illustrate the effect of field (or frequency) dependent phenomena on linewidths we parallel the procedure of Slichter (64). The transition probability between two spin states (k and m) is calculated using the density matrix formalism. Time rate of change of the density matrix to second order is given by

$$\frac{d\rho^*(t)}{dt} = \frac{i}{\hbar}[\rho^*(0), H_1^*(t)] + (\frac{i}{\hbar})^2 \int_0^t dt\Big[[\rho^*(0), \mathcal{H}_1^*(t')], \mathcal{H}_1^*(t)\Big]. \quad (36)$$

The asterisk refers to the interaction representation defined as

$$\rho^*(t) = e^{(i/\hbar)\mathcal{H}_0 t}\, \rho(t)\, e^{-(i/\hbar)\mathcal{H}_0 t}$$

$$\mathcal{H}_1^*(t) = e^{(i/\hbar)\mathcal{H}_0 t}\, \mathcal{H}_1(t)\, e^{-(i/\hbar)\mathcal{H}_0 t}$$

where ρ is the density matrix operator. If we assume only state k is occupied at $t = 0$ then

$$\frac{d}{dt}\langle m|\rho|m\rangle \propto W_{km}.$$

Under these circumstances the only non-vanishing element of the density matrix is $\langle k|\rho|k\rangle$. From the relation

$$\langle \eta|\rho^*|m\rangle = e^{(\frac{i}{\hbar})(E_n - E_m')t}\, \langle n|\rho|m\rangle \quad (37)$$

we have

$$\langle n|\rho^*(0)|m\rangle = \langle n|\rho(0)|m\rangle = 0. \tag{38}$$

Clearly for $n = m = k$

$$\langle k|\rho^*(0)|k\rangle = \langle k|\rho(0)|k\rangle = 1 \tag{39}$$

To compute the matrix element mn of Eq. (36), we apply the relations above, Eqs. (37), (38), (39) and obtain a simplified expression

$$\frac{d}{dt}\overline{\langle m|\rho|m\rangle} = \frac{1}{\hbar^2}\int_0^t \Big[\overline{\langle m|\mathcal{H}_1(t')|k\rangle}\,\overline{\langle k|\mathcal{H}_1(t)|m\rangle}\, e^{i(W_m-W_k)(t'-t)} + \overline{\langle m|\mathcal{H}_1(t)|k\rangle}\,\overline{\langle k|\mathcal{H}_1(t')|m\rangle}\, e^{i(W_m-W_k)(t-t')}\Big]dt'. \tag{40}$$

At this point the perturbation could be any time dependent phenomena and since this varies from one ensemble to another ensemble average was performed. For the case of a stationary perturbation we can define a correlation time

$$G_{mk}(\tau) \equiv \overline{\langle m|\mathcal{H}_1(t)|k\rangle\langle k|\mathcal{H}_1(t+\tau)|m\rangle} = G_{km}(-\tau) \tag{41}$$

with $\tau \equiv t - t'$

which is dependent only on τ, m, and k at $\tau = 0$, the correlation function is non-zero

$$G_{mk}(0) = \left|\overline{\langle k|\mathcal{H}_1(t)|m\rangle}\right|^2 \geq 0 \tag{42}$$

and suggests that the function $G_{mk}(\tau)$ falls off from this maximum and tends toward zero when $\tau > 0$ reaching its destination in a somewhat nebulous time characterized by τ_c, the so-called correlation time. This provides the physical picture of how a fluctuation dies away. Substitution of Eq. (41) into (40) yields

$$\frac{d}{dt}\overline{\langle m|\rho|m\rangle} = \frac{1}{\hbar^2}\int_{-t}^{t} G_{mk}(\tau)\, e^{-i(\omega_m-\omega_k)\tau}\, d\tau. \tag{43}$$

The expression is time dependent unless we assume that $t \gg \tau_c$. However, on the electron spin resonance time scale, we are concerned with the possibility that certain processes will not permit the use of this inequality in which case the line shapes will take on Gaussian Character. For the moment we assume that $t \gg t_c$ and then Eq. (43) can be written

$$W_{km} = \frac{d}{dt}\overline{\langle m|\rho|m\rangle} = \frac{1}{\hbar^2}\int_{-\infty}^{\infty} G_{mk}(\tau)\, e^{-i(\omega_m-\omega_k)\tau}\, d\tau \tag{44}$$

and is immediately recognized as a Fourier transform. By defining

$$J_{mk}(\omega) \equiv \int_{-\infty}^{\infty} G_{mk}(\tau)\, e^{-i\omega\tau}\, d\tau \tag{45}$$

the inverse Fourier transform is

$$G_{mk}(\tau) = \frac{1}{2\pi} \int_{-\infty}^{\infty} J_{mk}(\omega) e^{i\omega\tau} d\omega . \tag{46}$$

This is the power spectrum which roughly describes how much "fluctuation" is available to induce a transition as a function of frequency. $G_{mk}(\tau)$ has a characteristic power cut-off at $\omega \sim 1/\tau_c$. ω is the Larmor frequency for the $m \rightarrow k$ transition.

In the $MnBr_4^=$ exchange study, dipolar broadening and large frequency effects are observed. Thus, it is appropriate to consider the problem through a very general and simplified treatment to extract the qualitative features of the interaction.

The magnitude of dipolar interaction is essentially dependent on the radius vector between two spin systems and their relative orientations. On the other hand, duration of any particular value depends directly on the rate of diffusion. Therefore it is correlated in this respect and is clearly uncoupled to intramolecular rotational correlation times. Therefore we see that

$$G_{mk}(0) = \left| \overline{\langle m | \mathcal{H}_1(t) | k \rangle} \right|^2 \tag{47}$$

and further that it is not correlated. For this condition Eq. (46) gives

$$G_{mk}(0) = \frac{1}{2\pi} \int_{-\infty}^{\infty} J_{mk}(\omega)\, d\omega \tag{48}$$

and it is apparent that spectral density area remains constant as τ_c varies. This is illustrated in Fig. 3 for various τ_c's which may arise in an experiment by changing temperature or altering the macroscopic viscosity by changing solute-solvent ratios. The important feature here is that the spectral density exhibits a maximum when $\omega\tau_c \approx 1$ and this condition provides the most efficient transfer of energy between two connected levels. To be more specific we take the perturbation imposed by dipolar interaction to be a coupling between a fluctuating magnetic field and the spin system

$$\mathcal{H}_1(t) = g\beta \sum_q' H_q(t)\, S_q \qquad (49)$$

$$q = x, y, z .$$

From the definition of a correlation time, Eq. (47) and the above specific perturbation give

$$G_{mk} = g^2\beta^2 \sum_{q,\,q'}' \langle m|S_q|k\rangle\langle k|S_{q'}|m\rangle\, \overline{H_q(t)\, H_{q'}(t+\tau)} . \qquad (50)$$

Providing components of the perturbation are independent which is reasonable for a diffusing system, then $q = q'$ and we define

$$j^q_{mk}(\omega) = g^2\beta^2 \left| \langle m|S_q|k\rangle \right|^2 \int_{-\infty}^{\infty} H_q(t)\, H_q(t+\tau)\, e^{-i\omega t}\, d\tau \qquad (51)$$

and the transition probability is

FIGURE 3

Spectral density area remains constant as τ_c changes illustrating in an arbitrary fashion that $J_{mk}(\omega_1)$ has a maximum value for a curve of some intermediate τ_c.

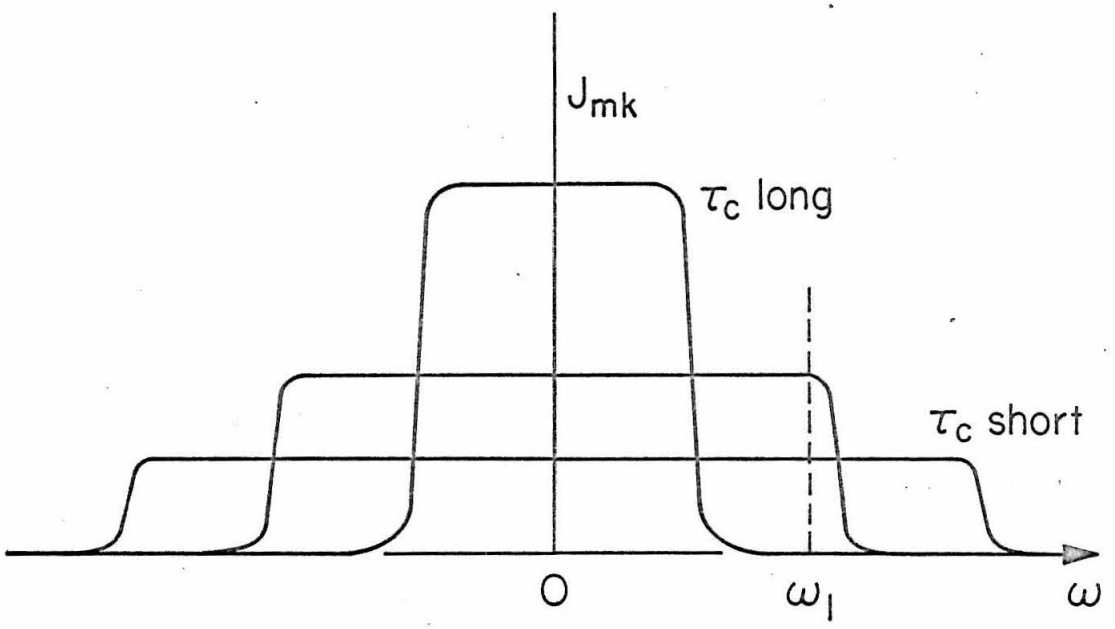
J_{mk}
τ_c long
τ_c short
0
ω_1
ω

$$W_{km} = \frac{1}{\hbar^2} \sum_q j^q_{mk} (\omega_m - \omega_k). \tag{52}$$

Appealing to a previous argument, it is assumed that $H_q(t)\, H_q(t+\tau)$ takes on an exponential form according to Eq. (19). This is certainly a weak point in relaxation theory but is mathematically expedient and demonstrates some validity on the grounds of success. Bearing this in mind, we assume

$$\overline{H_q(t)\, H_q(t+\tau)} = h_q\, e^{-\frac{|\tau|}{\tau_c}}. \tag{53}$$

Insertion of Eq. (53) into (51) and utilizing Eq. (52) provides the final result

$$W_{km} = \left[\sum_q g^2 \beta^2 \left| \langle m | S_q | k \rangle \right|^2 \right] \frac{2\tau_c}{1 + \omega^2 \tau_c^2}. \tag{54}$$

The relationship between W_{km} and T_1 is not immediately obvious in a spin 5/2 case. Nevertheless, the general behavior of the transition probability under influence of a random force can be visualized from Eq. (54). It is evident that the T_1 part of the linewidth will go through a maximum when $\omega\tau_c \approx 1$. Furthermore, a strong frequency effect can be expected when the correlation time is in the right range. In addition, a temperature study of T_1 can provide information about the temperature dependence of the process producing the fluctuations.

3.4 Modified Bloch Equation

A set of equations was proposed by Bloch (63) on the basis of phenomenological arguments to explain the macroscopic dynamical magnetic behavior of interacting nuclear spins. These equations introduce both the longitudinal and transverse relaxation times as dynamical damping factors. Transverse relaxation may be different than longitudinal relaxation since the spins interact strongly with their environment. Typically electrons relax much more rapidly than nuclear spins but the formalism applies equally well to both cases. Although basically simple, these equations have proven to be very useful in describing magnetic phenomena in liquids.

McConnell (67) has shown how the Bloch equations can be directly generalized to include the effects of chemical exchange. The modified Bloch equations are used here to examine several important cases relevant to our observations for an exchanging two-state system.

As a matter of convenience it is expedient to treat the problem in the imaginary plane. Total magnetization is defined in the usual fashion

$$G = u + iv$$

where u = in-phase component of magnetization

and v = out-of-phase component of magnetization.

The Bloch equations in the rotating frame representation are

$$\dot{u} + \frac{u}{T_2} + (\omega_0 - \omega)v = 0 \qquad (55)$$

$$\dot{v} + \frac{v}{T_2} - (\omega_o - \omega)u + \gamma H_1 M_Z = 0 \tag{56}$$

$$\dot{M}_Z + \frac{M_Z - M_o}{T_1} - \gamma H_1 v = 0 \tag{57}$$

and the two modified equations of relevance to our specific application are

$$\dot{G}_A + \alpha_A G_A = -i\gamma H_1 M_{oA} + \frac{G_B}{\tau_B} - \frac{G_A}{\tau_A} \tag{58}$$

$$\dot{G}_B + \alpha_B G_B = -i\gamma H_1 M_{oB} + \frac{G_A}{\tau_A} - \frac{G_B}{\tau_B} \tag{59}$$

where

$$G = u + iv = G_A + G_B$$
$$\alpha_A = T_{2A}^{-1} - i(\omega_A - \omega)$$
$$\alpha_B = T_{2B}^{-1} - i(\omega_B - \omega)$$
$$M_{oA} = P_A M_o \text{ and } M_{oB} = P_B M_o$$

ω_A, ω_B are the Larmor frequencies of the two states; P_A and P_B are the magnetic mole fractions in the two states. Experiments are always conducted under slow passage conditions and provides a major simplification of the modified Eqs. (58) and (59).

$$\dot{G}_A = \dot{G}_B = 0 \tag{60}$$

In the case at hand we are considering a two state system in which the spin system alternates rapidly between two environments A and A, B.

The first-order life times of the spin states in A and A, B are τ_A and τ_B. Chemical equilibrium between the two states is represented by

$$A + B \underset{k_1}{\overset{k_2}{\rightleftharpoons}} A, B \tag{61}$$

where k_2 is a bimolecular rate constant and k_1 is a first-order rate constant. Total relaxation times of the paramagnetic components are T_{2A} and T_{2B} corresponding to species A and A, B; B is a diamagnetic component. We now write the mass equilibrium expression for the above exchange process designated in Eq. (61)

$$K_{eq} = \frac{k_2}{k_1} = \frac{[A, B]}{[A][B]}. \tag{62}$$

The probability of being in a particular state [A] or [A, B] is proportional to the life time of the respective states so that

$$\frac{P_A}{P_B} = \frac{\tau_A}{\tau_B} = \frac{[A]}{[A, B]}. \tag{63}$$

Substituting this into the above equilibrium expression (Eq. 59) relates the rate constants to the spin state life times

$$\frac{\tau_{AB}}{\tau_A[B]} = \frac{k_2}{k_1}.$$

Thus,

$$k_2 = \frac{1}{\tau_A[B]} \quad \text{or} \quad \frac{1}{\tau_A} = k_2[B]$$
$$k_1 = \frac{1}{\tau_B}. \tag{64}$$

From the bimolecular rate expression for the reaction in Eq. (61)

$$-[\dot{A}] = k_2[A][B] \tag{65}$$

the disappearance rate of A should be proportional to the product [A][B]. However, in an electron spin resonance experiment we monitor only the spin state life time of [A], assuming, of course, that [A, B] is unobservable, and barring other line broadening effects, we should observe a dependency due only to the concentration of the diamagnetic component [B]. So the rate constant extracted from experiment is the bimolecular rate constant k_2.

Assuming the slow passage situation shown in Eq. (60), Eqs. (58) and (59) are solved simultaneously in determinantel form to give the well-known expression

$$G = G_A + G_B = \frac{-i\gamma H_1 M_0 [\tau_A + \tau_B + \tau_A \tau_B (P_A \alpha_B + P_B \alpha_A)]}{(\alpha_A \tau_A + 1)(\alpha_B \tau_B + 1) - 1}. \tag{66}$$

It should be noted that the result reported in Pople, Schneider and Bernstein "High-Resolution Nuclear Magnetic Resonance", McGraw-Hill Co. Inc., 1959, pp. 221, eq. 10-14 is incorrect. Equation (66) is now separated into real and imaginary parts by standard procedures.

An expansion of terms and a convenient substituion: $\chi_A^{-1} = T_{2A}^{-1}\tau_A$, $\chi_B^{-1} = T_{2B}^{-1}\tau_B$, results in

$$G = -i\gamma H_1 M_0 \frac{(BD - AC) + i(AB + CD)}{B^2 + C^2} \tag{67}$$

where

$$A = \tau_A + \tau_B + \tau_A\tau_B(P_B T_{2A}^{-1} + P_A T_{2B}^{-1})$$

$$B = [(\chi_A^{-1} + 1)(\chi_B^{-1} + 1) - 1] - \tau_A\tau_B(\omega_A - \omega)(\omega_B - \omega)$$

$$C = \tau_A(\chi_B^{-1} + 1)(\omega_A - \omega) + \tau_B(\chi_A^{-1} + 1)(\omega_B - \omega)$$

$$D = \tau_A\tau_B[P_B(\omega_A - \omega) + P_A(\omega_B - \omega)].$$

For a line shape analysis we consider only the imaginary part of G, that is

$$v = -\gamma H_1 M_0 \frac{(AB + CD)}{B^2 + C^2}. \tag{68}$$

If terms of lower magnitude are neglected v can be beaten into Lorentzian form

$$v = -\gamma H_1 M_0 \frac{(\tau_A + \tau_B)[(\chi_A^{-1} + 1)(\chi_B^{-1} + 1) - 1]^{-1}}{1 + \dfrac{(\tau_A + \tau_B)^2}{[(\chi_A^{-1} + 1)(\chi_B^{-1} + 1) - 1]^2}(\omega_A - \omega)^2}. \tag{69}$$

Therefore,

$$T_2^2 = \frac{(\tau_A + \tau_B)^2}{[(\chi_A^{-1}+1)(\chi_B^{-1}+1) - 1]^2}. \qquad (70)$$

Upon slight rearrangement and assuming $2T_{2A}T_{2B}(1 + \chi_A + \chi_B)$ to be greater than other terms Eq. (70) can be transformed into a convenient form

$$T_2^2 = \left[\frac{T_{2B}(\chi_A+1) + T_{2A}(\chi_B+1)}{(1 + \chi_A + \chi_B)}\right]^2 - \frac{2T_{2A}T_{2B}}{(1 + \chi_A + \chi_B)} \qquad (71)$$

which allows us to investigate several important cases. As stated at the beginning we are using the subscript B to represent the paramagnetic state A, B and [B] to define the concentration of the diamagnetic component.

Case 1

Considering the equilibrium reaction represented by Eq. (61), high concentrations of the diamagnetic component [B] should favor the formation of [A, B]. If sizeable quantities of [A, B] can be formed, i.e., K_{eq} is large, then the linewidth should become typical of [A, B]. Since $T_{2B} < T_{2A}$ in any case, under the above circumstances, $\tau_B > \tau_A$, $T_{2B}\chi_A > T_{2A}\chi_B$, and $\tau_B \rightarrow T_{2B}$. Utilizing the mass equilibrium expression, Eq. (62), and the expressions for the rate constants, Eq. (64), the master Eq. (71) reduces to

$$\frac{1}{T_2} = \frac{1}{T_{2B}}\left(\frac{K_{eq}[B]}{1 + K_{eq}[B]}\right). \qquad (72)$$

In the limit of large $K_{eq}[B]$, T_2^{-1} approaches T_{2B}^{-1} as expected.

Case 2

For solutions less concentrated in [B] or smaller equilibrium constant, K_{eq}, and relaxation control [A, B]: $T_{2B} < T_{2A}$, $\tau_B < \tau_A$, and $T_{2B}\chi_A < T_{2A}\chi_B$. These approximations introduced into Eq. (71) give

$$\frac{1}{T_2} = \frac{1}{T_{2A}} + \left(\frac{k_2}{1 + \chi_B}\right)[B] \tag{73}$$

and it is seen that the slope of [B] predicts a rate constant less than or in the limit, equal to k_2.

Case 3

When $T_{2B} \ll \tau_B$ then Eq. (55) reduces to a particularly simple result

$$\frac{1}{T_2} = \frac{1}{T_{2A}} + k_2[B] \tag{74}$$

which predicts that the observed linewidth broadens linearly upon addition of the diamagnetic component [B]. From Eq. (64) it is apparent that this is equivalent to limiting the spin-state lifetime of the paramagnetic component [A].

Lifetime broadening, on the other hand, does not require a two state model involving a transient paramagnetic intermediate. The virtues of these two approaches will be considered in greater detail

in the $MnBr_4^{-2}$ section.

III. EXPERIMENTAL

Most electron spin resonance has been conducted at a frequency of 9 kMc (X-band) which provides an optimum situation between numerous experimental conditions. The inherent nature of the klystron and its supporting system makes it awkward to change frequencies over a suitable desirable range. Recently the 35 kMc (K-band) microwave bridge has become commercially available and the capability to perform experiments at two widely different frequencies has greatly expanded the utility of the technique to solve problems. Certainly, electron spin resonance at 35 kMc has many advantages in its own right. For example, a factor of 50 in sensitivity is easily obtained, second-order hyperfine effects are minimized, g-shifts stemming from more than one paramagnetic component are enhanced, and forbidden transitions are greatly reduced ($\propto H_0^{-2}$). Most important however, the ability to work at two frequencies provides a powerful means to study spin relaxation in liquids. In the last section we have demonstrated that spin-lattice (T_1) and spin-spin (T_2) relaxation can exhibit strong and characteristic frequency dependencies. To unravel these highly interwoven interactions in a complicated system it is absolutely essential to work at more than one frequency.

1. Magnetic Resonance Apparatus

The electron spin resonance system consisted of a standard V-4502 spectrometer suited for both 9 kMc (X-band) and 35 kMc

(K-band) operation. Initially, a high impedance Varian V-4007 six-inch electromagnet driven by a V-2200A regulated magnet power supply was used for experiments at 9 kHz. Most of the work, however, was performed with a twelve-inch low impedance Varian V-3603 electromagnet with a 45° canted fixed-yoke, and a lockable base ring permitting 360° operation about a vertical axis. Tapered pole caps provided a gap of $2\frac{5}{8}$" for X-band, and ring shim tips of 7/16" thickness fit into the existing pole faces dropping the gap to $1\frac{3}{4}$" for the high homogeneity required at K-band frequencies. A V-2503 solid-state regulated magnet power supply was used in connection with a Fieldial Magnetic Field Regulator Mark II providing direct magnetic field selection with visual readout of field intensity in kilogauss. Accurate magnetic field intensities were measured with an Alpha Scientific Laboratory NMR Gaussmeter (Al 675) containing a solid-state broad band amplifier (Fig. 4) to provide sufficient output to drive a Hewlett-Packard 5245-L counter. ^{1}H and ^{7}Li resonances were used to calibrate the 9 kHz (3400 gauss) and 35 kHz (12400 gauss) regions, respectively.

Two standard Varian microwave bridges were available for experiments: 1) X-band, Varian V-4500-41A low-high power bridge; 2) K-band, V-4561 bridge. An adjustable, motor-driven aluminum platform for the microwave bridges and auxiliary equipment was designed to facilitate allignment procedures and permit rapid interchange between X and K-band operation. The mechanism platform rides on a four-wheeled carriage that provides a three foot range in horizontal positioning. Tracks for the carriage are supported by a

FIGURE 4

Schematic circuit diagram of solid-state broad band amplifier to provide sufficient output from Model 675 NMR Gaussmeter to drive Hewlett-Packard frequency counter. Unit was built inside the Gaussmeter and uses the same B+.

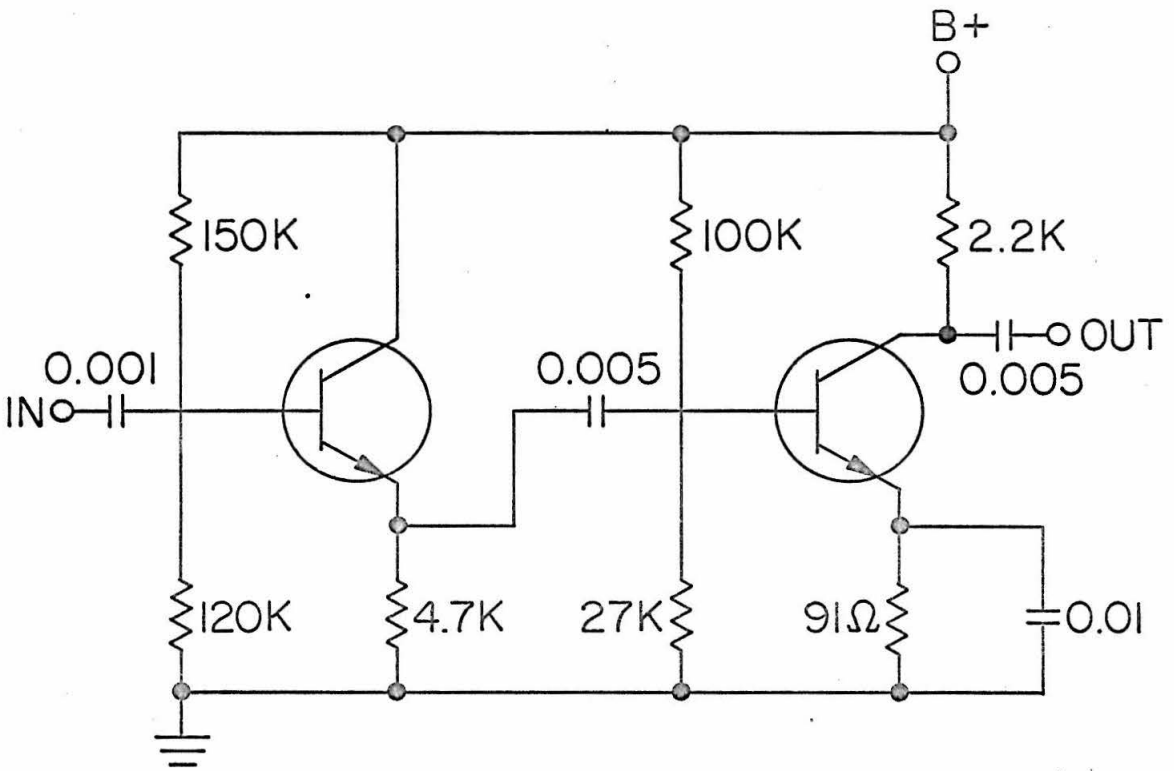

TRANSISTORS = 2N 3826

CAPACITORS = μfd

RESISTORS = 1/4 WATT

B+ = 8.4 VOLTS

INPUT = POINT Ⓐ MARKED ON GAUSSMETER SCHEM. C-3-0006

OUTPUT = HP COUNTER

metal framework that straddles the magnet. Three degrees of freedom are readily available for positioning experiments. Details of the system are illustrated in Figs. 5 and 6.

X and K-band experiments were conducted in cylindrical microwave cavities operated in a TE 011 mode with 100 K Hz Zeeman modulation. In this mode of operation an electric (E) field null runs axially through the cavity. At 9 G Hz sample tubes (pyrex) were typically 1-2 mm in outside diameter and were positioned axially to take advantage of the electric (E) field null. Rather minor dielectric losses permitted the solution length to traverse the entire cavity. However, at 35 G Hz sample requirements were much more demanding with respect to volume and positioning. Samples were contained in ~1 mm outside diameter capillaries and solution lengths were on the order of 1-3 mm. Positioning, of course, was much more critical for several reasons but mainly because the electric (E) field pattern was drastically altered by changes in magnetic susceptibility in the resonance region causing a corresponding variation in dielectric losses and thereby admixing dispersion and absorption modes. This generates asymmetric signals and requires considerable patience in aligning liquid samples to obtain a strictly pure absorption mode.

At X-band frequencies, temperature studies were performed with a standard Varian V-4540 temperature controller and quartz dewar. A variable temperature dewar was designed for the K-band cavity and is illustrated in Fig. 7. Modification of the microwave cavity was necessary to accommodate the dewar and allow tuning from

FIGURE 5

Mechanized dewar and microwave bridge support assembly.

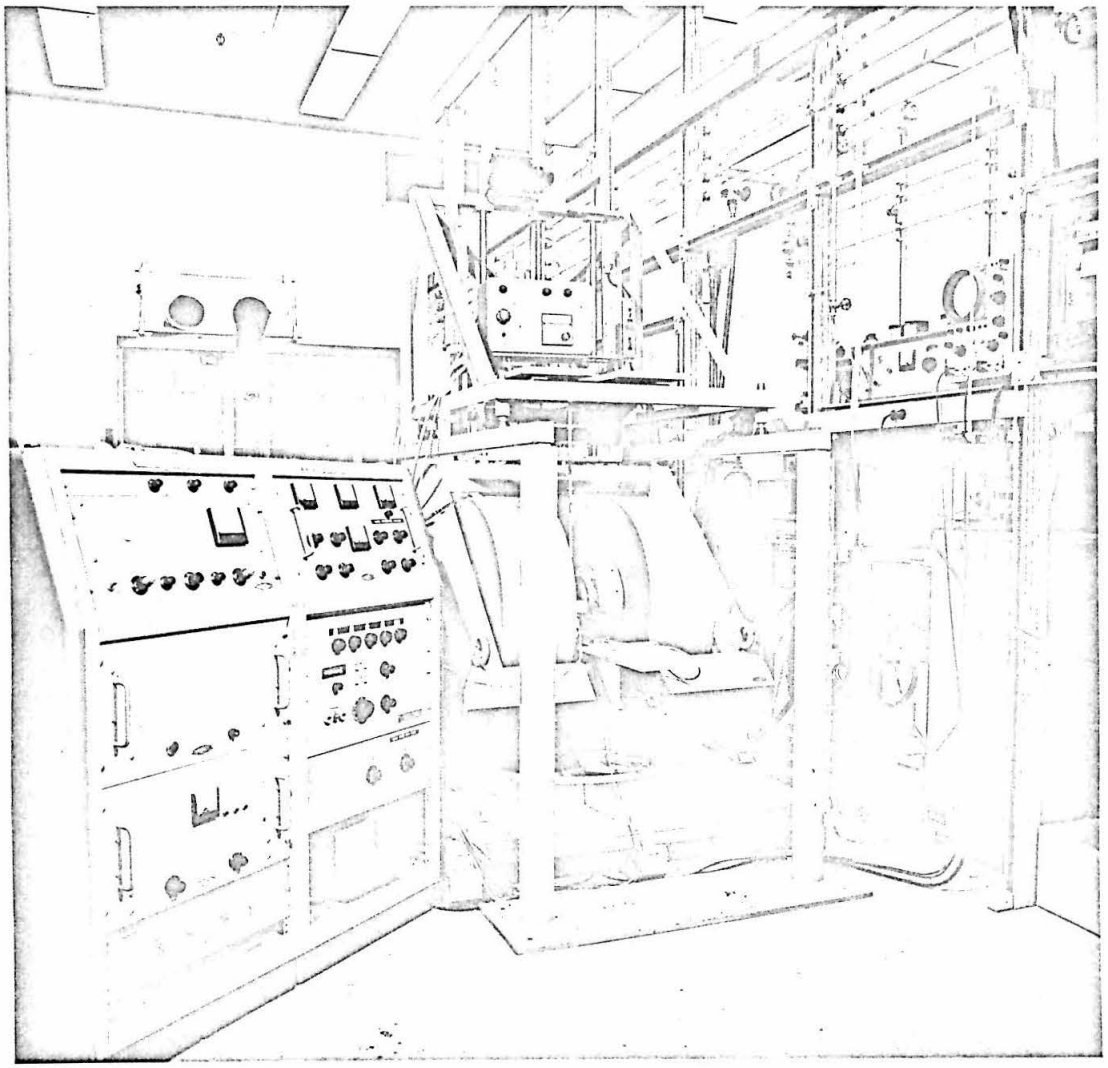

FIGURE 6

Support assembly carriage and framework.

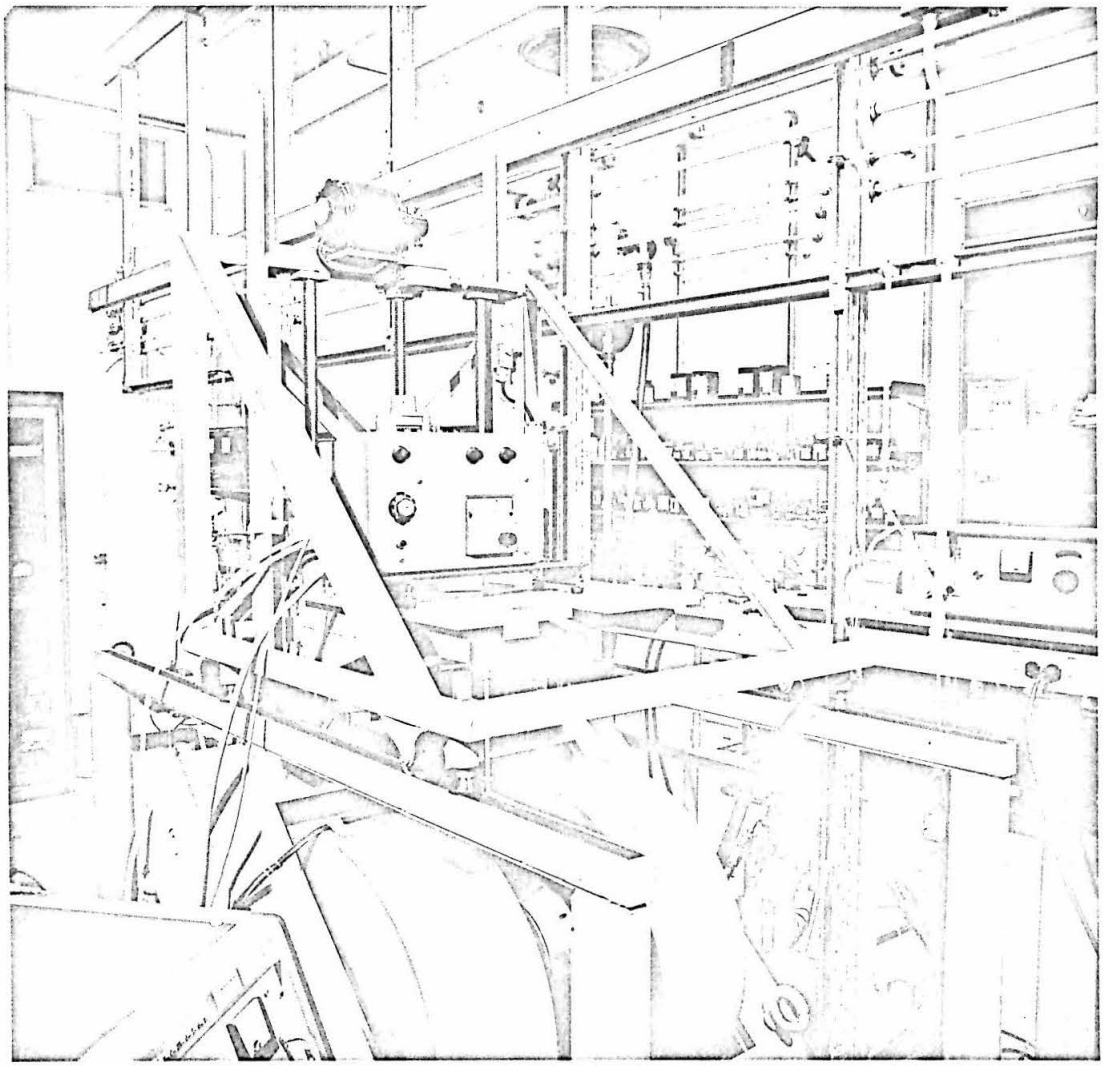

FIGURE 7

Variable temperature dewar for K-band microwave cavity. Unit was designed to operate with Varian 4540 variable temperature controller.

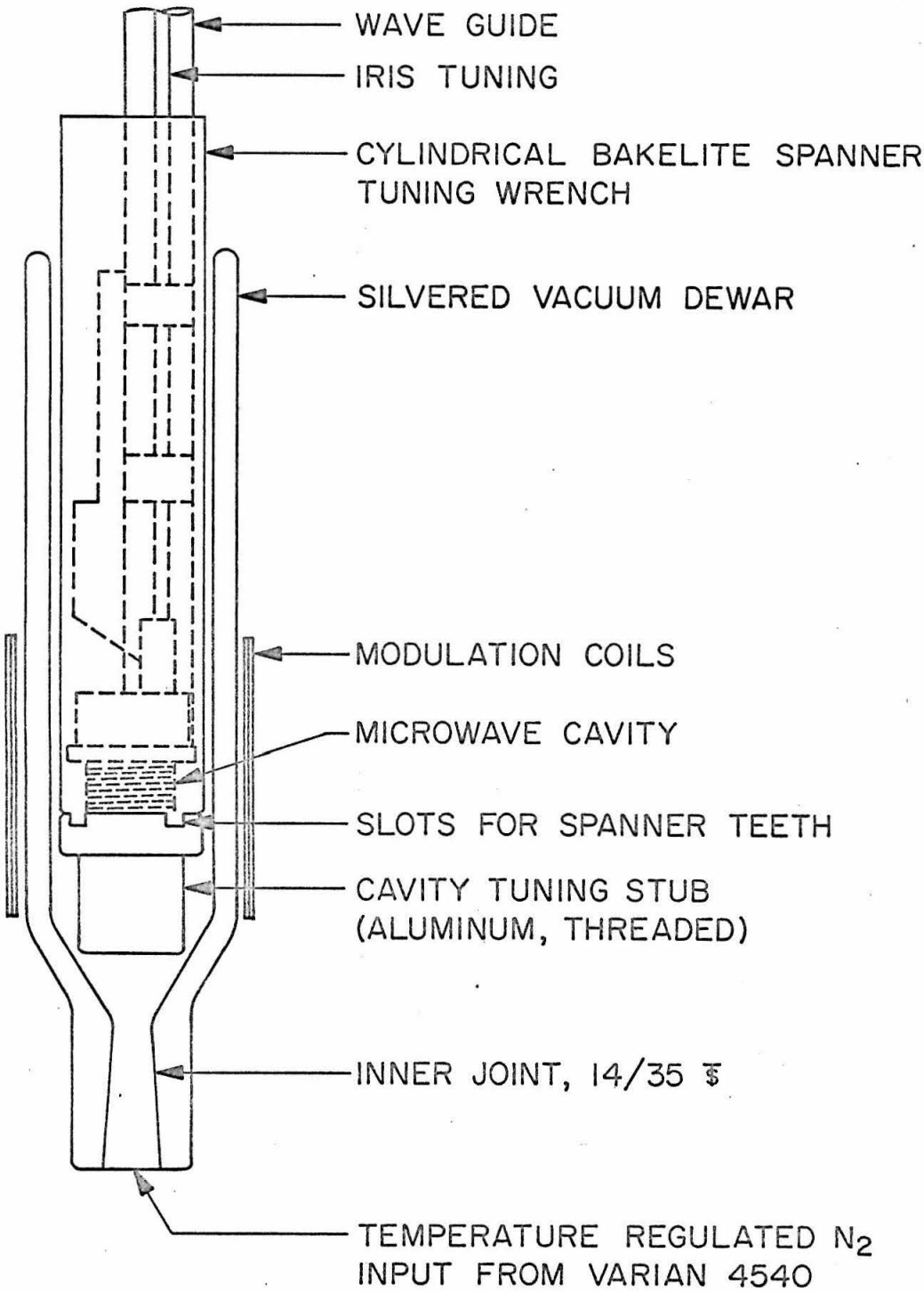
WAVE GUIDE
IRIS TUNING
CYLINDRICAL BAKELITE SPANNER TUNING WRENCH
SILVERED VACUUM DEWAR
MODULATION COILS
MICROWAVE CAVITY
SLOTS FOR SPANNER TEETH
CAVITY TUNING STUB (ALUMINUM, THREADED)
INNER JOINT, 14/35 ⅋
TEMPERATURE REGULATED N_2 INPUT FROM VARIAN 4540

the top. Temperature regulated nitrogen from the V-4540 wave swept around the entire cavity. Temperatures in both cavities were monitored with an iron-constantan thermocouple having an estimated $\pm 2^{\circ}C$ tolerance.

2. Density and Viscosity Measurements

A Weld specific gravity bottle was used to determine densities at room temperature; a set of hydrometers for other temperatures. Viscosity was measured in a standardized Ostwald viscometer suspended in a temperature regulated water bath.

3. Synthesis of Manganese(II) Complexes.

The anhydrous compounds $MnCl_2$ and $MnBr_2$ were obtained from their hydrates by heating under vacuum in two separate stages. Powdered hydrates were heated in a vacuum oven at $120^{\circ}C$ for 8 hours to remove the bulk of water. Final dehydration was accomplished by continuous pumping in a high vacuum system maintained at $190^{\circ}C$ for the chloride and $150^{\circ}C$ for the bromide over a 24 hour duration. Vapor pressures were monitored with a Veeco vacuum gauge Type RG-31X. In the case of $MnBr_2$ it was redissolved in acetonitrile, filtered, vacuum pumped, redissolved in water, filtered, and finally recrystallized from the aqueous medium. The dehydration procedure was then repeated and the compound was cycled in this fashion several times. This was necessary to remove organic matter and other insoluble solids, presumably oxyhalides and carbonates. Anhydrous $AgClO_4$ was also prepared from the hydrate by pumping at $90^{\circ}C$.

Higher temperatures caused the material to decompose and the red solids frozen in the liquid nitrogen trap suggested that one of the products was ClO_2--a very unstable and dangerous compound. Tetra-n-butylammonium bromide and tetraethylammonium chloride were analytical grade materials obtained from the Eastman Kodak Co. Tetra-n-butylammonium perchlorate was obtained from both Matheson-Bell and Southwestern Analytical Chemical Co. Prior to use, these compounds were recrystallized from acetonitrile, and dried in a vacuum oven at 60-70°C for roughly 24 hours. Matheson spectroscopic grade acetonitrile was used exclusively in this work.

The complexes were prepared under vacuum in a pyrex transfer apparatus suited for solution manipulation as shown in Fig. 8. Chemistry of formation for the tetrahedral complexes used in this study is shown as follows:

$$Bu_4NBr + MnBr_2 \xrightarrow{CH_3CN} 2\,Bu_4N^+ + MnBr_4^{-2}$$

$$Et_4NCl + MnCl_2 \xrightarrow{CH_3CH} 2\,Et_4N^+ + MnCl_4^{-2}.$$

For the tetrahedral halide complexes, weighed amounts of the manganese halide and corresponding tetraalkylammonium halide were placed in the vacuum apparatus and were heated for an hour at 90°C under constant evacuation to remove water picked-up during handling in air. Acetonitrile was weighed into a separate tube, containing P_2O_5, degassed by a repeated freeze-melt sequence under constant pumping and was finally distilled into the apparatus containing the weighed

FIGURE 8

Vacuum sample transfer apparatus. a) solid components are weighed into this section and degassed under vacuum; b) weighed solvent is vacuum transferred into round-bottom flask and degassed prior to mixing with solid components in (a); c) solution is decanted through valve into epr capillary tube that has been degassed; d) auxiliary tip containing glass filter for transfer of solutions prepared from reactions forming solid products.

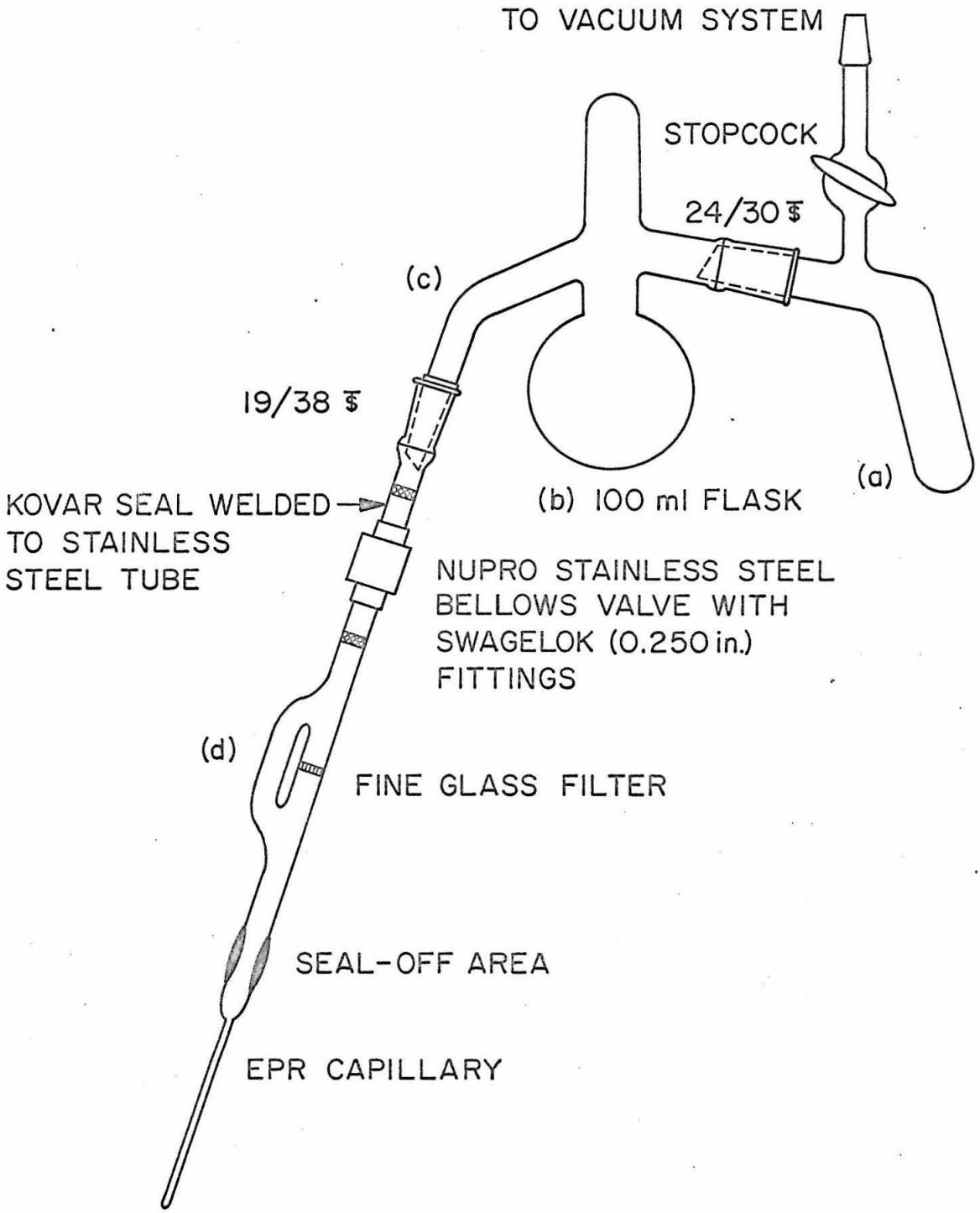
TO VACUUM SYSTEM
STOPCOCK
24/30 ⅁
(c)
19/38 ⅁
KOVAR SEAL WELDED
TO STAINLESS
STEEL TUBE
(b) 100 ml FLASK
(a)
NUPRO STAINLESS STEEL
BELLOWS VALVE WITH
SWAGELOK (0.250 in.)
FITTINGS
(d)
FINE GLASS FILTER
SEAL-OFF AREA
EPR CAPILLARY

solids. A magnetic stirring-bar was always included to insure proper mixing. Solutions were decanted under vacuum into an electron spin resonance capillary attached to the side of the apparatus through a stainless steel valve. The valve was then closed to prevent solvent transport; the capillary was frozen with liquid nitrogen and finally sealed-off under vacuum. Solvated manganese(II) was formed by similar chemistry involving a metathetical reaction requiring 2 parts (molar) $AgClO_4$ and 1 part $MnBr_2$

$$2\,AgClO_4 + MnBr_2 \xrightarrow{CH_3CN} Mn(CH_3CN)_6^{+2} + AgBr + 2\,ClO_4^-.$$

The bromide is preferred to the chloride because of its greater solubility in the solvent. It was prepared in the vacuum apparatus shown in Fig. 8 containing a glass filter to exclude any AgBr from the capillary.

IV. RESULTS AND DISCUSSION

1. $Mn(CH_3CN)_6^{+2}$

A spin relaxation study of the unique manganese(II) tetrahedral complexes, in particular the tetrabromide complex, is the main issue described in this research. Since the complexes are formed in acetonitrile and are known to exchange with the solvent, a brief re-examination of the solvated octahedral complex (55), $Mn(CH_3CN)_6^{+2}$, was conducted to carefully obtain constants of the spin Hamiltonian and resonance widths at both X and K-band frequencies. The effect on these parameters imposed by such phenomena as ion-pairing and exchange with the first and second coordination sphere is considered in this section as a preliminary step leading to the more detailed work on $MnCl_4^{-2}$ and $MnBr_4^{-2}$.

Electron spin resonance spectra of $Mn(CH_3CN)_6^{+2}$ taken at X and K-band frequencies are compared in Fig. 9. The line positions may be located by the eigenvalues of the spin Hamiltonian given in Eq. (13) where H_0 is the static magnetic field, g is the electron spectroscopic splitting factor, β is the Bohr magneton and A is the hyperfine coupling constant. In the octahedral complex, $^{55}Mn(II)$ is in the $^6S_{5/2}$ state and there are thirty fully allowed paramagnetic resonance transitions according to the selection rules ($\Delta m_S = \pm 1$, $\Delta m_I = 0$) with positions given adequately by the second-order expression rearranged from Eq. (13)

FIGURE 9

(a) Electron spin resonance spectrum taken at X-band frequencies of 0.005 m (0.0039 M) $Mn(CH_3CN)_6^{+2}$ in acetonitrile. (b) K-band (lower) spectrum. Sharp central peak is DPPH marker. H_0 increases to the left. Scale: 1 cm = 42 gauss.

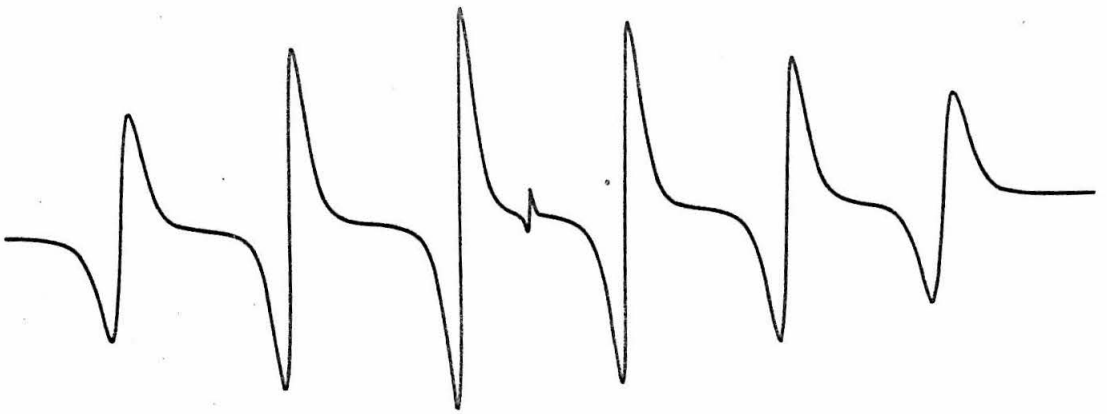

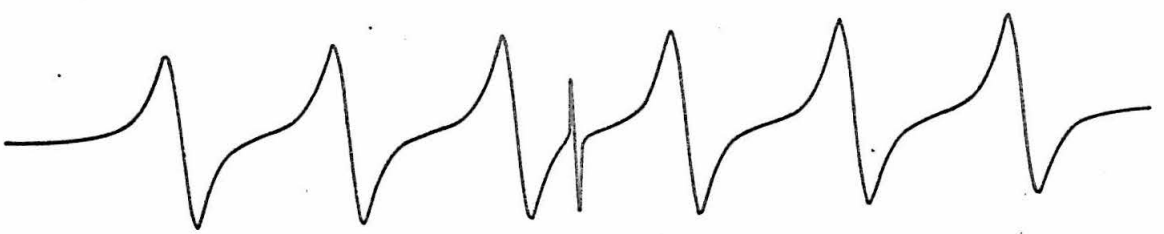

$$H_o(\text{gauss}) = \frac{1}{2}\left[\frac{\hbar\omega}{\langle g\rangle\beta} - \langle A\rangle m_I\right] \pm \frac{1}{2}\left\{\left[\langle A\rangle m_I - \frac{\hbar\omega}{\langle g\rangle\beta}\right]^2 - 2\langle A\rangle^2\left[I(I+1) - m_I^2 + m_I(2m_S+1)\right]\right\}^{\frac{1}{2}} \qquad (75)$$

where $m_I = -I, -I+1, \cdots I-1, I$ and $m_S = -S, -S+1, \cdots S-1, S$. From the above relation we see there are five $|m_S, m_I\rangle \rightarrow |m_S+1, m_I\rangle$ transitions for every m_I each appearing at slightly different positions. Since the angular momenta I and S are not completely decoupled at laboratory field strengths, second-order effects must be considered in the overall resonance width of each hyperfine component. However the second-order effects are small enough so that the $|m_S, m_I\rangle \rightarrow |m_S+1, m_I\rangle$ transitions are considered to be symmetrically disposed about the $|-\frac{1}{2}, m_I\rangle \rightarrow |\frac{1}{2}, m_I\rangle$ transition. Spin Hamiltonian parameters were extracted from the $|-\frac{1}{2}, \frac{1}{2}\rangle \rightarrow |\frac{1}{2}, \frac{1}{2}\rangle$ and $|-\frac{1}{2}, -\frac{1}{2}\rangle \rightarrow |\frac{1}{2}, -\frac{1}{2}\rangle$ transitions. Resonance widths were determined from the $|-\frac{1}{2}, \frac{1}{2}\rangle \rightarrow |\frac{1}{2}, \frac{1}{2}\rangle$ transition which provides the least amount of $m_S \rightarrow m_S + 1$ overlapping. The K-band spectrum shows six hyperfine components with nearly the same amplitude clearly reflecting a reduction in the second-order effect. Spin Hamiltonian parameters and resonance widths are presented in Table I. The g value reported in this work represents an average of a number of measurements and is definitely lower than the value reported by Chan, Fung and Lütje ($g = 2.003 \pm 0.001$ (Ref. 55)). The hyperfine constant was within the limits of error compared to the

Table I. Spin Hamiltonian Constants for $Mn(CH_3CN)_6^{+2}$ in Acetonitrile

Concentration (molal)		ΔH^* Gauss	$\langle g \rangle$	$\langle A \rangle$ Gauss
$Mn(CH_3CN)_6^{+2}$	Excess Bu_4NClO_4	±0.2	±0.0005	±0.2
0.005	0.000	8.7	2.0005	-93.1
0.005	0.110	9.8	2.0001	-93.0

*4th line; $|-\frac{1}{2}, \frac{1}{2}\rangle \rightarrow |\frac{1}{2}, \frac{1}{2}\rangle$ transition

former work (55). Using these parameters the thirty allowed line positions were computed from the second-order expression, Eq. (75), and the results for X-band frequencies are collected in Table II. These calculations confirm the symmetrical distribution of lines around the central $|-\frac{1}{2}, m_I\rangle \rightarrow |\frac{1}{2}, m_I\rangle$ transition and show that $m_I = \frac{1}{2}$ transitions have the narrowest range (5.2 gauss) of line positions.

An attempt was made to at least partially resolve the lines by running a dilute solution at elevated temperature where resonance widths were expected to be significantly narrowed by a decrease in viscosity. An experiment on 0.005 m stoichiometric $Mn(CH_3CN)_6^{+2}$ was conducted at 78°C and the spin Hamiltonian constants were: $\langle A \rangle = -93.2$ gauss, $\langle g \rangle = 2.0007$; the resonance width of the narrowest component (4th line) was 8.0 gauss. At these temperatures

Table II. $Mn(CH_3CN)_6^{+2}$ Line Positions in Gauss $|m_I, m_S\rangle \rightarrow |m_I, m_{S+1}\rangle$ Transitions

$\langle A \rangle = -93.1$, $\langle g \rangle = 2.0005$, $H_0 = 3270.9$

	m_S					$m_I > 0$ $\|m_S, m_I\rangle - \|m_{S+1}, m_I\rangle$
m_I	3/2	1/2	-1/2	-3/2	-5/2	$m_I < 0$ $\|m_S, m_I\rangle - \|m_{S-1}, m_I\rangle$
5/2	3488.1	3494.3	3500.6	3506.7	3512.9	6.2
3/2	3394.6	3398.4	3402.3	3406.1	3409.9	3.8
1/2	3303.7	3305.0	3306.3	3307.6	3308.9	1.3
-1/2	3215.6	3214.2	3212.9	3211.5	3210.2	1.4
-3/2	3130.6	3126.4	3122.2	3118.0	3113.9	4.2
-5/2	3048.8	3041.7	3034.6	3027.4	3020.2	7.2

it is conceivable that broadening mechanisms such as ligand exchange may become operative to frustrate our effort. We see at a glance from Table II that the close overlapping in the $m_I = 1/2$ component precludes resolution and that our only chance resides in the spectral wing, $m_I = \pm 5/2$, transitions. Unfortunately there was no evidence of partial resolution in any hyperfine component.

Experiments were conducted (68) on vacuum-prepared $Mn(CH_3CN)_6^{+2}$ to examine the response of the narrowest hyperfine component ($|-\frac{1}{2}, \frac{1}{2}\rangle \rightarrow |\frac{1}{2}, \frac{1}{2}\rangle$) to changes in concentration and frequency. Results of this study are summarized in Fig. 10 and indicate that resonance widths are essentially independent of frequency. However, they do increase with concentration (0.005 → 0.300 molal) and suggest that manganese spin-spin dipolar interactions are operative in this system.

Irreproducibility of resonance widths after brief exposure to air prompted a further investigation (68) into the role of water as a possible source of broadening. The comparison was made with $Mn(CH_3CN)_6^{+2}$ solutions prepared in air without special precautions toward moisture other than starting with dry reactants. The results are compiled in Table III and the response of resonance width to $Mn(CH_3CN)_6^{+2}$ concentration and to frequency are illustrated graphically in Fig. 11. Both X and K band widths increase with concentration. At higher concentrations a sizeable divergence occurs with $\Delta H_K > \Delta H_X$ which possibly reflects the presence of an additional paramagnetic component having a different g-value. Under these circumstances, the logical

FIGURE 10

Resonance width ($\left|-\frac{1}{2}, \frac{1}{2}\right\rangle \rightarrow \left|\frac{1}{2}, \frac{1}{2}\right\rangle$) as a function of $Mn(CH_3CN)_6^{+2}$ concentration at X (Δ) and K (O)-band frequencies.

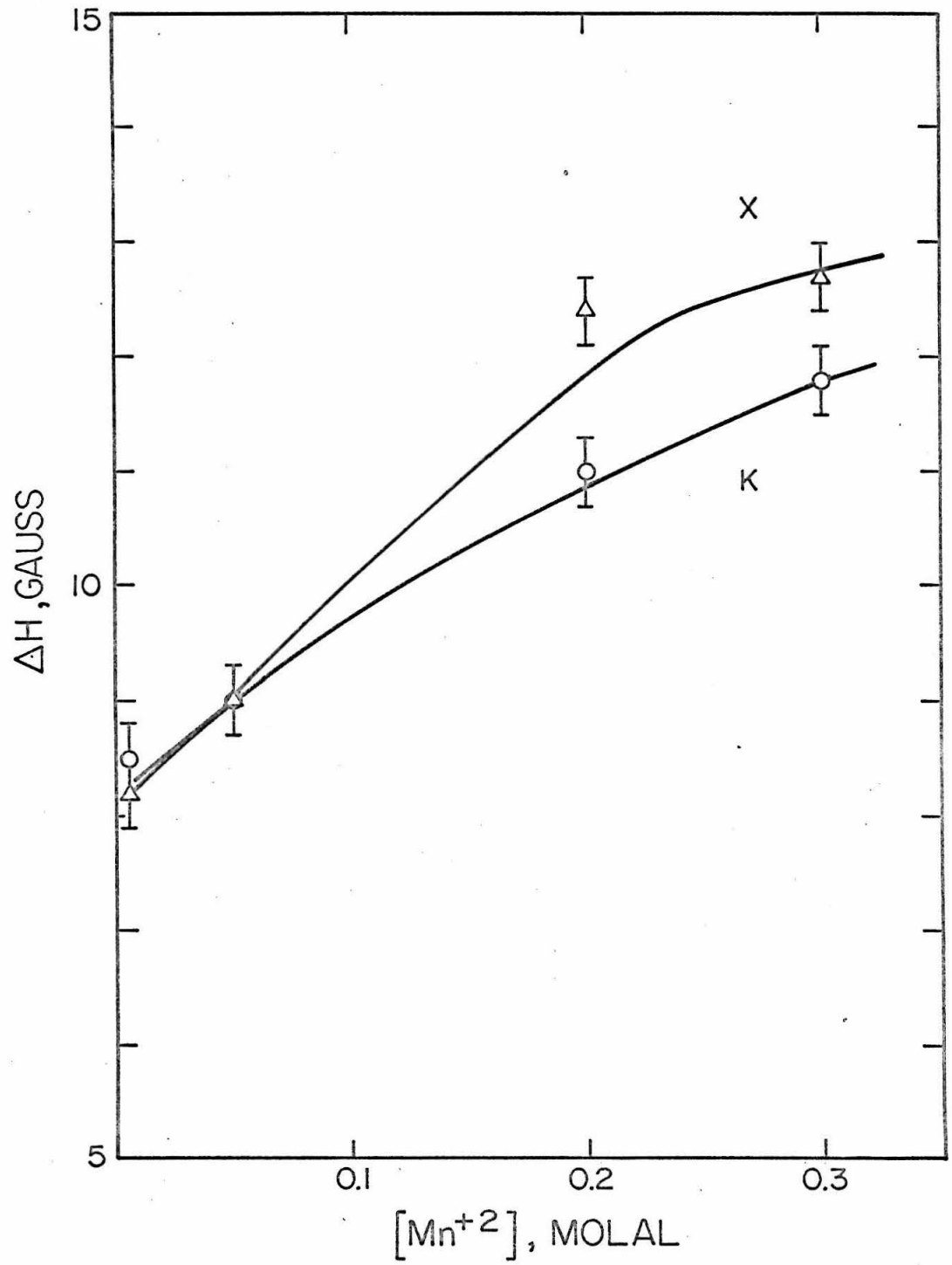
15
10
5
ΔH, GAUSS
X
K
0.1
0.2
0.3
[Mn+2], MOLAL

Table III. Resonance Widths and Spin Hamiltonian Constants as a Function of $Mn(CH_3CN)_6^{+2}$ Concentration

Concentration (molar) $Mn(CH_3CN)_6^{+2}$	X-band ΔH_4 gauss $\lvert -\frac{1}{2}, \frac{1}{2}\rangle \rightarrow \lvert \frac{1}{2}, \frac{1}{2}\rangle$	X-band $-\langle A\rangle$ ±0.2 gauss	X-band $\langle g\rangle$ ±0.0005	K-band ΔH_4 gauss $\lvert -\frac{1}{2}, \frac{1}{2}\rangle \rightarrow \lvert \frac{1}{2}, \frac{1}{2}\rangle$	K-band $-\langle A\rangle$ ±0.2 gauss	K-band $\langle g\rangle$ ±0.0005
0.005	8.3	92.9	2.000	9.4	39.7	2.0007
0.01	8.6	92.9	1.9999	10.6	94.0	2.0008
0.02	8.8	92.9	2.0000			
0.025	9.2	93.3	2.0001	10.4	93.8	2.0006
0.03	9.0	93.0	1.9997	10.8	92.9	2.0008
0.04	9.2	93.0	1.9999	10.7	93.9	2.0010
0.05	9.7	93.2	1.9998			
0.075	10.0	92.0	1.9999	11.4	93.8	2.0009
0.10	10.5	93.2	2.0004	11.4	93.5	2.0008
0.15	11.8	93.3	2.0004	14.0	94.9	2.0009
0.20	13.0	93.4	2.0004	19.8	94.2	2.0008

FIGURE 11

Resonance width ($|-\frac{1}{2}, \frac{1}{2}\rangle \rightarrow |\frac{1}{2}, \frac{1}{2}\rangle$) as a function of $Mn(CH_3CN)_6^{+2}$ concentration at X and K-band frequencies.

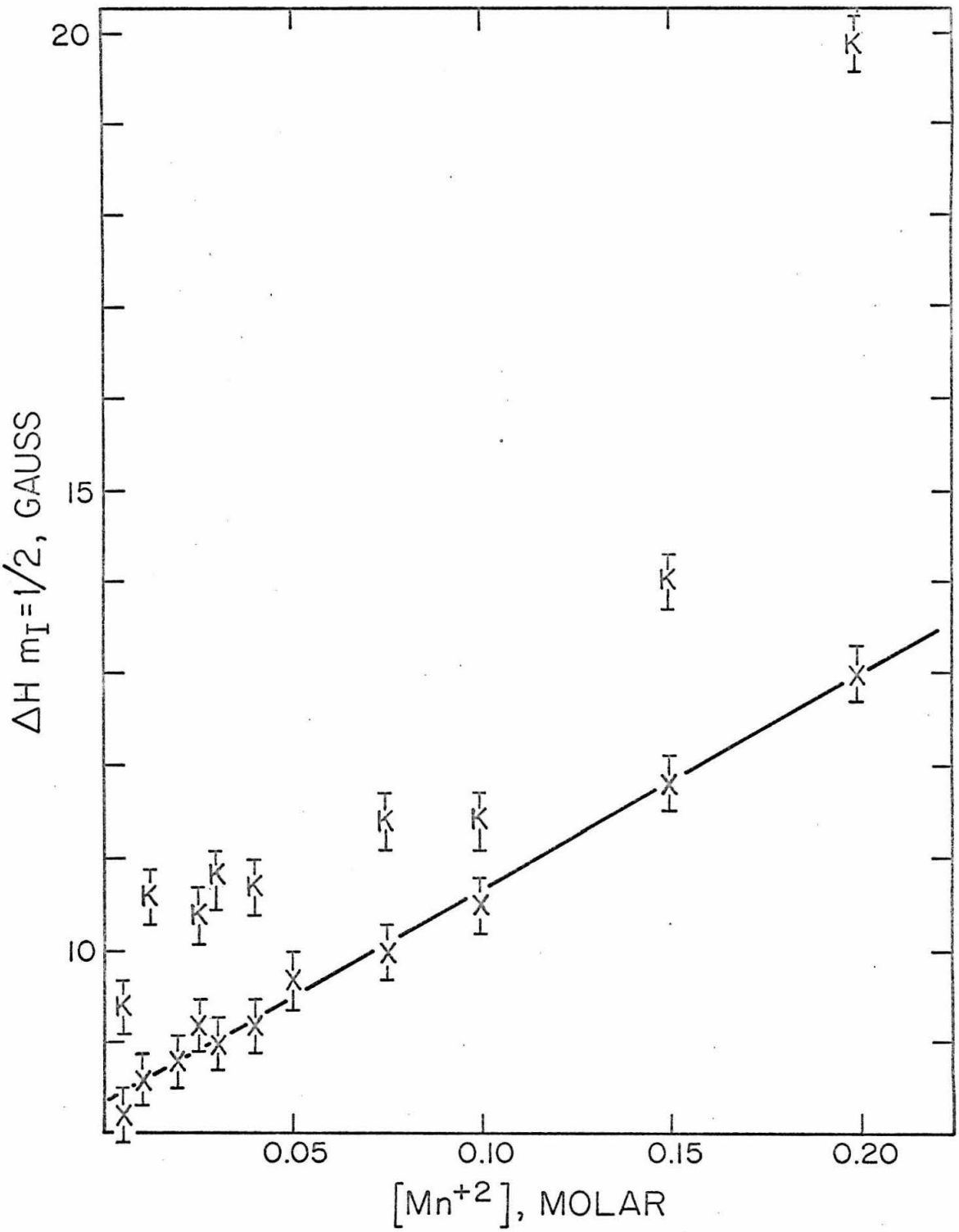
20
15
10
0.05
0.10
0.15
0.20
ΔH m_I=1/2, GAUSS
[Mn^{+2}], MOLAR

suspect is the hexaaqueous complex, $Mn(H_2O)_6^{+2}$. In order to impose such a large effect, water must be coming in with the dried components which, in fact, are known to be hygroscopic. Since the solid components were not redried under vacuum it is reasonable to expect considerable amounts of water to be present and this is consistent with the effect becoming more noticeable at higher salt concentrations. At high concentration the solution may also be very hygroscopic. Let us now calculate the shift in band centers, ΔH, arising from a change of frequency using the simple relation

$$\Delta H = H_2 - H_1 = \frac{h\nu}{\beta}\left(\frac{1}{g_2} - \frac{1}{g_1}\right). \tag{76}$$

Taking g_2, $Mn(CH_3CN)_6^{+2} = 2.0005$ and g_1, $Mn(H_2O)_6^{+2} = 2.0023$, we find $\Delta H_X = 3.1$ gauss and $\Delta H_K = 11.2$ gauss. As usual h represents Plank's constant, ν is the frequency (Hz) and β is the Bohr magneton. Clearly, a Δg of this magnitude can, indeed, account for a large frequency effect and consequently presents a plausible explanation for the observed results. Further experiments conducted by J. E. Crawford (68) in which water was deliberately added to the complex verified these suspicions. In any event, special precautions are required to insure the absence of water to obtain meaningful spin Hamiltonian constants for the solvated complex, $Mn(CH_3CN)_6^{+2}$.

Since ClO_4^- provides the counterion partner for the paramagnetic complex, a brief study was deployed on the interaction between the two ionic components and its effect on the effective spin

Hamiltonian constants and resonance widths. Excess Bu_4NClO_4 was added to a solution containing 0.005 molal (M) $Mn(CH_3CN)_6^{+2}$ and the effects on the m = $\frac{1}{2}$ hyperfine component resonance widths are reported in Fig. 12. Excess Bu_4NClO_4 is defined as $[ClO_4^-]/[Mn^{+2}] > 2$. A slight increase in resonance width with increasing excess Bu_4NClO_4 concentration was observed. Above 0.10 M excess Bu_4NClO_4 the resonance width increase appears to level off at approximately 10.5 gauss. At any rate the effect is small and definitive information would certainly be obscured by uncertainties in the measurements. Furthermore, there were no significant effects observed on the effective spin Hamiltonian constants within the concentration ranges examined.

2. $[MnCl_4]^{-2}$

A study of the $[MnCl_4]^{-2}$ complex in acetonitrile was carried out to provide a comparison for the subsequent work described on $[MnBr_4]^{-2}$. Relaxation processes are frequently interwoven with the detail of several phenomena and it is sometimes helpful to have "chemical" arguments at hand to gain more insight on the situation. On these grounds it is anticipated that a parallel study between the tetrachloro and tetrabromomanganese(II) complexes in the same solvent may provide this sort of information. Bearing this in mind, experiments on the chloride system were designed to investigate ion-pairing, chemical exchange, dipolar interactions and frequency or field effects under conditions very much analogous to the bromide

FIGURE 12

Resonance width, ΔH ($|-\frac{1}{2}, \frac{1}{2}\rangle \rightarrow |\frac{1}{2}, \frac{1}{2}\rangle$), of 0.005 M $Mn(CH_3CN)_6^{+2}$ as a function of Bu_4NClO_4 concentration.

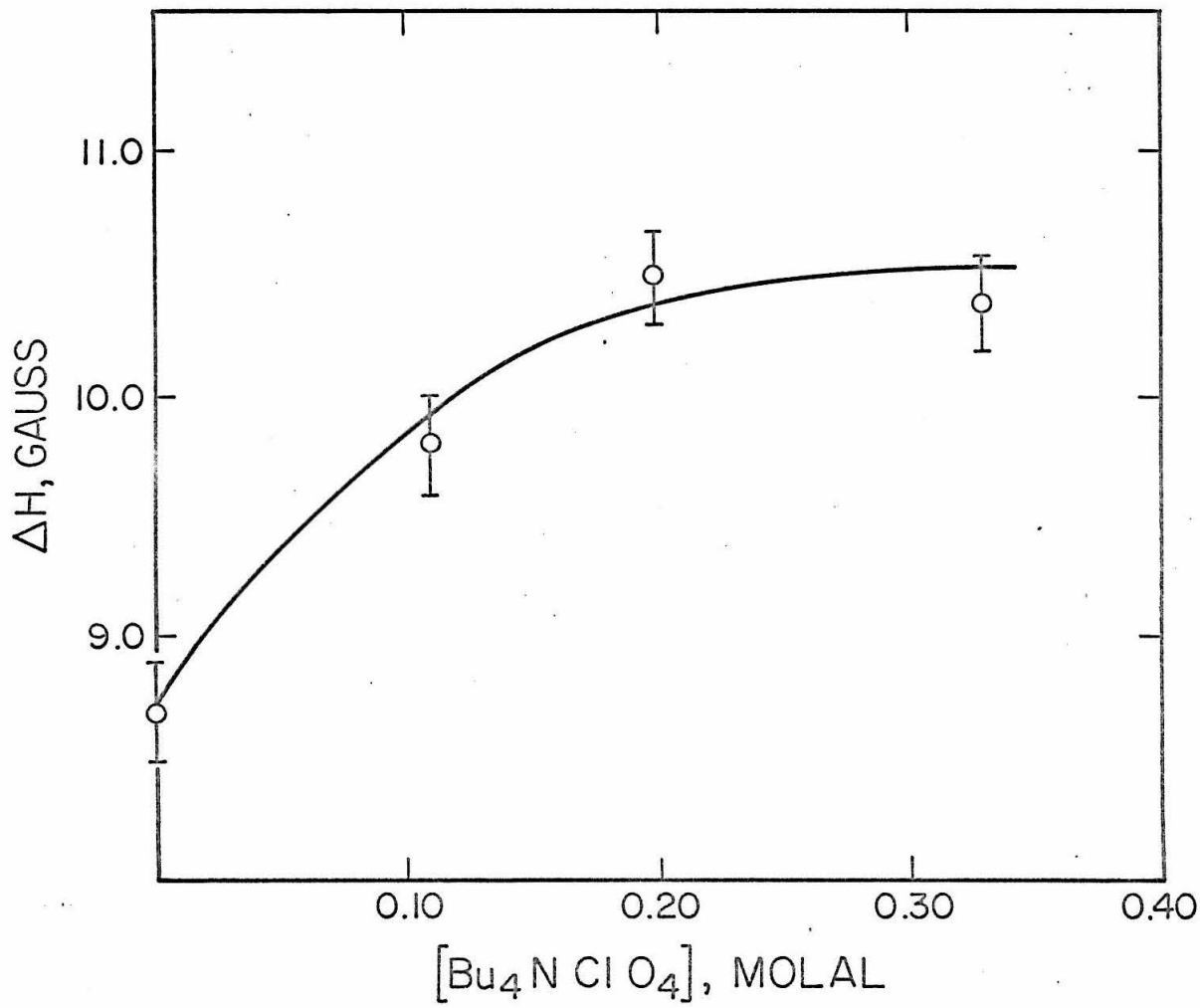
11.0
10.0
9.0
ΔH, GAUSS
0.10
0.20
0.30
0.40
[Bu4 N Cl O4], MOLAL

studies.

Typical electron spin resonance spectra of $[MnCl_4]^=$ with a tetraethylammonium, Et_4N^+, counterion taken at X and K-band frequencies are presented in Fig. 13. Spectra may be explained quite adequately on the basis of the effective spin Hamiltonian and its eigenvalues taken to second order as given in Eqs. (12), (13) and (75). In this case also, the effective spin Hamiltonian parameters were extracted from the $|-\frac{1}{2}, -\frac{1}{2}\rangle \rightarrow |\frac{1}{2}, -\frac{1}{2}\rangle$ and $|-\frac{1}{2}, \frac{1}{2}\rangle \rightarrow |\frac{1}{2}, \frac{1}{2}\rangle$ transitions. Resonance widths were determined from the $|-\frac{1}{2}, \frac{1}{2}\rangle \rightarrow |\frac{1}{2}, \frac{1}{2}\rangle$ transition which provides the least amount of $m_S \rightarrow m_S + 1$ overlapping. Again, as in the solvated complex case, the K-band spectrum shows six hyperfine components with nearly the same amplitude reflecting reduction in the second-order effects. A careful determination of the g-value was made by comparison to purified DPPH diluted with KCl contained in sealed capillaries and also from accurate field and frequency measurements. All resonance widths in the chloride series were determined from the least overlapped hyperfine component, $m_I = \frac{1}{2}$, which consequently displays the most Lorentzian character. Constants of the effective spin Hamiltonian computed from a wide range of experimental parameters utilized in this study are presented in Table IV. Our g-values were much lower than the value reported by Chan, Fung and Lütje ($g = 2.007 \pm 0.001$) (55). The hyperfine constant was within the limits of error compared to the former work (55). Using these constants the thirty allowed line positions were computed from the second-order expression given in Eq. (75) and the

FIGURE 13

(a) X-band electron spin resonance spectrum of 0.0039 M $MnCl_4^{-2}$ in acetonitrile.

(b) K-band spectrum.

H_o increases to the right. Scale: 1 cm = 34 gauss.

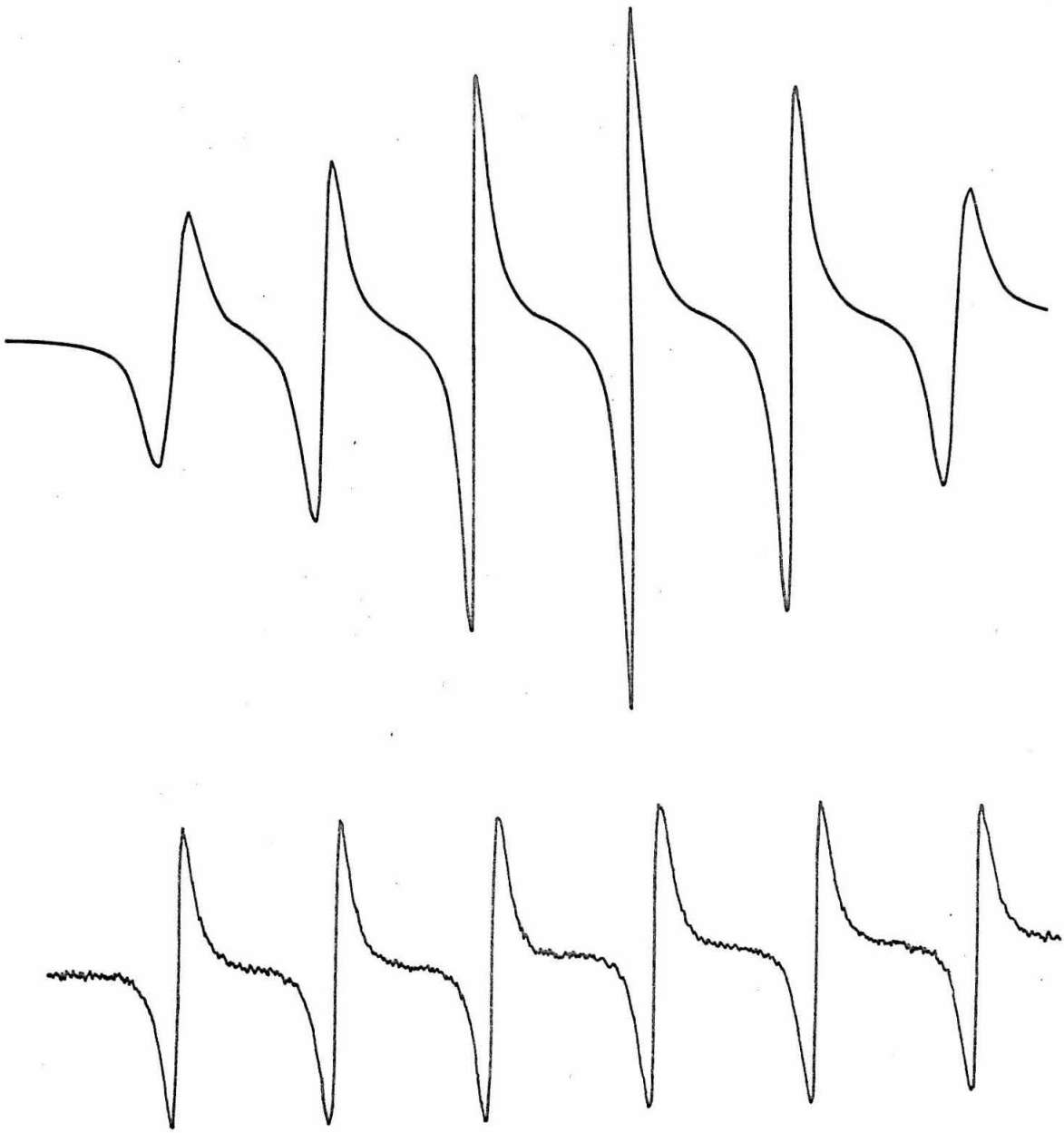

Table IV. Spin Hamiltonian Constants for $MnCl_4^=$ in Acetonitrile

Concentration (molal)			Frequency	⟨A⟩	⟨g⟩
$[MnCl_4^=]$	Excess $[Et_4NCl]$	Excess $[Et_4NClO_4]$	range	gauss ±0.2	±0.0005
0.005	0.000	0.000	K	-79.3	2.0026
0.005	0.113	0.000	K	-79.1	2.0027
0.005	0.113	0.000	K	-79.6	2.0025
0.005	0.000	0.101	K	-78.9	2.0027
0.005	0.000	0.101	K	-79.4	2.0027
0.005	0.000	0.682	K	-78.9	2.0027
0.050	0.000	0.000	X	-79.8	2.0021
0.052	0.040	0.000	X	-79.5	2.0024
0.00005	0.000	0.000	K	-79.8	
0.00017	0.000	0.000	K	-79.6	
0.00025	0.000	0.000	K	-79.7	
0.0005	0.000	0.000	K	-79.8	
0.005	0.000	0.000	K	-79.7	

results for X-band frequencies are summarized in Table V. As in the solvated complex case, these calculations demonstrate the symmetrical deployment of lines around the central $|-\frac{1}{2}, m_I\rangle \rightarrow |\frac{1}{2}, m_I\rangle$ transition and show that $m_I = \frac{1}{2}$ transitions have the narrowest (3.7 gauss) range of line positions. Partial resolution of individual lines was neither anticipated nor observed.

Tabie V. $MnCl_4^{-2}$ Line Positions in Gauss $|m_S, m_I\rangle \rightarrow |m_S+1, m_I\rangle$ Transition

Mn^{+2} epr line positions in gauss m_S to m_S+1 transitions

A = -79.5 gauss frequency = 9.555 GHz $\langle g \rangle$ = 2.002

m_S =	+3/2	+1/2	-1/2	-3/2	-5/2
m_I = 5/2	3597.8	3602.2	3606.6	3611.0	3615.4
m_I = 3/2	3518.1	3520.8	3523.5	3526.2	3528.9
m_I = 1/2	3440.2	3441.1	3442.0	3442.9	3443.9
m_I = -1/2	3364.2	3363.3	3362.3	3361.4	3360.4
m_I = -3/2	3290.3	3287.5	3284.6	3281.7	3278.8
m_I = -5/2	3218.7	3213.8	3208.9	3203.9	3199.0

Returning to Table IV we notice that the hyperfine coupling constant $\langle A \rangle$ decreases from -79.7 ± 0.2 gauss for dilute stoichiometric 0.005 M $MnCl_4^{-2}$ to -78.9 ± 0.2 gauss for 0.005 M $MnCl_4^{-2}$ with

0.682 M excess Et_4NClO_4. Therefore upon increasing the Et_4N^+ concentration to favor the presence of our hypothetical ion-pair, we observe a slight decrease in $\langle A \rangle$, greater than the limit of error. Assuming that ClO_4^- does not interact with the complex, the increase of Et_4N^+ counterion concentration may expand the complex slightly through an electrostatic interaction thus provoking a decrease in hyperfine coupling. In addition, the $\langle g \rangle$ values do not change under any experimental circumstance and we may conclude that the interactions are isotropic.

Variation in resonance widths of solutions containing stoichiometric $MnCl_4^{-2}$ with tetraethylammonium providing the counterion were examined over a wide manganese concentration range at both X and K-band frequencies. The results are presented in Tables VI and VII and are illustrated graphically in Figs. 14 and 15. There were no significant changes in the hyperfine coupling constant or g-value over the entire concentration range and little, if any, resonance width dependency on frequency. Inspection of the two plots reveal the same interesting general behavior. Starting from the dilute side the sequence is: (1) constant resonance width, ΔH, up to about 0.01 or 0.02 Molar $MnCl_4^{-2}$, (2) a sharp increase of ΔH between 0.1 or 0.02 M and 0.05 M $MnCl_4^{-2}$, (3) constant ΔH between 0.05 and 0.075 to 0.10 M $MnCl_4^{-2}$ and, finally, (4) a continuous increase above these concentrations. The initial rise in the observed resonance width, ΔH, commencing about 0.01 M $MnCl_4^{-2}$ may be caused by the onset of a new paramagnetic component having a slightly smaller relaxation time.

Table VI. X-Band Resonance Width Dependence on Concentration of Stoichiometric $MnCl_4^{-2}$ at 298°K

Concentration (Molar) $[Mn^{+2}]$	ΔH (Gauss) $\left\|-\frac{1}{2}, \frac{1}{2}\right\rangle \rightarrow \left\|\frac{1}{2}, \frac{1}{2}\right\rangle$	Concentration (Molar) $[Mn^{+2}]$	ΔH (Gauss) $\left\|-\frac{1}{2}, \frac{1}{2}\right\rangle \rightarrow \left\|\frac{1}{2}, \frac{1}{2}\right\rangle$
0.01	8.6	0.075	10.8
0.02	9.2	0.10	12.0
0.03	9.8	0.15	13.8
0.04	10.1	0.20	14.8
0.05	10.3		

Table VII. K-Band Resonance Width Dependence on Concentration of Stoichiometric $MnCl_4^{-2}$ in Dilute Range at 298°K

Concentration (Molar) $[Mn^{+2}]$	ΔH (Gauss) $\left\|-\frac{1}{2}, \frac{1}{2}\right\rangle \rightarrow \left\|\frac{1}{2}, \frac{1}{2}\right\rangle$	Hyperfine Constant $-\langle A \rangle$
3.9×10^{-5}	9.9 *	79.8
1.3×10^{-4}	8.3	79.6
1.9×10^{-4}	9.3	79.7
3.9×10^{-4}	8.7	79.8
3.9×10^{-3}	8.9	79.7

* High modulation level requirement for weak signal may have saturated resonance.

FIGURE 14

X-band resonance width as a function of stoichiometric $MnCl_4^{-2}$ concentration.

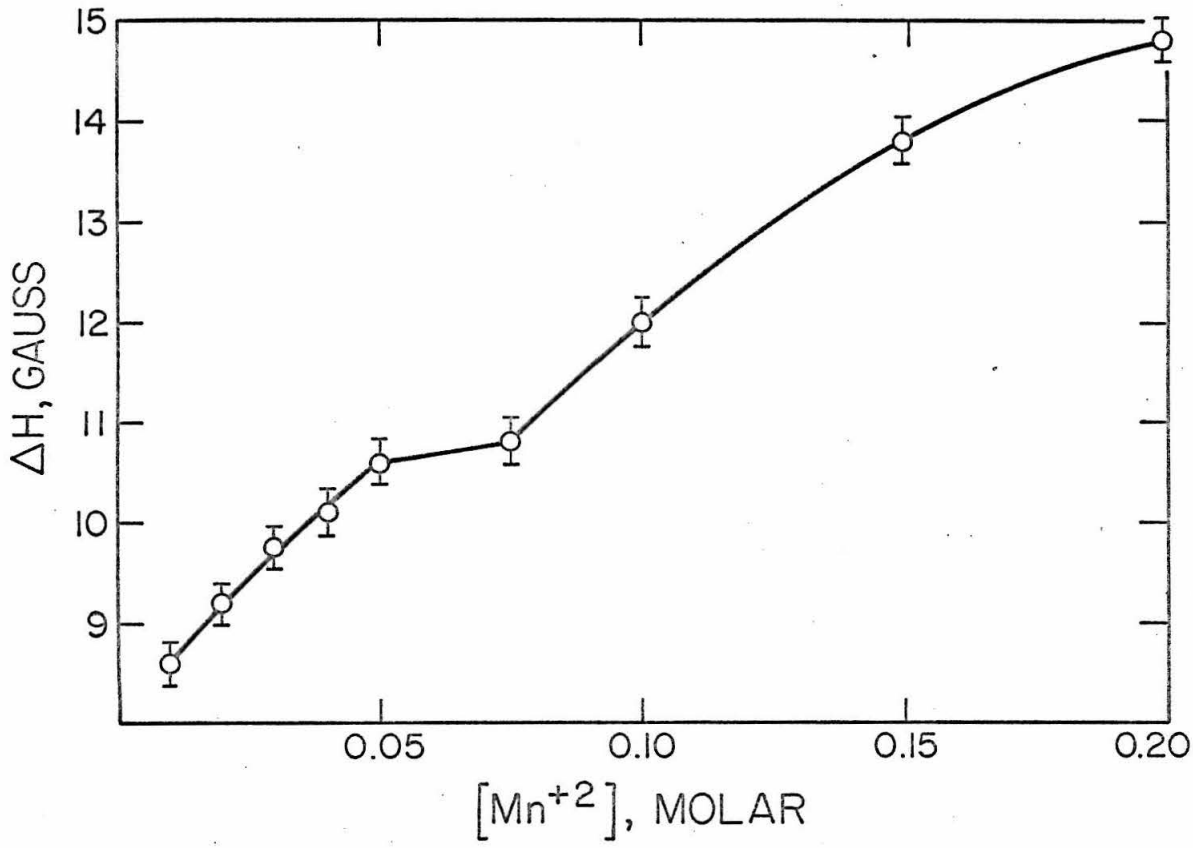
15
14
13
12
11
10
9
ΔH, GAUSS
0.05
0.10
0.15
0.20
[Mn+2], MOLAR

FIGURE 15

K-band resonance width as a function of stoichiometric $MnCl_4^{-2}$ concentration.

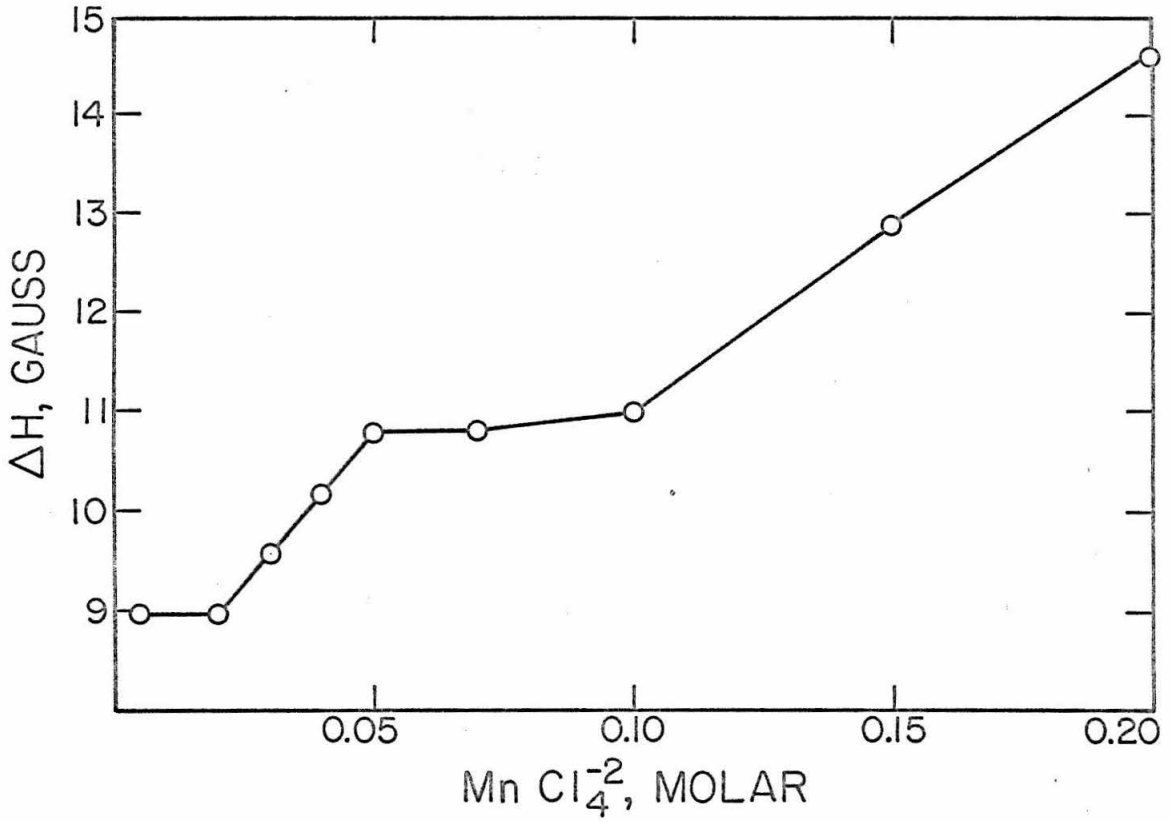
15
14
13
12
11
10
9
ΔH, GAUSS
0.05
0.10
0.15
0.20
Mn Cl$_4^{-2}$, MOLAR

A possible candidate is an ion-pair consisting of a relatively short range electrostatic marriage between the paramagnetic anion and its counterion. The interaction may be represented by a simple equilibrium model

$$\underset{A}{MnCl_4^{=}} + \underset{C}{Et_4N^+} \overset{K_a}{\rightleftharpoons} \underset{B}{[Et_4N^+ \cdots MnCl_4^{=}]}$$

or possibly by

$$[Et_4N^+ \cdots MnCl_4^{=}] + Et_4N^+ \overset{K_a}{\rightleftharpoons} [Et_4N^+ \cdots MnCl_4^{=} \cdots Et_4N^+].$$

In the absence of structural detail in solution which electron spin resonance cannot provide, let us, for the moment, choose the simpler equilibria as our model. A dynamical association between components A and C may lead to spin relaxation through distortions imposed on the paramagnetic complex by the counterion. Since states A and B are almost magnetically equivalent it would be difficult to assign a rapid exchange limit to the dynamical process. Nevertheless, there are several experimental approaches that should inject additional insight into our proposal that ion pairing is responsible for electron spin relaxation. We, first, explore the effect of Et_4N^+ counterion from two different sources on the resonance width by changing the counterion concentration relative to $MnCl_4^{-2}$. Secondly, we shall "freeze-in" the anticipated broadening effect due to viscosity in order to get a better look at ion-pairing.

The first study was performed with 0.05 M $MnCl_4^=$ solutions and excess Et_4N^+ was provided by tetraethylammonium chloride. Chloride ion concentrations in excess of the stoichiometric 4:1 ratio were taken to be "excess" concentrations. Resonance width dependency on excess chloride concentration at three different temperatures is compiled in Table VIII. In Figs. 16 and 17 we have plotted the variation of resonance width vs. excess Et_4NCl concentration at X-band frequency for the two sharpest hyperfine components. Addition of excess chloride causes an initially rapid increase in resonance width which gradually diminishes at higher concentrations. There is virtually no difference between the results depicted in Figs. 16 and 17. As can be seen the broadening effect increases with decreasing temperature and probably reflects a significant viscosity change. A plot of the chloride curve (Fig. 16) compensated for the association of Et_4NCl in acetonitrile at 26°C (K_d = 0.029) is shown in Fig. 18 and it is apparent that there is still a small initial increase in the curve before straightening out. Recalling Figs. 14 and 15 we notice that stoichiometric 0.05 M (0.039 M) $MnCl_4^=$ solutions are nearly converted to the ion-pair so that we cannot expect a large initial rise in ΔH due to a "chemical-shove" in favor of the ion-pair predicated by the mutual counterion upon addition of Et_4NCl. The effect of excess Et_4NCl on the resonance width is small amounting only to 3-4 gauss over a wide range of concentration and viscosity.

Table VIII. $MnCl_4^{-2}$ Resonance Width as a Function of Excess $[Cl^-]$

Excess Concentration (Molal)		$\|-\frac{1}{2}, m_I\rangle \rightarrow \|+\frac{1}{2}, m_I\rangle$ Resonance Widths (Gauss)																	
		T = 268°K						T = 299°K						T = 355°K					
$[Cl^-]_d$	$[Cl^-]_a$	-5/2	-3/2	-1/2	1/2	3/2	5/2	-5/2	-3/2	-1/2	1/2	3/2	5/2	-5/2	-3/2	-1/2	1/2	3/2	5/2
0.00	0.00	13.7	11.3	10.0	10.0	10.7	13.7	13.6	11.5	10.3	9.4	9.9	12.8	13.7	11.0	9.3	8.7	9.9	12.7
0.004	0.004	14.9	12.7	11.2	10.4	11.6	13.4	14.1	11.7	10.3	9.8	10.8	13.7	13.8	11.8	9.6	9.9	10.2	13.3
0.140	0.0518	16.1	14.4	13.3	12.9	13.3	15.3	14.4	12.4	11.2	11.0	11.6	13.7	14.1	12.0	10.5	10.7	11.1	13.5
0.610	0.129	17.2	15.3	14.9	14.4	15.2	16.0	15.2	13.5	12.4	12.1	12.6	14.3	14.6	12.2	10.6	10.7	11.7	13.2
0.983	0.173	17.9	17.0	16.3	16.0	16.4	17.8	15.6	14.1	12.8	12.8	12.9	15.2	14.4	12.8	11.9	11.5	12.2	14.4

$[Cl^-]$ subscripts designate Et_4NCl to be (d) completely dissociated in CH_3CN and (a) partially associated.

FIGURE 16

Variation in resonance width, ΔH (gauss, $|-\frac{1}{2}, \frac{1}{2}\rangle \rightarrow |\frac{1}{2}, \frac{1}{2}\rangle$) of 0.05 M $MnCl_4^{-2}$ with excess molal Et_4NCl at 268°, 299° and 355°K.

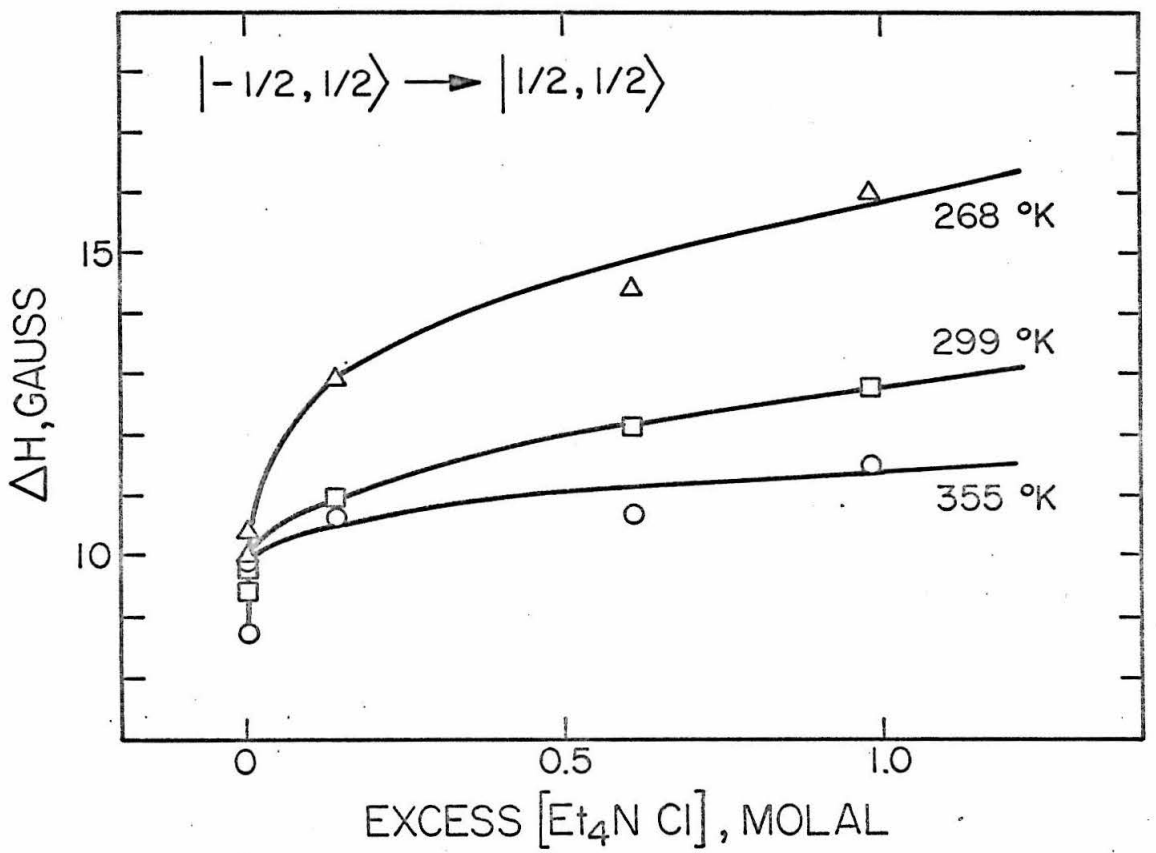
|-1/2, 1/2⟩ → |1/2, 1/2⟩
268 °K
299 °K
355 °K
ΔH, GAUSS
15
10
0
0.5
1.0
EXCESS [Et4N Cl], MOLAL

FIGURE 17

Variation in resonance width, ΔH (gauss, $|-\frac{1}{2}, -\frac{1}{2}\rangle \rightarrow |\frac{1}{2}, -\frac{1}{2}\rangle$) of 0.05 M $MnCl_4^{-2}$ with excess molal Et_4NCl at 268°, 299° and 355°K.

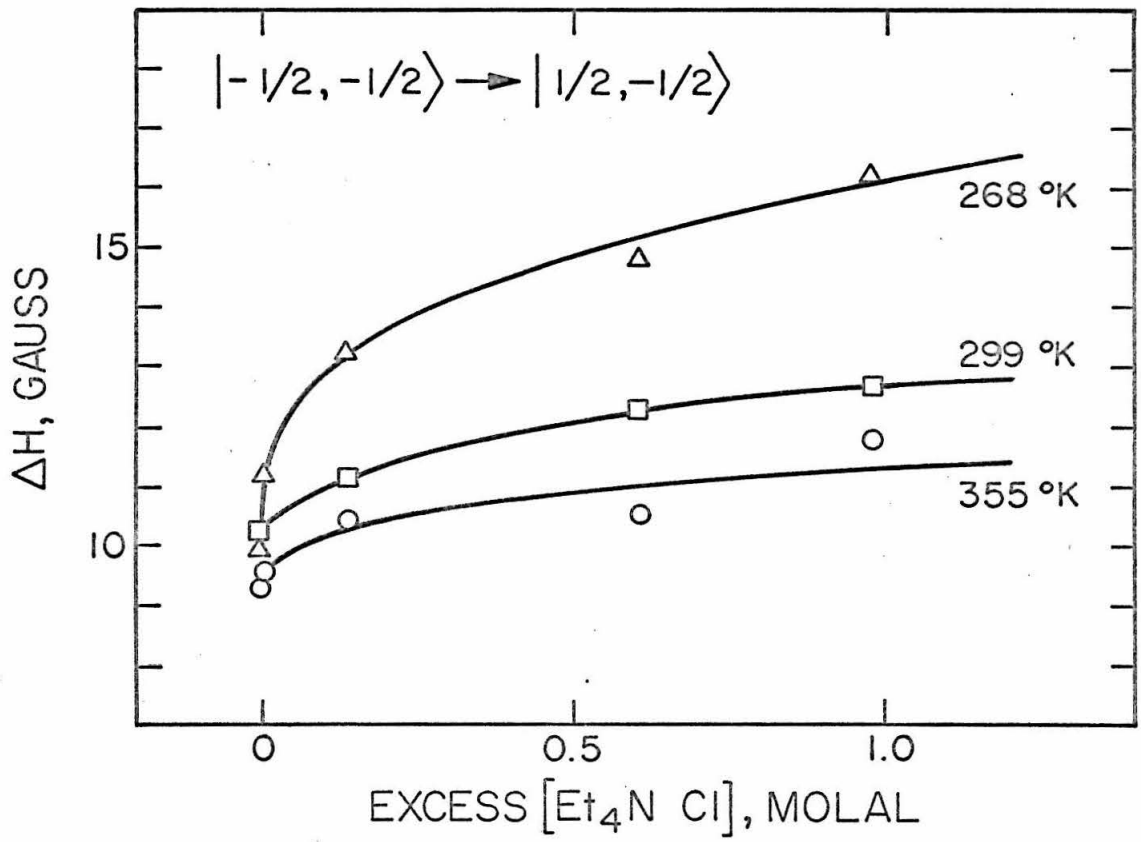
|-1/2,-1/2⟩ → |1/2,-1/2⟩
268 °K
299 °K
355 °K
ΔH, GAUSS
15
10
0
0.5
1.0
EXCESS [Et4N Cl], MOLAL

FIGURE 18

Variation in resonance width, ΔH (gauss, $|-\frac{1}{2}, \frac{1}{2}\rangle \rightarrow |\frac{1}{2}, \frac{1}{2}\rangle$) of 0.05 M $MnCl_4^{-2}$ with excess molal Et_4NCl compensated for association at 299°K.

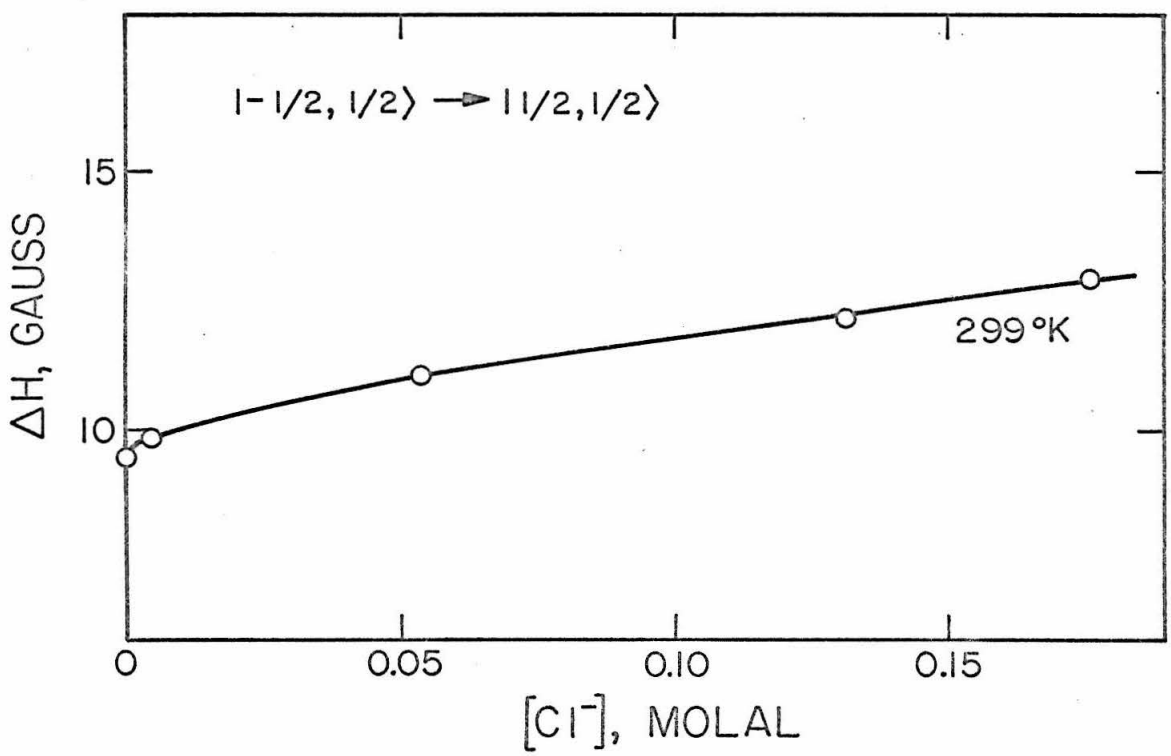
|-1/2, 1/2⟩ → |1/2, 1/2⟩
15
10
ΔH, GAUSS
299°K
0
0.05
0.10
0.15
[Cl⁻], MOLAL

A parallel experiment using tetraethylammonium perchlorate was performed by J. E. Crawford (68) and the results were superimposable with the 299°K curve in Fig. 16. If we assume that the ClO_4^- exchange rate to be slower than Cl^-, we may conclude that chemical exchange between Cl^- and $MnCl_4^=$ is not on the electron spin resonance time scale and, as a result, does not significantly contribute to spin relaxation.

Garrett and Morgan (52) have established that electron spin relaxation of the unpaired electrons in solvated manganese(II) complexes arises principally through spin-orbit interaction caused by modulation of the ligand field resulting from transient distortions of the complex by solvent fluctuations in the immediate surroundings of the paramagnetic ion. If this mechanism were the only one operative here, the resonance widths would vary linearly with the correlation time characteristic of the solvent fluctuations and would not be strongly dependent upon excess chloride concentration. It has been suggested (52) that this correlation time is proportional to $\eta M/\rho T$, where η is the viscosity of the solution, M is the molecular weight of the solvent, and ρ is the density of the solvent at temperature T. In Table IX, we have shown the variation of the resonance widths vs. $\eta M/\rho T$ for five solutions, each containing a different excess chloride concentration (0, 0.004, 0.14, 0.61, 0.98 M. The results are plotted in Fig. 19. It is significant to note that, whereas the resonance widths for each of these solutions do vary linearly with $\eta M/\rho T$ as the solvent structural correlation time is varied with temperature, the

Table IX. $MnCl_4^{-2}$ Resonance Width as a Function of $\eta M/\rho T$ for Solutions Containing Excess Et_4NCl and 0.05 M (0.039 M) $MnCl_4^{-2}$

Excess Concentration (Molal)	η centipoise; ρ g/cm^3; ΔH gauss $\lvert -\frac{1}{2}, \frac{1}{2}\rangle \rightarrow \lvert \frac{1}{2}, \frac{1}{2}\rangle$											
	T = 268°K				T = 299°K				T = 355°K			
Et_4NCl	η	ρ	$\eta M/\rho T \times 10^2$	$\Delta H_{\frac{1}{2}}$	η	ρ	$\eta M/\rho T \times 10^2$	$\Delta H_{\frac{1}{2}}$	η	ρ	$\eta M/\rho T \times 10^2$	$\Delta H_{\frac{1}{2}}$
0.00	0.489	0.8160	9.172	10.0	0.353	0.7825	6.189	9.4	0.225	0.7262	3.580	8.7
0.004	0.490	0.8162	9.189	10.4	0.353	0.7827	6.187	9.8	0.226	0.7265	3.595	9.9
0.140	0.534	0.8215	9.949	12.9	0.378	0.7889	6.581	11.0	0.240	0.7326	3.785	10.7
0.610	0.684	0.8360	12.52	14.4	0.463	0.8055	7.886	12.1	0.289	0.7538	4.430	10.7
0.983	0.803	0.8475	14.50	16.0	0.532	0.8177	8.926	12.8	0.328	0.7676	4.937	11.5

FIGURE 19

Variation of resonance width, (ΔH gauss, $|-\frac{1}{2}, \frac{1}{2}\rangle \rightarrow |\frac{1}{2}, \frac{1}{2}\rangle$), of 0.05 M $MnCl_4^{-2}$ containing different concentration of excess M Et_4NCl as a function of $\eta M/\rho T$ for five solutions: Δ, 0.00 excess M Cl^-; $\times$, 0.004 excess M Cl^-; ∇, 0.14 excess M Cl^-; $\odot$, 0.61 excess M Cl^-; $\bullet$, 0.98 excess M Cl^-.

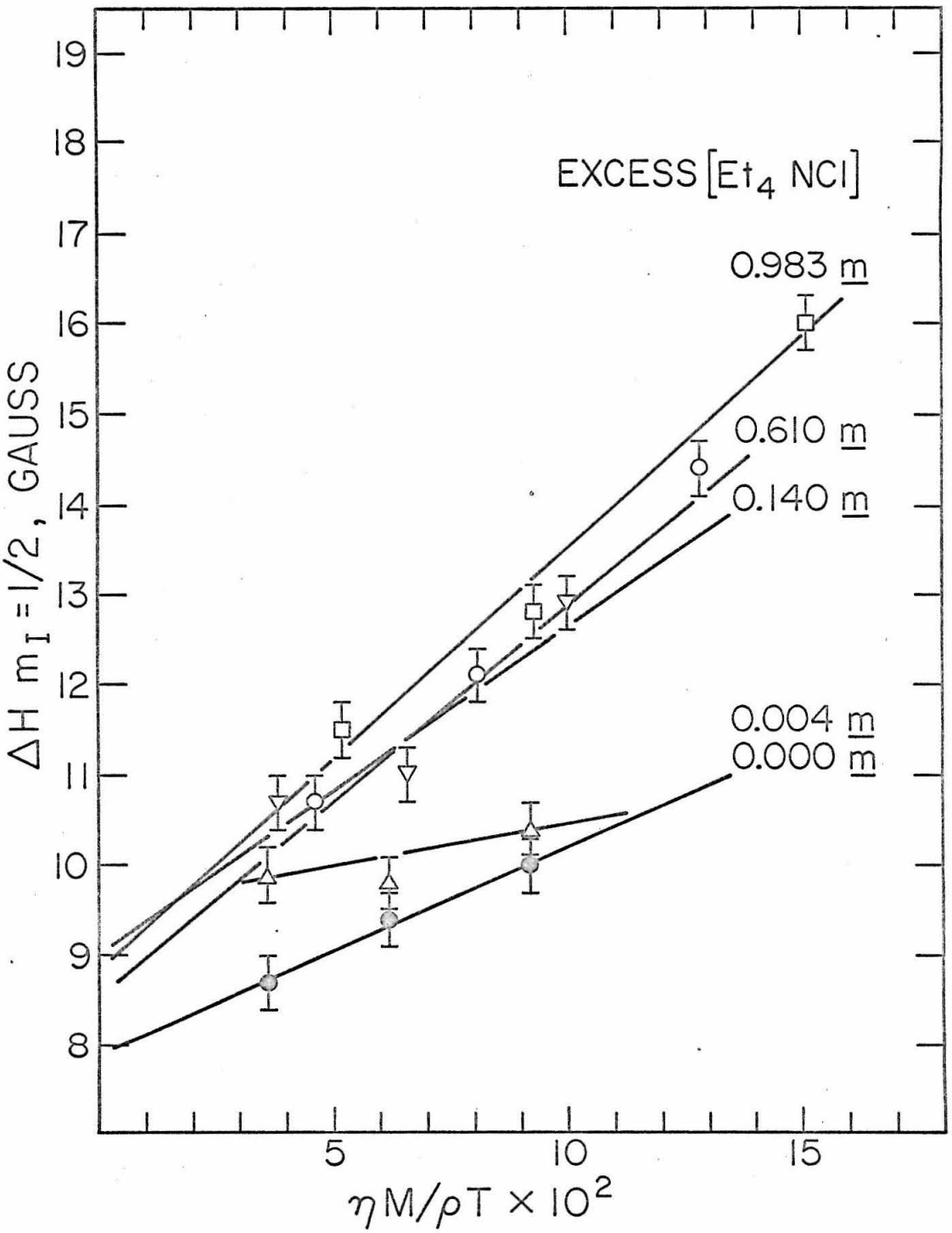
EXCESS [Et4 NCl]
0.983 m
0.610 m
0.140 m
0.004 m
0.000 m
ΔH mI=1/2, GAUSS
ηM/ρT × 10²
19
18
17
16
15
14
13
12
11
10
9
8
5
10
15

data points corresponding to different excess chloride concentrations fall into two major groups with one solution connecting both. The points in the higher concentration group fall almost on the same line and, hence, appear to vary linearly with the correlation time characteristic of solvent fluctuations and are clearly not strongly dependent on excess chloride concentration. The lower, zero-excess line displays the same general behavior and the 0.04 excess M points connect the two sets and intersects the resonance width axis approximately in the same region as the higher concentration lines at zero correlation. The latter may possibly be interpreted as a resonance width compensated for broadening imposed by solvent fluctuations. The lower "zero excess" line intersects the ΔH axis at about 8.1 gauss which is approximately 1.2 gauss lower than the other set of lines. This coupled with the results previously described and illustrated in Figs. 14 and 15 strongly suggests the existence of two paramagnetic components. The 0.004 M excess chloride line in Fig. 19 shows an intermediate case where considerable amounts of both components are present.

Based on experimental results, a plausible explanation for the two observable paramagnetic components would be a free or isolated $MnCl_4^{-2}$ anion at low manganese and counterion concentrations and a solvent separated or loosely bound ion-pair designated by $[Et_4N^+ \ldots MnCl_4^{-2}]$ at higher manganese concentration or counterion/manganese ratios. Equilibrium between the two states may be described by the simple reaction scheme

$$\underset{[A]}{MnCl_4^{-2}} + \underset{[C]}{Et_4N^+} \underset{}{\overset{K_a}{\rightleftharpoons}} \underset{[B]}{[Et_4N^+ \cdots MnCl_4^{-2}]}$$

and the mass action equilibrium constant for the process is approximated by

$$K_{association} = \frac{[Et_4N^+ \cdots MnCl_4^{-2}]}{[MnCl_4^{-2}][Et_4N^+]} = \frac{[B]}{[A][C]} \qquad (77)$$

If it is assumed that the ion-pairing is a fast process so that the spin state lifetimes of the paramagnetic components [A] and [B] are shorter than the inverse hyperfine splitting, the K_a may be determined from a simple rapid-exchange relationship

$$\frac{1}{T_2} = \frac{1}{T_{2A}} + \frac{[C]K_a}{1+[C]K_a}\left(\frac{1}{T_{2B}} - \frac{1}{T_{2A}}\right) \qquad (78)$$

where T_2^{-1} is the observed resonance width, T_{2A}^{-1} and T_{2B}^{-1} are the observed resonance widths for constituents [A] and [B] as defined above and [C] is the molar concentration of the counterion, Et_4N^+. The quantity $(T_{2B}^{-1} - T_{2A}^{-1})$ may be estimated consecutively from (1) the correlation function plots given in Fig. 19 and (2) the stoichiometric $MnCl_4^{-2}$ dilution study illustrated in Fig. 14. The correlation plots provide the ΔH between the completely ion-paired component and a "partially" ion-paired component existing at 0.05 M (0.039 M) $MnCl_4^{-2}$ in the absence of excess Et_4NCl ($\Delta H \approx 2.0$ gauss). Figure 14 then gives the ΔH between the "partially" ion-paired state at the

corresponding Mn^{+2} concentration and the "free" state, [A] ($\Delta H \approx$ 1.6 gauss). As a result, we estimate $(T_{2B}^{-1} - T_{2A}^{-1}) \approx 3.6$ gauss and the best match between calculation and observation provides us with $K_a \approx 20$.

In summary, the $MnCl_4^{-2}$ complex with Et_4N^+ as gegen ion in acetonitrile may best be interpreted in terms of two rapidly exchanging paramagnetic components whose equilibrium distribution is determined by both manganese concentration and Et_4N^+/Mn^{+2} ratio. Combined with an absence of frequency effects on resonance widths and the known dynamical behavior of ionic association in solution, a rapid exchange picture is probably a good approximation. The two components have been designated as (1) an isolated $MnCl_4^{-2}$ anion existing at low manganese concentration and Et_4N^+/Mn(II) ratios and (2) a solvent separated or loosely bound entity between complex and counterion $[Et_4N^+ \cdots MnCl_4^{-2}]$ existing at higher manganese concentration and Et_4N^+/Mn(II) ratios. A high resolution proton magnetic resonance study of the counterion, Et_4N^+, under parallel experimental conditions would strongly augment the electron spin resonance results by providing more definitive information on the structural nature of the ion-pair. Aside from the natural resonance widths of the two paramagnetic components, another relaxation mechanism appears to arise from the short range solvent fluctuation about the paramagnetic ion as described by Garrett and Morgan (52). Under all circumstances investigated in this work, the relaxation mechanisms and spin Hamiltonian constants are independent of frequency or field. Among

other things this suggests that the correlation time of events leading to relaxation are short and that the observations to a very good approximation are in the limit of extreme narrowing, i.e., $\omega\tau_c \ll 1$. Finally, from a sizeable number of experiments, the average values for the spin Hamiltonian constants are: (1) $MnCl_4^{-2}$, $\langle A \rangle$ = -79.7 ± 0.2 gauss, $\langle g \rangle = 2.0027 \pm 0.0005$; (2) $[Et_4N^+ \cdots MnCl_4^{-2}]$, $\langle A \rangle = -78.9 \pm 0.2$ gauss, $\langle g \rangle = 2.0027 \pm 0.0005$.

As the $MnCl_4^{-2}$ concentration is increased beyond 0.1 M (Figs. 14 and 15) the resonance width increases rapidly and becomes much larger than the ΔH in comparable counterion studies (Figs. 17/299°K and 18) in which ion-association should be favored by virtue of mass equilibria. Consequently, it would be difficult to rationalize the sizeable ΔH increase above 0.10 M $MnCl_4^{-2}$ in terms of an ion-pairing model, but it is certainly dependent on the manganese concentration. A possible candidate for spin relaxation is a dipolar mechanism and this, in fact, has been reported to be operable in other manganese(II) complexes at relatively low concentrations (69), i.e., 0.01 M. Examination of the spectra at 0.2 M $MnCl_4^{-2}$ indicated a definite asymmetry of the hyperfine components, particularly in the extremes. The high field side of the hyperfine components are clearly spread-out farther then the low field side. From the moment ratios of the dipolar interaction given by Hinckley and Morgan (69), it is seen that the individual m_S transition linewidths are not equal and, thus, are not symmetrically disposed about the $|-\frac{1}{2}, m_I\rangle \rightarrow |\frac{1}{2}, m_I\rangle$ transition as anticipated for an intramolecular process. A dipolar process will

indeed cause a spreading out of the high field side transitions ($|-5/2, \frac{1}{2}\rangle \rightarrow |-3/2, \frac{1}{2}\rangle$ and $|-3/2, \frac{1}{2}\rangle \rightarrow |-\frac{1}{2}, \frac{1}{2}\rangle$) and this is consistent with our observation.

2.1 $MnCl_4^{-2}$ in Other Environments

An attempt to answer the question concerning the influence of environment on the natural resonance width and on the spin Hamiltonian constants of $MnCl_4^{-2}$ prompted us to briefly explore the possibility of forming this complex in other solvents and phases. In view of the well-known solvent capabilities of N, N-dimethylformamide (DMF), it should provide a good candidate for comparison with acetonitrile. Furthermore, since DMF tolerates a much wider range of materials in solution than acetonitrile, it appears to be well suited for ion-pair studies involving different types of counterions.

Anhydrous $MnCl_2$ dissolved readily in DMF (68) and the electron spin resonance spectrum as shown in Fig. 20 was complex and reminiscent of the $MnBr_2$–CH_3CN system in which two components coexisted in a slow exchange limit. Possibly, then, in a similar fashion an octahedral and tetrahedral manganese(II) complex were simultaneously present in DMF. However, in the presence of DMF saturated with anhydrous LiCl, NaCl, CsCl, $CaCl_2$ and $AlCl_3$, the electron spin resonance spectra were all clearly characteristic of the $MnCl_4^{-2}$ complex. A quantitative solution containing the Li^+ counterion was prepared by vacuum techniques similar to those described in the experimental section. In this case, the $MnCl_2$ and LiCl were *simultaneously* heated at 150°C for two hours under constant pumping.

FIGURE 20

Electron spin resonance X-band spectra of $MnCl_2$ in DMF for different chloride to manganese ratios: [Cl]/[Mn] = 2 (≡2:1) and [Cl]/[Mn] = 4 (≡4:1) formed on addition of anhydrous excess LiCl. H_0 increases to the right. Scale: 1 cm = 46 gauss.

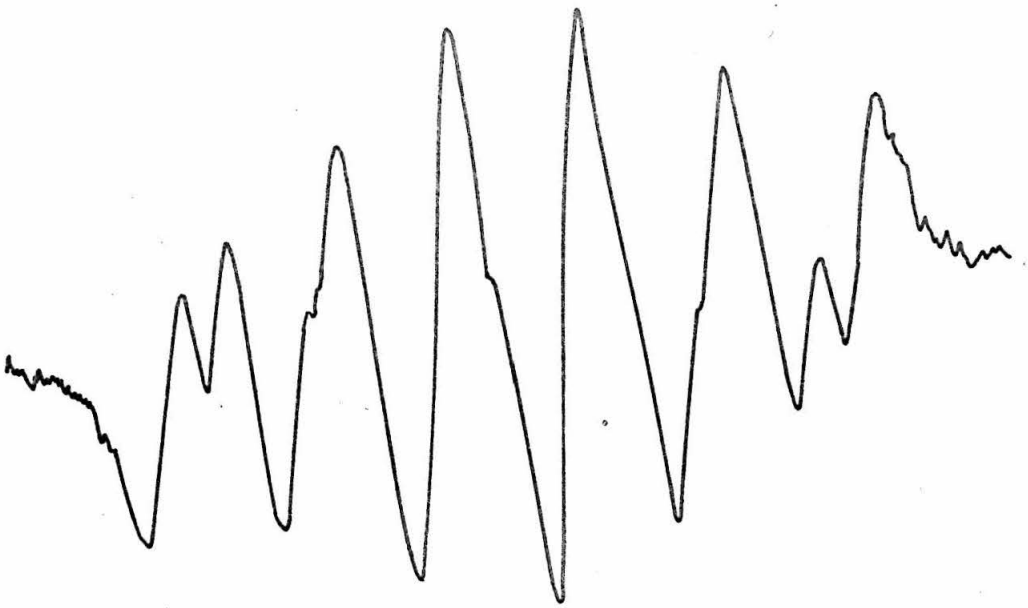

2:1

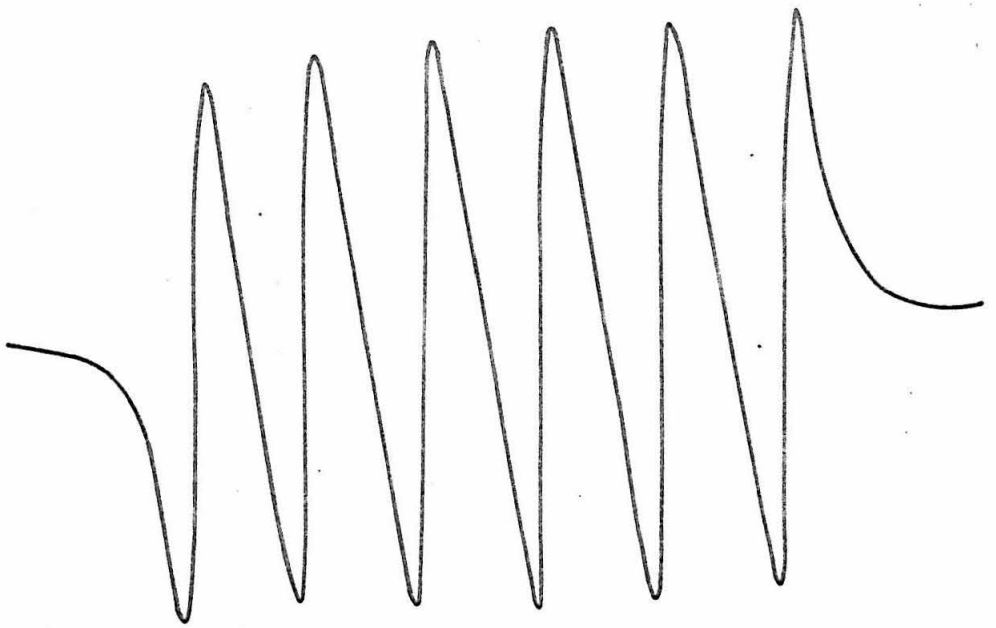

4:1

Drierite ($CaSO_4$) was added to the DMF prior to degassing and was present during the entire freeze-melt degassing procedure. The solvent was then transferred under vacuum onto the solids and the remaining sample preparation was the same as described in the experimental section. The X-band spectrum is presented in Fig. 21 and the resulting spin Hamiltonian constants and resonance widths are collected in Table X. The resonance width (14.9 gauss) was larger than a similar solution in acetonitrile (~ 9 gauss). This may stem from the greater viscosity imposed by DMF on the complex (a simple viscosity ratio $(\eta_{DMF}/\eta_{CH_3CN})\Delta H_{MnCl_4^{-2}}$ predicts ~16 gauss for $MnCl_4^{-2}$ in DMF) or from the increased polarizability due to the Li^+ counterion present in an ion-pair arrangement. The latter seems less feasible, however, since the Li^+ capability of polarizing the complex anion should be practically neutralized by the incorporation of large DMF molecules in the solvation sphere. Considerable experimental work would be required to answer this question but from

Table X. Spin Hamiltonian Constants for $[MnCl_4]^{-2}$ in Two Different Environments

State	M $MnCl_4^{-2}$	Excess M LiCl	⟨A⟩ ±0.2 gauss	⟨g⟩ ±0.0005	$\Delta H_{m_I=+\frac{1}{2}}$ gauss
DMF Solution	0.051	0.121	-79.4	2.0028	14.9
Et_4NCl crystal 0.2 wt% $MnCl_2$		0	-80.8	2.0018	12.3

FIGURE 21

Electron spin resonance X-band spectrum of 0.051 M $[Li^{+} \cdots MnCl_4^{-2}]$ in dimethylformamide. H_o increases to the right. Scale: 1 cm = 40 gauss.

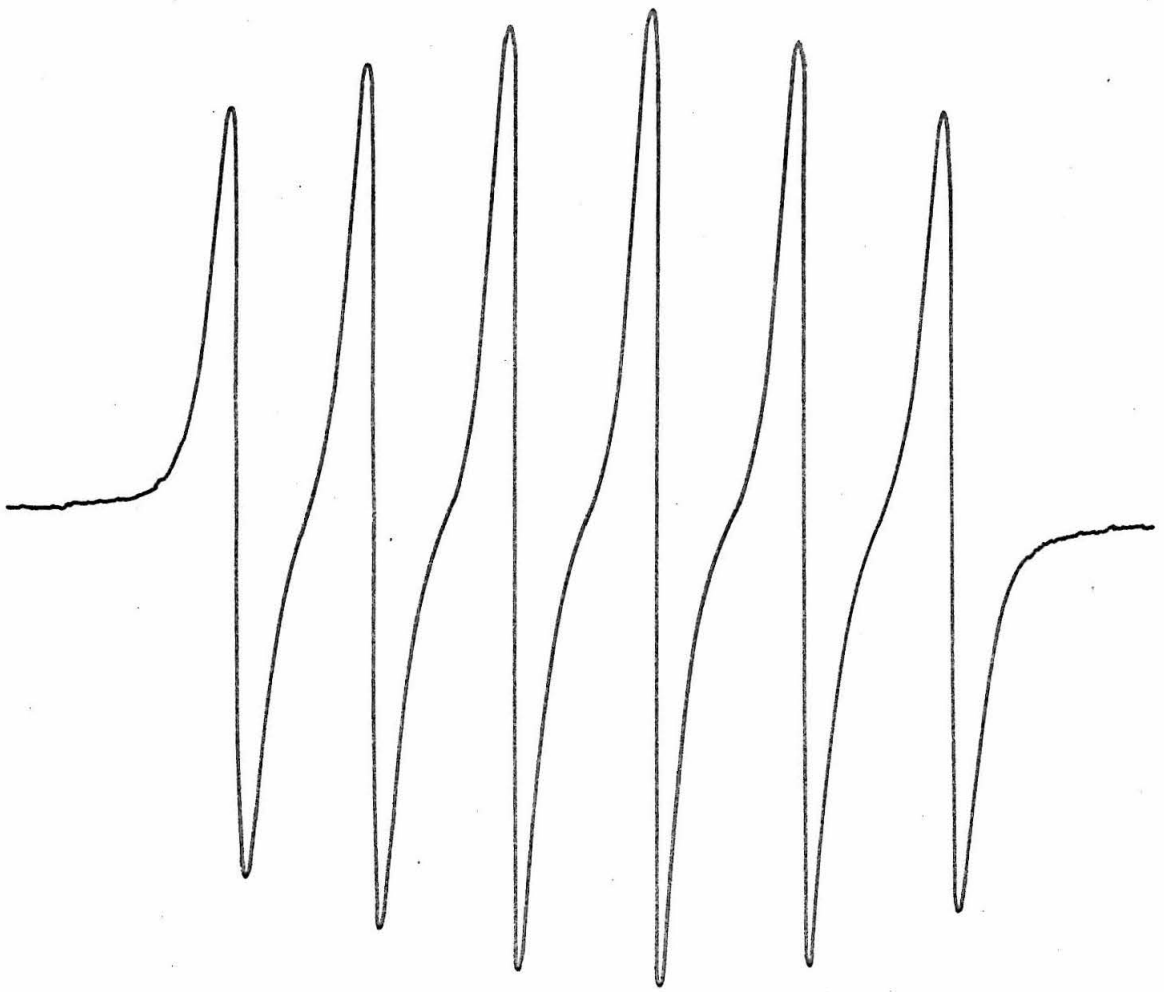

the spin Hamiltonian constants which are almost identical to those reported in acetonitrile we can conclude that the complex is tetrahedral.

Acetonitrile solutions of $MnCl_4^{-2}$ rapidly cooled to ~ 83°K do not display an electron spin resonance spectrum. On the other hand, frozen DMF solutions of $MnCl_4^{-2}$ exhibit a spectrum as shown in Fig. 22. Additional sets of lines are observed between the main hyperfine components and are probably due to the forbidden $\Delta m_S = \pm 1$, $\Delta m_I = \pm 1$ similar to those observed for manganese(II) in methanol (70). The relative intensities for these transitions are given by

$$I_r = \frac{\langle A \rangle^2 [I(I+1) - m_I(m_I+1)]}{2(g\beta H_0)^2} \tag{79}$$

and it is evident that the relative intensity is proportional to H_0^{-2} and that the center components having low m_I, i.e., $m_I = \pm \frac{1}{2}$ will be the most intense. Excluding second-order effects the lines will be located roughly at field positions

$$H_{m_I} = \frac{h\nu}{\langle g \rangle \beta} - \langle A \rangle (m_I \pm \tfrac{1}{2}). \tag{80}$$

These effects are in qualitative agreement with the observed spectrum. Using the $m_I = \pm \frac{1}{2}$ hyperfine components according to the second-order relation in Eq. (71) the hyperfine coupling constant, $\langle A \rangle$ for the frozen complex was estimated to be -94.9 gauss. This should not be taken seriously as an accurate value due to the overlaped

FIGURE 22

Electron spin resonance X-band spectrum of 0.039 M $MnCl_4^{-2}$ in DMF at ~83°K. H_0 increases to the left. Scale: 1 cm = 48 gauss.

nature of the spectrum but it does seem to indicate that the manganese complex is octahedrally coordinated in the solid phase at ~83°K. Unfortunately, nothing can be concluded about the nature of the ligand in this state. One may speculate that in the process of cooling, solvation energies of the components may direct the chemistry in favor of LiCl and $Mn(DMF)_6^{+2}$. Furthermore, the solid was colorless in contrast to the typically colored tetrahedral Mn(II) complexes.

Large crystals were also grown from acetonitrile solutions containing $MnCl_2$ and Et_4NCl. An electron spin resonance spectrum of a crystal taken at K-band is shown in Fig. 23 and demonstrates that Mn^{+2} ions have indeed been incorporated in the structure. The spin Hamiltonian constants have been included in Table X and clearly indicate that Mn^{+2} resides in a tetrahedral environment. Although we cannot be certain about the nature of the ligand, most probably the paramagnetic ion is surrounded by four chloride ions and the larger hyperfine coupling constant suggests that the complex may be more tightly compressed in the crystal than in solution. Spectra taken at ~83°K had the same appearance and indicated that Mn^{+2} was included in the solid as opposed to being occluded in pockets of solvent at room temperature. Further investigation showed no additional lines between 0 and 19 kgauss and rotation of the field with respect to crystalline axes had no effect on the line positions. Resonance widths were almost the same as observed in acetonitrile. It may be concluded that crystal and zero field splittings are negligible. Therefore the complex may be considered to be dispersed randomly throughout a

FIGURE 23

Electron spin resonance K-band spectrum of Et_4NCl crystal containing Mn^{+2}.

H_0 increases to the right. Scale: 1 cm = 37 gauss.

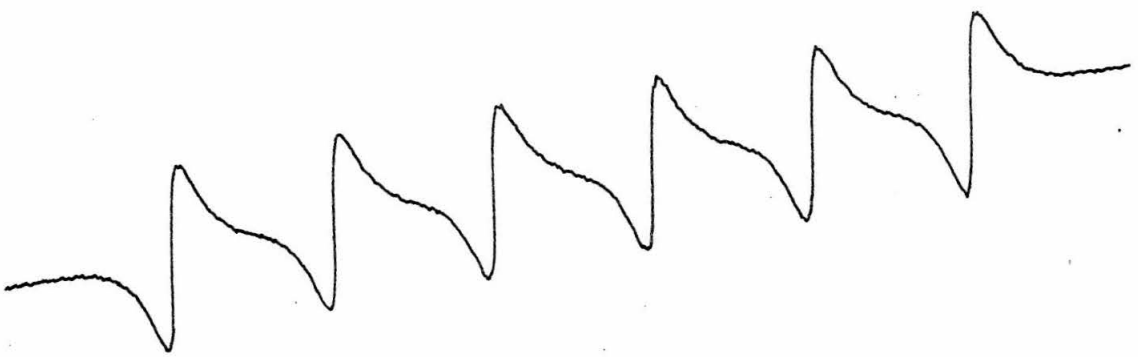

typically covalent organic crystal.

3. $MnBr_4^{-2}$

Electron spin relaxation studies of the $MnBr_4^{-2}$- acetonitrile system provide the central theme in this thesis. As stated earlier, the widths of the ^{55}Mn nuclear hyperfine components were found to be unusually broad, and a strong correspondence between broadening and bromide concentration was noted. It was suggested (55) that the bromide-dependent line broadening might be due to rapid ligand exchange occurring on the electron spin resonance time scale. In this section we set forth evidence to confirm this interpretation. As the problem unraveled it became apparent there were several important cooperative relaxation processes contributing to the overall relaxation picture. Although, at first glance, the exchange part appeared to be straightforward, in practice the system was complicated by important equilibria that determine the component distribution and that most certainly influence the dynamical properties.

Preparation of the $MnBr_4^{-2}$complex in acetonitrile was described in the Experimental section. Bromide ion concentrations in excess of the stoichiometric 4:1 ratio were taken to be the excess concentration. It was discovered that vacuum preparation of the $MnBr_4^{-2}$ was not critical as long as the reactants and solvent were anhydrous. Even in this case, however, sample capillaries were sealed-off immediately to prevent further interaction with moisture.

Electron spin resonance spectra observed for $MnBr_4^{-2}$ in acetonitrile were also treated adequately with the effective spin Hamiltonian and its eigenvalues to second order as given, respectively, in

Eqs. (12) and (13). However in the case of unusually broad $MnBr_4^{-2}$ lines, the individual hyperfine components are highly overlapped and their resonance widths may be considered to be equal. Since they are quite broad, the overlapping $|m_S, m_I\rangle \rightarrow |m_S+1, m_I\rangle$ is used to locate the hyperfine component line positions and line shapes are assumed to be Lorentzian. A Fortran IV program for this procedure is shown in Fig. 24. By comparing computer synthesized and experimental spectra, it was possible to extract the resonance width, ΔH, hyperfine coupling constant $\langle A \rangle$, and the spectroscopic splitting factor, $\langle g \rangle$. The spin Hamiltonian constants are: $\langle A \rangle$ = -76 gauss; $\langle g \rangle$ = 2.007. Within a range of 50-95 gauss the spectral characteristics were quite sensitive to the resonance width of the hyperfine components and the estimated error is ±1 gauss. Outside this range, the resonance width is somewhat more uncertain. Typical spectra of $MnBr_4^{-2}$ taken at X and K-band are illustrated in Fig. 25. Agreement between experimental and computer simulated spectra was excellent throughout the wide range of conditions investigated in this study and clearly justified our basic assumptions. Comparison of the X and K-band spectra in Fig. 25 illustrates the presence of a second-order effect reflected in the asymmetry of the X-band envelope. In contrast, the K-band spectra is quite symmetrical due to attenuation of the second-order effect.

In the absence of excess bromide ion and, hence, possible chemical exchange broadening, the stoichiometric complex (Br/Mn = 4.0) still has an unusually broad resonance width. For example,

FIGURE 24

Fortran IV computer program for generating $MnBr_4^{-2}$ electron spin resonance spectra.

```
$ID                SICMN2, CH25000, 2, 25
$IBJOB
$IBF13 MSS
C       PROGRAM TO SYNTHESIZE EPR SPECTRA OF MN(II)BR4
C       INPUT DATA - HZ, M, L, R, A  HZ=COMPUTED MAG FIELD
        POSITIONS IN GAUSS
C       A=END PEAK AMPL IN HALF INCHES   R=STARTING POINT
        FOR SCAN OF LINE WIDTH
C       M=SOLUTION NUMBER  L=APPROXIMATE TEMPERATURE
C       THE PROGRAM IS SET UP TO RUN 6 SETS OF DATA AT ONE
        TIME
C       ENDS OF PLOTS MADE TO AGREE WITH CALIBRATION OF
        EXPERIMENTAL FIELD
        DIMENSION HZ(6), H(2004), SSUM(2004), SUM(2204)
        DIMENSION DD(3)
        DD(1)=0
        DD(3)=1
C       H(J) GENERATES FIELD INTERVALS IN GAUSS
        H(1) = 2971.0
        DO 20 J=2, 2000
    20  H(J) = H(J-1) + 0.387
        DO 11 N=1, 6
        READ(5, 50)M, L, R, A
        READ(5, 40)HZ
        WRITE(6, 60)
        WRITE(6, 70)HZ
        WRITE(6, 80)A
        DO 11 I=1, 6
        XI=I
C       DH = BAND WIDTH IN GAUSS
        DH=R-1.+XI
        DO 10 J=1, 2000
        DY = 0.0
        DO 15 K = 1, 6
    15  DY=DY-(1.3333/(DH)**2)*(H(J)-HZ(K))/(1.0+(1.3333/(DH)**2)
       *(H(J)1-HZ(K))**2)**2
    10  SUM (J) = DY
        DO 13 J=200, 550
        IF(ABS(SUM(J))-ABS(SUM(J+1)))13, 12, 12
    12  S=A/SUM(J)
        GO TO 14
    13  CONTINUE
    14  DO 16 J=1, 2000
    16  SSUM(J)=-S*SUM(J)
C       AUTOMATIC NORMALIZATION OF CURVES. S = SCALING
        FACTOR.
        WRITE (6, 90) DH
```

```
      CALL PRTNUM(11.0, 9.5, 0.25, DH, 23H(13HLINE WIDTH = ,
     F5.1), 0.)
      CALL PRTNUM(11.0, 9.0, 0.25, M, 18H(10HSOLUTION C, I2), 0.)
      CALL XYPLOT (984, H, SSUM, 2971.0, 3352.0, -10.0, 10.0, DD, 1)
      CALL XYPLOT(1016, H(985), SSUM(985), 3352.0, 3745.0, -10.0,
     10.0, DD, 1)
11 CONTINUE
40 FORMAT (6F10.3)
50 FORMAT(2I5, 2F10.3)
60 FORMAT (46H1INPUT DATA FOR SYNTHESIS OF MN(II)BR4
   SPECTRA)
70 FORMAT(6H0H(K)=, 6F10.3)
80 FORMAT(6H0  A =, F10.3)
90 FORMAT (6H0 DH =, F6.0)
      STOP
      END
```

FIGURE 25

(a) Electron spin resonance X-band spectrum of 0.039 M $MnBr_4^{-2}$ in acetonitrile.

(b) K-band (lower) spectrum of 0.0019 M $MnBr_4^{-2}$ in acetonitrile.

H_0 increases to the right. Scale: 1 cm = 66 gauss.

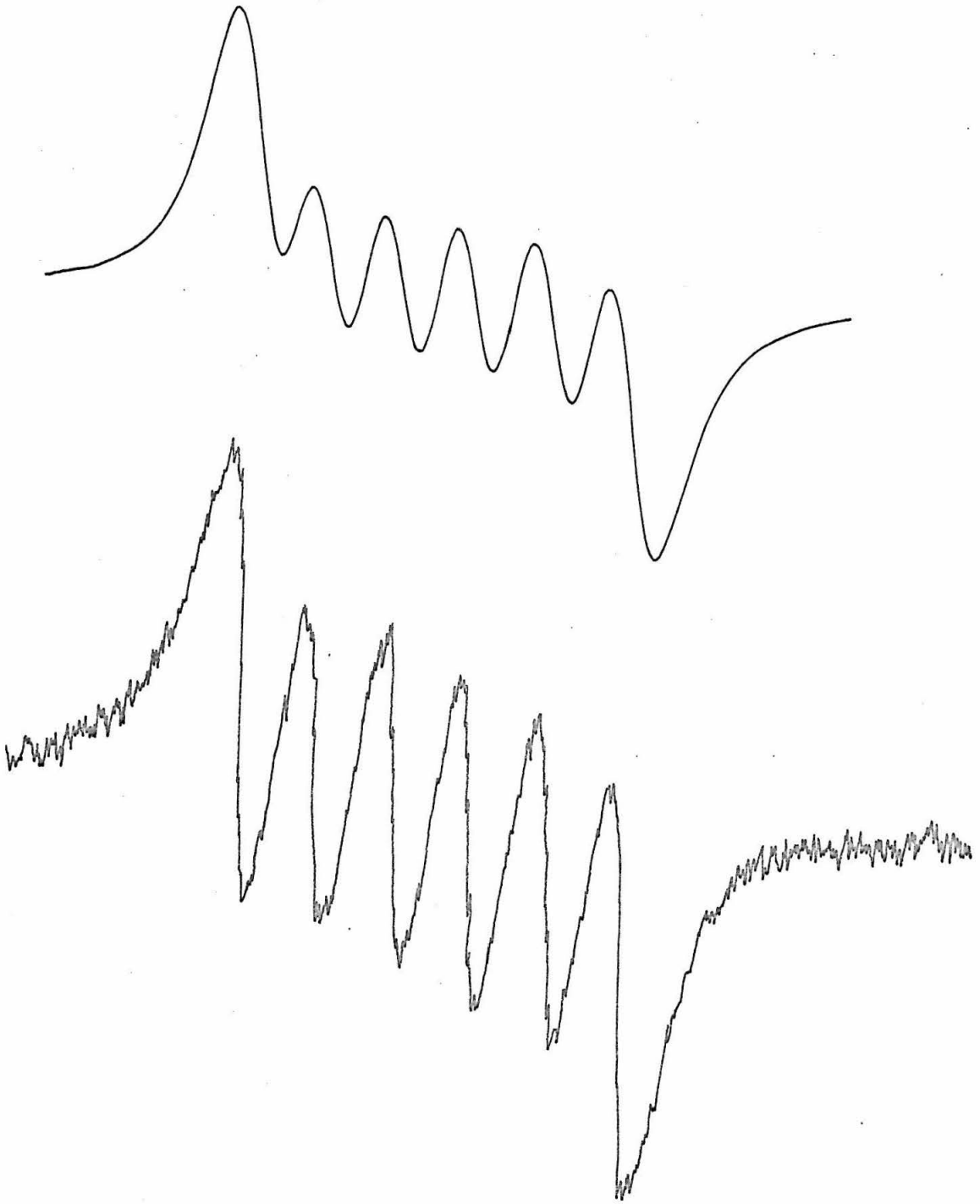

a 0.05 M (0.039 M) solution of $MnBr_4^{-2}$ displays a resonance width of 60 gauss (X-band result) compared to 9 gauss for the chloride analogue. To further amplify on the anomalous broadening problem, a study was initiated to investigate the effect of stoichiometric $MnBr_4^{-2}$ concentration on the overall resonance width and the results are depicted in Fig. 26 at both X and K-band frequencies. It is seen that the resonance widths are dependent on both Mn^{+2} concentration and frequency. Thus, we prematurely conclude that dipolar interactions will play an important part in determining the overall resonance widths at higher Mn^{+2} concentrations but a discussion on this subject will be deferred until later. For the moment we consider only the lower concentration portion of the curves where dipolar interactions are diminished but are certainly not insignificant. Based on previous intensity measurements (55), the actual $MnBr_4^{-2}$ concentration must surely be modified by the presence of chemical intermediates. Unfortunately, it is not possible to identify the paramagnetic intermediates since they must possess less than cubic symmetry leading to very short relaxation times and extremely broad and probably unobservable resonance widths. A reasonable conjecture on a possible dissociation reaction is

$$MnBr_4^{-2} + CH_3CN \rightleftharpoons Mn(CH_3CN)Br_3^{-} + Br^{-}. \qquad (81)$$

Consequently, the mass action equilibrium expression is given by

FIGURE 26

Resonance width, ΔH (gauss), as a function of stoichiometric $MnBr_4^{-2}$ concentration at two frequencies:
○, X-band; Δ, K-band.

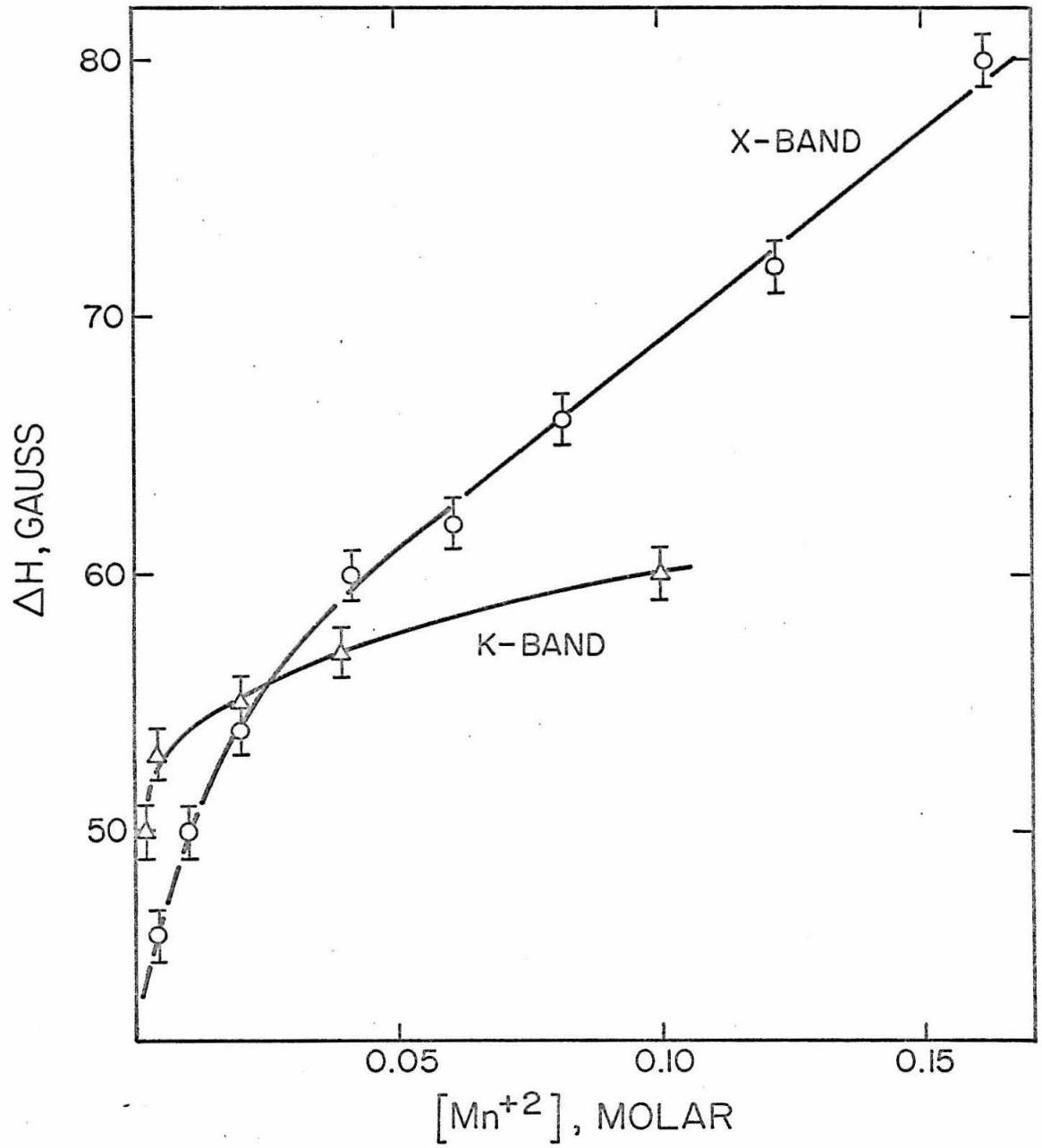
80
70
60
50
ΔH, GAUSS
X-BAND
K-BAND
0.05
0.10
0.15
[Mn+2], MOLAR

$$K_d = \frac{[Mn(CH_3CN)Br_3^-][Br^-]}{[MnBr_4^{-2}]} \qquad (82)$$

and from the intensity data published earlier (55), we estimate $K_d = 5 \times 10^{-3}$. Based on this value we have computed the extent of dissociation over the range of stoichiometric $MnBr_4^{-2}$ concentrations anticipated in this work and the results are summarized in Table XI. As can be seen, dissociation of stoichiometric $MnBr_4^{-2}$ is significant throughout the entire concentration range. Since resonance widths are strongly $MnBr_4^{-2}$ concentration dependent, dissociation plays an important role in the interpretation of the exchange data at X and K-band frequencies to be presented later.

In Fig. 26 we notice that the curve slope increases markedly in the dilute range. To better illustrate this observation we have extended and magnified the K-band results in Fig. 26 and replotted them in Fig. 27. The K-band results were chosen since dipolar effects are attenuated at this frequency (to be discussed at greater length in the next section) and other electron spin relaxation mechanisms can be seen more directly. More specifically, we can examine two important issues germane to the interpretation of our exchange data: (1) the effect of the counterion, Bu_4N^+, on resonance widths at high concentrations and (2) the effect of ion-pairing on resonance widths.

Table XI. Distribution of Components Due to Dissociation of Stoichiometric $MnBr_4^{-2}$

Concentration (Molar)			
Total [Mn]	$[MnBr_4^{-2}]$	$[Mn(CH_3CN)Br_3^-]$ or $[Br^-]$	% of $MnBr_4^{-2}$ dissociated
0.0001	2.1×10^{-6}	9.8×10^{-5}	98.0
0.0019	0.0004	0.0015	79.0
0.005	0.002	0.003	60.0
0.010	0.005	0.005	50.0
0.039	0.028	0.012	30.8
0.050	0.037	0.013	26.0
0.081	0.064	0.017	21.0
0.100	0.080	0.020	20.0
0.150	0.125	0.025	16.7
0.200	0.171	0.029	14.5

FIGURE 27

Response of K-band resonance width, ΔH (gauss), to stoichiometric $MnBr_4^{-2}$ concentration at low concentration levels.

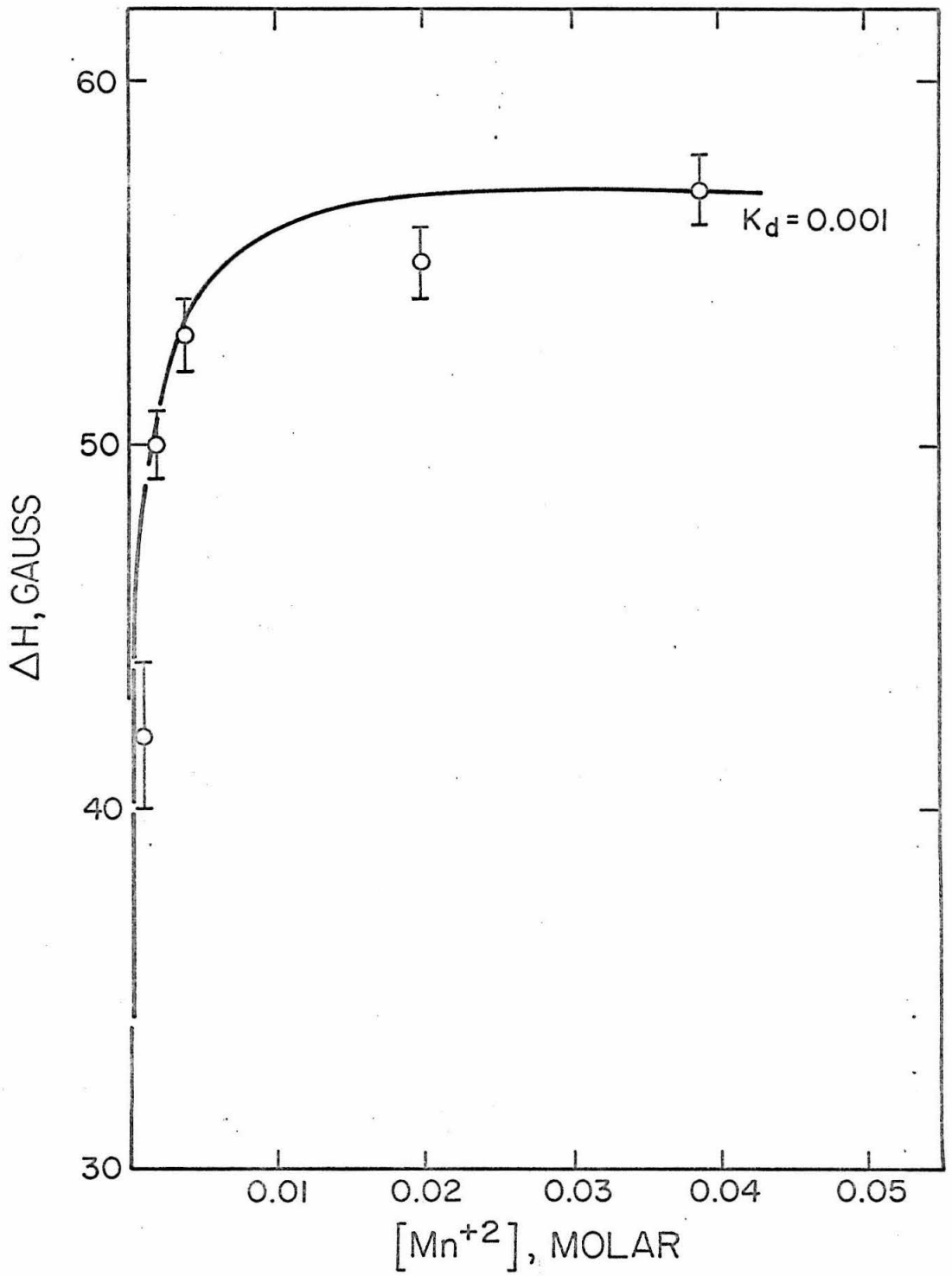
60
50
40
30
ΔH, GAUSS
$K_d = 0.001$
0.01
0.02
0.03
0.04
0.05
$[Mn^{+2}]$, MOLAR

It is evident from Figs. 26 and 27 that resonance width remains relatively constant for the K-band data between 0.1 and 0.0039 M Mn^{+2}. Below this concentration the resonance width drops sharply to 42 ± 2 gauss at 0.001 M Mn^{+2}. Unfortunately, the signal intensity is low at this concentration and after much experimentation with sample geometry, placement and adjustment of electronic parameters, it was evident that the lower limit of observation had been attained. The most important feature of this series is the constancy of resonance width above 0.0039 M Mn^{+2}. Between 0.02 M and 0.1 M Mn^{+2} the counterion concentration correspondingly increases from 0.04 to 0.2 M. Yet, the change in resonance width is only 5 gauss and, moreover, part of this can be attributed to the increase of Mn^{+2} concentration. Therefore, we reach the very important conclusion that the Bu_4N^+ counterion interactions do not provide an important electron spin relaxation mechanism in solutions containing more than 0.02 M Mn^{+2}.

We may then interpret the results shown in Fig. 27 as signifying the presence of two degenerate paramagnetic components having quite different relaxation times. It is difficult to accurately assess the exchange rate limit under these circumstances but the fact that the spectra maintain Lorentzian character and spin Hamiltonian constants do not change suggests a rapid exchange limit for the two paramagnetic components. A plausible model for the two exchanging species would involve a free or isolated $MnBr_4^{-2}$ anion at low manganese concentrations ($\leq$ 0.002 M) and counterion concentrations and a solvent

separated or loosely bounded ion pair designated by $Bu_4N^+ \cdots MnBr_4^{-2}$ at higher manganese (> 0.0039 M) concentrations or counterion/manganese ratios. Equilibrium between the two states may be written as

$$\underset{B}{Bu_4N^+ \cdots MnBr_4^{-2}} \rightleftharpoons \underset{A}{Bu_4N^+ + MnBr_4^{-2}} \tag{83}$$

and, consequently, the mass action equilibrium constant defining the dissociation of the ion pair may be approximated by

$$K_d = \frac{[Bu_4N^+][MnBr_4^{-2}]}{[Bu_4N^+ \cdots MnBr_4^{-2}]} \cdot \tag{84}$$

Assuming the rapid exchange picture for states A and B and noting that $T_{2B} < T_{2A}$, the dissociation constant may be estimated from the relation

$$\frac{1}{T_2} = \frac{1}{T_{2A}} + \frac{[C]}{[C]+K_d}\left(\frac{1}{T_{2B}} - \frac{1}{T_{2A}}\right) + \sum_i T_{2i}^{-1} \tag{85}$$

where T_2^{-1} is the overall resonance width, T_{2A}^{-1} and T_{2B}^{-1} are the resonance widths estimated from the data shown in Fig. 27 based on the two-state model represented by the ion-pairing equilibrium in Eq. (83), [C] is the molar concentration of the counterion, Bu_4N^+, and the summation runs over all other, as yet undetermined, relaxation processes contributing to the overall resonance width.

Presuming that ion-pairing equilibria dominates the relaxation picture at low Mn^{+2} concentrations and assuming reasonable values for T_{2A}^{-1}, T_{2B}^{-1} and $\sum_i T_{2i}^{-1}$, the distribution of components was calculated for a wide range of dissociation constants. In the face of all this uncertainty, the best match between theory and observation was obtained by taking $K_d = 10^{-3}$ and this generated the solid line included in Fig. 27. Since the formation of chemical intermediates undoubtedly reduces the apparent $MnBr_4^{-2}$ concentration, the dissociation constant for the ion-pair equilibrium must only be considered as an upper-limit, order-of-magnitude value. Again, a high resolution proton nuclear magnetic resonance study of the Bu_4N^+ counterion under parallel experimental conditions would strongly augment the present results by providing more definitive information on the structural nature of the ion pair.

It seems clear that dynamical association of the counterion, Bu_4N^+, to form an ion-pair plays a significant role in determining the overall resonance width for stoichiometric solutions containing less than 0.02 M $MnBr_4^{-2}$. Of course, Bu_4N^+ from other sources also favors the ion-paired state. These effects will become quite apparent during the interpretation of subsequent data in support of our hypothetical ion-pair model.

As mentioned earlier in the section on the $MnCl_4^{-2}$ complex, Garrett and Morgan (52) have established that electron spin relaxation of the $3d^5$ electrons in solvated manganese(II) complexes arises from solvent fluctuations in the immediate surroundings of the paramagnetic

ion. If this mechanism were the only one operative here, the resonance widths would vary linearly with the correlation time characteristic of the solvent fluctuations and would not be strongly dependent upon the bromide concentration. It has been suggested that this correlation time is proportional to $\eta M/\rho T$ where the constituents were defined in the $MnCl_4^=$ section. In Figs. 28-31, variation of the overall electron spin resonance widths were plotted against the correlation function, $\eta M/\rho T$, for twelve solutions (71) containing 0.05 M (0.039 M) manganese(II) tetrabromide and different bromide ion concentrations ranging from zero to 0.304 M excess bromide ion. The data are compiled in Table XII. In this series bromide ion was supplied by tetra-n-butylammonium bromide which is quite soluble and strongly dissociated in acetonitrile. It is interesting that, whereas the resonance widths for each of these solutions do vary linearly with $\eta M/\rho T$ as the solvent structural correlation time is varied with temperature, the data points corresponding to different excess bromide ion concentration do not fall on the same line. This clearly indicates the onset of a new relaxation mechanism which is dependent upon the excess bromide concentration. The result is in sharp contrast to the $MnCl_4^{-2}$ system where the correlation plots showed a very weak dependency (if any) on excess chloride ion over a wide range of concentration (0.14 to 0.98 M).

In Fig. 32, the excess widths attributable to the new bromide-dependent relaxation are plotted vs. the excess bromide concentration at six different temperatures from the data summarized in Table XIII.

Table XII. Summary of Data. The Resonance Width Dependence on Excess Bromide Ion Concentration, Viscosity and Temperature. All Solutions Contained 0.039 M $MnBr_4^{-2}$

Excess concentration (molar) $[Br^-]_d$	$[Br^-]_a$	η c.p.	T°K	$\frac{\eta(10^3)}{T}$	ΔH
0.000	0.000	0.5083	268	1.932	71
0.000	0.000	0.4007	289	1.388	66
0.000	0.000	0.3622	300	1.207	64
0.000	0.000	0.3097	317	0.978	61
0.000	0.000	0.2626	337	0.780	59
0.000	0.000	0.2270	354	0.641	58
0.0215	0.0180	0.5188	268	1.936	75
0.0209	0.0175	0.4080	289	1.412	69
0.0206	0.0172	0.3683	300	1.228	65
0.0201	0.0168	0.3149	317	0.993	62
0.0196	0.0164	0.2670	337	0.792	60
0.0191	0.0160	0.2307	354	0.652	59
0.0610	0.0485	0.5384	268	2.009	80
0.0594	0.0473	0.4218	289	1.460	71
0.0585	0.0467	0.3800	300	1.267	69
0.0572	0.0457	0.3250	317	1.025	65
0.0557	0.0446	0.2757	337	0.818	62
0.0544	0.0436	0.2378	354	0.672	61

Table XII. (Cont'd)

Excess concentration (molar) $[Br^-]_d$	$[Br^-]_a$	η c.p.	T°K	$\frac{\eta(10^3)}{T}$	ΔH
0.0651	0.0515	0.5402	268	2.016	84
0.0635	0.0504	0.4230	289	1.464	78
0.0625	0.0496	0.3810	300	1.270	72
0.0611	0.0486	0.3259	317	1.028	70
0.0595	0.0474	0.2765	337	0.820	66
0.0581	0.0464	0.2384	354	0.673	64
0.1138	0.0855	0.5650	268	2.108	84
0.1108	0.0835	0.4401	289	1.523	77
0.1092	0.0824	0.3956	300	1.319	72
0.1068	0.0808	0.3382	317	1.067	71
0.1040	0.0789	0.2871	337	0.852	67
0.1077	0.0814	0.2472	354	0.698	65
0.1240	0.0922	0.5701	268	2.127	89
0.1200	0.0896	0.4438	289	1.536	79
0.1190	0.0889	0.3986	300	1.329	74
0.1160	0.0870	0.3410	317	1.076	73
0.1140	0.0856	0.2890	337	0.858	71
0.1110	0.0836	0.2491	354	0.706	68
0.1770	0.1255	0.5975	268	2.23	87
0.1720	0.0896	0.4630	289	1.60	78
0.1700	0.1212	0.4150	300	1.38	78
0.1660	0.1188	0.3550	317	1.12	73
0.1620	0.1163	0.3013	337	0.89	67
0.1580	0.1139	0.2590	354	0.73	66

Table XII. (Cont'd)

Excess concentration (molar) $[Br^-]_d$	$[Br^-]_a$	η c.p.	T°K	$\frac{\eta(10^3)}{T}$	ΔH
0.1840	0.1296	0.6019	268	2.246	93
0.1790	0.1267	0.4658	289	1.612	82
0.1770	0.1255	0.4172	300	1.391	75
0.1730	0.1230	0.3570	317	1.126	73
0.1680	0.1200	0.3033	337	0.900	70
0.1650	0.1182	0.2603	354	0.735	66
0.1930	0.1350	0.6070	268	2.26	90
0.1880	0.1320	0.4693	289	1.62	80
0.1860	0.1308	0.4202	300	1.40	79
0.1820	0.1284	0.3596	317	1.13	79
0.1770	0.1255	0.3055	337	0.91	72
0.1730	0.1230	0.2620	354	0.74	73
0.2240	0.1528	0.6240	268	2.328	105
0.2190	0.1500	0.4811	289	1.665	93
0.2160	0.1483	0.4102	300	1.367	87
0.2110	0.1454	0.3681	317	1.161	84
0.2060	0.1426	0.3129	337	0.929	77
0.2020	0.1402	0.2682	354	0.758	76
0.2400	0.1618	0.6335	268	2.36	104
0.2340	0.1584	0.4840	289	1.68	88
0.2310	0.1568	0.4330	300	1.44	83
0.2260	0.1540	0.3730	317	1.18	80
0.2210	0.1511	0.3170	337	0.94	73
0.2160	0.1483	0.2715	354	0.77	70

[d] Bu_4NBr assumed to be completely dissociated in CH_3CN.

[a] Bu_4NBr assumed to be partially dissociated in CH_3CN with $K_d = 0.5/25°C$.

FIGURES 28-31

Variation of X-band resonance width of 0.039 M $MnBr_4^{-2}$ containing different concentrations of excess Bu_4NBr as a function of $\eta M/\rho T$. Concentrations are indicated on plots. Broken line indicates stoichiometric (0.000 M) solution for comparison.

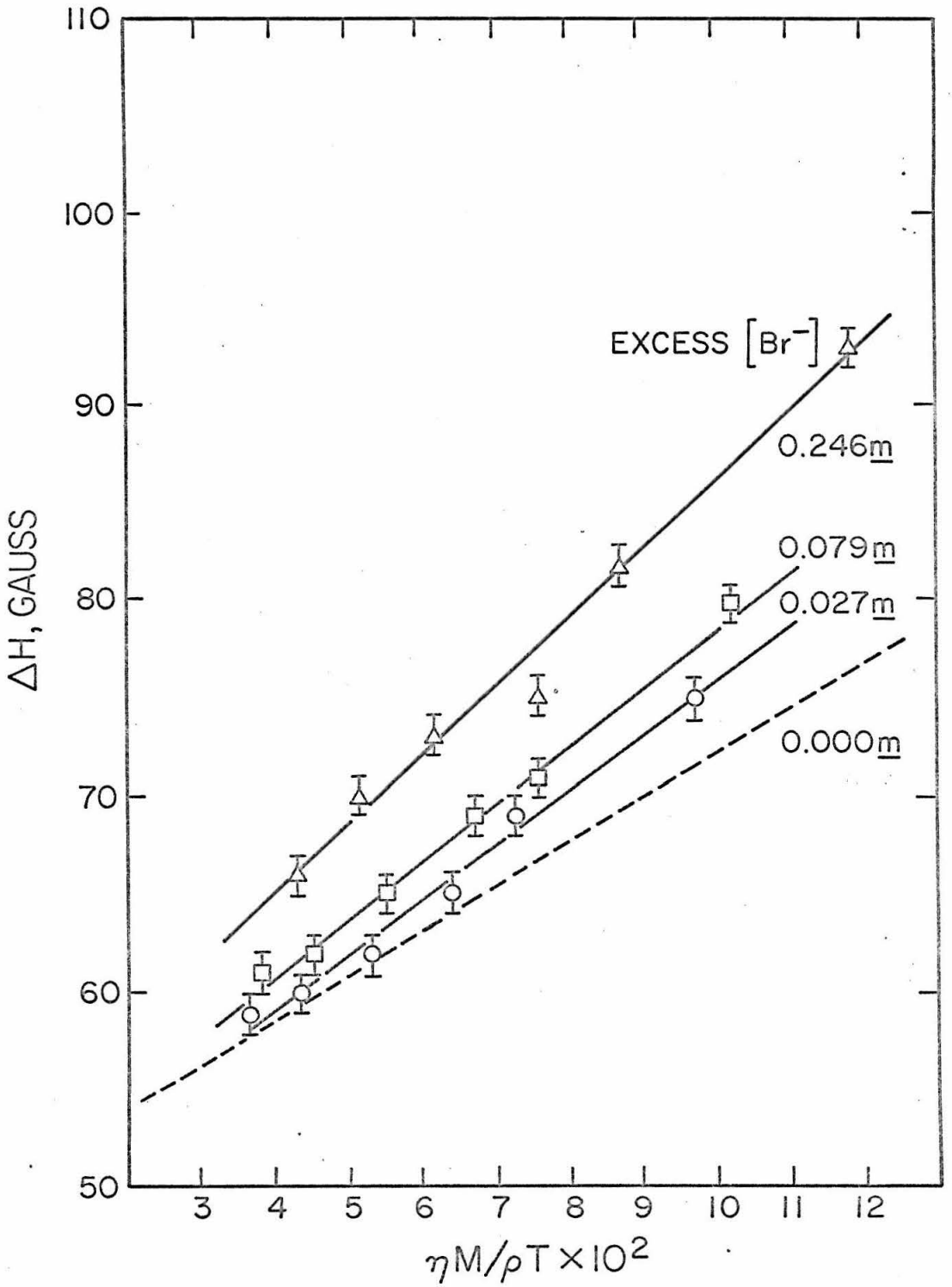
110
100
90
80
70
60
50
ΔH, GAUSS
3
4
5
6
7
8
9
10
11
12
ηM/ρT×10²
EXCESS [Br⁻]
0.246m
0.079m
0.027m
0.000m

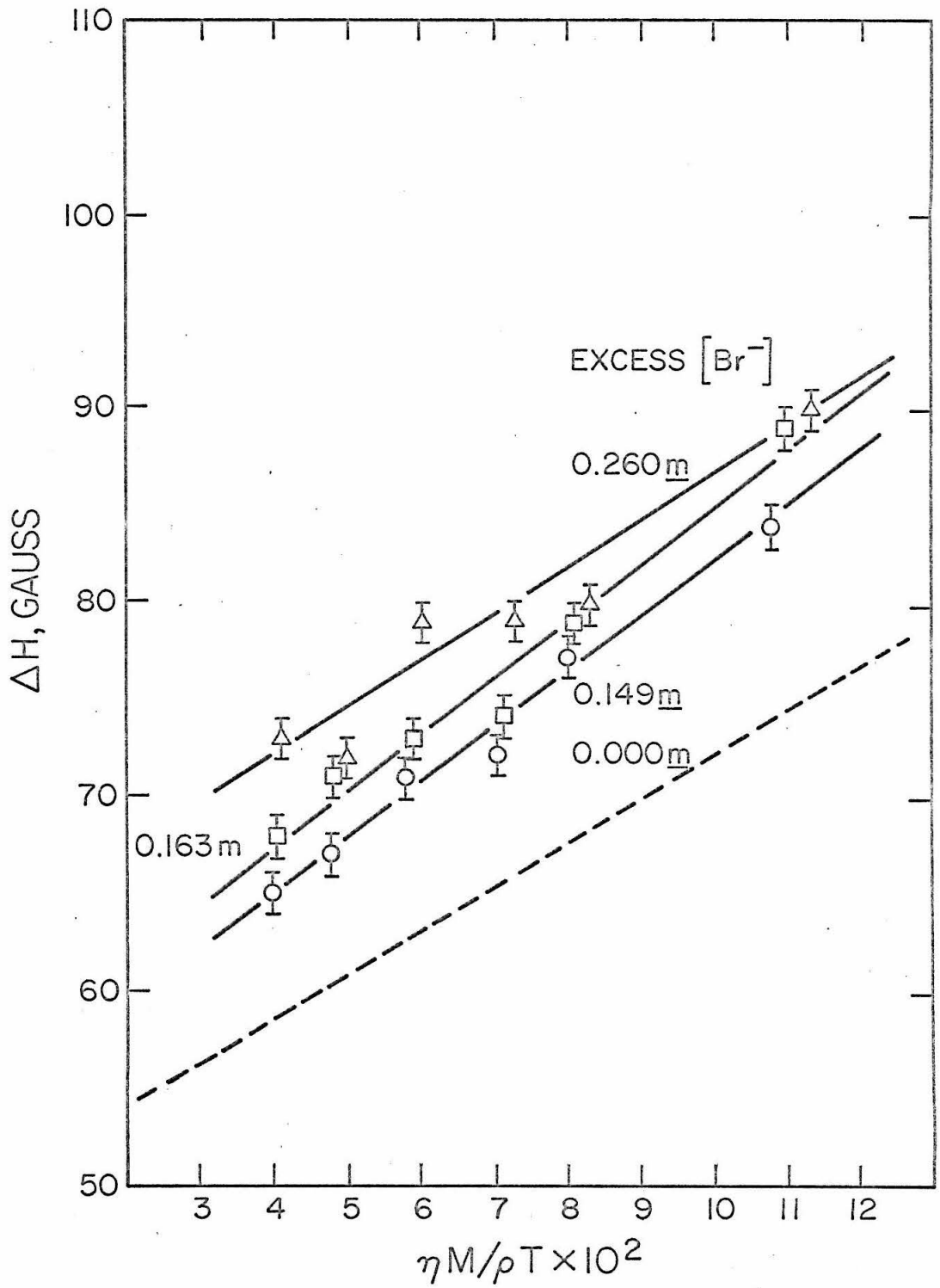
110
100
90
80
70
60
50
ΔH, GAUSS
EXCESS [Br⁻]
0.260 m
0.149 m
0.000 m
0.163 m
3
4
5
6
7
8
9
10
11
12
ηM/ρT×10²

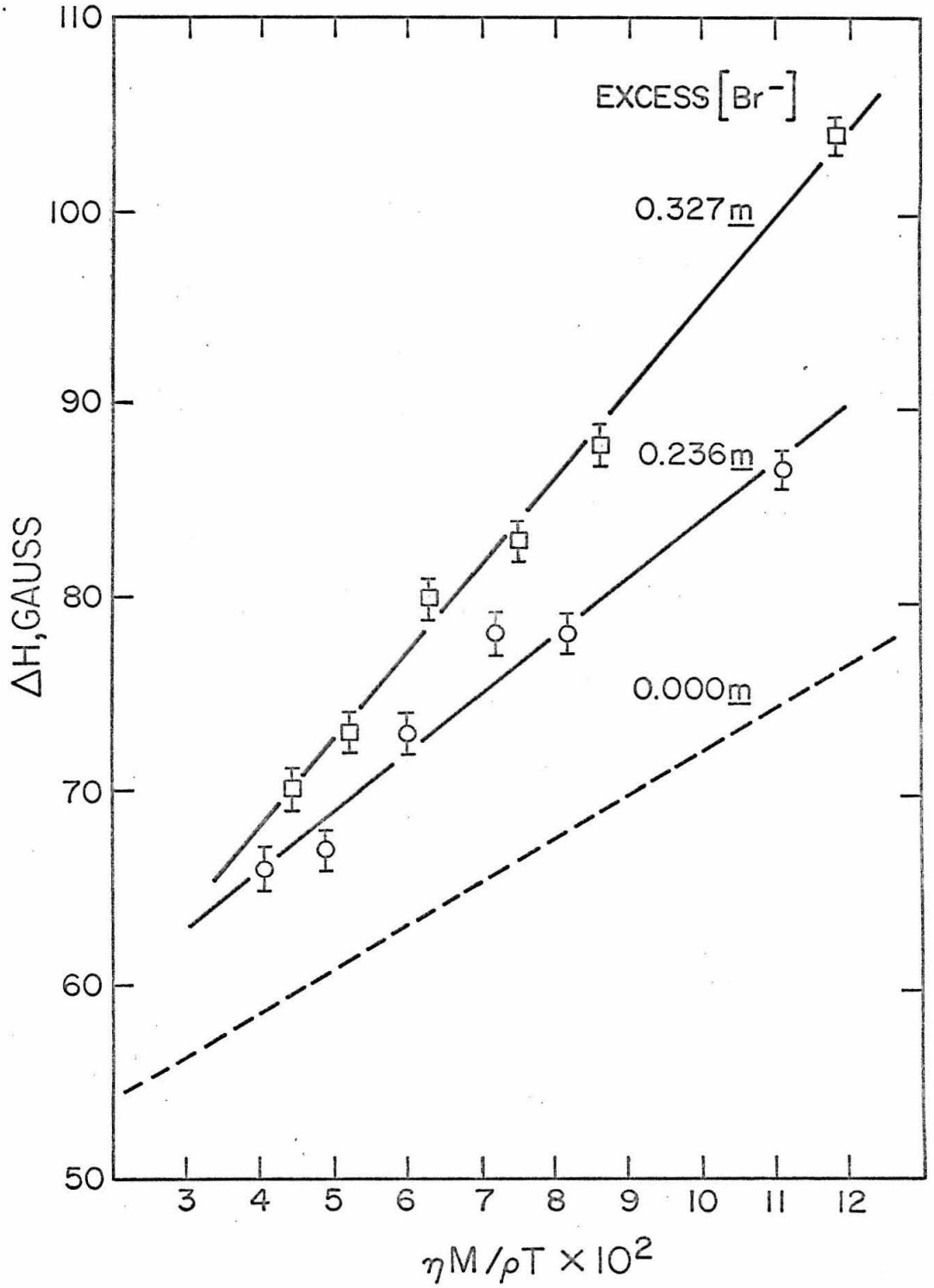
EXCESS [Br⁻]
0.327m
0.236m
0.000m
ΔH, GAUSS
110
100
90
80
70
60
50
3
4
5
6
7
8
9
10
11
12
ηM/ρT × 10²

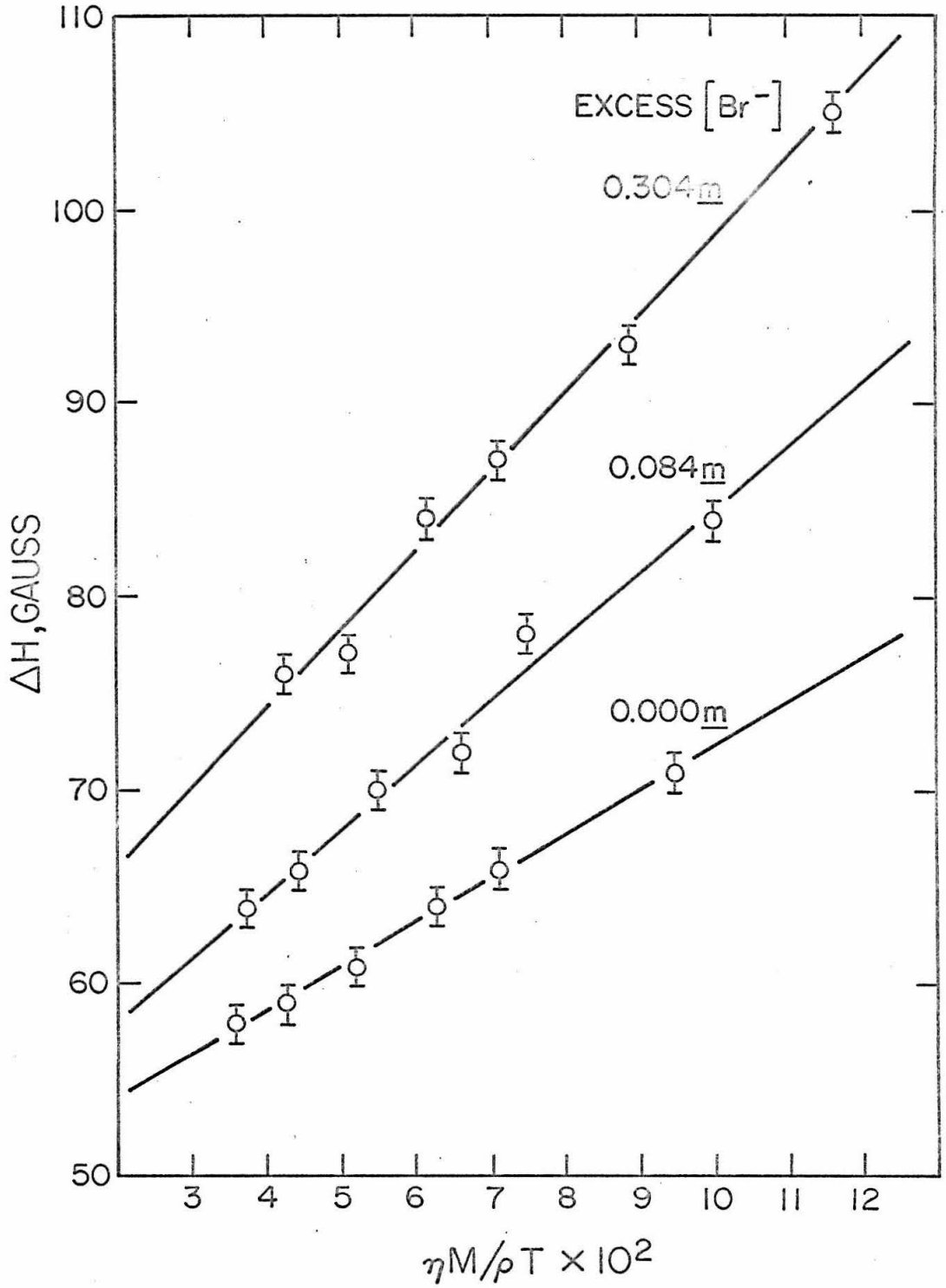
EXCESS [Br⁻]
0.304m
0.084m
0.000m
ΔH, GAUSS
ηM/ρT × 10²
110
100
90
80
70
60
50
3
4
5
6
7
8
9
10
11
12

Table XIII. Summary of Data. The Exchange Resonance Width Dependence on Excess Bromide Ion Concentration and Temperature. All Solutions Contained 0.039 Molar $MnBr_4^{-2}$.

T = 268°K

Excess concentration (molar) $[Br^-]_d$	$[Br^-]_a$	ΔH (gauss)	ΔH_c (gauss)	ΔH_{ex} (gauss)
0.000	0.000	71	71	0
0.0215	0.0180	75	72	3
0.0610	0.0485	80	72	8
0.0651	0.0515	84	72	12
0.1138	0.0855	84	73	11
0.1240	0.0922	89	74	15
0.1770	0.1255	87	75	12
0.1840	0.1296	93	75	18
0.1930	0.1350	90	75	15
0.2240	0.1528	105	76	29
0.2400	0.1618	104	76	28

$k_{2d} = 1.53 \times 10^9$ and $k_{2a} = 2.27 \times 10^9$ ℓ mole^{-1} sec^{-1}.

d) Bu_4NBr assumed to be completely dissociated in CH_3CN.

a) Bu_4NBr assumed to be partially dissociated in CH_3CN with $K_d = 0.5/25°C$.

c) Resonance width corrected for broadening due viscosity.

Table XIII. (Cont'd)

T = 289°K

Excess concentration (molar) $[Br^-]_d$	$[Br^-]_a$	ΔH (gauss)	ΔH_c	ΔH_{ex}
0.000	0.000	66	66	0
0.0209	0.0175	69	66	3
0.0594	0.0473	71	66	5
0.0635	0.0504	78	67	11
0.1108	0.0835	77	67	10
0.1200	0.0896	79	67	12
0.1720	0.1224	78	68	10
0.1790	0.1267	82	68	14
0.1880	0.1320	80	68	12
0.2190	0.1500	93	69	24
0.2340	0.1584	88	69	19

$K_{2d} = 1.16 \times 19^9$ and $k_{2a} = 1.72 \times 10^9$ ℓ mole^{-1} sec^{-1}.

T = 300°K

0.000	0.000	64	64	0
0.0206	0.0172	65	64	1
0.0585	0.0467	69	64	5
0.0625	0.0496	72	64	8
0.1092	0.0824	72	65	7
0.1190	0.0889	74	65	9
0.1700	0.1212	78	66	12
0.1770	0.1255	75	66	9
0.1860	0.1308	79	66	13
0.2160	0.1483	87	66	21
0.2310	0.1568	83	66	17

$k_{2d} = 1.15 \times 19^9$ and $k_{2a} = 1.69 \times 19^9$ ℓ mole^{-1} sec^{-1}.

Table XIII. (Cont'd)

T = 317°K

Excess concentration (molar) $[Br^-]_d$	$[Br^-]_a$	ΔH (gauss)	ΔH_c	ΔH_{ex}
0.000	0.000	61	61	0
0.0201	0.0168	62	62	0
0.0572	0.0457	65	62	3
0.0611	0.0486	70	62	8
0.1068	0.0808	71	62	9
0.1160	0.0870	73	62	11
0.1660	0.1188	73	63	10
0.1730	0.1230	73	63	10
0.1820	0.1284	79	63	16
0.2110	0.1454	84	63	21
0.2260	0.1540	80	63	17

$k_{2d} = 1.22 \times 10^9$ and $k_{2a} = 1.80 \times 10^9$ ℓ mole^{-1} sec^{-1}.

T = 337°K

0.000	0.000	59	59	0
0.0196	0.0164	60	59	1
0.0557	0.0446	62	60	2
0.0595	0.0474	66	60	6
0.1040	0.0789	67	60	7
0.1140	0.0856	71	60	11
0.1620	0.1163	67	60	7
0.1680	0.1200	70	61	9
0.1770	0.1255	72	61	11
0.2060	0.1426	77	61	16
0.2210	0.1511	73	61	12

$k_{2d} = 0.93 \times 10^9$ and 1.37×10^9 ℓ mole^{-1} sec^{-1}.

Table XIII. (Cont'd)

T = 354°K

Excess concentration (molar) $[Br^-]_d$	$[Br^-]_a$	ΔH (gauss)	ΔH_c	ΔH_{ex}
0.000	0.000	58	58	0
0.0191	0.0160	59	58	1
0.0544	0.0436	61	58	3
0.0581	0.0464	64	58	6
0.1077	0.0814	65	58	7
0.1110	0.0836	68	58	10
0.1580	0.1139	66	59	7
0.1650	0.1182	66	59	7
0.1730	0.1230	73	59	14
0.2020	0.1402	76	59	17
0.2160	0.1483	70	59	11

$k_{2d} = 0.93 \times 10^9$ and $k_{2a} = 1.37 \times 10^9$ ℓ mole^{-1} sec^{-1}.

FIGURE 32

Ligand exchange widths, $\Delta H_{exchange}$ (gauss) vs. the excess bromide concentration at several temperatures. All solutions contained 0.05 M manganese in acetonitrile and spectra were taken at X-band frequencies.

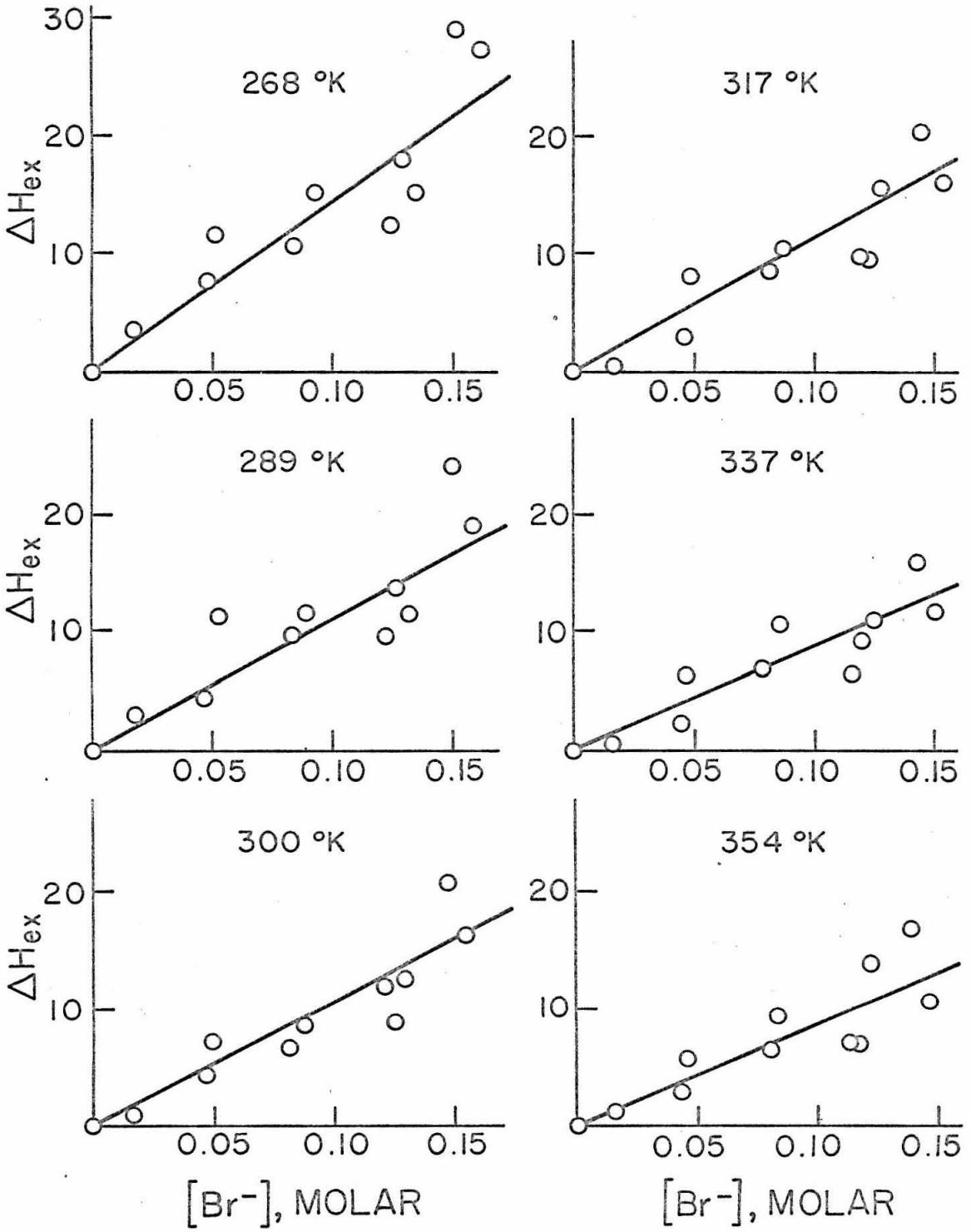
268 °K
317 °K
289 °K
337 °K
300 °K
354 °K
ΔHex
30
20
10
0.05
0.10
0.15
[Br⁻], MOLAR

These widths have been corrected for small variations in the solvent viscosity resulting from the addition of the excess bromide. The corrections amounted, at most, to several gauss and hence do not affect the final data significantly. The excess bromide concentrations have also been compensated for the incomplete dissociation of tetra-n-butylammonium bromide in acetonitrile. The known dissociation constant of 0.5 (72) reported at 25°C was used at all temperatures since temperature data concerning the dissociation of this salt were unavailable.

A plausible interpretation of the significant bromide-dependent resonance widths is bromide ligand exchange. Presumably, the electronic distortion imposed by ligand exchange is strong, so that the lifetimes of the spin states, and hence both the longitudinal and transverse relaxation times, are limited to the chemical lifetime of the complex. The linear variation of the bromide-dependent widths with excess bromide concentration depicted in Fig. 32 suggests that the ligand exchange is bimolecular, involving one bromide ion and one $MnBr_4^{-2}$ in which the initial and final states are the same:

$$MnBr_4^{-2} + Br^- \rightleftharpoons MnBr_4^{-2} + Br^- . \qquad (86)$$

Analysis of the data according to the well-known expression

$$\left(\frac{1}{T_2}\right)_{ex} = k[Br^-] = \sqrt{3}\,\beta\pi\,(g/h)\,\Delta H_{ex} \qquad (87)$$

yielded a set of bimolecular rate constants at six different

temperatures and the results are summarized in Table XIV. As a comparison, the results computed for completely dissociated Bu_4NBr are included and provide a set of smaller bimolecular rate constants. If we consider the influence of activity on the dissociation of Bu_4NBr, we may expect our results to lie somewhere in between the extreme values reported in Table XIV. We have used the extended Debye-Hückel limiting law which compensates for the finite size of ions to calculate the mean activity coefficient of Bu_4NBr in CH_3CN at 300°K. Recalculation with the activities of $[Br^-]$ then gives $k_2 = 1.6 \times 10^9$ ℓ mole^{-1} sec^{-1} at 300°K. Uncertainties in the Bu_4NBr dissociation constant and lack of its temperature dependency does not warrant further extension of these calculations.

Based on earlier observations, the exchange interaction at this concentration level (0.039 M Mn^{+2}) is presumably between a bromide ion and the ion-paired state of $MnBr_4^{-2}$. The rate constants deduced suggest that the kinetics of ligand exchange is probably diffusion controlled. Consequently, analysis of the kinetic data by classical transition state theory has questionable validity. When the standard Arrhenius plot is made as illustrated in Fig. 33, one obtains an apparent enthalpy of activation of -1 kcal/mole, and apparent entropy of activation of -22 e.u. The small and negative apparent energy of activation is not too meaningful. However, the large and negative apparent entropy of activation is consistent with an associative mechanism for the ligand-exchange process. Apparent negative activation energies have been reported for electron-transfer reactions

Table XIV. The Bimolecular Rate Constants at Six Temperatures. Thermodynamic Properties of the Activated Complex.

Bu_4NBr in CH_3CN assumed to be	T°K	k_2 $\times 10^{-9}$	$\Delta S^{\circ\ddagger}$ e.u.	$\Delta G^{\circ\ddagger}$ kcal	$K_c^{\ddagger}$ $\times 10^4$	E_a kcal
completely dissociated	268	1.53	-22.1	4.37	2.74	
	289	1.16	-22.5	4.91	1.92	
	300	1.15	-22.5	5.13	1.84	
	317	1.22	-22.3	5.42	1.84	
	337	0.93	-22.7	5.98	1.33	
	354	0.93	-22.7	6.31	1.27	-1.01
partially dissociated with $K_d = 0.5$	268	2.67	-22.4	4.16	4.06	
	289	1.72	-21.8	4.69	2.85	
	300	1.69	-21.8	4.90	2.71	
	317	1.80	-21.6	5.17	2.72	
	337	1.37	-22.0	5.72	1.96	
	354	1.37	-22.0	6.04	1.85	-1.03

FIGURE 33

Arrhenius plot of $\ell n\ k_2$ vs. $10^3/T°K$ for chemical exchange bimolecular rate constants.

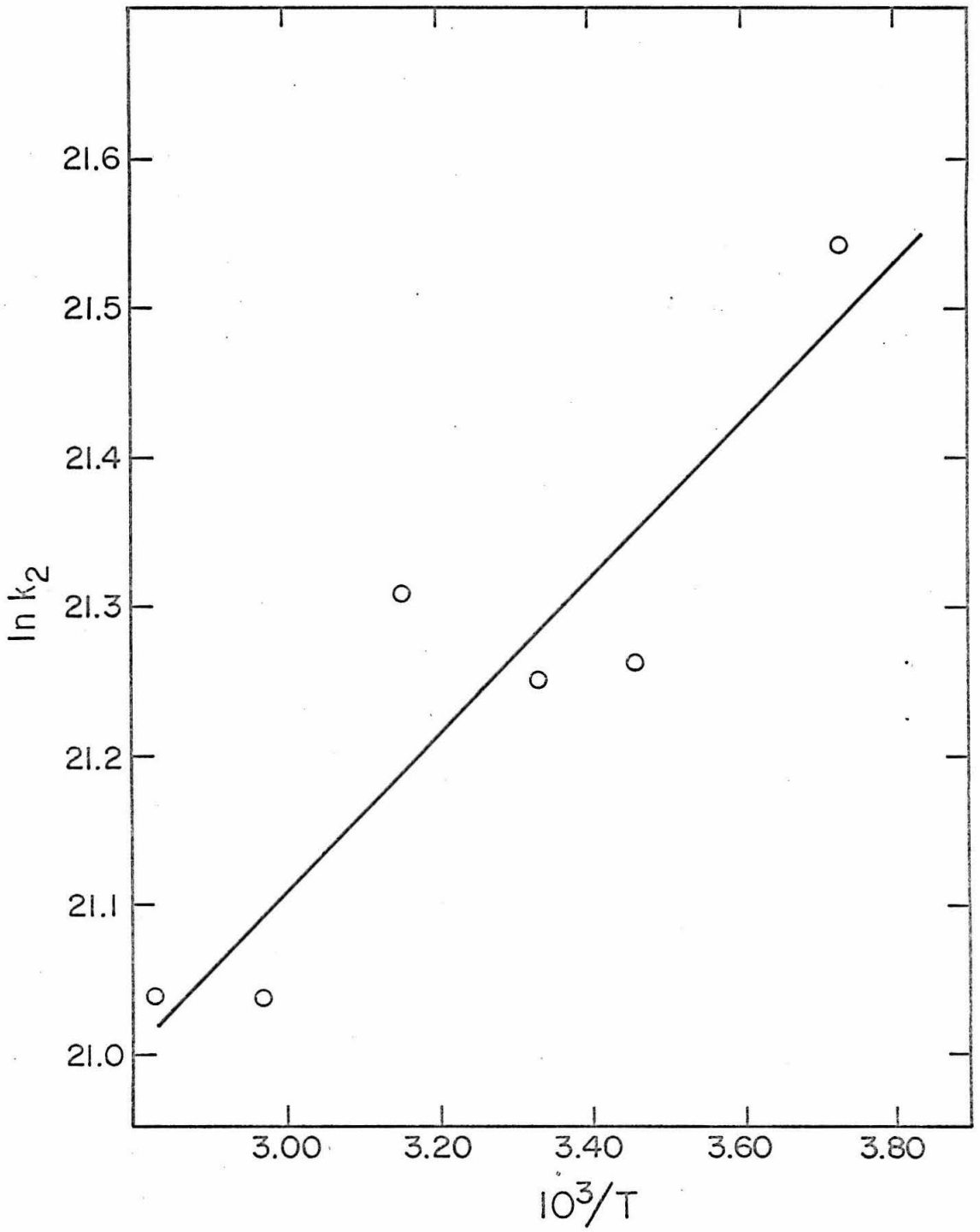
21.6
21.5
21.4
21.3
21.2
21.1
21.0
ln k2
3.00
3.20
3.40
3.60
3.80
10^3/T

on several occasions (46, 73).

Previous studies on relaxation in manganese(II) solutions dealt exclusively with octahedrally coordinated complexes. Tetrahedral complexes, in general, are known to ligand exchange more rapidly than octahedral complexes. Ligand exchange in tetrahedral complexes is believed to proceed through the "classical" five-coordinated activated complex proposed as an intermediate. The large resonance width variation in response to bromide ion concentration may be interpreted as a case of high ligand lability in which exchange is indeed very rapid. Reaction is occurring in the ten nanosecond region amenable to the electron paramagnetic resonance time scale.

Since we are measuring resonance widths reflecting the manganese(II) spin-state lifetime we cannot obtain direct information on structure or lifetime of the activated complex nor on the fate of the interacting bromide ion. All we know is that the manganese electronic energy manifold has experienced a large perturbation that did not occur in the analogous $MnCl_4^{-2}$ system under similar conditions. Armed with this chemical argument, let us propose that the colliding bromide ion reaches the manganese first coordination sphere to generate a transient reaction intermediate. Let us now consider the fate of the transient intermediate. There are several possibilities open: (1) the same ion can leave the activated complex or, (2) a different ion can leave. If the activated complex is isotropic, the probability of any group leaving will be equal and cases (1) and (2)

will be indistinguishable provided exchangeable ions are the same, although, technically speaking only case (2) presents a true exchange process. In the situation where the entering group forms an anisotripic intermediate, case (1) will be operative and this is tantamont to a distortion as opposed to exchange. It must be born in mind that our spin relaxation experiments cannot discriminate between these possibilities. As we shall see in the next section, there is further reason to suspect a chemical exchange process. In the meantime we shall refer to our new mechanism as chemical exchange in the spirit of mild speculation.

Since we are measuring resonance widths presumably reflecting the manganese(II) spin-state lifetimes, the same mechanism causing a strong perturbation of the electronic system should then provide a channel for spin relaxation. That is to say, colliding or exchanging bromide ions can provide a sink for the excited-state paramagnetic anion and, therefore, we may think of this as a spin-lattice relaxation or a T_1 process.

We can also treat the data by invoking a two-state model which includes a paramagnetic intermediate or "activated" complex. The chemistry may then be represented by

$$\underset{A}{MnBr_4^{-2}} + Br^- \underset{k_1}{\overset{k_2}{\rightleftharpoons}} \underset{B}{[MnBr_4^{-2} \cdots Br^-]^*} \qquad (88)$$

where k_2 is the bimolecular rate constant and k_1 is the unimolecular

rate constant characterizing dissociation of the activated complex. Thus, Mn^{+2} resides in two exchanging states A and B (in keeping with our former nomenclature). Although we did not observe any additional broad spectra due to state B, this does not preclude its existence. Accordingly, we were motivated to examine the consequences of this model and the derivations leading to three important cases were included in the Theoretical Section. Assuming, then, that state B, the paramagnetic "activated" complex, has an extremely short relaxation time and, thus, is very broad, we can rule out case (1) which predicts curvature between exchange resonance width and excess bromide ion. On similar grounds we can probably eliminate case (2). That leaves us with case (3) which predicts a linear relationship between exchange resonance width and bromide ion concentration

$$\frac{1}{T_2} = \frac{1}{T_{2A}} + \frac{1}{\tau_A} \tag{89}$$

in agreement with experimental observation. Moreover, we arrive at the same conclusion as in our primitive quantum mechanical treatment. However, the present phenomenolical approach is somewhat more sophisticated in the sense that we now require a two-state system interacting in the slow exchange limit, $\omega_i < |\omega_A - \omega_B|$.

3.1 Frequency Dependence of Resonance Widths

Reviving an earlier observation in Fig. 26 depicting the response of resonance width to $[Mn^{+2}]$ concentration, we notice an additional dependence on frequency for solutions containing more than 0.03 M $MnBr_4^{-2}$ in the absence of excess $[Br^-]$ ion. This surprising effect marks the onset of another important relaxation mechanism whose origin appears to lie in the manganese concentration and probably involves a dipolar interaction. It suggested a way to untangle some of the relaxation mechanisms in this complicated system. Consequently, a thorough study was launched to explore the frequency effect of manganese concentration at constant, excess bromide ion concentration and variable excess bromide ion concentration at various levels of constant manganese concentration on electron spin resonance widths.

Since dipolar interactions effecting line shapes can be expected in solutions containing more than 0.01 M manganese(II) (69), an initial experiment was performed with 0.0025 M (0.0019 M) $MnBr_4^=$ in order to more or less guarantee the absence of dipolar broadening. In any event, this concentration was found to be the lower limit providing resonance widths that were dependably reproducible. In Fig. 33, the variation of resonance width vs. excess bromide ion concentration has been plotted at X and K-band frequencies from the data summarized in Table XV. As before, the bromide ion concentration in acetonitrile has been corrected for association at 25°C and is included in Table XV. Furthermore, our experience in the first exchange

Table XV. Resonance Width Dependence on Excess Molar Bromide Concentration and Frequency at 300°K. Bimolecular Rate Constants Calculated from Least-Square Treatment of Data.

Molar concentrations			Resonance width (gauss)	
$MnBr_4^{-2}$	Br^- (D)	Br^- (A)	ΔH_X	ΔH_K
0.0019	0.0005	0.0005	44	49
	0.0005	0.0005		49
	0.004	0.004	47	
	0.010	0.010	49	57
	0.051	0.046		58
	0.052	0.047	55	
	0.099	0.084		63
	0.102	0.086	58	
	0.153	0.122		63
	0.154	0.123	60	
	0.201	0.153		67

Bimolecular Rate Constants, ℓ $mole^{-1}$ sec^{-1}

	k_2 (D) $\times 10^{-9}$	k_2 (A) $\times 10^{-9}$
X	0.75	1.01
K	0.81	1.15

(D) Bu_4NBr assumed completely dissociated; (A) Br^- concentration compensated for partial association with $K_d = 0.5$; (X) Experiments conducted at X-band frequencies ~9.5 &Hz; (K) at K-band frequencies ~34.7 &Hz.

FIGURE 33

Resonance width, ΔH (gauss), variation of 0.0019 M $MnBr_4^{-2}$ as a function of excess molar Bu_4NBr at X and K-band frequencies.

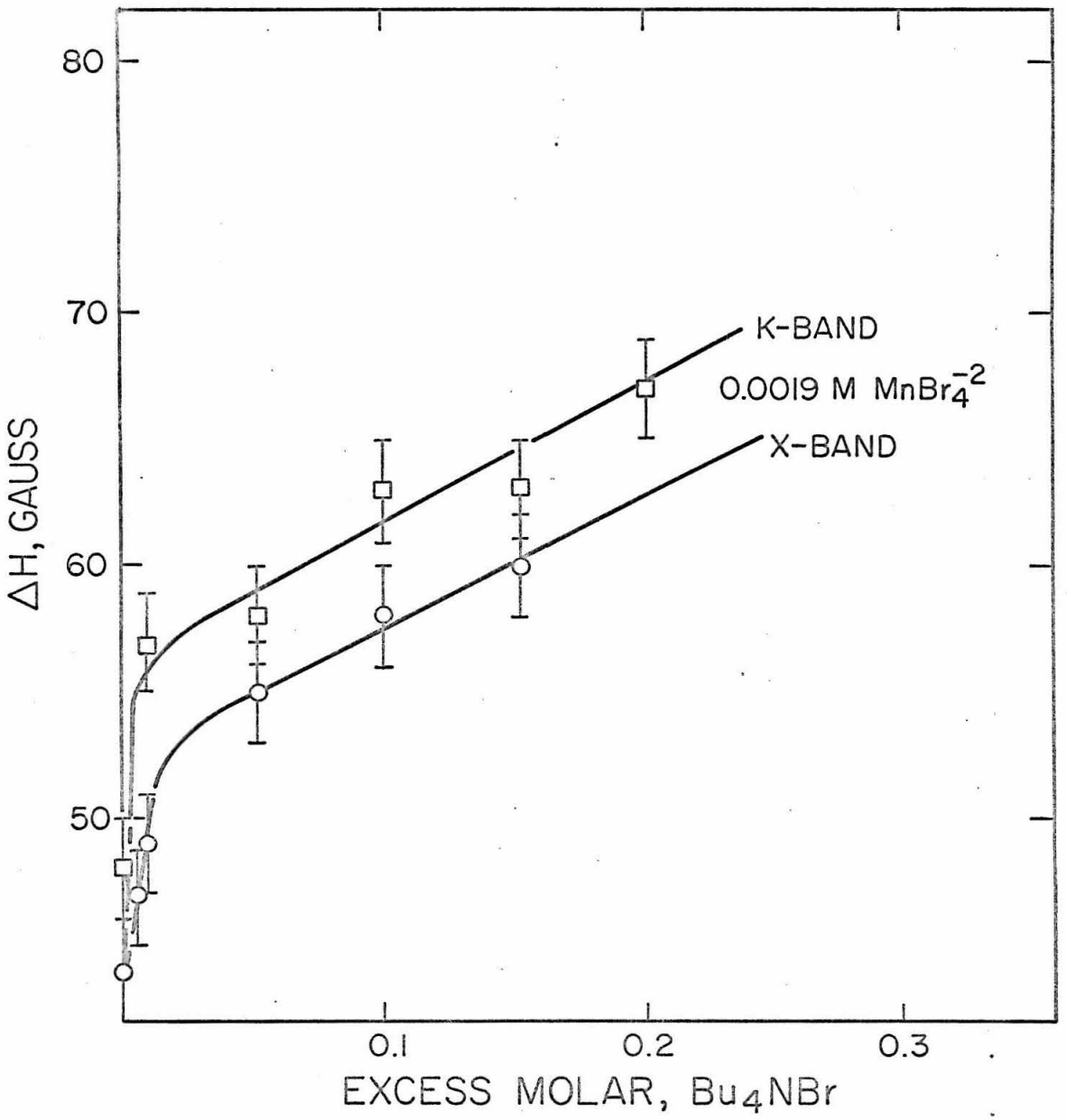
80
70
60
50
ΔH, GAUSS
K-BAND
0.0019 M $MnBr_4^{-2}$
X-BAND
0.1
0.2
0.3
EXCESS MOLAR, Bu_4NBr

study demonstrated that solvent viscosity contributes relatively little to the overall resonance width and hereafter shall be ignored. The plots show a similar trend to the 0.05 M (0.039 M) $MnBr_4^{-2}$ exchange study depicted in Fig. 32. In both cases an increase of resonance width accompanies increasing excess molar bromide ion concentration and the slopes are almost the same. Analysis of the data obtained from the linear portion of the curve according to Eq. (87) yielded the bimolecular rate constant, k_2, and the results are included in Table XV. However there are several important differences: a) the X-band resonance widths are slightly smaller than the K-band results in the linear portion but the difference may not be real in view of error tolerances at this level of concentration; b) the linear portion of the X and K-band plots are from 8 to 14 gauss lower than the 0.05 M (0.039 M) $MnBr_4^{-2}$ exchange study; c) an abrupt increase of resonance width occurs on addition of a slight Bu_4NBr excess before a constant slope is attained. The latter observation is consistent with our ion-pair model at a concentration level where resonance width responds rapidly to changes imposed by equilibria according to Eqs. (81) and (83). Point b), however, raises interesting questions regarding the source of the large discrepancy in resonance widths for exchange studies conducted at different manganese concentrations and supplied the impetus to explore the problem more deeply.

The next exchange study was performed with 0.0037 M $MnBr_4^{-2}$ and at this concentration resonance widths were easier to measure and the confidence level of the result was higher. It should be

mentioned that in all frequency effect studies, X and K-band samples were prepared simultaneously from a given solution. Variation of resonance width vs. excess bromide ion concentration at both X and K-band frequencies has been plotted from the data collected in Table XVI and the results are presented in Fig. 34. As usual, increase in resonance widths follows from addition of excess bromide ion. Non-linear behavior in both plots at low bromide ion concentrations is observed in agreement with our ion-pair arguments but persistence of curvature may result from additional complications inherented from complex-solvent intermediates previously illustrated in Eqs. (81) and (82). The latter effect becomes more prominent at higher manganese concentrations and will be considered in greater detail in subsequent exchange studies. At zero excess bromide ion concentration, X and K-band resonance widths are essentially the same but as concentration is increased the plots steadily diverge to approximately 5 gauss at 0.1 excess molar bromide concentration and, thereafter, remain parallel displaying the same slope as their predecessors. A frequency effect is now quite visible and definite with the X-band resonance width being larger than the K-band result. Bimolecular rate constants are extracted from the linear portion of the two plots according to Eq. (87) and are included in Table XVI.

Another exchange study was performed with solutions containing 0.05 M (0.039 M) $MnBr_4^{-2}$ in order to enhance the frequency effect. In Fig. 35, we have plotted the variation of electron spin resonance width vs. excess bromide ion concentration at both X and K-band

Table XVI. Resonance Width Dependence on Excess Molar Bromide Concentration and Frequency at 300°K. Bimolecular Rate Constants Calculated from Least-Square Treatment of Data.

Molar concentration			Resonance width (gauss)	
$MnBr_4^{-2}$	Br^- (D)	Br^- (A)	ΔH_X	ΔH_K
0.0037	0.000	0.000	48	48
	0.030	0.028	53	52
	0.073	0.065	59	57
	0.109	0.092	65	59
	0.146	0.118	67	63
	0.215	0.162	73	68
	0.246	0.181	75	69
	0.306	0.214	79	73

Bimolecular Rate Constants, ℓ $mole^{-1}$ sec^{-1}

	k_2 (D) $\times 10^{-9}$	k_2 (A) $\times 10^{-9}$
X	1.12	1.81
K	1.07	1.68

(D) Bu_4NBr assumed completely dissociated; (A) Br^- concentration compensated for partial association with $K_d = 0.5$;
(X) experiments conducted at X-band frequencies ~9.5 GHz;
(K) at K-band frequencies ~34.7 GHz.

FIGURE 34

Variation of resonance width of 0.0037 M $MnBr_4^{-2}$ as a function of excess molar Bu_4NBr at X and K-band frequencies.

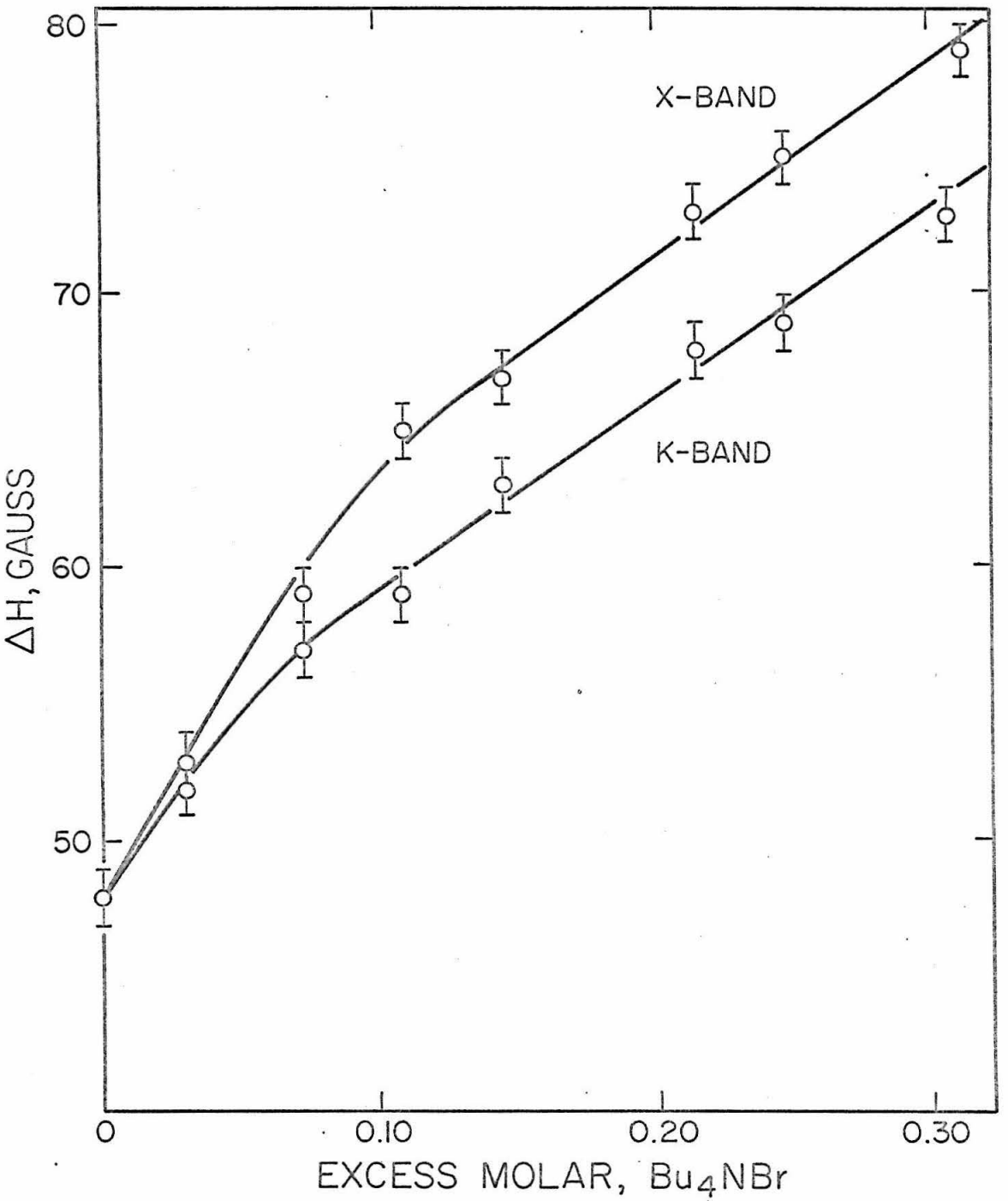
80
70
60
50
ΔH, GAUSS
X-BAND
K-BAND
0
0.10
0.20
0.30
EXCESS MOLAR, Bu4NBr

frequencies from the data compiled in Table XVII. As we already know from the initial exchange studies, increase in resonance widths accompanies increasing bromide ion concentrations. According to earlier experiments and our ion-pairing model, the complex resides in the ion-paired state at this level of manganese concentration even in the absence of excess Bu_4NBr. Then as the bromide ion concentration is increased the plots diverge dramatically from three to about 12 gauss at 0.06 excess molar bromide reflecting attenuation of solvation intermediates, and, thereafter, remain parallel displaying the same slope as their predecessors. Bimolecular rate constants were obtained from the linear portion of both plots by the previously discussed formalism and are also included in Table XVII. It is now evident that the overall observed resonance width depends strongly on both the manganese concentration and the H_1 frequency. The initial rise in X-band resonance width above those at zero excess bromide concentration implies that broadening imposed by manganese originates directly from the complex form, $MnBr_4^{-2}$, whose concentration in the stoichiometric region is strongly influenced by complex-solvent equilibria of the type

$$MnBr_4^{-2} + CH_3CN \rightleftharpoons Mn(CH_3CN)Br_3^- + Br^-$$

proposed earlier as a possible explantion for the intensity behavior in this system (55). The effect is striking here, but was not obvious by inspection in the last exchange study conducted at 0.0037 M manganese concentration in the presence of ion-pairing effects.

Table XVII. Resonance Width Dependence on Excess Molar Bromide Concentration and Frequency at 300°K. Bimolecular Rate Constants Calculated from Least-Square Treatment of Data

Molar concentration			Resonance Width (gauss)	
$MnBr_4^{-2}$	Br^- (D)	Br^- (A)	ΔH_X	ΔH_K
0.039	0.000	0.000	60	57
	0.046	0.037	65	60
	0.067	0.053	73	63
	0.104	0.079	75	65
	0.129	0.096	78	68
	0.161	0.116	80	67
	0.226	0.154	84	72
	0.305	0.197	90	78

Bimolecular Rate Constants, ℓ $mole^{-1}$ sec^{-1}

	k_2 (D) $\times 10^{-9}$	k_2 (A) $\times 10^{-9}$
X	1.09	1.81
K	0.98	1.60

(D) Bu_4NBr assumed completely dissociated; (A) Br^- concentration compensated for partial association with $K_d = 0.5$;
(X) experiments conducted at X-band frequencies ~9.5 Mc Hz;
(K) at K-band frequencies ~34.7 Mc Hz.

FIGURE 35

Variation of resonance width of 0.039 M $MnBr_4^{-2}$ as a function of excess molar Bu_4NBr at X and K-band frequencies.

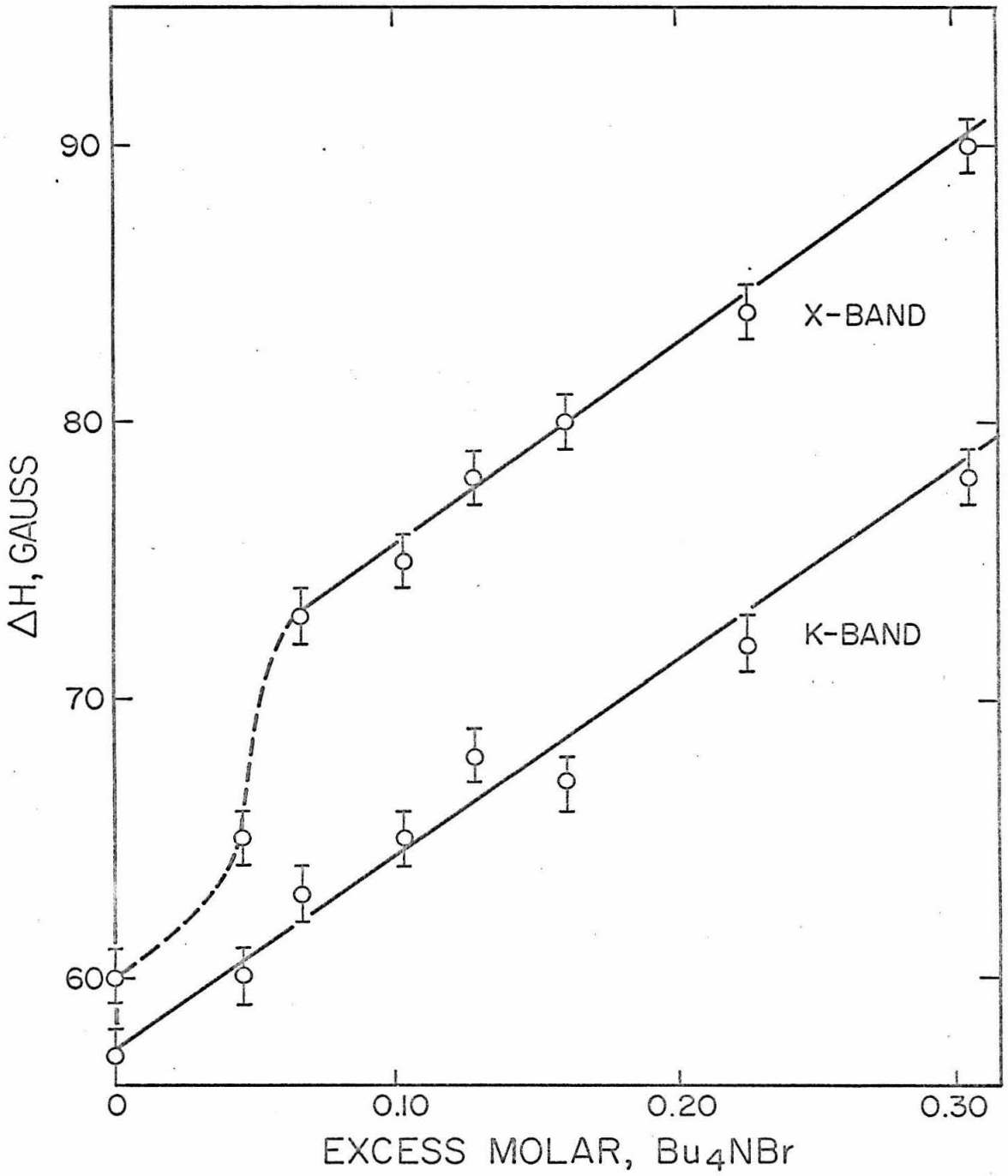
90
80
70
60
ΔH, GAUSS
X-BAND
K-BAND
0
0.10
0.20
0.30
EXCESS MOLAR, Bu4NBr

In parallel to these exchange studies, the analogous chloride system was investigated at both X and K-band frequencies. A solution containing 0.039 M $MnCl_4^{-2}$ and 0.375 M excess Et_4NCl in acetonitrile displayed the following resonance widths for two separate hyperfine components: $|-\frac{1}{2}, \frac{1}{2}\rangle \rightarrow |\frac{1}{2}, \frac{1}{2}\rangle$, $\Delta H_X = 12.0$, $\Delta H_K = 12.5$; $|-\frac{1}{2}, -\frac{1}{2}\rangle \rightarrow |\frac{1}{2}, -\frac{1}{2}\rangle$, $\Delta H_X = 12.3$, $\Delta H_K = 12.1$ gauss. Within experimental error, a resonance width dependency on frequency is not observed in this system nor in the previously described experiments appearing in the $MnCl_4^{-2}$ section. Although dipolar interactions leading to line broadening are probably operative in the chloride system, it is evident that dipolar interactions in the bromide system behave quite differently. This fascinating comparison suggests that the dipolar interactions leading to line broadening may operate on entirely different time scales leading to the possibility of unraveling some of the more intricate details of electron spin relaxation in the chemically exchanging $MnBr_4^{-2}$ system.

The exchange series was further extended to examine solutions containing 0.100 M $MnBr_4^{-2}$. In Fig. 36, we have compared the resonance width as a function of excess bromide ion concentration at both X and K-band frequencies from data summarized in Table XVIII. At this level of manganese concentration and zero excess bromide the complex should be in the ion-paired state and sufficiently concentrated to observe a frequency effect on the resonance widths even in the presence of some solvent intermediates. Figure 36 supports this contention and depicts the line broadening with increasing bromide ion

Table XVIII. Resonance Width Dependence on Excess Molar Bromide Concentration and Frequency at 300°K. Bimolecular Rate Constants Calculated from Least-Square Treatment of Data

Molar concentration			Resonance width (gauss)	
$MnBr_4^{-2}$	Br^- (D)	Br^- (A)	ΔH_X	ΔH_K
0.100	0.000	0.000	74	60
	0.027	0.026	76	61
	0.058	0.039	78	62
	0.084	0.056	80	64
	0.113	0.073	83	66
	0.161	0.101	87	69
	0.200	0.122	90	72
	0.229	0.137	93	76
	0.298	0.171	96	79

Bimolecular Rate Constants, ℓ mole^{-1} sec^{-1}

	k_2 (D) $\times 10^{-9}$	k_2 (A) $\times 10^{-9}$
X	1.20	2.18
K	1.12	2.03

(D) Bu_4NBr assumed completely dissociated; (A) Br^- concentration compensated for partial association with $K_d = 0.5$;
(X) experiments conducted at X-band frequencies ~9.5 GHz;
(K) at K-band frequencies ~34.7 GHz.

FIGURE 36

Variation of resonance width of 0.10 M $MnBr_4^{-2}$ as a function of excess molar Bu_4NBr at X and K-band frequencies.

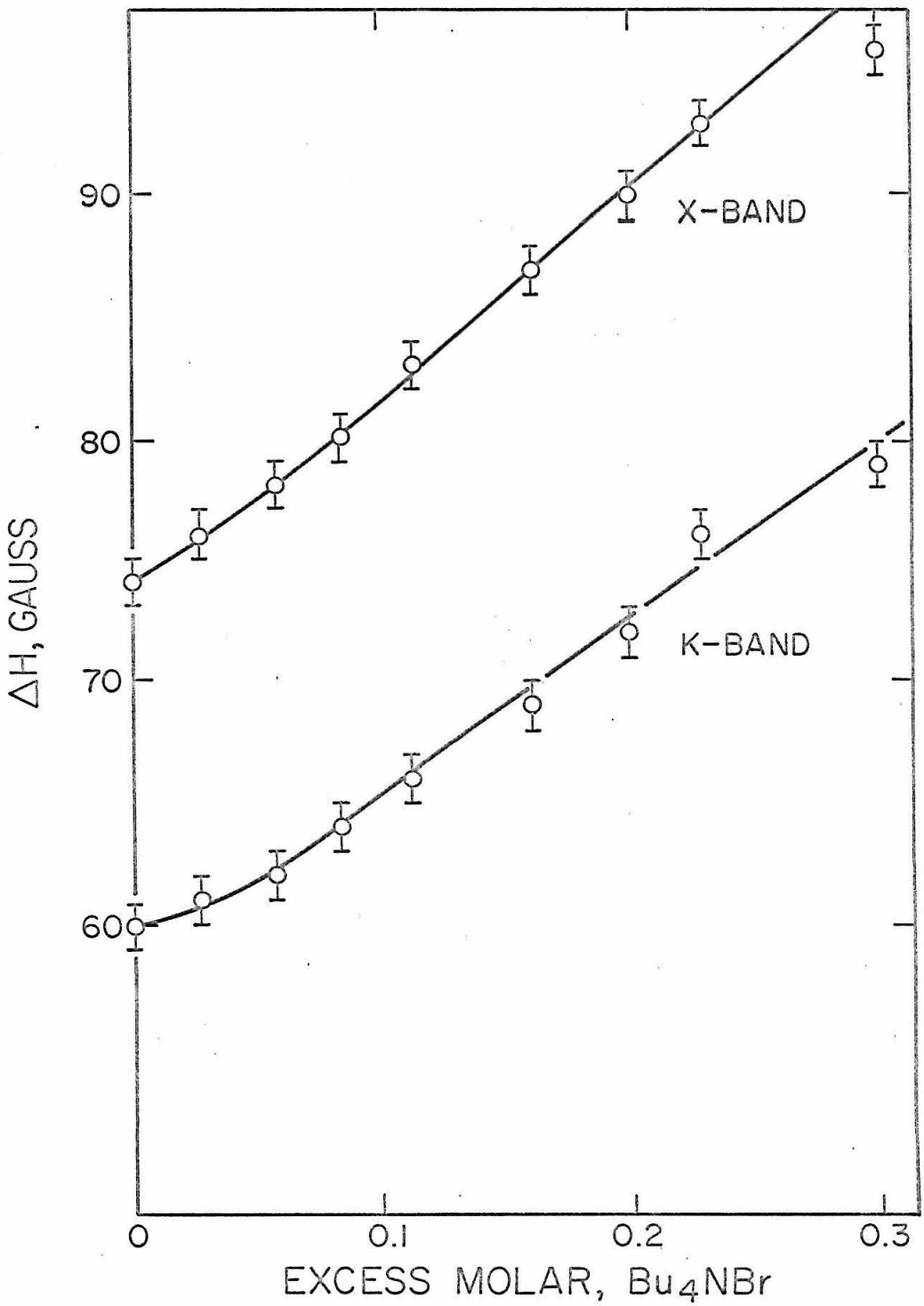
90
80
70
60
ΔH, GAUSS
X-BAND
K-BAND
0
0.1
0.2
0.3
EXCESS MOLAR, Bu4NBr

concentration as usual. X-band resonance widths are greater than K-band widths over the entire concentration range starting from a difference of 14 gauss at zero excess bromide and gradually increasing to 16-18 gauss at 0.05 molar excess bromide ion concentration; the plots remain essentially parallel thereafter at higher concentration. In the diverging region a small curvature is observed, although above 0.05 molar excess bromide, the plots are relatively linear. Bimolecular rate constants were extracted from the linear portions of both plots as before and the results are included in Table XVIII. Trends in the exchange studies have developed in a consistent manner and frequency dependent line broadening is clearly associated with $MnBr_4^{-2}$ concentration.

The experimental situation was then inverted to study line broadening imposed by $MnBr_4^{-2}$ in a system containing constant 0.15 excess molar bromide ion concentration. On the basis of foregoing results, bromide concentration was adjusted to a region where the state of the complex was well defined and where the contribution from bromide ion ligand exchange to resonance width was known. Furthermore, this compromise permits an extension of the line broadening studies to higher manganese concentrations. In Fig. 37, we show the variation of electron spin resonance width vs. the complex, $MnBr_4^{-2}$, concentration containing 0.15 excess molar Bu_4NBr at both X and K-band frequencies. Line broadening occurs with increasing $MnBr_4^{-2}$ concentration as anticipated from the previous exchange studies. Both plots are approximately linear but have different positive slopes

FIGURE 37

Variation of resonance width as a function of $MnBr_4^{-2}$ concentration at constant 0.15 M excess Bu_4NBr. Response compared at X and K-band frequencies.

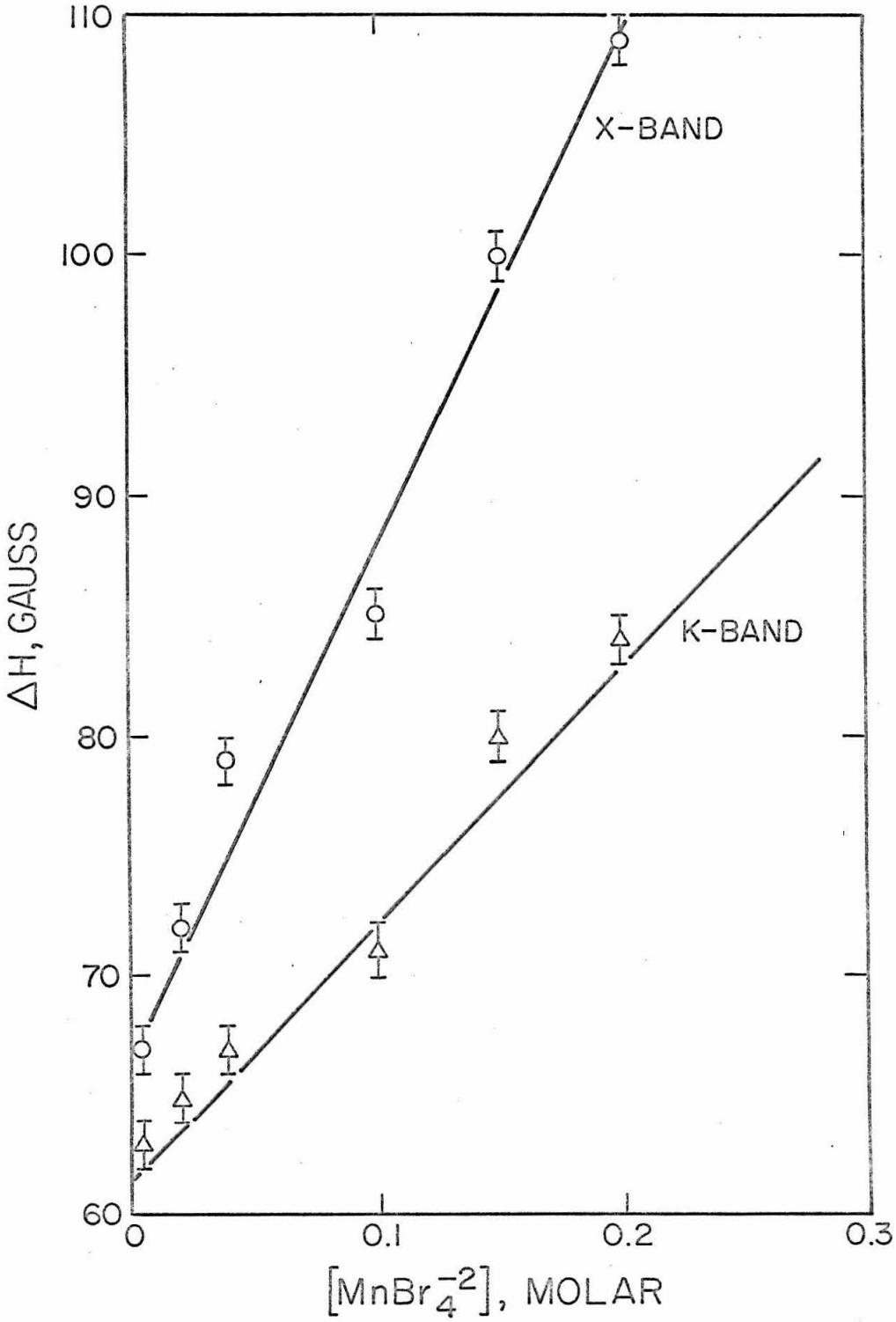
110
100
90
80
70
60
ΔH, GAUSS
X-BAND
K-BAND
0
0.1
0.2
0.3
[MnBr$_4^{-2}$], MOLAR

with the X-band possessing the larger of the two: (1) X-band, $\Delta H_{ex}/[Br^-] = 211$ gauss/mole; (2) K-band, $\Delta H_{ex}/[Br^-] = 105$ gauss/mole. The difference between them is 4 gauss at 0.0037 M $MnBr_4^{-2}$ and 25 gauss at 0.2 M $MnBr_4^{-2}$. Resonance widths beyond 110 gauss cannot be analyzed with much accuracy so we set this value arbitrarily as a practical upper limit for meaningful results. It should be noted by comparison to the previous exchange studies presented in Figs. 31-34 that manganese dependent broadening at X-band frequencies is considerably greater than bromide ion-ligand exchange broadening.

In view of these experimental results, a possible mechanism for line broadening is superexchange induced by transmission of paramagnetism through diamagnetic carriers, in this case, bromide ions. The superexchange Hamiltonian or sometimes referred to as the Heisenberg exchange Hamiltonian has the form

$$H_{ex} = \sum_{j,k} \vec{J}(r_{jk})\, \vec{S}_j \cdot \vec{S}_k \qquad (85)$$

and the extent of interaction can depend on concentration of both the paramagnetic and diamagnetic components. $J(\vec{r}_{jk})$ is the coupling constant characterizing the interaction between the exchanging spins $\vec{S}_j$ and $\vec{S}_k$ over a distance $\vec{r}_{jk}$. Superexchange phenomena are typified by collapse of hyperfine structure, that is, reduction of $\langle A \rangle$, coupled with a general broadening of the entire spectrum up to a certain point followed by exchange narrowing upon further increase of concentration.

These effects have been reported for $MnCl_2$ in molten LiCl (74) and molten LiCl-KCl eutectics (75) where manganese concentrations (0.15-0.30 M) are similar to those reported in the present work although the halide ion concentration was more than an order of magnitude higher. Nevertheless, a careful determination of the effective spin Hamiltonian constants for two $MnBr_4^{-2}$ solutions spanning a significant manganese concentration range was performed and the values are compared in Table XIX. Within experimental tolerances, a decrease in the hyperfine coupling constant was not observed, however, the magnitude of collapse could be small enough to be obscured by the accuracy of our measurements. In addition, the quantitative effect imposed by superexchange mechanisms on the collapse of hyperfine structure, line narrowing, and intricate details of line shape, particularly in liquid media, is still open to question. Even so, under the experimental circumstantial evidence at hand, we suspect that superexchange does not provide a significant relaxation

Table XIX. Spin Hamiltonian Constants and Resonance Widths for $MnBr_4^{-2}$ Solutions in Acetonitrile

Molar concentration/26°C $[MnBr_4^{-2}]$	ex$[Br^-]$	ΔH_K (gauss)	$\langle g \rangle$ ±0.001	$\langle A \rangle$ ±0.5 gauss
0.0047	0.149	68	2.007	-76
0.200	0.150	84	2.007	-76

mechanism for $MnBr_4^{-2}$ within the concentration range investigated in the present work.

Returning to Fig. 37, depicting the manganese dependent broadening, it is seen that the X and K-band plots converge and almost coincide on approaching zero manganese concentration. Extrapolation of these lines through the ordinate axis gives nearly coincident intercepts within experimental error and defines an "average" overall resonance width in the absence of manganese dependent broadening. Since the average overall resonance width is now accountable to previously discussed mechanisms including intrinsic contributions, we can assign broadening above the point of convergence to interactions involving only manganese. The dividing line between these two major relaxation mechanisms may be envisioned in Fig. 37 as an imaginary absicca extending through the averaged point of convergence.

Comparison of Fig. 37 to Figs. 33-36 depicting bromide ligand exchange effects, clearly demonstrates that manganese dependent interactions provide the dominant relaxation mechanism in this system.

Looking back on the experimental results, we can now represent the overall resonance width in the exchanging system by the incorporation of two new terms

$$\frac{1}{T_2} = \frac{1}{T_{2A}} + k_2[Br^-] + [k_2' + D(\omega)][MnBr_4^{-2}] \qquad (90)$$

where T_{2A}^{-1} contains all intrinsic contributions to broadening mentioned earlier. The first of these new terms is a bimolecular rate constant, k_2', to account for the possibility of an exchange process between two like paramagnetic anions in which the spin-state lifetime is limited by the interaction and is formulated by the following quasi-reaction

$$MnBr_4^{-2} + MnBr_4^{-2} \underset{k_1'}{\overset{k_2'}{\rightleftharpoons}} [MnBr_4^{-2} \cdots MnBr_4^{-2}]^* \qquad (91)$$

The second term, $D(\omega)$, represents the frequency dependent dipolar interaction term having the general form

$$D(\omega) = K\left(\frac{g^4\beta^4}{\hbar^2 r^6}\right)\left[a\tau_d + \frac{b\tau_b}{1+C\omega_o^2\tau_d^2} + \frac{d\tau_d}{1+\ell\omega_o^2\tau_d^2} + \cdots\right] \qquad (92)$$

where a, b, $\cdots \ell$ are generally small integers, τ_d is the translational correlation time, r is the average mean distance between interacting dipoles and the other symbols bear their usual significance. It is impractical to bring this expression into closed form for two interacting sextet state ions. However, the operator formalism introduced by McLachlan (25) provides numerical solutions for T_2 by diagonalization of an appropriate relaxation matrix. The line shapes, however, are still dependent on the assignment of a correlation time, τ_d, and when $\omega_o\tau_d \approx 1$ they assume their most complex form. As in all relaxation treatments when $\omega_o\tau_d > 1$, the theory is not valid and line

shapes deviate from Lorentzian character (25). In view of theoretical uncertainties it is probably uneconomical to pursue a solution under the present circumstances.

The plots of ΔH (X and K band) as a function of $[Br^-]$ shown in Figs. 33-36 contained different concentrations of manganese and, yet, they all had essentially the same slope. This is clearly consistent with our interpretation that the slope characterizes a dynamical exchange process between free Br^- and $MnBr_4^{-2}$ occurring on a time scale amenable to electron spin resonance. It further suggests under these conditions that the factor $[k_2' + D(\omega)]$ and therefore its components, are apparently independent of viscosity changes. At constant $[Br^-]$ and variable $[MnBr_4^{-2}]$ concentrations the resonance width also responded in linear fashion but their slopes depended markedly on the exciting H_1 frequency, ω_0. It is interesting to recall that analogous experiments on Et_4NCl-$MnCl_4^{-2}$ showed no such concentration or frequency dependency. We propose that the frequency dependent resonance widths have their origin in dynamical dipolar interactions between the paramagnetic anions. Since the $MnBr_4^{-2}$ complex is larger than its chloride analogue, it is perfectly reasonable on an intuitive level to expect the larger specie to move more slowly through solution. Consequently, dipolar interactions between Mn^{+2} ions in the larger complex can persist over a longer period of time. Moreover, the tetraalkyl ammonium counterions probably diffuse in a cooperative fashion along with the complex to further modify dynamical processes. In Table XX we have listed the

Table XX. Molecular Radii of Tetrahedral Mn(II) Complexes and Their Ion-Pairs

Complex	Radius a (Å)
* $MnCl_4^{-2}$	4.02
$Et_4N^+ \cdots MnCl_4^{-2}$	8.13
* $MnBr_4^{-2}$	4.30
$Bu_4N^+ \cdots MnBr_4^{-2}$	11.49

* Estimated from Pauling ionic radii.

molecular dimensions of the complexes based on the additivity of ionic and covalent radii. Lack of structural information about the ion-paired states, of course, renders these dimensions rather speculative. Nevertheless, they are useful in estimating the "residence" or correlation time of the dipolar interactions. To simplify the calculations we treat the ion-pairs as rigid spheres interacting in a viscous medium having a macroscopic viscosity, η. If we assume the diffusion equation to apply at the molecular level, a relation can be established between the minimum distance of approach, d, the self-diffusion coefficient, D, and the translational correlation time, τ_d

$$\tau_d = \frac{d^2}{2D} . \tag{93}$$

In terms of molecular radii, a, this becomes

$$\tau_d = \frac{2a}{D} \tag{94}$$

and assuming the Stokes relation for D

$$D = \frac{kT}{6\pi a \eta} \tag{95}$$

the combination of these equations leads to the familiar translational correlation time

$$\tau_d = \frac{12\pi a^3 \eta}{kT} . \tag{96}$$

Therefore, the correlation times for $MnBr_4^{-2}$ and $MnCl_4^{-2}$ are related through their molecular radii, a, and macroscopic viscosity, η

$$\frac{\tau_d(MnBr_4^{-2})}{\tau_d(MnCl_4^{-2})} = \left(\frac{a_{Br}}{a_{Cl}}\right)^3 \left(\frac{\eta_{Br}}{\eta_{Cl}}\right) . \tag{97}$$

More specifically we estimate this ratio for the ion-paired states from the values listed in Table XX

$$\frac{\tau_d(Bu_4N^+ \cdots MnBr_4^{-2})}{\tau_d(Et_4N^+ \cdots MnCl_4^{-2})} = 2.98 \tag{98}$$

Let us now rewrite Eq. (92) in a convenient and simplified form ignoring the higher order terms

$$\frac{1}{T_2} = C\tau_d + \frac{C\tau_d}{1+\omega_0^2\tau_d^2} + \cdots \qquad (99)$$

where T_2^{-1} is the observed linewidth (gauss), C is a constant (gauss/sec), ω_0 is the Larmor angular frequency and τ_d is the translational correlation time (sec). Although the exact weighting of these two terms is not known, we can, at least, examine the frequency dependent resonance width behavior in a qualitative fashion by assuming reasonable values for molecular radii. As a first approximation we assign a reasonable τ_d for $[Et_4N^+ \cdots MnCl_4^{-2}]$ that gives rise to a small frequency effect (at K-band) through the frequency term in Eq. (99). A resonance width at X-band is then computed with the same relation. Using our ratio relation given in Eq. (98) we extract a τ_d for $[Bu_4N^+ \cdots MnBr_4^{-2}]$ and then calculate a set of resonance widths at two frequencies. Several sets of resonance widths have been computed in this way for various τ_d's and the results are summarized in Table XXI. It is evident in all cases that $T_{2X}^{-1} > T_{2K}^{-1}$ for translational correlation times in the 10^{-11} to 10^{-12} second range. Clearly the $(\omega_0\tau_d)^2$ term in Eq. (99) responds sharply to the magnitude of its components. At X and K-band frequencies, τ_d's $\geq 10^{-12}$ seconds make the denominator aware of the squared term. The ability to work at two frequencies also grants us a factor of sixteen in the

Table XXI. Theoretical Resonance Widths According to Dynamical Dipolar Model

	Complex (ion-paired) 0.039 M Mn^{+2};	$\tau_d \times 10^{12}$ (sec)	$C\tau_d$ (gauss)	K-band $\omega_0^2\tau_d^2$	K-band $\frac{C\tau_d}{1+\omega_0^2\tau_d^2}$ (gauss)	K-band T_{2K}^{-1} (gauss)	X-band $\omega_0^2\tau_d^2$	X-band $\frac{C\tau_d}{1+\omega_0^2\tau_d^2}$ (gauss)	X-band T_{2X}^{-1} (gauss)	$T_{2X}^{-1} - T_{2K}^{-1}$ (gauss)
1	$Et_4N^+ \cdots MnCl_4^{-2}$	1.04 (a)	5	0.0526	4.75	9.75	0.0039	4.98	9.98	0.2
2	$Bu_4N^+ \cdots MnBr_4^{-2}$	3.13 (c)	40	0.474	27.1	67.1	0.0349	38.6	78.6	11.5
3	$Et_4N^+ \cdots MnCl_4^{-2}$	1.52 (a)	5	0.111	4.5	9.5	0.0082	4.96	9.96	0.5
4	$Bu_4N^+ \cdots MnBr_4^{-2}$	4.55 (c)	40	1.0	20.0	60.0	0.0737	37.3	77.3	17.0
5	$Et_4N^+ \cdots MnCl_4^{-2}$	2.82 (a)	5	0.25	4.0	9.0	0.0182	4.93	9.93	0.9
6	$Bu_4N^+ \cdots MnBr_4^{-2}$	6.84 (c)	40	2.26	12.3	52.3	0.1660	34.3	74.3	22.0

(a) Assumed value; (c) Calculated value; T_{2K}^{-1} resonance width at K-band frequency; T_{2X}^{-1} resonance width at X-band frequency.

denominator and plays an important role in displaying the dynamical nature of dipolar interactions. Thus a barely perceptable frequency effect in $[Et_4N^+ \cdots MnCl_4^{-2}]$ resonance widths due to a judicious choice of τ_d predicts a strong effect in $[Bu_4N^+ \cdots MnBr_4^{-2}]$. For example, calculations in lines 1 through 4 in Table XXI closely parallel the experimental results, and consequently we have reason to assign a value of approximately 5×10^{-12} seconds for the translational correlation time.

The frequency dependent resonance widths appear to originate from the dipolar interactions as modulated by the relative motions of the paramagnetic anions. A temperature study of resonance widths should then reveal the usual predictable behavior expected of a diffusion controlled process. Moreover, we can test the relative importance of the $\omega_0 \tau_d$ term in Eq. (99) since it is also temperature dependent. In other words, we have two ways of changing $\omega_0 \tau_d$ at our disposal and we shall exploit them both in the following section to gain deeper insight on the dynamical nature of molecular interactions.

3.2 Temperature Dependence of Resonance Widths

If the dominant electron spin relaxation mechanisms are diffusion controlled processes, we may examine the temperature behavior of resonance widths according to a simple liquid model proposed by Frenkel (76). It is assumed, in this case, that the mean life, $\langle \tau \rangle$ of an atom or molecule in a definite equilibrium position approximates the correlation time, τ_d, for the diffusional process which, in turn, may be related to the self diffusion constant, D

$$\tau_d = \frac{\delta^2}{6D} \tag{100}$$

where δ represents the minimum interaction distance. Applying the well-known temperature dependent relation for the self diffusion coefficient

$$D = \frac{\delta^2}{6\tau_0} e^{-\frac{W}{kT}} \tag{101}$$

to the above equation we find

$$\tau_d = \tau_0 e^{\frac{W}{kT}} \tag{102}$$

where τ_0 is a constant representing the free vibrational period of the diffusing component about an equilibrium position in a quasi-lattice; W is the standard activation energy required for transport into an adjacent site; the other parameters have their usual meanings. In the limit of extreme narrowing ($\omega^2 \tau_d^2 \ll 1$) which should be more applicable to the X-band results, the resonance width is proportional to the diffusional correlation time and we may rewrite Eq. (102) to give the very familiar relation

$$\ell n \Delta H = \text{Const.} + \frac{W}{kT}. \tag{103}$$

In Figs. 38 and 39 we have plotted the log of ΔH vs. $10^3/T$ for two solutions containing the same concentration of excess bromide ion

FIGURE 38

$\ell n\ \Delta H$ vs. $10^3/T°K$ for solution containing 0.2 M $MnBr_4^{-2}$ and 0.15 M excess Bu_4NBr.

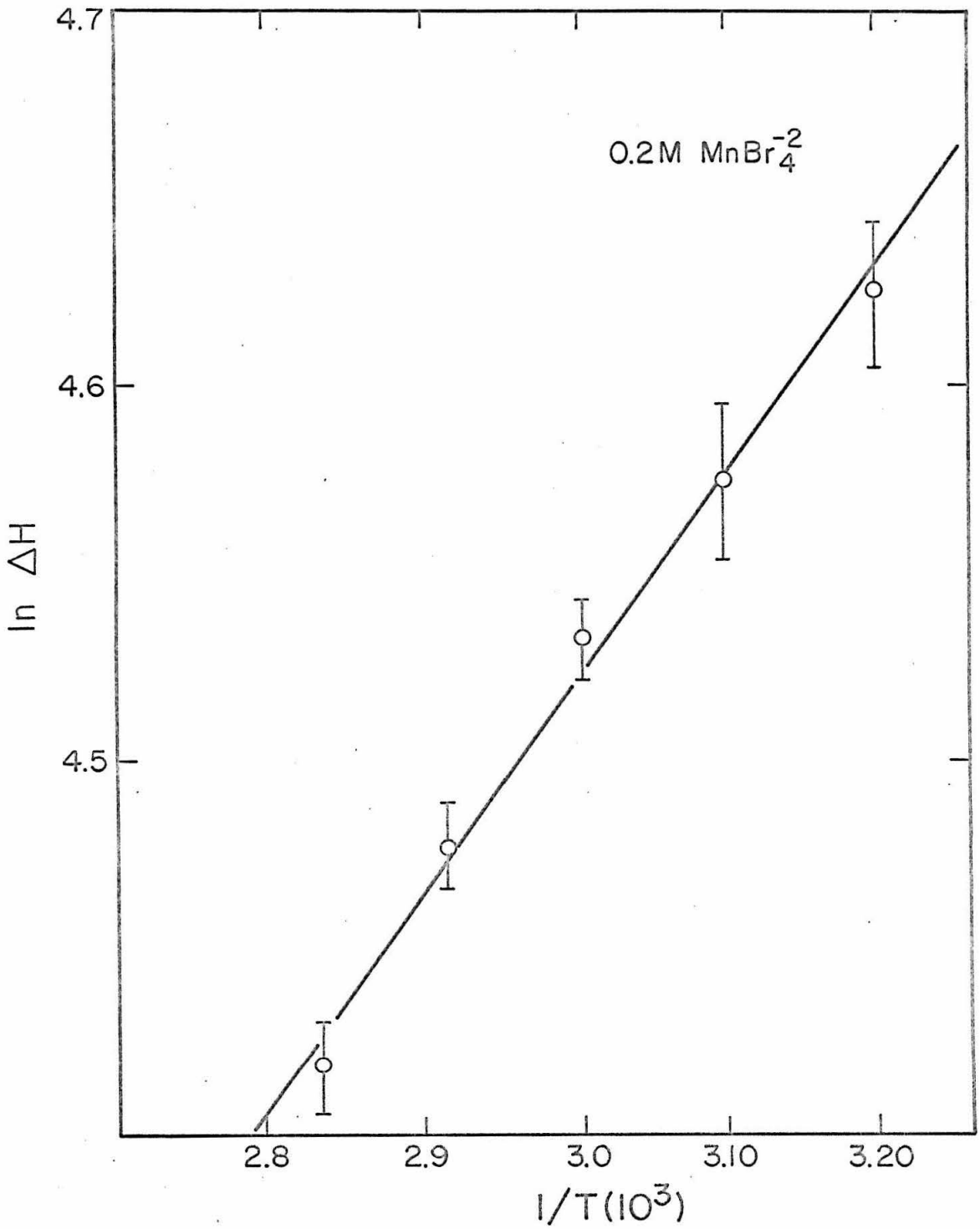
4.7
4.6
4.5
ln ΔH
0.2M $MnBr_4^{-2}$
2.8
2.9
3.0
3.10
3.20
1/T(10³)

FIGURE 39

$\ell n\ \Delta H$ vs. $10^3/T°K$ for solution containing 0.1 M $MnBr_4^{-2}$ and 0.15 M excess Bu_4NBr.

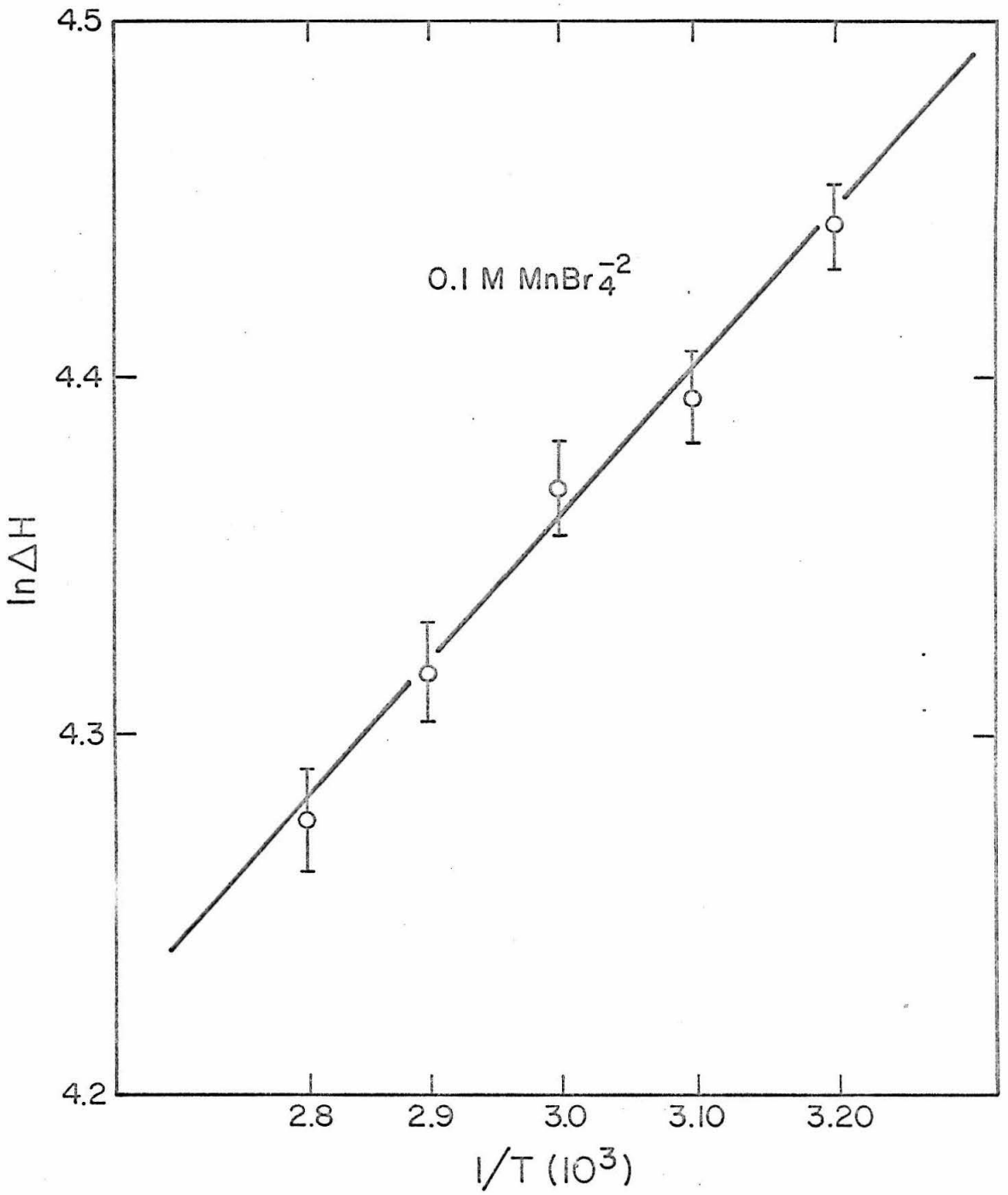
4.5
4.4
4.3
4.2
0.1 M $MnBr_4^{-2}$
ln ΔH
2.8
2.9
3.0
3.10
3.20
1/T (10^3)

but different concentrations of $MnBr_4^{-2}$. Excess bromide ion not only guarantees the state of the manganese but also provides an exchanging system exhibiting considerable line broadening. A linear relationship is observed in each case and the diffusional activation energies for 0.1 and 0.2 molar concentrations of $MnBr_4^{-2}$ are 5.0 and 6.4 kcal/mole, respectively, compared with 3 kcal/mole observed for water (17). As expected, the decrease in activation energy, W, probably reflects a decrease in viscosity, although it is conceivable that an admixture of dipolar and exchange relaxation could lead to the same effect.

To further illustrate the dynamical nature of the dipolar interactions we have plotted in Fig. 40 the X and K-band resonance widths as a function of temperature for a solution containing 0.039 M (0.05 M) $MnBr_4^{-2}$ and 0.150 excess M Bu_4NBr (68). As expected, resonance widths respond inversely to changes in temperature. The most significant feature of this experiment, however, is that the difference in X and K-band resonance widths diminishes with increasing temperature and practically vanishes at the highest temperature (73°C). From previous data we know that η/T typically decreases by a factor of three over this temperature interval. Accordingly, we expect the $\omega^2\tau_d^2$ term in Eq. (99) to reflect this change as a factor of nine. Hence, for K-band observations at the high temperature end (73°C), we expect this change to partially neutralize ω_k^2 so that once more the extreme narrowing case is realized, i.e., $\omega_k\tau_d < 1$. Referring, again, to Eq. (99) we note that change in τ_d ($\tau_d \propto \eta/T$)

FIGURE 40

X and K-band resonance widths, ΔH gauss, as a function of temperature. Solution contained 0.039 M $MnBr_4^{-2}$ and 0.150 M excess Bu_4NBr. Experimental work was performed by J. E. Crawford.

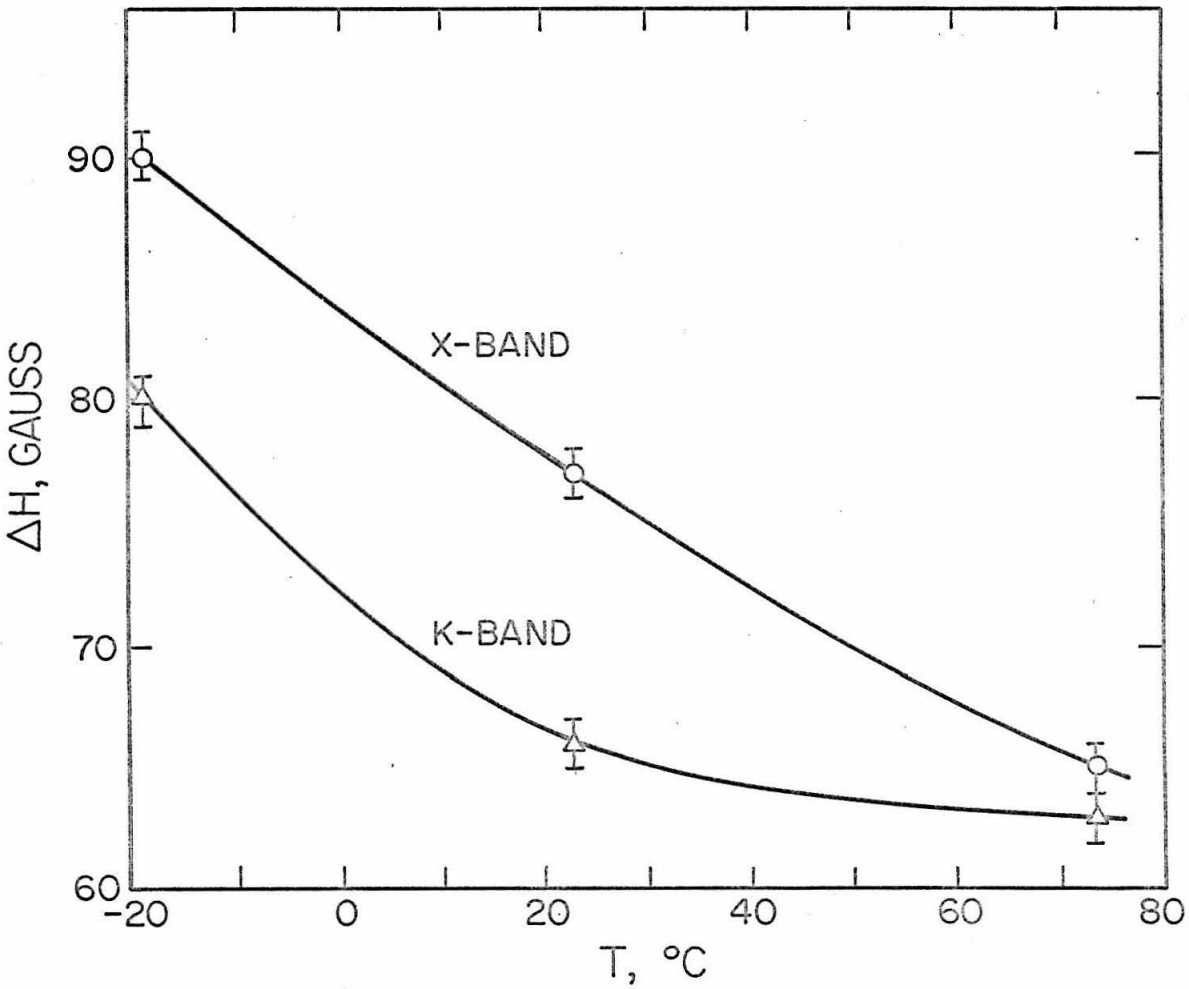
90
80
70
60
ΔH, GAUSS
X-BAND
K-BAND
-20
0
20
40
60
80
T, °C

imposed by adjusting temperatures elicits a particularly important effect at K-band frequencies due to the magnitude of $\omega_k^2\tau_d^2$. We predict that X and K-band resonance widths converge at higher temperatures and this was, indeed, borne-out experimentally as shown in Fig. 40. More precisely, at elevated temperatures

$$\frac{C\tau_d}{1+\omega_k^2\tau_d^2} \longrightarrow \frac{C\tau_d}{1+\omega_x^2\tau_d^2} \tag{104}$$

with

$$\frac{1+\omega_k^2\tau_d^2}{1+\omega_x^2\tau_d^2} \geq 1.$$

In conclusion, the results contribute very significantly to our arsenal of support for the dynamical model. We have demonstrated by two different approaches that the frequency dependent dipolar relation shown in Eq. (92) qualitatively accounts for the behavior of the $MnBr_4^{-2}$ system. In the wake of establishing dipolar relaxation as the dominating source of resonance broadening in this system, we were able to assign a translational correlation time for the diffusion process and deduce the activation energy associated with the molecular motion.

3.3 Formation of $MnBr_4^{-2}$ in Other Media. Counterion Effect.

An attempt to understand the anomolous resonance width of $MnBr_4^{-2}$ in acetonitrile prompted us to explore several new paths: (1) the possibility of forming this complex in solvents other than acetonitrile; (2) preparation of frozen $MnBr_4^{-2}$–CH_3CN solutions and (3) doping Mn^{+2} into crystal sites tetrahedral with respect to bromine. All these methods were aimed at preventing or, at least, altering solvent exchange with the complex.

In view of the well-known solvent capabilities of N, N-dimethylformamide, we felt this may provide a workable solvent for $MnBr_4^{-2}$. In fact, we demonstrated earlier that $MnCl_4^{-2}$ was indeed stable in this solvent in the presence of a variety of counterions. Unfortunately, Bu_4NBr-$MnBr_2$-DMF prepared under vacuum in a sealed tube did not produce a spectrum characteristic of a tetrahedral complex but rather of an ill-defined system perhaps containing a mixture of tetrahedral and octahedral complex. It is conceivable that the complex $Mn(DMF)_6^{+2}$ is much more stable than $MnBr_4^{-2}$ in DMF or perhaps the spectrum is excessively broadened through solvent exchange. At any rate the results were uninformative. Addition of excess LiBr to DMF containing $MnBr_2$ produced a spectrum consisting only of a single, broad line and consequently did not provide any information about solvent exchange.

Attempts to obtain spectra of $MnBr_4^{-2}$-CH_3CN frozen at low temperature by conventional techniques failed. However, a spectrum was obtained by very rapid freezing. This was performed by allowing

a single drop of solution to fall into a small, pointed cavity in a brass block maintained at 77°K. Under these circumstances heat exchange is very fast. The frozen drop was transferred under nitrogen into a cooled K-band capillary and then into the K-band cavity maintained near 77°K. The spectrum is shown in Fig. 41 and is typical of a "glassy" spectrum which is clearly a Mn^{+2} spectrum but has a hyperfine component $\langle A \rangle \approx -95$ gauss characteristic of an octahedral complex. Perhaps, as in the case of $MnCl_4^{-2}$-DMF, solvation energetics demand disproportionation of the complex into Bu_4NBr and $Mn(CH_3CN)_6^{+2}$. We also notice that the "forbidden" transitions at K-band frequencies occurring between the hyperfine components have been greatly attenuated as predicted by Eq. (79).

Tetramethylammonium bromide crystals doped with Mn^{+2} were grown from a 25 ml CH_3CN solution containing 0.0055 g $MnBr_2$ and 6.54 g Me_4NBr. An electron spin resonance spectrum characteristic of tetrahedrally coordinated Mn^{+2} was obtained with the following spin Hamiltonian constants: $\langle A \rangle = -81.5$ gauss and $\langle g \rangle = 2.0015$. The narrowest resonance widths were: $|-\frac{1}{2}, \frac{1}{2}\rangle \rightarrow |\frac{1}{2}, \frac{1}{2}\rangle$, 15.3 gauss; $|-\frac{1}{2}, -\frac{1}{2}\rangle \rightarrow |\frac{1}{2}, -\frac{1}{2}\rangle$, 10.9 gauss. Crystal spectra were not field orientation dependent and suggested that crystal field effects were very small. Unfortunately, it was not possible to repeat the experiment to investigate other parameters although many attempts were made. It has been said by some, who regard crystal growing as an art form rather than science, that such experiences are not uncommon. Although this isolated success appears to support our contention that

FIGURE 41

Electron spin resonance K-band spectrum of 0.039 M $MnBr_4^{-2}$ at ~77°K. H_o increases to the right. Scale: 1 cm = 40 gauss.

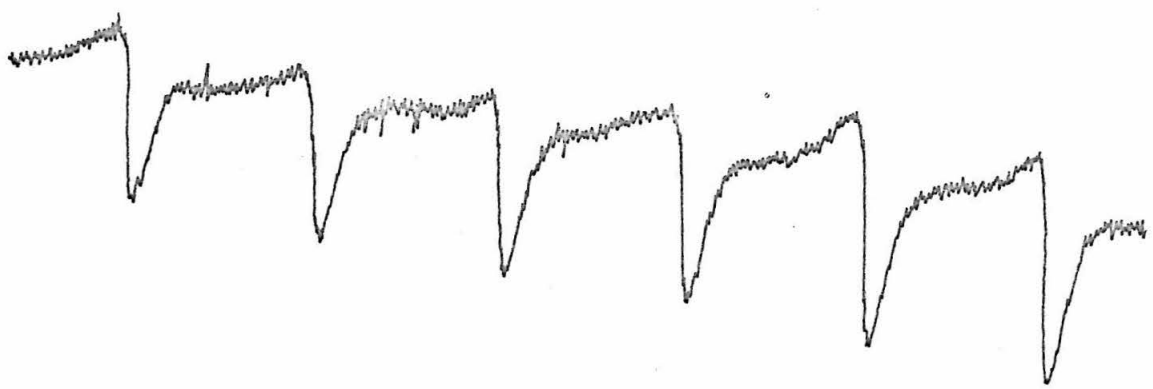

solvent exchange may contribute to the anomalous resonance broadening of $MnBr_4^{-2}$, we cannot actually extrapolate the results to reach this conclusion because the nature of forces in crystalline and liquid states are quite different.

Another source of line broadening, as discussed earlier, may stem from distortions imposed on $MnBr_4^{-2}$ by the counterion. We briefly explored this possibility by comparing resonance widths of the complex in the presence of several different counterions. Lithium bromide dissolves readily in acetonitrile and generates $MnBr_4^{-2}$ upon addition of $MnBr_2$. A solution containing 0.05 M $MnBr_4^{-2}$ plus 0.005 excess M LiBr gives an electron spin resonance spectrum virtually identical to the Bu_4NBr-$MnBr_4^{-2}$ system with the same spin Hamiltonian constants: $\langle A \rangle$ = -76 gauss; $\langle g \rangle$ = 2.007. Response of resonance width to stoichiometric $[Li \cdots MnBr_4]$ concentration is shown in Fig. 42 and bears a strong resemblance to the parallel study with Bu_4N^+ counterion illustrated in Fig. 27. J. E. Crawford (68) has extended the work to include a resonance width study as a function of excess LiBr and made the interesting discovery that excess LiBr does not effect the lines with the possible exception of a small viscosity broadening. We reach the conclusion, then, that the change in resonance width depicted in Fig. 42 results from the onset of an ion pair between $MnBr_4^{-2}$ and probably a "solvated" lithium ion. The excess bromide study suggests that LiBr may not be dissociated to any extent in the solvent and that ionic components are necessary for an exchange process. Further work (68) indicated that the counterions NH_4^+,

FIGURE 42

Resonance width as a function of stoichiometric $[Li^{+} \cdots MnBr_4^{-2}]$ concentration in acetonitrile.

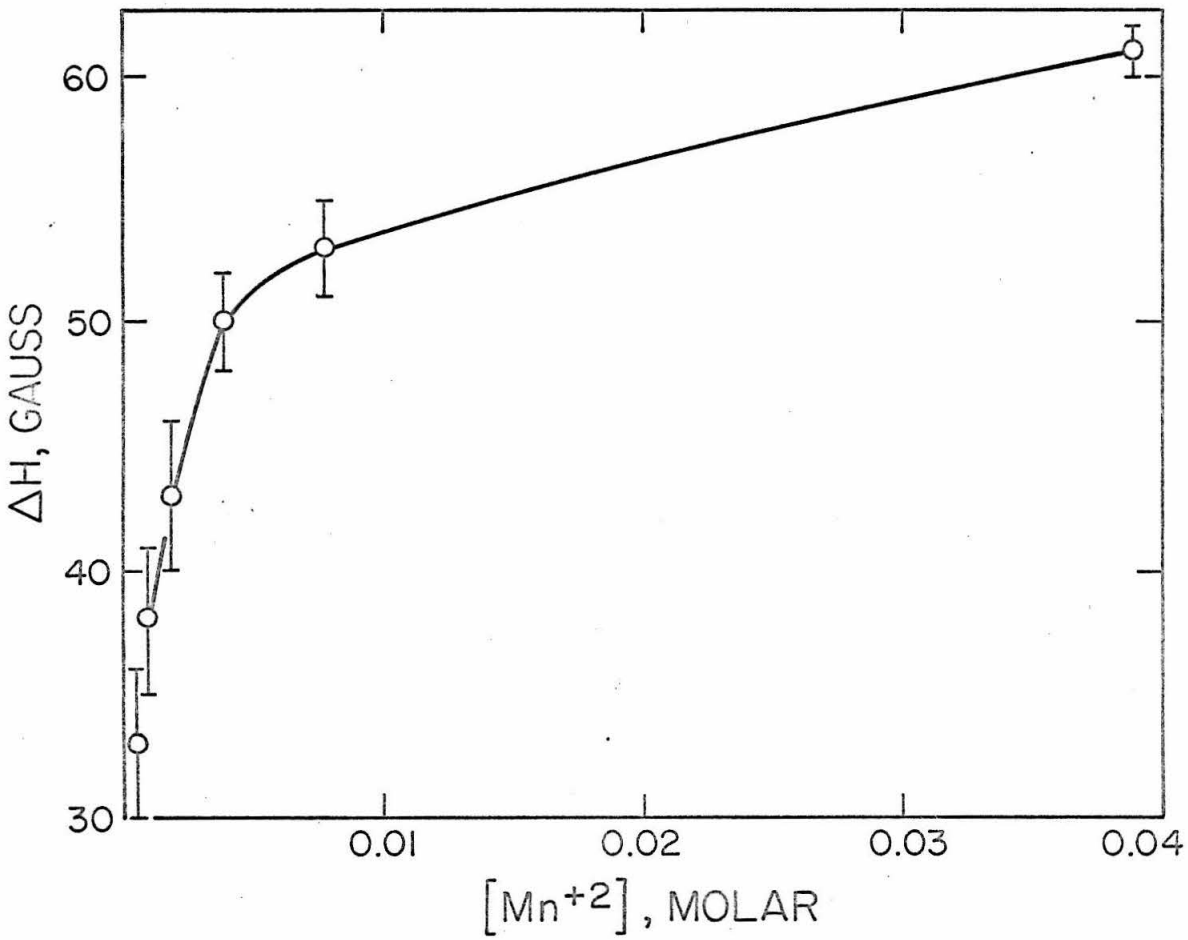
60
50
40
30
ΔH, GAUSS
0.01
0.02
0.03
0.04
[Mn+2], MOLAR

Me_4N^+, Et_4N^+ also did not substantially alter $MnBr_4^{-2}$ resonance widths. Finally, from these observations and appeal to chemical arguments, we draw the general conclusion that counterion interactions are not responsible for the broadening mechanisms assigned earlier to ligand exchange.

4. Conclusions

A study of electron spin relaxation of three manganese(II) complexes in acetonitrile has given us deeper insight on the structure and dynamical behavior of ionic complexes in liquids. We were able to utilize the $3d^5$ spin system of the manganese as a probe to investigate dynamical processes occurring on the nanosecond time scale. Information about the reaction kinetics of tetrahedral transition-metal complexes and other phenomena occurring at this time scale are, indeed, scarce.

The main effort centered around the unusual resonance broadening observed in the tetrahedral complex, $MnBr_4^{-2}$, imposed by experimental parameters. Parallel studies were conducted on the analogous tetrahedral chloride complex, $MnCl_4^{-2}$, and also the octahedral complex, $Mn(CH_3CN)_6^{+2}$. In all three cases, the ionic nature of the complex requires the presence of counterions which are naturally interwoven into the interpretation of the results.

The initial step, of course, was a careful re-evaluation of the effective spin Hamiltonian constants for all three complexes. For the system Et_4NCl-$MnCl_4^{-2}$ we found several relaxation mechanisms

leading to line broadening. One source appears to arise through spin-orbit interaction caused by modulation of the ligand field resulting from transient distortions of the complex imparted by solvent fluctuations in the immediate surroundings of the paramagnetic ion. An additional spin relaxation mechanism was assigned to the formation of ion-pairs. Although exact structural parameters for the loosely associated pairs are unavailable from spin relaxation measurements because of the stochastic nature of the system, we were, at least, able to tell qualitatively that the paramagnetic anion and its counterion are interacting at short range to produce electron spin relaxation. Moreover, we can define the experimental parameters leading to the apparent dynamical association and assign an equilibrium constant for the process.

The Bu_4NBr-$MnBr_4^{-2}$ study was considerably more interesting. As in the former case, solvent fluctuations and ion-pairing of the paramagnetic complex provide significant relaxation for the electronic spin system. Most interesting, without doubt, is the onset of a new relaxation mechanism leading to significant resonance broadening which is best interpreted as chemical exchange. Thus, assuming that resonance widths were simply governed by electron spin state lifetimes, we were able to extract dynamical information from an interaction in which the initial and final states are the same. The bimolecular rate constants were obtained at six different temperatures and their magnitudes suggested that the exchange is probably diffusion controlled with essentially a zero energy of activation. Further,

the entropy of activation suggests an associative S_N2 mechanism for the process in line with current theories proposing the existence of five-coordinate intermediates in reactions involving tetrahedrally coordinated complexes. An important feature of the spin-state lifetime approach is that the mathematical treatment does not require a transient reaction intermediate. On the other hand, regulation of spin-state lifetime requires the formation of a short-lived intermediate. Moreover the intermediate must have an entirely different electronic energy manifold to provide the required strong perturbation and efficient spin-flipping during exchange. If this is indeed the case we must conclude that chemical exchange causes spin-flipping and relaxation proceeds through spin-lattice interactions--a T_1 effect.

We can also arive at these same conclusions by invoking a two-state model including an intermediate activated complex whose short relaxation time prevents detection. Although we did not observe any additional broad spectra, this does not preclude its existence and, in fact, we cannot really distinguish between our two models. Fortunately, this is not a requisite for understanding the system since they both lead to the same relations for the bimolecular rate constant.

The most important source of spin relaxation in this system stems directly from dipolar interactions between the manganese $3d^5$ electrons. Moreover, the dipolar broadening is strongly frequency dependent indicating a deviation between the transverse and longitudinal relaxation times. We are then led to the conclusion that the $3d^5$ spin states of the ion-paired $MnBr_4^{-2}$ are significantly correlated so

that dynamical processes are also entering the picture.

Finally, we conclude that the $MnBr_4^{-2}$ complex consists of a loosely-knit ensemble of ions held together by weak electrostatic forces. The potential barrier for a negative ion forming an intermediate state is evidently quite low due to the electrostatic and stereochemical accessibility of the central positive manganese ion. By the same token, the leaving group can diffuse away with very little change in energy and consequently we have a sufficient condition for high ligand lability.

REFERENCES

(1) B. R. McGarvey, J. Phys. Chem. 60, 71 (1956); 61, 1232 (1957).

(2) H. M. McConnell, J. Chem. Phys. 25, 709 (1956); 24, 632, 764 (1956); 28, 1188 (1958).

(3) R. Kubo and K. Tomita, J. Phys. Soc. Japan 9, 888 (1954).

(4) D. Kivelson, J. Chem. Phys. 27, 1087 (1957); 33, 1094 (1960).

(5) J. W. H. Schreurs, G. E. Blomgren, and G. K. Fraenkel, J. Chem. Phys. 32, 1861 (1960).

(6) J. W. H. Schreurs and G. K. Fraenkel, J. Chem. Phys. 34, 756 (1961).

(7) J. P. Lord and G. E. Pake, Phys. Rev. 94, 579 (1954).

(8) M. J. Stephen and G. K. Fraenkel, J. Chem. Phys. 32, 1435 (1960).

(9) M. J. Stephen, J. Chem. Phys. 34, 484 (1961).

(10) Y. Ayant, J. Phys. Radium 16, 411 (1955).

(11) F. Bloch, Phys. Rev. 102, 104 (1956).

(12) A. G. Redfield, IBM J. Res. Develop. 1, 19 (1957).

(13) A. Abragam, The Principles of Nuclear Magnetism, Oxford University Press, London, 1961.

(14) J. H. Freed and G. K. Fraenkel, J. Chem. Phys. 39, 326 (1963); 41, 699, 3623 (1964).

(15) H. M. McConnell, Ann. Rev. Phys. Chem. 8, 105 (1957).

(16) H. M. McConnell, Proc. Natl. Acad. Sci. U.S. 43, 721 (1957).

(17) H. S. Jarrett, J. Chem. Phys. 25, 1289 (1956).

(18) P. Brovetto and S. Ferroni, Nuovo Cimento 5, 142 (1957).

(19) S. I. Weissman, J. Chem. Phys. 23, 890 (1956).

(20) R. Bersohn, J. Chem. Phys. 24, 1066 (1956).

(21) H. M. McConnell and D. B. Chesnut, J. Chem. Phys. 27, 984 (1957); 28, 107 (1958).

(22) H. M. McConnell and H. H. Dearman, J. Chem. Phys. 28, 51 (1958).

(23) A. Carrington and H. C. Longuet-Higgins, Mol. Phys. 5, 447 (1962).

(24) R. K. Wangsness and F. Bloch, Phys. Rev. 89, 728 (1955).

(25) A. D. McLachlan, Proc. Roy. Soc. A, 280, 271 (1964).

(26) A. Carrington and G. R. Luckhurst, Mol. Phys. 8, 125 (1964).

(27) J. D. Currin, Phys. Rev. 126, 1995 (1962).

(28) C. S. Johnson, Jr., Mol. Phys. 12, 25 (1967).

(29) J. H. Freed, J. Chem. Phys. 45, 3452 (1966).

(30) G. K. Fraenkel, J. Phys. Chem. 71, 139 (1967).

(31) W. Plachy and D. Kivelson, J. Chem. Phys. 47, 3312 (1967).

(32) A. Hudson and G. R. Luckhurst, Mol. Phys. 16, 395 (1969).

(33) R. N. Rodgers and G. E. Pake, J. Chem. Phys. 33, 1107 (1960).

(34) F. C. Adam and S. I. Weissman, J. Am. Chem. Soc. 80, 1518 (1958).

(35) E. deBoer, Rec. Trav. Chim. 84, 609 (1965).

(36) R. Catterall, M. C. R. Symons, and J. Tipping, J. Chem. Soc. 4342 (1966).

(37) P. W. Atkins, N. Keen, and M. C. R. Symons, J. Chem. Soc. 2873 (1962).

(38) N. Hirota and R. Krulick, J. Am. Chem. Soc. 88, 614 (1966)

(39) T. E. Gough and M. C. R. Symons, Trans. Faraday Soc. 62, 271 (1966).

(40) N. M. Atherton and S. I. Weissman, J. Am. Chem. Soc. 83, 1330 (1961).

(41) T. Kitagawa, T. Layloff, and R. N. Adams, Anal. Chem. 36, 925 (1964).

(42) N. Hirota and S. I. Weissman, J. Am. Chem. Soc. 86, 2537 (1964).

(43) R. L. Ward and S. I. Weissman, J. Am. Chem. Soc. 79, 2086 (1957).

(44) I. M. Brown, S. I. Weissman, and L. C. Snyder, J. Chem. Phys. 42, 1105 (1965).

(45) N. Hirota and S. I. Weissman, J. Am. Chem. Soc. 86, 2538 (1964).

(46) N. Hirota, J. Phys. Chem. 71, 127 (1967).

(47) R. G. Pearson and T. Buch, J. Chem. Phys. 36, 1277 (1962).

(48) M. Eigen, Z. physik. Chim. 1, 176 (1954).

(49) A. A. Frost and R. G. Pearson, Kinetics and Mechanism, J. Wiley and Sons, 2nd ed., New York, 1961, Chapter 11.

(50) M. Tinkham, R. Weinstein, and A. F. Kip, Phys. Rev. 84, 848 (1951).

(51) N. Bloembergen and L. O. Morgan, J. Chem. Phys. 34, 842 (1961).

(52) B. B. Garrett and L. O. Morgan, J. Chem. Phys. 44, 890 (1966).

(53) V. I. Avvakumov, N. S. Garif'yanov, B. M. Kozyrev, and P. G. Tishov, J. E. T. P. 37, 1110 (1960).

(54) R. G. Hayes and R. J. Meyers, J. Chem. Phys. 40, 877 (1964).

(55) S. I. Chan, B. M. Fung, and H. Lütje, J. Chem. Phys. 47, 2121 (1967).

(56) B. Bleaney and D. J. E. Ingram, Proc. Roy. Soc. 205A, 336 (1951).

(57) T. P. P. Hall, W. Hayes and F. I. B. Williams, Proc. Phys. Soc. 78, 883 (1961).

(58) A. Abragam, Phys. Rev. 79, 534 (1950).

(59) A. Abragam, J. Horowitz and M. H. L. Pryce, Proc. Roy. Soc. (London), A230, 169 (1955).

(60) V. Heine, Phys. Rev. 107, 1002 (1957); J. H. Wood and G. W. Pratt, Jr., Phys. Rev. 107, 995 (1957); R. E. Watson and A. J. Freeman, Phys. Rev. 120, 1134 (1960); A. J. Freeman and R. E. Watson, Phys. Rev. 123, 2027 (1961).

(61) O. Matamura and R. S. Title, Phys. Rev. 130, 17 (1963).

(62) G. E. Pake, Paramagnetic Resonance, W. A. Benjamin, Inc., New York, 1962, Chapter 5.

(63) F. Bloch, Phys. Rev. 70, 460 (1946).

(64) C. P. Slichter, Principles of Magnetic Resonance, Harper and Row, New York, Evanston, and London, 1963, Chapter 5.

(65) C. J. Gorter, Paramagnetic Relaxation, Elsevier Publ. Co., Inc., 1947, pp. 127.

(66) N. Bloembergen, E. M. Purcell and R. V. Pound, Phys. Rev. 73, 679 (1948).

(67) H. M. McConnell, J. Chem. Phys. 28, 430 (1958).

(68) J. E. Crawford, private communcation.

(69) C. C. Hinckley and L. O. Morgan, J. Phys. Chem. 44, 898 (1966).

(70) B. T. Allen and D. W. Nebert, J. Chem. Phys. 41, 1983 (1964).

(71) J. E. Crawford determined η and ρ.

(72) D. F. Evans, C. Zawoyski and R. L. Kay, J. Phys. Chem. 69, 3878 (1965).

(73) P. J. Zandstra and S. I. Weissman, J. Am. Chem. Soc. 84, 4408 (1962).

(74) L. S. Singer and M. C. Haun, Bull. Am. Phys. Soc. 7, 200 (1962).

(75) L. Yarmus, M. Kukk and B. R. Sundheim, J. Chem. Phys. 40, 33 (1964); T. B. Swanson, J. Chem. Phys. 45, 179 (1966).

(76) J. Frenkel, Kinetic Theory of Liquids, Dover Publications, Inc., New York, 1952.

PART II

I. INTRODUCTION

The electron spin relaxation study described in Part I provided us with considerable insight about the unique dynamical nature of the paramagnetic anion, $MnBr_4^{-2}$. As in any scientific endeavor, one specific technique most certainly will have limitations and it is always desirable to examine the problem from another point of view. Wide line nuclear magnetic resonance provides this other view and it is particularly amenable to the problem since both bromine isotopes (^{79}Br and ^{81}Br) have observable resonances and should provide additional information about the complex. Therefore we turn the problem inside-out and now focus attention on the bromide ion whose nuclear spin is being shared in the same unique system.

Nuclear magnetic resonance techniques have given us a powerful means for studying molecular rate processes in gases, liquids and solids. Of particular interest to the chemist are the dynamical processes occurring in solution such as intramolecular rotations and exchange via chemical reaction. Dynamical effects manifest themselves in both resonance line shifts and line widths and, accordingly, require detailed analyses to extract the desired information. Sometimes the analysis is complicated and not very definitive presenting us only with a hazy picture about the molecular rate process. More often it provides precise rate constants and activation energies for chemical processes that could not be obtained by any other method.

Chemical exchange can be described by a nuclear spin residing in several different sites where it has different Larmor frequencies. These sites may be in different states in the same molecule such as

tautomers, conformers, cis-trans isomers and so on. In chemical reactions intermolecular sites may include intermediate transition states in addition to the initial and final states. When the exchange frequency is smaller than the nuclear magnetic resonance line separations, the spectrum consists of distinct lines corresponding to the number of available sites. In the rapid exchange limit, the nuclear spin feels only an average environment and a single line is observed. Of course, an exchange process can proceed somewhere between these two well-defined limits and naturally the spectrum becomes more complicated.

A quantitative description of an exchanging system can be handled with a suitable modification of the phenomenological Bloch equations (1) and, historically speaking, Gutowsky, McCall and Slichter (2) were the first to use this approach on a chemical system. Subsequently, McConnell (3) reduced the treatment to almost trivial algebraic operations and this has since served as a theoretical framework generally adaptable to many types of conditions and systems. The method, however, suffers from the lack of quantum mechanical rigor and although its general application has been justified on the grounds of success, discretion must be exercised in extending it to quantum mechanical problems. A more sophisticated quantitative treatment was developed utilizing the density matrix which deals directly with the quantum mechanical problem and is simply a variation of time-dependent perturbation theory. A more general treatment of this approach followed from the ideas of Wangsness and Bloch (4, 5) who proposed that for a complete description of spin motion one must consider the rate

of change of both the diagonal and off-diagonal elements of the density matrix. These ideas were further generalized and placed in a more elegant mathematical format by Fano (6). Redfield (7) recast the conventional theories of time proportional transition probabilities into a more useful form in which relaxation of a system by its thermal environment can be expressed in terms of a linear matrix operator. By using this technique complicated problems can be handled with ease, and both longitudinal and transverse relaxation terms in addition to the Bloch equations unfold in a very natural fashion.

An enormous number of exchange studies have been performed by nuclear magnetic resonance techniques since the original work of Gutowsky, Slichter and McCall. Most of the work, however, has been restricted to spin-half ($I = \frac{1}{2}$) nuclei, and within this group the proton has been, by far, the leading subject for dynamical studies for obvious reasons. In contrast, similar studies on systems containing nuclei with $I > \frac{1}{2}$ are relatively scarce and this is unfortunate because most elements belong to this class. Clearly more information on this subject would lead to new insight on chemical systems. Nuclei with $I > \frac{1}{2}$ possess quadrupole moments which can interact strongly with field gradients from external sources and provide a powerful relaxation mechanism leading to line broadening. The extent of quadrupole relaxation varies greatly from one nuclei to another and, although onset of an additional relaxation mechanism could conceivably complicate matters, in many cases it dominates the linewidth and actually simplifies the treatment.

There are important properties of $I > \frac{1}{2}$ nuclei that lend them-

selves beautifully to dynamical and structural problems in chemical systems. For example, quadrupole nuclei placed in a cubic environment such as a tetrahedral or octahedral complex experience near zero electric field gradients and the ensuing resonance lines are relatively sharp depending, of course, on other sources of relaxation. However, when the cubic symmetry is degraded, a field gradient appears at the nucleus, interacts with the quadrupole and causes line broadening. The extent of the field gradient depends also on the nature of bonding involved in the partnership. Covalent bonding with the nucleus generates enormous electric field gradients and causes rapid relaxation through the quadrupole mechanism leading to extreme line broadening. On the other hand, ionic-bound nuclei usually experience much smaller field gradients due to symmetrical electron shielding and correspondingly tend to have narrower lines. This tendency has been demonstrated from a ^{35}Cl and ^{37}Cl magnetic resonance study of simple chlorine compounds traversing from covalent CCl_4 to the more ionic CH_3Cl (8). Apparently, then, information on the nature of bonding can be gleaned from a line shape analysis. As can be seen, these properties of quadrupole nuclei provide a way to examine some of the more elusive and esoteric structural and dynamical features of molecules and complexed ions in solution. Certainly, these topics are of great interest and importance to liquid structure, reactions in solution and, perhaps most interesting, the role of ionic phenomena in biological systems. Unfortunately, few workers have taken advantage of quadrupole nuclei properties and the field in general has been overshadowed by the more glamorous proton magnetic resonance. Nevertheless, a number of

important experiments have been performed to illustrate the general utility of wide-line spectroscopy. A cross-section of examples relevant to our work are included in the following paragraphs.

In a series of papers Wertz (9) and Jardetzsky (10-13) studied the nuclear magnetic resonance of sodium ion in aqueous solution. Line broadening was observed for numerous weakly complexing anions such as phosphates, hydroxy and keto acids or alcohols. These effects were thought to arise from interaction between quadrupole and electric field gradients imposed by the slightly asymmetric environment about the sodium ion. Although the magnitude of linewidths indicated that they were almost certainly modulation-broadened and thus obscuring a great deal of information, the potential application of this technique to chemical and biological systems was quite evident.

Wide line nuclear magnetic resonance techniques have also been applied to the task of determining ionic solvation structure (coordination numbers) in non-aqueous, aqueous and mixed medias. Recently, Hon (14) studied the $LiCl-AlCl_3-CH_3CN$ system in which two ^{27}Al resonances were clearly evident. Addition of LiCl led to increased intensity of one line while the other vanished. Both lines were quite narrow reflecting the absence of a quadrupole-field gradient interaction and suggested the aluminum site symmetry was tetragonal or greater. From stoichiometry it was concluded the two species were $Al(CH_3CH)_6^{+3}$ and $AlCl_4^-$.

The very clever work of Baldeschwieler and coworkers (15) has demonstrated wide-line nuclear magnetic resonance of halide ions such as ^{35}Cl ($I = 3/2$) may serve as a valuable probe for investigating

the gross physical characteristics and specific reactivities of large biological molecules in solution. An extension of this work by Bryant (16) reports an observation of the well-substantiated helix-coil transition in synthetic poly-l-glutamate using ^{35}Cl resonance. The glutamate was labeled with -SHgCl and exchange occurred with Cl^- ions in solution. In fact it was possible to monitor extremely small quantities (10^{-3} M) of the macromolecule in the presence of 2 M aqueous NaCl. A plot of linewidth vs pH indicated a width of 90 Hz at low pH corresponding to the coiled configuration, and a sharp transition at pH ~ 7 to 75 Hz in the random phase reflecting that the ^{35}Cl probe lives in two covalent states with different field gradients. When the ^{35}Cl atom is covalently bound, the magnitude of e^2qQ is quite large compared to the free $^{35}Cl^-$ ion. Hence the resulting linewidths depend on the spin mole fractions of the sites, the values of e^2qQ and τ_c at each site and, of course, the rate of spin exchange. Further studies were performed on hemoglobin and again demonstrated the utility of the ^{35}Cl probe in biological sites at low concentration with the rapid spin exchange process functioning as a "chemical amplifier."

There are indeed very few examples of kinetic information derived from wide-line nuclear magnetic resonance spectroscopy. Several pertinent cases will be stated here in the following paragraphs.

Hertz (17) actually deserves the credit for inventing the halogen probe or so-called "chemical amplifier" mentioned by Baldeschwieler and coworkers (15) in his original and important contribution to the application of wide-line spectroscopy to problems in chemical dynamics. From the nuclear magnetic resonance linewidths of ^{81}Br, ^{79}Br and ^{127}I,

reaction rates were determined for rapid exchange of the type

$$MeX_{i-1} + X^- \underset{k_{2i}}{\overset{k_{1i}}{\rightleftharpoons}} MeX_i^- \qquad (i = 1 \rightarrow 4)$$

in aqueous solution where Me represents a metal and X the complexing halogen ligand (17). The substances investigated were: $CdBr_2$, $HgBr_2$, $ZnBr_2$, CdI_2 and ZnI_2 which form a full range of complexed ions up to MeX_4^{-2}. Addition of small quantities ($\sim 10^{-3}$ M) of the above substances generated very pronounced line broadening in the resonance of Br^- and I^- in solutions of the completely dissociated electrolytes (KBr and KI). Reported rate constants were $k_{14} = 1.2 \times 10^7$, 4.6×10^8 and 1.4×10^9 (together), 8×10^7, $\geq 1.5 \times 10^8$ and $\leq 7 \times 10^8$ (together), and 7×10^6 mole ℓ^{-1} sec^{-1} for the forward reaction and $k_{24} = 6.0 \times 10^6$, 2.5×10^7, 2.0×10^7, 1.5×10^7 and 3×10^7 sec^{-1} for the back reaction corresponding to the complexes: $CdBr_4^{-2}$, $HgBr_4^{-2}$, $ZnBr_4^{-2}$, CdI_4^{-2} and ZnI_4^{-2}, respectively.

Solvation exchange rates between bulk solution and the first coordination sphere of hydrated paramagnetic ions Mn^{+2}, Fe^{+2}, Co^{+2}, Ni^{+2} and Cu^{+2} were determined from the nuclear magnetic relaxation studies of ^{17}O in water (18). Temperature dependence of linewidths was required to extract rate constants and various mechanisms controlling the relaxation. Rate constants, k_1 (sec^{-1} at 298°C) on the order of $3 - 4.0 \times 10^7$ were obtained with a corresponding activation energy of ~8 kcal.

Exchange of water (^{17}O) and chloride ions between the bulk solvent and the first coordination sphere of ferric-chloro complexes

has been the subject of several wide-line nuclear magnetic resonance studies (19, 20). Zeltmann and Morgan (21) extended the work to include complexes formed in concentrated aqueous hydrochloric acid. The linewidth was controlled by chemical exchange of H_2O or Cl^- at low HCl concentration, presumably containing the lower chloro-complexes, and dominated by relaxation rates at higher concentrations in which $FeCl_4^-$ was present. At intermediate HCl concentrations several chloro-complexes were present and both mechanisms were operative in determining the linewidth. Riding on assumptions regarding the stoichiometry and distribution of halogenated complexes, they were able to estimate the Cl^- exchange rate constant for $FeCl_4^-$, $k_{Cl} = 1.17 \times 10^5$ ℓ mole^{-1}sec^{-1} at 26°C, and determine the nuclear spin-electron spin coupling constant, $A/\hbar = 7.0 \times 10^7$ radians/sec or 1.1×10^7 radians/sec depending on whether the spin exchange correlation time was identified with ligand residence time or the electronic longitudinal relaxation time, T_1, respectively.

In Part II we study nuclear magnetic relaxation of bromide ions in the $MnBr_4^{-2}$–Bu_4NBr–CH_3CN system. Essentially, we monitor the ^{79}Br and ^{81}Br linewidths in response to the $[MnBr_4^{-2}]/[Br^-]$ ratio with the express purpose of supporting our contention that exchange is occurring between "free" bromide ions in the solvent and bromine in the first coordination sphere of the paramagnetic anion. The problem is complicated by possibly several dynamical processes in addition to the presence of a paramagnetic component. Consequently, the study is divided into two separate parts dealing, first, with Bu_4NBr–CH_3CN and then with the system $MnBr_4^{-2}$–Bu_4NBr–CH_3CN. As a prelude to the

detailed experimental description, we discuss several important mechanisms leading to nuclear spin relaxation anticipated in these systems.

II. THEORY

1. Correlation Times

There is a body of evidence that shows the Debye model for correlation time does not apply to small molecules such as CH_4 (22, 23). It has further been demonstrated that relaxation times of spherical or nearly spherical molecules are much less dependent on viscosity than nonsymmetrical molecules which require displacement of their neighbors in order to rotate. Cole (24) has tied these results together into a straightforward theory which proposed that when rotational reorientation is very rapid or when the rotational friction coefficient is small the correlation time becomes independent of the macroscopic viscosity, η, and assumes a particularly simple form

$$\tau \cong \left(\frac{I}{kT}\right)^{\frac{1}{2}} \qquad (1)$$

where I is the moment of inertia. The theory appears to apply well to gases and some non-viscous liquids such as CH_4 in which case molecules can rotate with a definite angular momenta. Consequently, this is referred to as the "inertial" limit for rotational correlation times.

By contrast, when molecules are trapped in specific potential-wells they can be treated as spheres in a viscous medium by simple hydrodynamic arguments according to Debye. If experimental results agree with this model so that the molecular states are well characterized in terms of orientation with respect to a laboratory coordinate system, we then say that correlation times are in the "Debye" limit.

1.1 Rotational Correlation Time in the Debye Limit

As mentioned in Part I the autocorrelation function of $\mathcal{H}_1$, the Hamiltonian representing the interaction giving rise to relaxation, has the general form

$$G_{mk}(\tau) = \overline{\langle m|\mathcal{H}_1(t)|k\rangle \langle k|\mathcal{H}_1(t+\tau)|m\rangle} \qquad (2)$$

with m and k as eigenstates of the stationary Hamiltonian. As usual, to evaluate this quantity we must have some information regarding the time dependence of the relaxation-producing interactions. The autocorrelation function can be written

$$\overline{\langle m|\mathcal{H}_1(0)|k\rangle \langle k|\mathcal{H}_1(\tau)|m\rangle} = \overline{\langle m|\mathcal{H}(0)|k\rangle}^2 \cdot e^{-|t|/\tau_c} \qquad (3)$$

and the exponential factor, $\exp -|t|/\tau_c$, is a natural consequence of the standard diffusion equation. It should be mentioned that there are several theoretical approaches leading to this exponential factor as discussed in Part I. The solution leads to

$$\tau_c = \frac{8\pi a^3 \eta}{\ell(\ell+1)kT} \qquad (4)$$

where ℓ represents rank of the interaction tensor. In magnetic resonance the interactions involve second rank tensors which are spherical harmonics of the second order and the expression above takes the usual form

$$\tau_c = \frac{4\pi a^3 \eta}{3kT} \qquad (5)$$

1.2 Translational Correlation Time in the Debye Limit

In the case of translational diffusion, the Stokes relation for the self diffusion coefficient, D, is given by

$$D = \frac{kT}{6\pi a\eta} \tag{6}$$

and is valid for a rigid sphere in a viscous medium according to the Debye model. Translational encounter times are then assumed to be the same as translational correlation times and are given by the relation

$$\tau_d = \frac{2a^2}{D} \tag{7}$$

and combination with the last expression yields

$$\tau_d = \frac{12\pi a^3 \eta}{kT} \tag{8}$$

The relation between rotational and translational correlation time is

$$\tau_d = 9\tau_c \tag{9}$$

and we notice that translational correlation times can persist almost an order of magnitude longer than rotational correlation times.

In view of all the theoretical uncertainties at the molecular level, the numerical factors associated with the correlation times may bear little meaning. More significant, perhaps, is the η/T dependence found experimentally for T_1^{-1} in many cases. On the contrary, for the bromides and iodides of Cs^+, Rb^+ and K^+, the viscosity dependence on

concentration demonstrates a minimum which is not reflected in T_2^{-1} linewidth measurements thus giving a non-linear plot against η/T (25, 26). It is clear that the disparity between the "inertial" and Debye limits as well as the observed experimental discrepancies in relating macroscopic variables to the correlation times prompts us to apply such theories with discretion.

2. Quadrupole Relaxation

Abragam and Pound (27) developed a theory of line broadening for nuclei of spin I in a liquid where relaxation results from fluctuating electric quadrupole interactions. The Hamiltonian representing the electric quadrupole energy of a rotating molecule having spin I with the field applied along the z-axis written in the molecular coordinate system is given by

$$\hbar\mathcal{H} = \frac{eQ}{4I(2I-1)}\left(\frac{\partial^2 V}{\partial z^2}\right)\left\{A^{(0)} + \frac{\eta}{\sqrt{6}}\left(A^{(2)} + A^{(-2)}\right)\right\} \qquad (10)$$

where the appropriate spin operators are

$$A^0(I) = 3I_Z^2 - I(I+1)$$

$$A^{(\pm 1)}(I) = \tfrac{1}{2}\sqrt{6}\,(I_Z I_\pm + I_\pm I_Z)$$

$$A^{(\pm 2)}(I) = \tfrac{1}{2}\sqrt{6}\,I_\pm^2$$

An asymmetry parameter, η, is defined as

$$\eta = \frac{\partial^2 V/\partial x^2 - \partial^2 V/\partial y^2}{\partial^2 V/\partial z^2}$$

and the components V_{xx}, V_{yy} and V_{zz} are simply the field gradients along the respective coordinate axes. We see that $0 \leq \eta \leq 1$ and in the case at hand, $\eta = 0$. In the limit of extreme narrowing ($\omega\tau_c \ll 1$) the linewidth due to quadrupole relaxation in liquids through molecular reorientation can be written

$$\frac{1}{T_1} = \frac{3}{40} \cdot \frac{2I+3}{I^2(2I-1)} \left(1 + \frac{\eta^2}{3}\right) \left(\frac{eQ}{\hbar} \frac{\partial^2 V}{\partial z^2}\right)^2 \tau_c \qquad (11)$$

Rearranged in a more convenient form with $\eta = 0$ we have

$$\frac{1}{T_1} = \left(\frac{3}{40}\right) \frac{[4I(I+1) - 3]}{I^2(2I-1)^2} \tau_c \left(\frac{eQ}{\hbar}\right)^2 \left\langle \left(\frac{\partial^2 V}{\partial z^2}\right) \right\rangle_{av}^2 \qquad (12)$$

where $q^2 \equiv \langle (\partial^2 V/\partial z^2)^2 \rangle_{av}$ is the mean square field gradient; eqQ is the nuclear quadrupole coupling constant and τ_c, as usual, is the correlation time for the interactions giving rise to the variation in the field gradient. In turn, the coupling constant, eqQ, is proportional to the average radial distribution of the electron

$$eqQ = eQ \frac{\ell+1}{2\ell-1} \frac{2\ell}{2\ell+3} \langle r^{-3} \rangle_{av} R' \qquad (13)$$

where r is distance from the nucleus and $\langle r^{-3} \rangle_{av}$ is the average of r^{-3} over the electron's radial wave function, ℓ is the usual orbital electron angular momentum and R′ is a relativistic factor discussed by Das and Hahn (28).

To examine the effect of symmetry on the field gradient, we perform the usual multipole expansion. The classical electrostatic interaction energy between the nucleus and its electron cloud charge

distribution may be written as

$$E = \int \rho_n(r_n)\, V(r_n)\, dr_n \tag{14}$$

where ρ_n is the charge distribution at the nucleus and r is the radial distance from the nucleus. With the origin defined at the nucleus, we expand the potential at the nucleus, V(r), in a Taylors series

$$V(r) = V(0) + \sum x_j \left(\frac{\partial V}{\partial x_j}\right)_0 + \frac{1}{2!} \sum_{j,k} x_j x_k \left(\frac{\partial^2 V}{\partial x_j \partial x_k}\right)_0 + \tag{15}$$

Substitution of Eq. (15) into Eq. (14) gives the interaction energy in the desired expanded form

$$E = V(0) \int \rho_n(r_n)\, dr_n + \sum_j \left(\frac{\partial V}{\partial x_j}\right)_0 \int \rho_n(r_n) x_j dr_n$$

$$+ \frac{1}{2!} \sum_{j,k} \left(\frac{\partial^2 V}{\partial x_j \partial x_k}\right)_0 \int \rho_n x_j x_k dr_n \tag{16}$$

The third term on the right is defined as the quadrupole term. Since the potential principal axis system can always be adjusted we can locate the condition where

$$\left(\frac{\partial^2 V}{\partial x_j \partial x_k}\right) = 0 \qquad (j \neq k) \tag{17}$$

Laplace's equation must satisfy the potential, V,

$$\nabla^2 V(r) = 0 \tag{18}$$

and evaluation at the origin, i. e., $\nabla^2 V(0) = 0$, provides the useful relation

$$\sum_j \left(\frac{\partial^2 V}{\partial x_j \partial x_j}\right) = \sum_j \left(\frac{\partial^2 V}{\partial x_j^2}\right) = 0 \qquad (19)$$

Evidently, then, for cases of cubic and spherical symmetry it follows from Laplace's equation that

$$\left(\frac{\partial^2 V}{\partial x^2}\right) = \left(\frac{\partial^2 V}{\partial y^2}\right) = \left(\frac{\partial^2 V}{\partial z^2}\right) = 0 \qquad (20)$$

This emphasizes again the important impact imposed by structure, or short range environment, on the linewidth for spin $I > \frac{1}{2}$ nuclei according to Eq. (12) above.

The nature of chemical bonding to the quadrupole nuclei also influences the field gradient according to the qualitative relation presented in Eq. (13), thereby leading to changes in linewidths. Covalent bonding permits the existence of large field gradients at the nucleus usually leading to extreme line broadening according to Eq. (12). As a bond becomes less covalent and more ionic through some form of external interaction or chemical subsitution, the field gradient diminishes and resonance linewidths correspondingly decrease. In a purely ionic state the field gradients imposed by external sources are usually small in the absence of dipole-dipole and strong solvent-dipole interactions, and this is reflected by relatively narrow resonance lines.

3. Nuclear Spin Relaxation in the Presence of Paramagnetism

The effect of paramagnetism on nuclear magnetic resonance linewidths and chemical shifts in exchanging systems has been the subject of numerous investigations (29-36). Paramagnetic ions

typically have larger magnetic moments than nuclear moments and consequently, the interaction energy $\mu_p\mu_d/r^3$ is about three orders of magnitude larger than μ_d^2/r^3 where μ_p and μ_d are the paramagnetic and diamagnetic moments. In order to treat the problem at hand, the dipolar spin-spin interaction and spin-exchange interaction must both be considered. The Hamiltonians representing these interactions are:

$$\mathcal{H}_1 = -\left(\frac{\hbar^2\gamma_I\gamma_S}{r^3}\right)\left[3(\vec{I}\cdot\vec{r})(\vec{S}\cdot\vec{r}) - \vec{I}\cdot\vec{S}\right] \tag{21}$$

$$\mathcal{H}_2 = A\vec{I}\cdot\vec{S} \tag{22}$$

For isotopic molecules, a chemical shift is frequently observed and may be represented by (32)

$$\frac{\Delta\nu}{\nu} = \frac{4}{9}\, I(I+1)S(S+1)\frac{\gamma_\ell}{\gamma_N}\frac{A}{kT} \tag{23}$$

where I is the nuclear spin of the diamagnetic ion and S is the electron spin of the paramagnetic ion; γ_N and γ_ℓ are the corresponding gyromagnetic ratios; A is the isotropic (scalar) hyperfine coupling constant.

In addition to chemical shifts, line broadening is also anticipated and the magnitude depends partially on the residence time of the exchanging spins. According to Bernheim et al. (34) the linewidths due to transverse and longitudinal relaxation can be written

$$\frac{1}{T_1} = \frac{4}{30}\cdot\frac{S(S+1)\gamma_{N(I)}^2 g^2\beta^2 p}{r^6}\left[3\tau_c + \frac{7\tau_c}{1+\omega_S^2\tau_c^2}\right] \tag{24}$$

and

$$\frac{1}{T_2} = \frac{1}{3} \frac{S(S+1)A^2}{\hbar^2} \tau_\ell \qquad (25)$$

These relations, of course, pertain to protons with $I = \frac{1}{2}$; p is proportional to ionic concentration, A is the scalar hyperfine coupling constant, τ_c is the correlation time for the dipolar interaction, τ_ℓ is the correlation time for the exchange interaction, and the other symbols bear their usual meaning. In the present situation we may estimate line broadening for the more general case to include nuclei with $I > \frac{1}{2}$

$$\frac{1}{T_2} = \frac{4}{9} I(I+1) S(S+1) \left(\frac{A}{\hbar}\right)^2 \tau_{\ell x} \qquad (26)$$

where $\tau_{\ell x}$ is the spin exchange correlation time. Finally, it is evident that the presence of paramagnetic components in solution must be carefully addressed in the process of unraveling the relaxation mechanisms effecting linewidths in exchanging systems.

4. Ion-Ion and Solvent-Ion Relaxation

Interactions responsible for nuclear magnetic resonance line broadening in halide ion solutions have been the subject of several studies (25, 37-41). However, the interpretations regarding the source of broadening have not been consistent but at least have suggested that ion-solvent and, in some cases, ion-ion interactions are important. A detailed study by L. Lin (40) on the nuclear magnetic resonance of alkali halide solutions brings out the features leading to relaxation rather clearly. Linewidth studies of ^{81}Br and ^{127}I ions in the presence

of varying concentrations of foreign cations derived from LiCl, $NaClO_4$ and $MgCl_2$ indicate negligible ion-ion interactions due to field gradient alterations and demonstrates a correlation time, τ_c, effect in accordance with Eq. (12). In agreement with Richards (25) and others (26) cesium ions were found to contribute to line broadening through changes in both correlation time and field gradient (ion-ion) interactions. Several models have been proposed for ionic structure in a solvent but, in view of current affairs, the ion-complex model brought forth by Iwamasa (42) appears to be most compatible with experimental results. The complex-ion model was further supported by examining the halide linewidths in the presence of mixed solvents displaying rather wide ranges of dipole moments. If the solvent molecules could move about the halide ion at short range in random fashion, linewidth would then be proportional to the dipole moment squared. Experimental results neatly disposed of this possibility and provided additional testimony in favor of the complex-ion theory. In mixed solvents, then, line broadening apparently results from the replacement of a solvating molecule in the first coordination sphere by a non-equivalent molecule that creates a resultant large average mean field gradient at the nucleus under study as modified by an appropriate correlation time. This effect will have a particularly important bearing on the work to be described in the experimental section.

5. Exchange Effects

As previously stated, exchange phenomena have a profound influence on nuclear magnetic resonance linewidths depending on many factors such as number and separation of exchange sites, relative

concentrations, temperature and correlation times. In the slow exchange limit broadening results from restriction of the nuclear spin-state lifetimes and, in transit, the commuting spin loses all phase coherence between exchange sites. Naturally, the linewidths corresponding to the various sites may be quite different depending, of course, on the intrinsic spin-state relaxation time in the site. Slow exchange is, by far, the most useful situation with respect to gaining quantitative kinetic information and the general relationships connecting linewidths and rate constants are available through the Bloch equations modified for chemical exchange (3) as described earlier in Part I of this thesis.

An appropriate calculation similar to our treatment in Part I was provided by Swift and Connick (18) who have further generalized McConnell's treatment to include three exchanging components and the experimental half-width at half-height to give

$$T_2^{-1} = T_{2a}^{-1} + \sum_{j=b}^{c} \frac{\frac{1}{T_{2j}^2} + \frac{1}{T_{2j}\tau_{ja}} + \Delta\omega_j^2}{\left(\frac{1}{T_{2j}} + \frac{1}{\tau_{ja}}\right)^2 + \Delta\omega_j^2} \qquad (27)$$

However, this relation is only valid under rather specialized concentration conditions, i. e., [a] $\gg$ [b] or [c]. Components are defined as follows:

T_{2a} = transverse relaxation time in state a

τ_{aj} = lifetime in state aj

T_{2j} = transverse relaxation time in state j

τ_{ja} = lifetime in state ja

$\Delta\omega_j$ = difference between the resonance frequency for j and the observed frequency in the mixed system

The slow exchange result modified for convenience with the problem at hand may be represented in the general form

$$\frac{1}{T_2} = \frac{1}{T_{2A}} + \sum_j R X_j N_j \left(\frac{1}{\tau_j + T_{2j}} \right) \tag{28}$$

where T_{2A} = intrinsic relaxation time of the diamagnetic ion

R = mole ratio of paramagnetic to diamagnetion ion

X_j = mole fraction of paramagnetic component j

N_j = coordination number of exchanging ion in paramagnetic component j

τ_j = correlation or residence time of diamagnetic ion in paramagnetic site j

T_{2j} = relaxation time of diamagnetic ion in paramagnetic component j

If the residence time τ_j of the diamagnetic ion in the paramagnetic component j far exceeds its relaxation time ($\tau_j \gg T_{2j}$), we then anticipate chemical exchange controlled linewidths leading to the usual expression

$$\frac{1}{T_2} = \frac{1}{T_{2A}} + \frac{1}{\tau} \tag{29}$$

for a two-state system with negligible paramagnetic interactions.

In the rapid exchange limit, the frequency of interaction exceeds the difference in Larmor frequencies of the various sites and the

exchanging spin experiences an average environment without loss of phase coherence. As a result the lines coalesce into a single line whose position and width are governed by the relative mole fractions, the positions and intrinsic linewidths of the non-exchanging components. The well-known rapid exchange expressions for line positions and widths are

$$\frac{1}{T_2} = \sum_i X_i T_{2i}^{-1}$$

$$\omega = \sum_i X_i \omega_i \qquad (30)$$

where $\frac{1}{T_2}$ = observed linewidth

X_i = mole fraction of component i

T_{2i} = relaxation time of component i

ω = observed angular Larmor frequency

ω_i = angular Larmor frequency of component i

In the intermediate exchange region, however, the quantitative treatment has its most complex form and the full expression for the relaxation time according to Eq. (66) Part I must be used.

Finally, analysis of ^{81}Br and ^{79}Br ion nuclear magnetic resonance linewidths in the presence of the paramagnetic anion, $MnBr_4^{-2}$, requires the consideration of all the aforementioned relaxation mechanisms. Linewidths arising from the individual mechanisms entwined with their correlation times act in parallel to define the overall linewidths, T_2^{-1}. As a result, it is left as a challenge for experiment to discover and assign the mechanisms responsible for line broadening. It should be possible, in favorable cases, to gain

information about the molecular rate process as a further dividend and secure deeper insight into the nature of chemical reactions. The remainder of the thesis is devoted to this task.

III. EXPERIMENTAL

1. Synthesis of $MnBr_4^{-2}$ Complex

The chemistry involved in the preparation of the $MnBr_4^{-2}$ complex in acetonitrile was described previously in Part I, but success in obtaining useful wide-line resonance results rests critically on a more demanding procedure than before and, consequently, shall be covered in considerable detail.

Hydrated manganous bromide and tetra n-butylammonium bromide were obtained from Inorganic Chemicals Co. and the Eastman Kodak Co., respectively. Dehydration and purification procedure was described in Part I in the experimental section and the products were stored in teflon stoppered flasks kept in a vacuum desiccator. From time to time the entire purification procedure was repeated to insure the absence of carbonates and perhaps oxybromides accumulated by frequent, although brief, exposures to air during sample weighing and handling. At first, preparation of $MnBr_4^{-2}$ solutions included brief exposure of all components to air. However, the ^{81}Br resonance linewidths were from 2000 Hz to unobservable and in all cases, the results were not reproducible. A vacuum technique was then introduced in which the reacting salts could be redried after weighing, the solution degassed by the standard freeze-thaw procedure and the sample tubes sealed-off under vacuum. Again the results were not satisfactory. Finally, it was discovered that the solvent, acetonitrile, had to be "super-dried" and never exposed to air in addition to other precautions. After a large investment in time and experimentation, a successful procedure was developed and is now presented in detail: (1) Dehydrated

$MnBr_2$ and Bu_4NBr were weighed into a 1.5 (O.D.) × 15 cm degassed pyrex tube precalibrated with a marker for 5.0 mℓ volume. It was attached through a 14/35 T joint to a high vacuum line. Under constant pumping, the salts were heated and the evolved gases were monitored continuously with the Veeco vacuum gauge. Initially, the pressure rose to around 200 μ followed by a sudden and dramatic decrease indicating complete dehydration of the salts. Heating was continued well after "zero pressure" was attained and was then extended to the glass above the salts as well. Upon cooling, the tube was isolated from the vacuum line by a stopcock; (2) About 10 grams of P_2O_5 was added to a 50 mℓ round-bottom flask fitted with a standard joint to accommodate the vacuum line. A teflon-coated stirring bar was attached internally to the neck of the flask just below the joint by a powerful horseshoe magnet taped externally to the flask. The flask was attached to the vacuum line, pumped carefully and the P_2O_5 was heated rather strongly with a oxy-gas torch until sublimation was evident and degassing as observed on the Veeco vacuum gauge had ceased. After cooling, the externally positioned magnet was removed allowing the stirring bar to drop into the dehydrated and degassed P_2O_5. Approximately 30-35 mℓ of spectroscopic grade CH_3CN was then distilled under vacuum onto the P_2O_5 maintained at -196°C. On returning to ambient temperature the P_2O_5/CH_3CN was thoroughly agitated with the stirring bar from an external motor; this was repeated prior to every solution preparation. In addition, the CH_3CN was degassed by the usual freeze-pump-melt cycle. If this is not done, transport under vacuum becomes impeded by traces of out-gassed material; (3) Super-dry CH_3CN is then distilled

onto the salts by cryogenic pumping and the correct volume is obtained by patiently manipulating the pumping, warming and solvation until the liquid level coincides with the 5.0 mℓ fiducial mark. At this point, the solution is refrozen to -196°C and the tube is separated from the vacuum line at a thickened seal-off area.

The role of sample preparation is critical to the success of this exchange study and cannot be overemphasized. For example, a typical solution carefully prepared by the above routine was measured before and after a brief (about one minute) exposure to air followed quickly by transfer to a new tube, freezing, degassing and encapsulation. The ^{81}Br nuclear magnetic resonance linewidth more than doubled after this brief exposure. Previous experience with acetonitrile following purification procedures indicated that water content was no greater than 10^{-4} M on brief exposures to air (typically longer than one minute) during the course of a Karl-Fischer analysis (43). This emphasizes the devastating effect imposed by water on the results. Although the exact water concentration in unknown, it is probably well below the level attainable by conventional "wet" analytical techniques ($\sim 10^{-4}$ M). At any rate, the solvent cannot be dehydrated more efficiently by any currently known method.

2. Instrumentation

The bromine resonances were recorded with a Varian V 4311 fixed-frequency (6.53 M Hz) transmitter-receiver and V 4331A probe. Receiver output was coupled to a Princeton Applied Laboratory Model HR-8 precision lock-in amplifier whose reference channel was driven by a Varian V 4250A sinusoidal sweep generator and amplifier

providing modulation to the sample. The HR-8 operates essentially as a phase sensitive detector tunable from 1.5 Hz to 150 k Hz with an exceedingly narrow equivalent noise bandwith. A signal 59 dB below ambient white noise in a 1 k Hz bandwidth centered around the signal frequency can be recovered with a signal-to-noise ratio of one. In typical experiments the V 4311 receiver was operated at very low gain to take advantage of the HR-8 high S/N characteristics.

A Varian flux-stabilized V 4013A twelve-inch electromagnet driven by a V 2100A regulated power supply was used in all experimental work. Field scans were made with a Varian V 3507 slow sweep unit. Spectra were calibrated frequently with a standard sideband technique provided by an audio signal generator and a Hewlett Packard 5245 L counter. Spectra were presented as derivatives of the absorption mode. The nuclear properties of bromine are presented in Table I along with the field requirements for the experimental work.

Solutions were sealed under vacuum in cylindrical tubes with a 1.5 cm O.D. and 1.3 cm I.D.; spinning was not required and spectra were recorded at 26 ± 1°C. R.F. power, modulation frequency and amplitude were optimized to avoid anomolous broadening through saturation, side band components or modulation. Typically, 20 Hz field modulation plus the 0.1 modulation field attenuator was required for the narrowest resonance lines and 80 Hz without attenuation for the widest lines. R.F. power attenuation was needed only for the narrowest lines. Time constants and scan rates were also carefully adjusted for optimum resolution and signal-to-noise ratios. The estimations of errors in linewidth measurements are included in all subsequent figures. Since the relatively large linewidths precluded

Table I. Nuclear Properties of Bromine and Experimental Field Requirements

Isotope	Natural abundance %	Magnetic moment μ (in multiples of $e\hbar/2Mc$)	Nuclear spin I (in multiples of $\hbar$)	Electric quadrupole moment Q (in multiples of $e \times 10^{-24} cm^2$)	Approx. field required for $\nu = 6.53$ M Hz (gauss)
^{79}Br	50.57	2.0991	3/2	0.34	6122
^{81}Br	49.43	2.2626	3/2	0.28	5679

the use of an internal reference standard, it was necessary to guarantee zero field drift prior to chemical shift experiments which were always conducted in a consecutive manner.

3. Viscosity and Density Measurements

Viscosity was measured in a standardized Ostwald viscometer suspended in a temperature bath regulated at 26 ± 1°C.

4. Attempted Variable Temperature Experiments

Construction of the Varian V 4331A probe precludes the use of a standard Varian variable-temperature dewar. A heat exchanging device must enter and leave through the hole at the top of the probe provided for sample tubes. Under our demanding experimental requirements, the heat exchanging element must also be contained under vacuum along with the sample. Hence, we built a doubled-walled vacuum jacketed heat exchanging device somewhat like the unit described by Swift and Connick (18). In our version, however, the upper structure contained a side arm in which the required intricate chemistry could be performed under vacuum. Decantation then delivered the solution into the sample area. Solution temperature was adjusted by a stream of nitrogen from the Varian temperature controller. Unfortunately, due to severe noise problems, even with tuned phase-sensitive detection, a signal could not be recorded with this device. Another attempt was made to control the temperature of the entire probe (ambient to 50°C) with a stream of nitrogen entering around the sample through an external tube injected concentrically into the probe. Thermal equilibrium was unattainable at any temperature even after two hours and, further, it was impossible to tune the probe paddles at 50°C.

IV. RESULTS AND DISCUSSION

The experimental work suffers from two major limitations which severely restrict the range of parameters that can be studied and these are: (1) the modest solubility of the paramagnetic complex $(Bu_4N^+)_2\ MnBr_4^{-2}$ in acetonitrile amounting to 0.4 – 0.5 molar concentration at 25°C and (2) the lower limit of bromide ion (symmetrically solvated or "free" ion) detection which is about 0.1 molar concentration. Although these limitations cannot easily be overcome, it is frequently advantageous to operate at low concentrations in order to minimize line broadening induced by dipolar interactions. Consequently, we are faced with striking a compromise between all of these factors and the bromine resonance signal-to-noise ratio.

The anhydrous exchanging system involves several equilibria that conceivably can contribute to bromine linewidth and the two leading candidates are

$$Bu_4N^+ \cdots MnBr_4^{-2} + Br^- \rightleftharpoons Bu_4N^+ \cdots MnBr_4^{-2} + Br^- \text{ (exchange)} \qquad (31)$$

and

$$Bu_4NBr \rightleftharpoons Bu_4N^+ + Br^- \text{ (dissociation-association)} \qquad (32)$$

Linewidth contributions arising through solvation interactions such as

$$MnBr_4^{-2} + CH_3CN \rightleftharpoons Mn(CH_3CN)Br_3^- + Br^- \qquad (33)$$

are attenuated by adjusting concentrations so that $[Br]/[Mn] > 4$ according to previous results discussed in Part I.

As the problem unfolds, it is evident there are at least three sites in which bromine nuclei can reside and before this complicated

system can be adequately analyzed, we must investigate the nature of Bu_4NBr/CH_3CN line broadening in the absence of the paramagnetic complex. Since bromine linewidth contribution from Bu_4NBr/CH_3CN is relatively large, it will obviously be important to understand the dynamical properties of the dissociation and the mechanism leading to broadening.

1. Bromine Linewidth Study of Tetrabutylammonium Bromide in Acetonitrile

A set of experiments was designed to investigate the response of ^{79}Br and ^{81}Br linewidths to changes in the Bu_4NBr concentration and the results are summarized in Table II. We have also considered the possibility that activities of the components in solution may influence the results and have included a new distribution of mole fractions in Table III to provide a comparison. Measurements were conducted at 27°C and the concentrations encompass the viscosity range anticipated in subsequent experiments containing the paramagnetic anion. A single, non-shifting resonance line possessing Lorentzian character was observed throughout the concentration range under study. Linewidth and concentration increase together but the linewidth relationship with η/T depicted in Figure 1 is clearly non-linear and the ^{79}Br and ^{81}Br curves are almost parallel. Evidently a single state for the bromide ion and a simple rotational diffusional correlation time, $\tau_c = 4\pi a^3\eta/3kT$, for modulation or frequency spectrum of the nuclear quadrupole--solvent dipole interaction does not present an accurate model for relaxation. An attractive candidate, then, is a two-state, rapid-exchange picture

Table II. Effect of concentration on ^{81}Br and ^{79}Br linewidths in the anhydrous Bu_4NBr/CH_3CN system.

Solution	Molar Conc. Bu_4NBr	Distribution of Components in Mole Fractions, K_d=0.5		Viscosity η(c.p.)	$\frac{\eta(10^3)}{T°K}$	Linewidth (Hz) ± 20 Hz	
		$X_A(Br^-)$	$X_B(Bu_4NBr)$			$^{81}T_2^{-1}$	$^{79}T_2^{-1}$
1	0.098	0.856	0.144	0.367	1.226	131	
2	0.204	0.763	0.237	0.403	1.343	204	277
3	0.397	0.657	0.343	0.485	1.617	260	363
4	0.697	0.561	0.439	0.710	2.367	349	467
5	0.815	0.534	0.466	0.807	2.690	384	504

Table III. Effect of activities on ^{81}Br and ^{79}Br linewidths in the anhydrous Bu_4NBr/CH_3CN system.

Solution	Molar Conc. Bu_4NBr	Distribution of Components in Mole Fractions of Total Br^-		Viscosity η(c. p.)	$\frac{\eta(10^3)}{T}$	Linewidth (Hz) ± 20 Hz	
		X_A	X_B			$^{81}T_2^{-1}$	$^{79}T_2^{-1}$
1	0.098	0.926	0.074	0.367	1.226	131	
2	0.204	0.881	0.119	0.403	1.343	204	277
3	0.397	0.821	0.179	0.485	1.617	260	363
4	0.697	0.753	0.247	0.710	2.367	349	467
5	0.815	0.731	0.269	0.807	2.690	384	504

The mole fraction distribution has been compensated for partial association and ionic activities using an extended Debye-Hückel theory that accounts for the finite sizes of ions. Accordingly, the corrected dissociation constant, K_d', becomes $K_d' = K_d/\gamma_\pm^2$ where $\gamma_\pm$ is the mean activity coefficient and $K_d = 0.5/25°C$. X_A = mole fraction of $[Br^-]$ and X_B = mole fraction of $[Br_4NBr]$.

FIGURE 1

Nuclear magnetic resonance study of Bu_4NBr in anhydrous CH_3CN conducted at 300°K. ^{79}Br and ^{81}Br nuclear magnetic resonance linewidths (Hz) are plotted against $\eta(10^3)/T$.

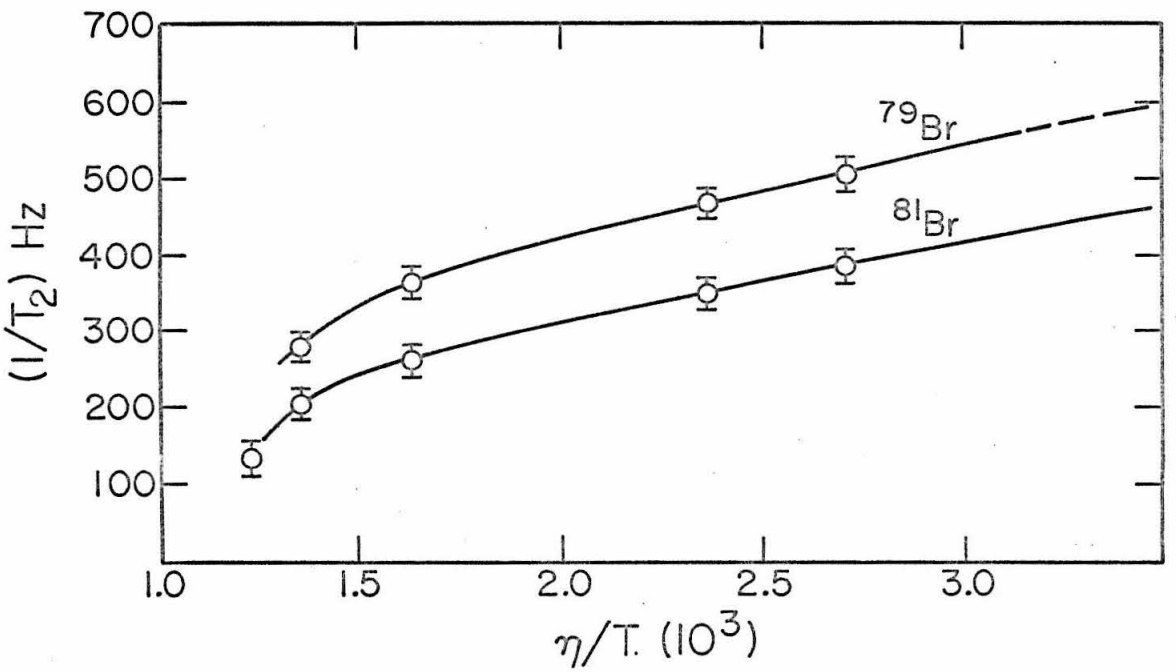
700
600
500
400
300
200
100
(1/T2) Hz
79Br
81Br
1.0
1.5
2.0
2.5
3.0
η/T. (10^3)

$$\underset{\text{state B}}{Bu_4N^+ \cdots Br^-} \underset{k_2}{\overset{k_1}{\rightleftharpoons}} \underset{\text{state A}}{Bu_4N^+ + Br^-} \qquad (34)$$

and to treat this case we rewrite Eq. (12) in a rapid exchange framework assuming, as usual, $\tau_c = 4\pi a^3 \eta / 3kT$

$$\frac{1}{T_2} = \frac{2\pi}{15k}\left(\frac{eQ}{\hbar}\right)^2 \left[a_A^3 q_A^2 + (a_B^3 q_B^2 - a_A^3 q_A^2) X_B\right] \frac{\eta}{T} \qquad (35)$$

where a_A = bromine radius in state A

q_A = bromine field gradient in state A

a_B = bromine radius in state B

q_B = bromine field gradient in state B

and the other terms have their usual significance. In Figure 2, it is seen that the expected linear relationship between a "viscosity-normalized" linewidth, $(T_2\eta)^{-1}$, and X_B, the mole fraction in state B does not materialize, but instead, generates a curve with a maximum $(T_2\eta)^{-1}$. It is seen that the activity compensated results have the same general appearance except for a reduced Bu_4NBr (X_B) mole fraction range. The results cast serious doubt on the foregoing model although, for the moment, it seems more reasonable to accept the rapidly exchanging two-state picture and pin the blame on the correlation time. Without further indulgence into the frailties of rotational correlation time as applied at the molecular level, let us suppose that in a rapidly exchanging system the lifetime of bromine nuclei in state A and B is sufficiently short to modulate the quadrupole interaction energy. If cooperative interactions due to rotation and lifetime are coupled, the

FIGURE 2

Nuclear magnetic resonance study of Bu_4NBr in anhydrous CH_3CN conducted at 300°K. Viscosity normalized a) ^{79}Br and b) ^{81}Br nuclear magnetic resonance linewidths (Hz deg/poise) are plotted against the mole fraction, X_B, of Bu_4NBr.

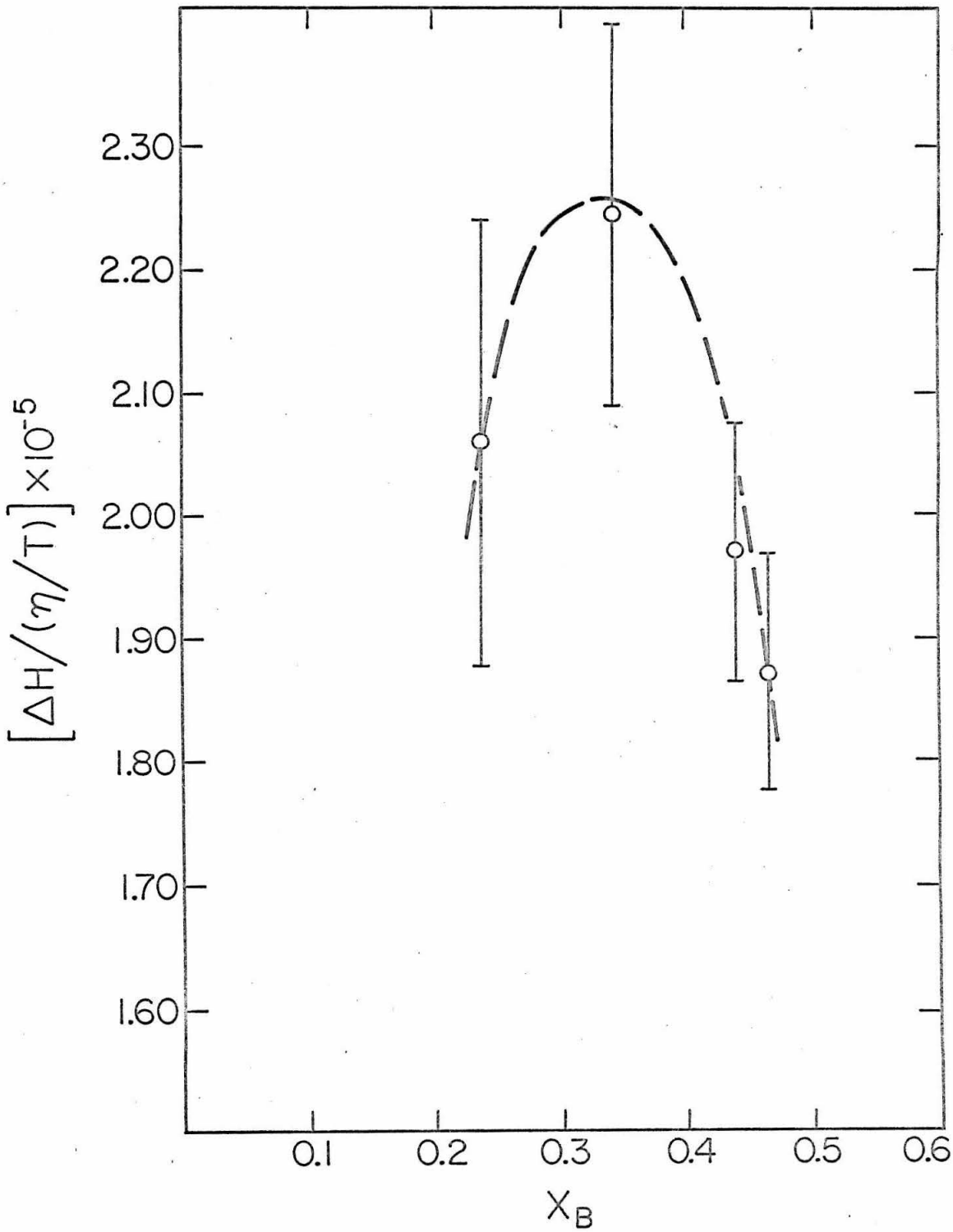
2.30
2.20
2.10
2.00
1.90
1.80
1.70
1.60
$[\Delta H/(\eta/T)] \times 10^{-5}$
0.1
0.2
0.3
0.4
0.5
0.6
X_B

(a)

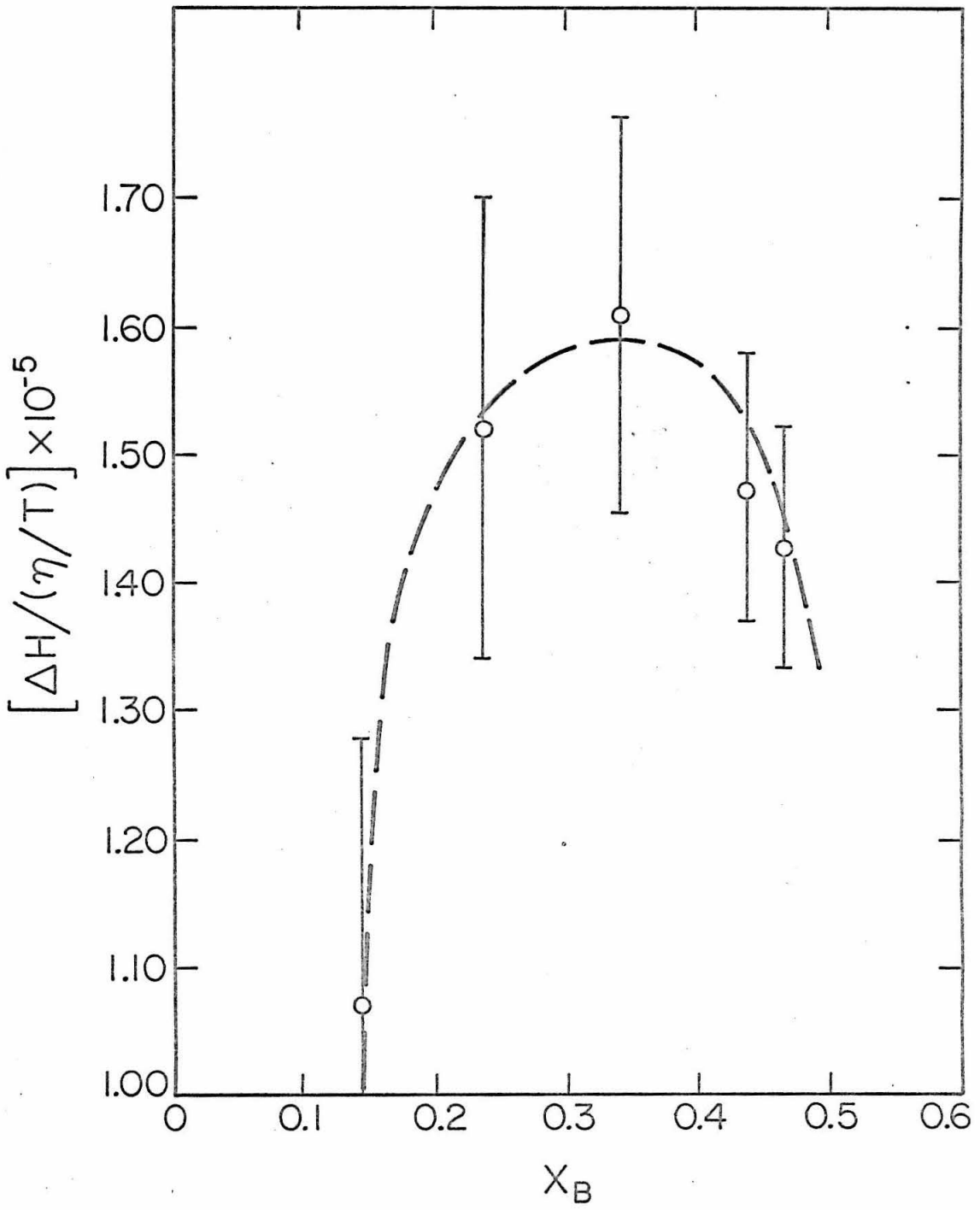
1.70
1.60
1.50
1.40
1.30
1.20
1.10
1.00
$[\Delta H/(\eta/T)] \times 10^{-5}$
0
0.1
0.2
0.3
0.4
0.5
0.6
X_B

(b)

FIGURE 2

Nuclear magnetic resonance study of Bu_4NBr in anhydrous CH_3CN conducted at 300°K. Viscosity normalized c) ^{79}Br and d) ^{81}Br nuclear magnetic resonance linewidths (Hz deg/poise) are plotted against mole fraction, X_B, of Bu_4NBr compensated for activities.

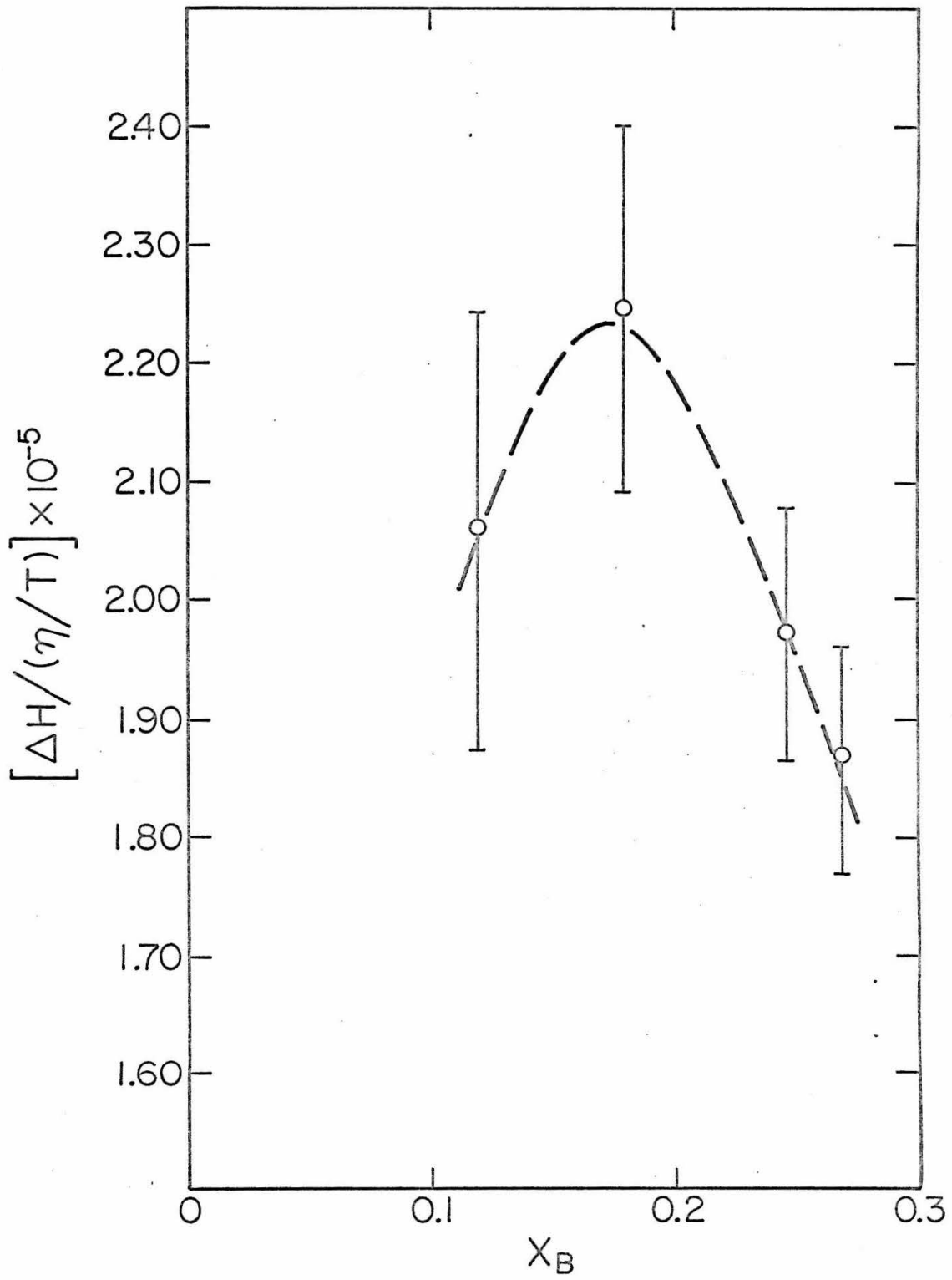
2.40
2.30
2.20
2.10
2.00
1.90
1.80
1.70
1.60
$[\Delta H/(\eta/T)] \times 10^{-5}$
0
0.1
0.2
0.3
X_B

(c)

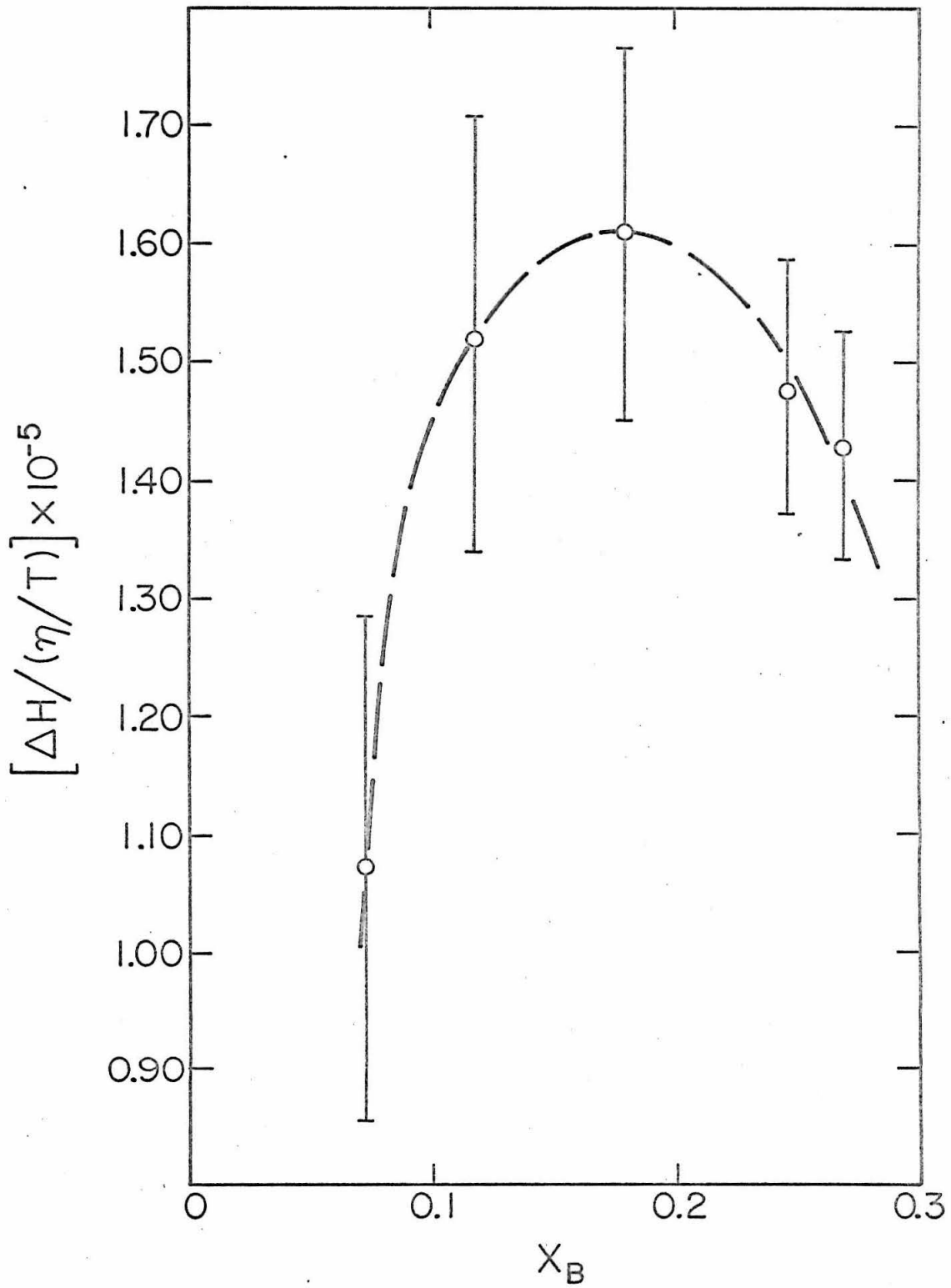
1.70
1.60
1.50
1.40
1.30
1.20
1.10
1.00
0.90
$[\Delta H/(\eta/T)] \times 10^{-5}$
0
0.1
0.2
0.3
X_B

(d)

correlation time may be expressed as

$$\tau_c^{-1} = \tau_r^{-1} + \tau_\ell^{-1} \tag{36}$$

where τ_r = rotational correlation time of either state

τ_ℓ = lifetime of bromine in either state

According to the Debye model, the correlation time for bromine nuclei in states A and B then take on the form

$$\tau_{cA} = \frac{1}{\frac{3k}{4\pi a_A^3}\left(\frac{T}{\eta}\right) + k_2[Bu_4N^+]} \tag{37}$$

and

$$\tau_{cB} = \frac{1}{\frac{3k}{4\pi a_B^3}\left(\frac{T}{\eta}\right) + k_1} \tag{38}$$

where k_1 and k_2 are unimolecular and bimolecular rate constants as defined in Eq. (34) for the dissociation of Bu_4NBr in acetonitrile; τ_{cA} and τ_{cB} are the correlation times for bromine nuclei in states A and B, respectively. Upon making several reasonable assumptions and approximations it is possible to examine the qualitative behavior of τ_{cA} and τ_{cB}. In diffusion controlled processes uni and bimolecular rate constants (k_1 and k_2) are typically on the order of $10^{10} \rightarrow 10^{11}$ ℓ mole^{-1} sec^{-1}. Invoking reasonable approximations for bromine radii in sites A and B we notice that denominator terms in τ_{cA}, Eq. (37), may have, in fact, the same order of magnitude. Furthermore, these two terms behave diametrically in response to changes in concentration as well as

viscosity and if the terms are in the proper range, we may expect the correlation time, τ_{cA}, to be roughly constant. Similarly, in a qualitative fashion, the properties of τ_{cB} may be inspected. Since $k_1 = 2k_2$ (for $K_d = 0.5/25°C$) and upon assuming $a_B \gg a_A$ it is reasonable to expect $k_1 > 3kT/4\pi a_B^3\eta$ over the entire experimental concentration range thus leading to a constant correlation time, τ_{cB}. In effect we are proposing that the so-called associated form, $Bu_4N^+ \cdots Br^-$, rotates slowly compared to the lifetime of the state. Hence in Eq. (38), k_1 (a constant) becomes the dominating factor in determining the correlation time and we estimate $k_1 \geq 3kT/4\pi a_B^3\eta \geq 9 \times 10^9$ moles sec^{-1}. Consequently, if this correlation model is operative, a significant simplification in Eq. (35) is realized

$$\frac{1}{T_2} = \frac{1}{10}\left(\frac{eQ}{\hbar}\right)^2 \left\{ q_A^2\tau_{cA} + (q_B^2\tau_{cB} - q_A^2\tau_{cA})X_B \right\} \qquad (39)$$

and, hence, we anticipate a linear relationship between the linewidth, T_2^{-1}, and mole fraction, X_B. In Figure 3 we have plotted these two parameters from the data contained in Tables II and III for both bromine isotopes and a linear relationship is indeed observed. Experimental results are consistent with the rapid exchange-constant correlation time model. Again, activity compensated data as shown in Figures 3c and d bear the same general appearance and results. Extrapolation of the least-squared lines in Figure 3 provide linewidths for the pure components, Br^- and Bu_4NBr, in acetonitrile. These results are summarized in Table IV for all cases corresponding to the plots in Figure 3. If the "free" solvated bromide ion is symmetrically surrounded by the

FIGURE 3

Nuclear magnetic resonance study of Bu_4NBr in anhydrous CH_3CN conducted at 300°K. a) ^{79}Br and b) ^{81}Br nuclear magnetic resonance linewidths (Hz) are plotted against the mole fraction, X_B, of Bu_4NBr.

$$\underset{\text{State:}}{\underset{}{Bu_4N^+ + Br^-}} \underset{k_1}{\overset{k_2}{\rightleftharpoons}} \underset{}{Bu_4N^+ \cdots Br^-}$$

A B

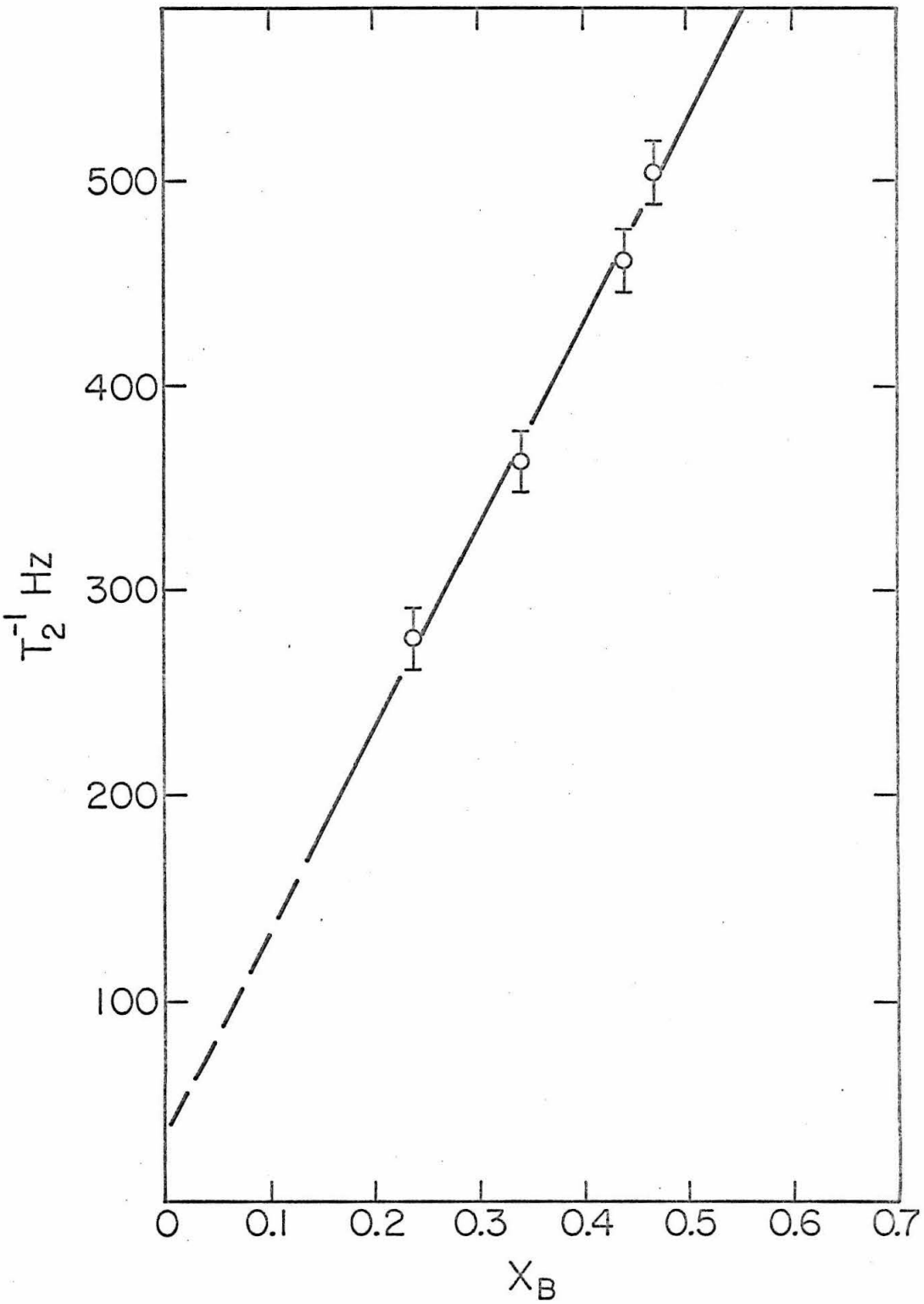

(a)

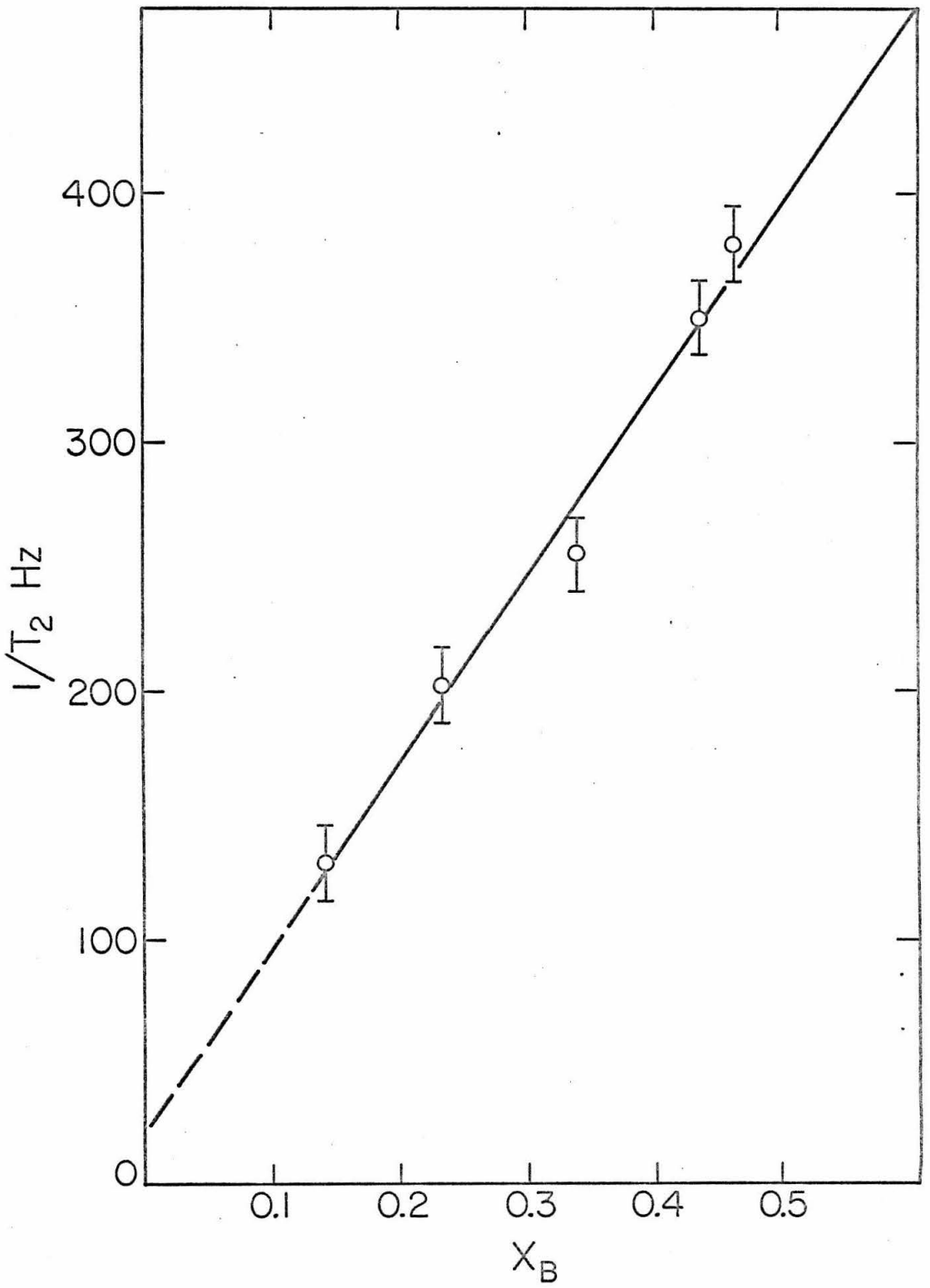

(b)

FIGURE 3

Nuclear magnetic resonance study of Bu_4NBr in anhydrous CH_3CN conducted at 300°K. c) ^{79}Br and d) ^{81}Br nuclear magnetic resonance linewidths (Hz) are plotted against the mole fraction, X_B, of Bu_4NBr compensated for the activity of the components.

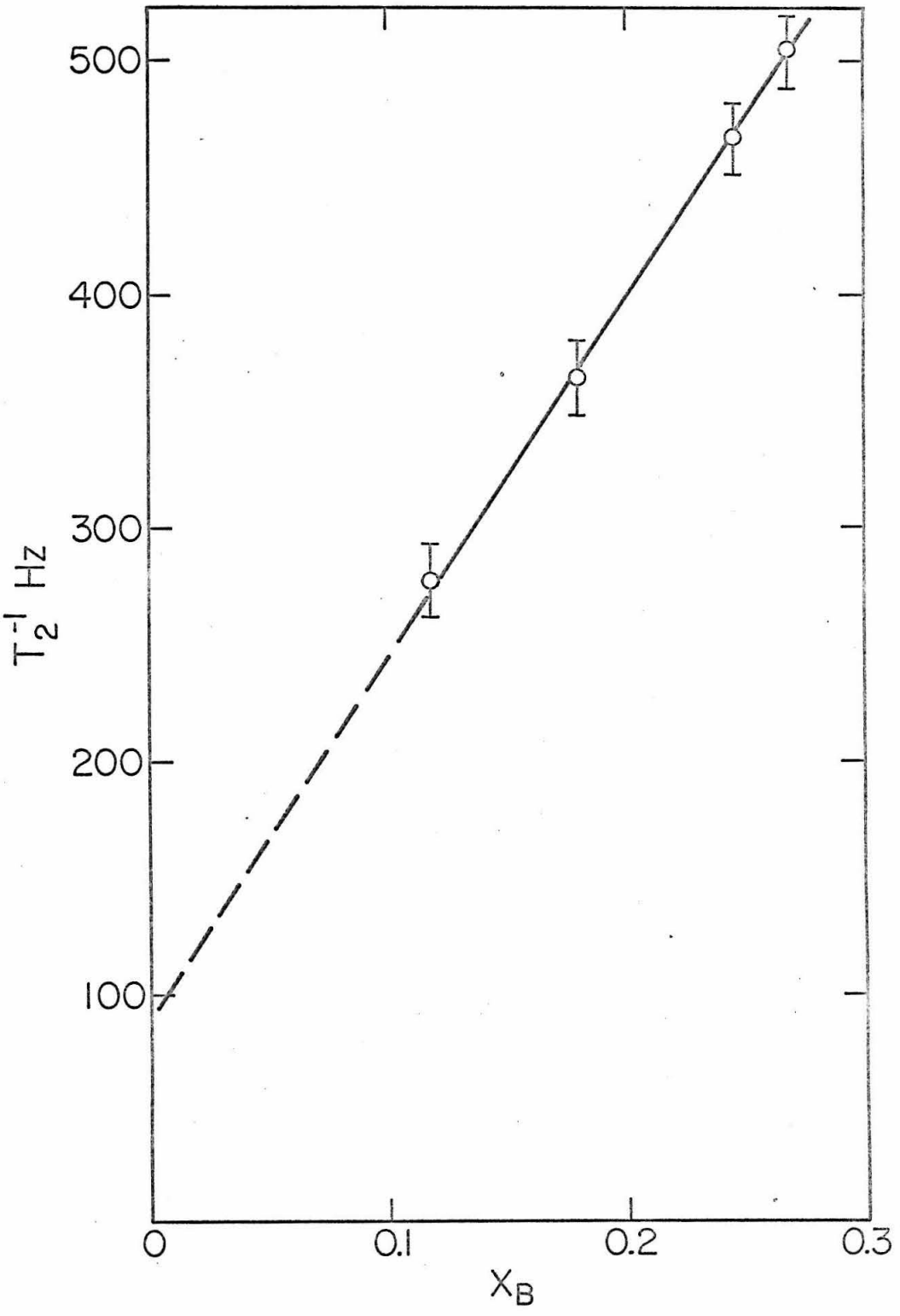

(c)

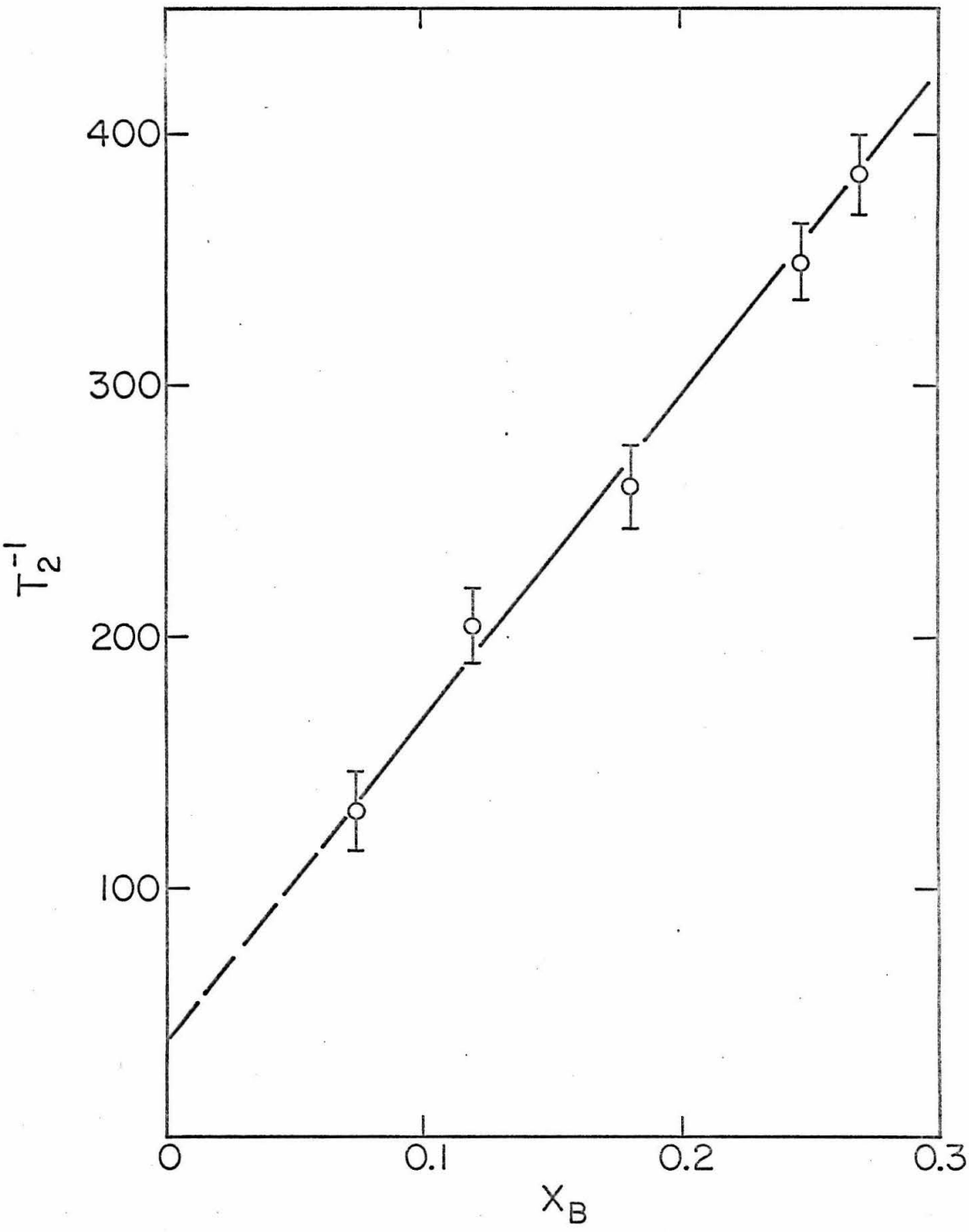

(d)

Table IV. Linewidths of the pure components, Br^- and Bu_4NBr, in acetonitrile.

Isotope	Figure	Linear Expression	Linewidths (Hz) of Components (X_A, X_B=1) (A) Br^-	(B) Bu_4NBr	$\left(\frac{^{79}Q}{^{81}Q}\right)^{2*}$	$\left(\frac{^{79}T_2^{-1}B}{^{81}T_2^{-1}B}\right)$
^{79}Br	3a	$T_2^{-1} = 989\ X_B + 35$	35	1024	1.434	1.33
^{81}Br	3b	$T_2^{-1} = 743\ X_B + 21$	21	764		
$^{79}Br(\gamma_{\pm}corr)$	3c	$T_2^{-1} = 1540\ X_B + 88$	88	1628	1.434	1.23
$^{81}Br(\gamma_{\pm}corr)$	3d	$T_2^{-1} = 1290\ X_B + 38$	38	1328		

*Reference (44).

solvent molecule, the nucleus should experience almost zero field gradient. Experimental linewidths obtained by extrapolation at $X_B = 0$ are indeed small and support this model, although the extrapolated values cannot be taken seriously in view of the systematic error in the measurements. Furthermore, there is a relation between measured relaxation times and chemical shifts in bromine nuclei. Chemical shift, σ, is the sum of a diamagnetic contribution, σ_d, which is always positive and of a paramagnetic contribution, σ_p, which vanishes for electronically closed shells typical for an ionic structure. An ionic model for the associated and dissociated compound is thus reasonable although lack of an observable chemical shift does not preclude the possibility of some covalent coupling in the associated state. The field gradient existing at the bromine nucleus depends on the bromide-counterion separation, r, as $r^{-\rho}$, $\rho \geq 3$, and the quadrupole broadened linewidth falls off as $r^{-2\rho}$ and it is evident that the interaction is short-ranged.

Furthermore, the agreement between theory and experiment attained for the squared quadrupole ratio suggests that quadrupole interactions provide the dominant relaxation mechanism in the Bu_4NBr/CH_3CN system. Moreover, absence of a viscosity dependence has been attributed to the very rapid dynamical association of Bu_4NBr in this solvent. As a consequence it was possible to estimate a lower limit for the unimolecular rate constant, k_1. To our knowledge, this marks the first reported case where a dynamical association process is modulating the linewidth. It clearly suggests new vistas for nuclear magnetic resonance in the study of very rapid phenomena in liquids

and should augment other fast techniques such as ultrasonic absorption and fluorescence.

Armed with these preliminary measurements and dynamical insight we may now proceed more effectively to the system containing the paramagnetic anion, $MnBr_4^{-2}$.

2. Bromine Linewidth Study in the $MnBr_4^{-2}$-Bu_4NBr-CH_3CN System

The ^{79}Br and ^{81}Br nuclear magnetic resonance linewidths in the anhydrous system $MnBr_4^{-2}$-Bu_4NBr-CH_3CN were studied as a function of several solution parameters. Excess bromide ion was supplied by Bu_4NBr hence sharing a common counterion, Bu_4N^+, with the paramagnetic anion. By manipulating concentrations of the components it was possible to examine the response of linewidths to reasonably wide ranges of $MnBr_4^{-2}$ mole fraction, X_{MB}, and $[MnBr_4^{-2}]/[Br^-]$ ratios. Concentrations were restricted within practical limits to coincide with mole fractions and viscosities exhibited in the preliminary work on the Bu_4NBr-CH_3CN system.

Since the Bu_4N^+ counterion associated with the paramagnetic anion may influence the $[Br^-]$ - $[Bu_4NBr]$ distribution through mass equilibria we must carefully consider the effect of such coupling on the bromine linewidths. Naturally, the extent of coupling is not immediately apparent and both extremes are considered to provide a comparative basis for analyzing the data. Experimental results for the exchanging $MnBr_4^{-2}$-Bu_4NBr-CH_3CN system are collected in Table V through IX and are treated for both the coupled and uncoupled models. Activity compensated data are included in Tables VI and IX. Treatment of data and extraction of results contained in these tables will become apparent as

Table V. Nuclear magnetic resonance study of $MnBr_4^{-2}$ and Bu_4NBr in anhydrous CH_3CN conducted at 299°K. Concentration and distribution of components for the coupled and uncoupled systems.

Solution No.	Molar Concentration/299°K						η c.p.
	$MnBr_4^{-2}$	Br^- Total	Uncoupled		Coupled		
			Bu_4NBr	Br^-	Bu_4NBr	Br^-	
1	0.401	0.100	0.015	0.085	0.063	0.037	0.805
2	0.200	0.100	0.015	0.085	0.048	0.053	0.556
3	0.100	0.082	0.010	0.072	0.028	0.054	0.460
4	0.200	0.200	0.047	0.153	0.100	0.100	0.633
5	0.250	0.399	0.138	0.263	0.229	0.171	0.852
6	0.099	0.200	0.047	0.153	0.078	0.122	0.493
7	0.150	0.300	0.089	0.211	0.143	0.157	0.689
8	0.033	0.100	0.015	0.085	0.022	0.078	0.391
9	0.051	0.400	0.138	0.263	0.162	0.238	0.536

Table VI. Nuclear magnetic resonance study of $MnBr_4^{-2}$ and Bu_4NBr in anhydrous CH_3CN conducted at 299°K. Concentration and distribution of components for the coupled and uncoupled systems compensated for activity.

Solution No.	Molar Concentration/299°K						η c.p.
	$MnBr_4^{-2}$	Br^- Total	Uncoupled		Coupled		
			Bu_4NBr	Br^-	Bu_4NBr	Br^-	
1	0.401	0.100	0.0072	0.0928	0.0417	0.0583	0.805
2	0.200	0.100	0.0072	0.0928	0.0282	0.0718	0.556
3	0.100	0.082	0.0053	0.0767	0.0169	0.0651	0.460
4	0.200	0.200	0.0232	0.177	0.0573	0.143	0.633
5	0.250	0.399	0.0721	0.328	0.135	0.264	0.852
6	0.099	0.200	0.0232	0.177	0.0419	0.158	0.493
7	0.150	0.300	0.0453	0.255	0.0800	0.220	0.689
8	0.033	0.100	0.0072	0.0928	0.0254	0.0746	0.391
9	0.051	0.400	0.0721	0.328	0.0871	0.313	0.536

Table VII. Nuclear magnetic resonance study of $MnBr_4^{-2}$ and Bu_4NBr in anhydrous CH_3CN conducted at 299°K. Total and exchange linewidth (Hz) dependence on $MnBr_4^{-2}$ mole fraction, X_B, in the presence of Bu_4NBr. Linewidth correction due to presence of $Br^- - Bu_4N^+ \cdots Br^-$ exchange according to the uncoupled model is also included.

Solution No.	$MnBr_4^{-2}$ X_B	$\Delta H \pm 50$ Hz		$\Delta H_{corr} \pm 50$ Hz		$\Delta H_{ex} \pm 50$ Hz	
		^{81}Br	^{79}Br	^{81}Br	^{79}Br	^{81}Br	^{79}Br
1	0.800	1273	1634	129	179	1144	1455
2	0.666	970	1235	129	179	841	1055
3	0.549	759	983	114	159	645	824
4	0.500	733	1052	195	267	538	785
5	0.385	799	- -	277	- -	522	- -
6	0.330	573	709	195	267	378	442
7	0.330	662	- -	242	- -	420	- -
8	0.250	456	501	129	144	327	357
9	0.113	376	615	277	376	97	239

Table VIII. Nuclear magnetic resonance study of $MnBr_4^{-2}$ and Bu_4NBr in anhydrous CH_3CN conducted at 299°K. Total and exchange linewidth (Hz) dependence on $MnBr_4^{-2}$ mole fraction, X_B, in the presence of Bu_4NBr. Linewidth correction due to presence of $Br^- - Bu_4N^+ \cdots Br^-$ exchange according to the coupled model is also included.

Solution No.	$MnBr_4^{-2}$ X_B	$\Delta H \pm 50$ Hz		$\Delta H_{corr} \pm 50$ Hz		$\Delta H_{ex} \pm 50$ Hz	
		^{81}Br	^{79}Br	^{81}Br	^{79}Br	^{81}Br	^{79}Br
1	0.800	1273	1634	486	654	787	980
2	0.666	970	1235	375	505	595	730
3	0.549	759	983	278	369	480	614
4	0.500	733	1052	392	530	341	522
5	0.385	799	- -	446	- -	353	- -
6	0.330	573	709	311	423	262	286
7	0.330	662	- -	375	- -	287	- -
8	0.250	456	501	188	257	268	244
9	0.113	374	615	322	436	52	179

Table IX. Nuclear magnetic resonance study of $MnBr_4^{-2}$ and Bu_4NBr in anhydrous CH_3CN conducted at 299°K. Total and exchange linewidth (Hz) dependence on $MnBr_4^{-2}$ mole fraction, X_B, in the presence of Bu_4NBr. Linewidth correction due to presence of $Br^- - Bu_4N^+ \cdots Br^-$ exchange according to the coupled model is also included. Results are compensated for Bu_4NBr component activities.

Solution No.	$MnBr_4^{-2}$ X_B	$\Delta H \pm 50$ Hz		$\Delta H_{corr} \pm 50$ Hz		$\Delta H_{ex} \pm 50$ Hz	
		^{81}Br	^{79}Br	^{81}Br	^{79}Br	^{81}Br	^{79}Br
1	0.800	1273	1634	577	731	696	903
2	0.666	970	1235	402	523	568	712
3	0.549	759	983	304	405	455	578
4	0.500	733	1052	408	530	325	520
5	0.385	799	- -	474	- -	325	- -
6	0.330	573	709	309	411	264	298
7	0.330	662	- -	382	- -	280	- -
8	0.250	456	501	366	479	90	22
9	0.113	374	615	319	426	55	189

the discussion develops. A cursory examination of the results indicates that ^{79}Br and ^{81}Br linewidths broaden with increasing mole fraction, X_{MB}, of $MnBr_4^{-2}$ as expected. In addition, a wide magnetic field search produced only a single bromine resonance bearing Lorentzian character over the entire mole fraction range of the paramagnetic anion. Several solutions containing both low and high concentrations of the paramagnetic anion were compared directly for the bromine chemical shifts and none were observed. This significant result immediately implies that the isotropic nuclear-electron coupling constant, A, characterizing the $A\vec{S}\cdot\vec{I}$ interaction, is small and broadening due to this mechanism is presumably within our experimental error estimated to be ± 50 Hz. Assuming this tolerance to represent the chemical shift, we may calculate the line broadening via hyperfine interaction according to the Bernheim relation (34) shown in Eq. (26). The computed value is 5×10^{-6} Hz and clearly signifies that this mechanism provides a negligible contribution to the overall linewidth. To analyze the results and extract dynamical information, it is necessary to establish the exchange limit of the process. Since two separate states are usually non-degenerate, one expects a chemical shift to be characteristic of a rapid exchange process. In the present situation, however, the magnetic non-equivalence may induce effects that are small by comparison to the overall linewidth and, thus, a chemical shift may escape detection. On the other hand, in a slow exchange limit between two states it is also possible to have only one observable resonance. This case arises when the longitudinal or transverse relaxation times are quite different, for example, $T_{2MB} \ll T_{2A}$, so that the

resonance in site MB is broadened beyond detection. Therefore an exchange process occurring in either of the two limiting cases would be consistent with the experimental observation. The apparent dichotomy elicited a study of relative intensities designed to establish the exchange rate limit. Two solutions were prepared to magnify the characteristics expected in either exchange limit and their ^{81}Br resonance line intensities were compared. Experimental results are summarized in Table X. The resonance line intensity is defined as the area subtended by the absorption curve. Assuming the lines to be Lorentzian, intensity of the derivative curve is given by

$$I = \tfrac{2}{3}\sqrt{3}\,\pi\, y'_m \Delta H^2 \qquad (40)$$

where y'_m = maximum derivative amplitude

ΔH = peak-to-peak linewidth

Comparison was made between two solutions having the same Bu_4NBr concentration (~ 0.1 M) but different quantities of the paramagnetic anion. More specifically, solution (A) contained 0.2 M $MnBr_4^{-2}$ and solution (B) was void. From Table X we predict for the rapid exchange picture a minimum intensity enhancement of 9.0 for solution (A) over that of (B) and the experimental observation was 6.5 in fair agreement with the theoretical value. Although this procedure of intensity comparison in the absence of an internal standard is somewhat crude, it appears that the exchange process is in the rapid limit. The experiment was performed carefully with regard to electronic parameters, filling factors and anomolous broadening from r. f. saturation, sweep modulation, side bands, scan speeds and so on. Certainly, the intensity

Table X. Intensity Comparison

	Molar Concentrations in Anhydrous CH_3CN		Minimum Ratio $\frac{4[MnBr_4^{-2}] + [Br^-]}{[Br^-]}$	T_2^{-1} Hz	Relative Area Δ mm $\times 10^{-5}$	$I_{MnBr_4^{-2}} / I_{Bu_4NBr}$
	$[MnBr_4^{-2}]$	$[Bu_4NBr]$				
A	0.200	0.100	9.0	969	5.82	
				970	5.76	
					5.79 (ave)	6.5
B	0.000	0.098	1.0	136	1.124	
				126	0.920	
				126	0.725	
				133	0.810	
					0.895 (ave)	1

enhancement measurement was well beyond experimental error. By contrast, a slow exchange process between sites in which the bromine nuclei have quite different relaxation times, for instance $T_{2MB} \ll T_{2A}$, would lead to a marked apparent decrease of intensity for solution A provided only one line was observable. Obviously an intermediate exchange process or the case where the two sites provide $T_{2MB} \approx T_{2A}$ would be difficult to interpret in terms of intensity changes.

Intensity results imply that the exchange interaction frequency (ω_i) between solvated bromide ions (A) and the bromine residing in the manganese first coordination sphere (MB) is in a rapid exchange limit, that is to say, $\omega_i \gg |\omega_A - \omega_{MB}|$. The exchange linewidth for a two-state system according to Eq. (30) is given simply by

$$(T_2^{-1})_{ex} = T_2^{-1} - T_{2A}^{-1} = (T_{2MB}^{-1} - T_{2A}^{-1}) X_{MB} \qquad (41)$$

where $(T_2^{-1})_{ex}$ = exchange linewidth

T_{2A} = transverse relaxation time of bromine in free ionic state

T_{2MB} = transverse relaxation time of bromine in $MnBr_4^{-2}$

To extract $(T_2^{-1})_{ex}$ from the overall linewidths we must compensate for linewidth contributions from other sources such as (1) dynamical association in the $Bu_4N^+Br^- \rightleftharpoons Br^-$ interaction, (2) dipolar interactions and, (3) rotational correlation effects imposed by changes in macroscopic viscosity. At the experimental concentration levels employed in this study the latter two sources are probably negligible. Using the

rapid exchange-constant correlation model for dynamical association (1), the overall linewidth may be compensated for solutions containing the corresponding Bu_4NBr mole fractions to yield a "residual" linewidth. At this point it is not clear how coupling between equilibria will influence the distribution of components for which compensation is being made. Therefore, we shall consider both extreme cases, i.e., coupled and uncoupled, and will reserve judgment on this situation until the subject is further developed.

Kinetic information is not directly forthcoming from a system in the rapid exchange limit. Nevertheless, in some favorable situations it may be possible to estimate exchange rates or at least establish a lower limit for the process. The linewidths T_{2A}, T_{2MB}, for the bromine nuclei in the two-state system are almost certainly quadrupole controlled and have the general form

$$\frac{1}{T_2} = C\left|\langle E\rangle\right|^2 \cdot \tau_c \qquad (42)$$

where E is the interaction energy involving field gradients imposed by neighboring nuclei and τ_c is the correlation time for events leading to fluctuations in this energy manifold thus establishing a frequency spectrum of $\left|\langle E\rangle\right|^2$. We propose a correlation model for the two different bromine sites by the following exchange reaction scheme

$$Br^- + MnBr_4^{-2} \xrightarrow{k_2} [MnBr_4^{=} \cdots Br^-]^* \xrightarrow{k_1} Br^- + MnBr_4^{-2} \qquad (43)$$

in which k_2 is a bimolecular rate constant and k_1 is a unimolecular rate constant typifying the behavior of the activated complex. Correlation

times for coupled time-dependent events have the general form

$$\tau_c^{-1} = \sum_i \tau_i^{-1} \tag{44}$$

and provides the basis for our analysis of a two-state system.

Free Bromide Ion

The bromide ion in acetonitrile probably exists as a symmetrical complex composed of the solvent and this we define as the free bromide ion. Two possible dynamical events leading to fluctuations of quadrupole interaction energy are immediately apparent. They are: (1) the relative reorientations of the molecular framework imposed by stochastic processes and (2) the lifetime of bromine nuclei in this particular "free" ionic state. Correlation time for these two dynamical processes acting in parallel is given by

$$\tau_{cA}^{-1} = \tau_{\ell a}^{-1} + \tau_{ra}^{-1} \qquad \text{or}$$

$$\tau_{cA} = [\tau_{\ell a}^{-1} + \tau_{ra}^{-1}]^{-1} \tag{45}$$

where τ_{cA} = correlation time of "free" ionic state

$\tau_{\ell a}$ = lifetime of bromine nuclei in state A

τ_{ra} = rotational correlation time in state A

Assuming the relations provided for $\tau_{\ell a}$ and τ_{ra} in the theoretical section of Part I, Eqs. (74) and (32), respectively, the above equation may be written as

$$\tau_{cA} = \frac{1}{\frac{3k}{4\pi a_A^3}\left(\frac{T}{\eta}\right) + k_2[MnBr_4^{=}]} \qquad (46)$$

with the symbols bearing their usual significance. Applying the same arguments used for computing correlation time in the preliminary Bu_4NBr/CH_3CN study, we notice that the two denominator terms in Eq. (46) respond diametrically to changes in concentration and, therefore, viscosity. Provided the terms have the same order of magnitude, we may expect τ_{cA} to be roughly constant in this case also. In other words, a short lifetime of "free" ionic bromine nuclei will tend to dampen the linewidth effects caused by changes in viscosity.

Bromine Nuclei in $MnBr_4^{-2}$

Presence of the paramagnetic component, of course, complicates the picture since we must now account for the possibility of modulation arising through electron spin relaxation. In addition, we have three other dynamical processes that may conceivably generate fluctuations in the quadrupole energy manifold leading to relaxation. These are: (1) the lifetime of bromine nuclei in the paramagnetic complex, (2) the rotational correlation time of the complex and (3) according to the exchange reaction scheme denoted in Eq. (43), an exchange lifetime in which the bromine atoms are promoted into a transient structure defined as an activated complex and to repeat, (4) relaxation of bromine nuclei induced by electron spin-flipping of the central paramagnetic ion. It is reasonable to eliminate mechanism (3) on the grounds that the activated complex will be short-lived compared to the other three dynamical processes and thus will be inefficient

in producing fluctuations at the bromine nuclei. At this juncture, we cannot accurately judge the relative magnitudes of the remaining sources of dynamical fluctuations and must appeal to the experimental results at hand. However if processes (1) and/or (2) dominate the picture we can expect a concentration and viscosity dependence in the linewidth. In the event that manganese spin-flipping (4) induces relaxation and dominates the other fluctuation sources we anticipate a negligible effect on the overall correlation time from changes in viscosity and concentration of the components.

We examine the behavior of the exchange linewidth by allowing the correlation time, τ_{cB} associated with the paramagnetic complex, to take on the two extreme cases: (I) $\tau_{cMB} = \tau_{rmb} = 4\pi a_{mb}^3 \eta/3kT$ and (II) $\tau_{cMB} = C$, a constant with respect to changes in viscosity and concentration. At the same time we invoke parallel assumptions for τ_{cA}, the correlation time associated with the exchanging free bromide ion. It was shown that the free bromide ion linewidth was small relative to other sources. Therefore, the actual form of τ_{cA} will not greatly influence the exchange linewidth. Returning to the rapid exchange expression in Eq. (41) and injecting the relevant correlation times proposed above we obtain

Case I

$$(\eta T_2)_{ex}^{-1} = \frac{2\pi}{15kT}\left(\frac{e\,Q}{\hbar}\right)^2 (a_{MB}^3 q_{MB}^2 - a_A^3 q_A^2) X_{MB} \qquad (47)$$

and

Case (2)

$$(T_2^{-1})_{ex} = \frac{1}{10}\left(\frac{e\,Q}{\hbar}\right)^2 (q^2_{MB}\tau_{cMB} - q^2_A\tau_{cA})X_{MB} \qquad (48)$$

where a_{MB}, a_A are the radii of the paramagnetic anion (MB) and the "free" ion (A). X_{MB} is the mole fraction of $MnBr_4^{-2}$ with respect to total bromine nuclei.

From the data in Tables VII through IX, it is evident that the "residual" or exchange linewidth does not depend significantly on the concentrations (or viscosities) involved in establishing a particular $[MnBr_4^{-2}]/[Br^-]$ ratio (for example, compare solutions 3 and 4; 6 and 7) and we, therefore, propose that dipolar interactions and correlation effects due to viscosity may impose negligible contributions to the linewidths within the observed range of concentrations. Indeed, a plot of $(\eta T_2)^{-1}_{ex}$ against X_B according to Case (1), Eq. (47), is definitely non-linear and exhibits large scatter. In Figures 4 through 7 we have plotted ^{81}Br and ^{79}Br exchange linewidths in response to the mole fraction of the paramagnetic anion, X_{MB}. Figures 8 and 9 show the coupled ^{79}Br and ^{81}Br exchange data compensated for activities from results given in Table IX. In all cases, a linear relationship appears to describe the data quite well and suggests that Case (2), Eq. (48), provides an adequate model in exhibiting the nature of the system. From the preliminary study on dynamical association in Bu_4NBr/CH_3CN we deduced that the field gradient, q_A, experienced by "free" ionic bromine nuclei was small, as expected. Certainly, then, it is evident that $q_{MB} \gg q_A$ and thus $q^2_{MB}\tau_{cMB} \gg q^2_A\tau_{cA}$ so that any non-linearity occurring in the latter term will be highly attenuated as X_{MB} changes.

FIGURE 4

Nuclear magnetic resonance study of $MnBr_4^{-2}$ and Bu_4NBr in anhydrous CH_3CN conducted at 299°K. ^{79}Br exchange linewidth, T_2^{-1}, (Hz) as a function of $MnBr_4^{-2}$ mole fraction, X_B. Coupled equilibria.

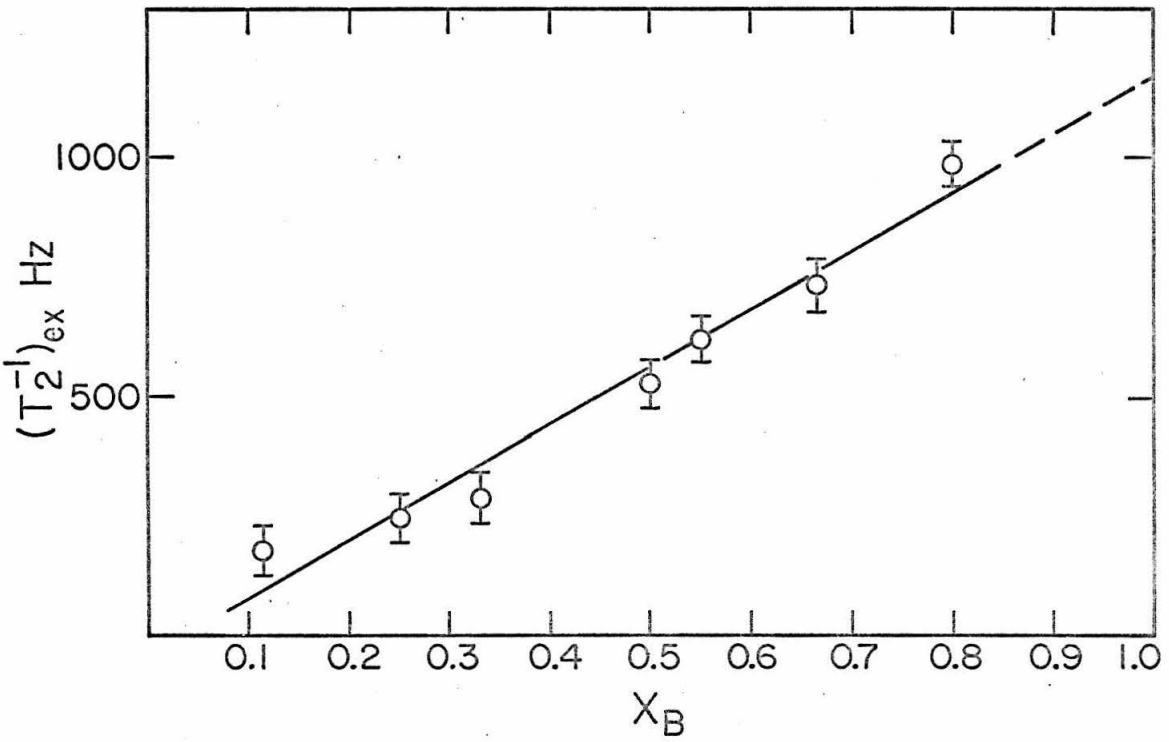
1000
500
$(T_2^{-1})_{ex}$ Hz
0.1
0.2
0.3
0.4
0.5
0.6
0.7
0.8
0.9
1.0
X_B

FIGURE 5

Nuclear magnetic resonance study of $MnBr_4^{-2}$ and Bu_4NBr in anhydrous CH_3CN conducted at 299°K. ^{81}Br exchange linewidth, T_2^{-1}, (Hz) as a function of $MnBr_4^{-2}$ mole fraction, X_B. Coupled equilibria.

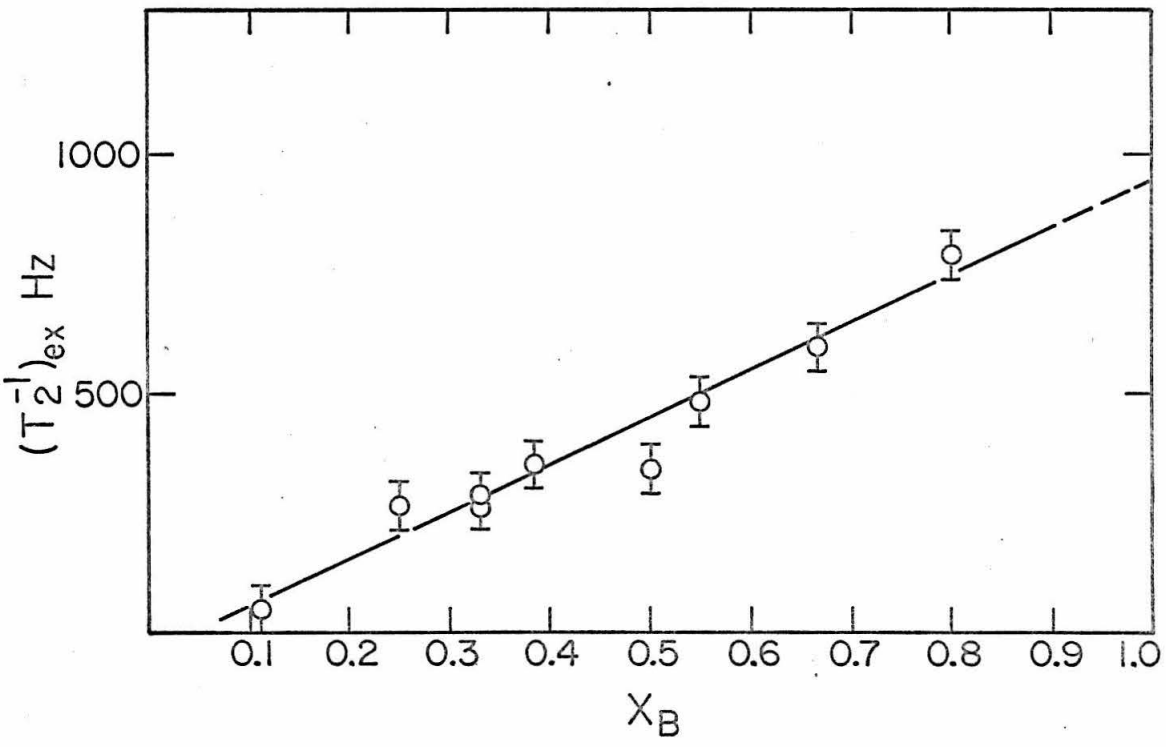
1000
500
$(T_2^{-1})_{ex}$ Hz
0.1
0.2
0.3
0.4
0.5
0.6
0.7
0.8
0.9
1.0
X_B

FIGURE 6

Nuclear magnetic resonance study of $MnBr_4^{-2}$ and Bu_4NBr in anhydrous CH_3CN conducted at 299°K. ^{79}Br exchange linewidths, T_2^{-1}, (Hz) as a function of $MnBr_4^{-2}$ mole fraction, X_B. Uncoupled equilibria.

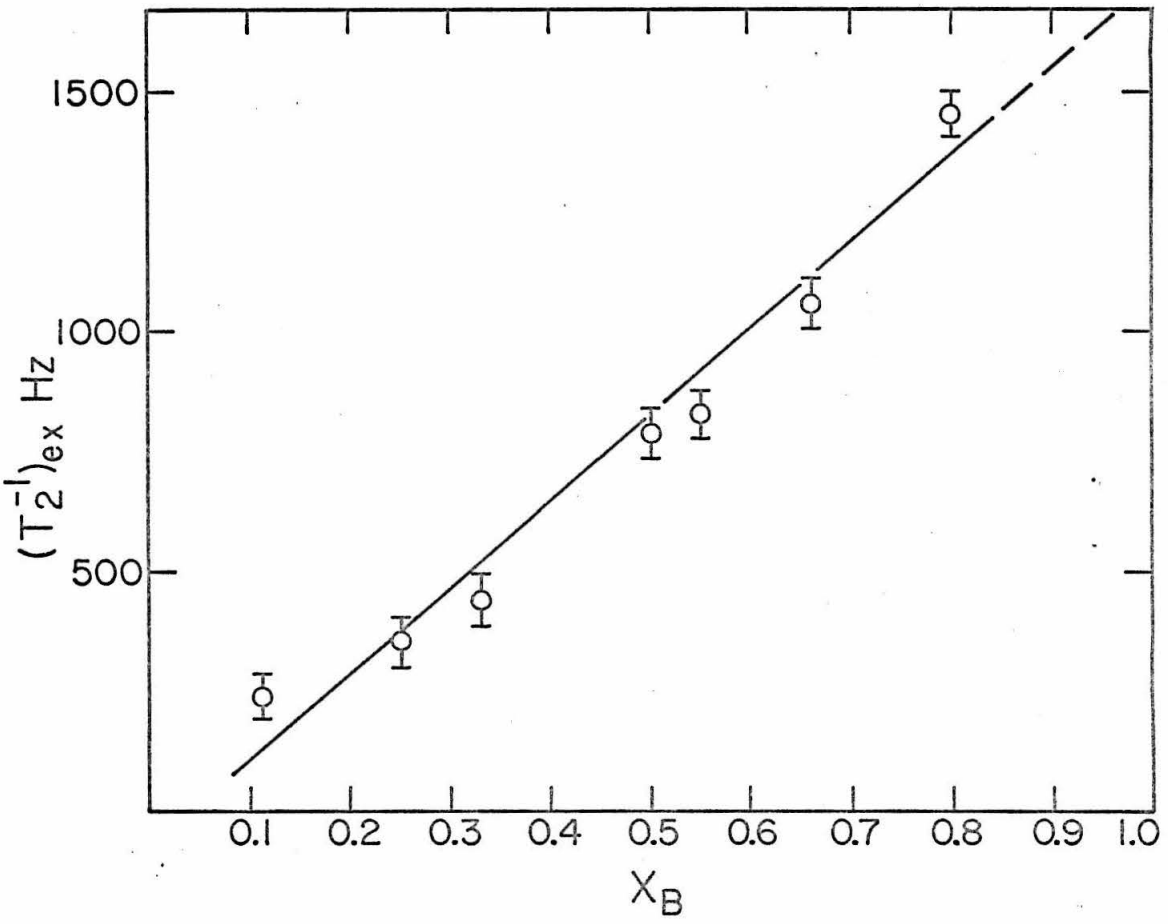
1500
1000
500
$(T_2^{-1})_{ex}$ Hz
0.1
0.2
0.3
0.4
0.5
0.6
0.7
0.8
0.9
1.0
X_B

FIGURE 7

Nuclear magnetic resonance study of $MnBr_4^{-2}$ and Bu_4NBr in anhydrous CH_3CN conducted at 299°K. ^{81}Br exchange linewidth, T_2^{-1}, (Hz) as a function of $MnBr_4^{-2}$ mole fraction, X_B. Uncoupled equilibria.

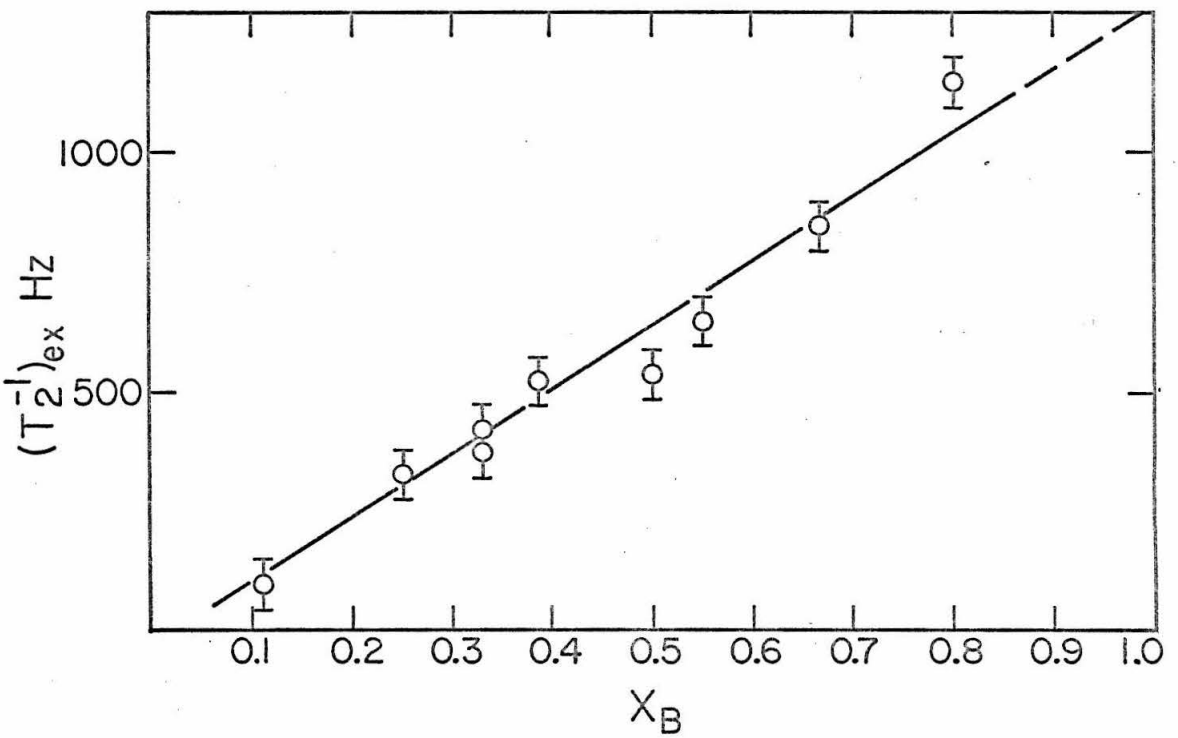
1000
500
$(T_2^{-1})_{ex}$ Hz
0.1
0.2
0.3
0.4
0.5
0.6
0.7
0.8
0.9
1.0
X_B

FIGURE 8

Nuclear magnetic resonance study of $MnBr_4^{-2}$ and Bu_4NBr in anhydrous CH_3CN conducted at 299°K. ^{79}Br exchange linewidths, T_2^{-1}, (Hz) as a function of $MnBr_4^{-2}$ mole fraction, X_B, compensated for activities.

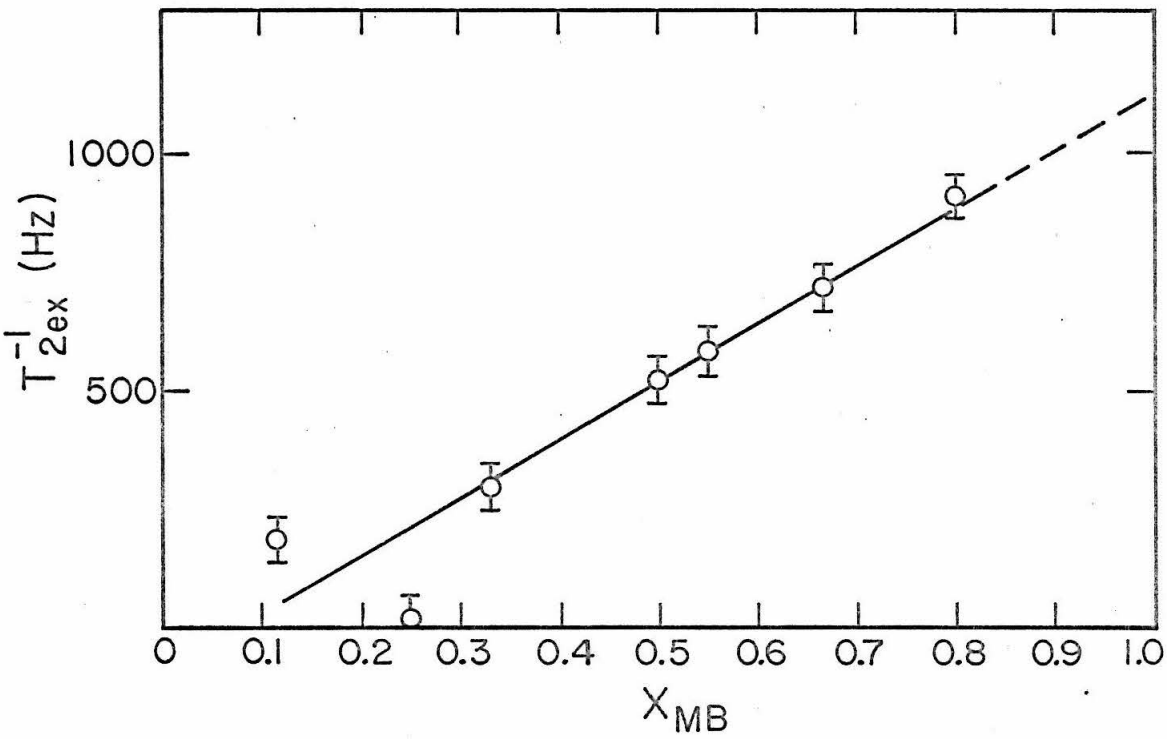
1000
500
T_{2ex}^{-1} (Hz)
0
0.1
0.2
0.3
0.4
0.5
0.6
0.7
0.8
0.9
1.0
X_{MB}

FIGURE 9

Nuclear magnetic resonance study of $MnBr_4^{-2}$ and Bu_4NBr in anhydrous CH_3CN conducted at 299°K. ^{81}Br exchange linewidths, T_2^{-1}, (Hz) as a function of $MnBr_4^{-2}$ mole fraction, X_B, compensated for activities.

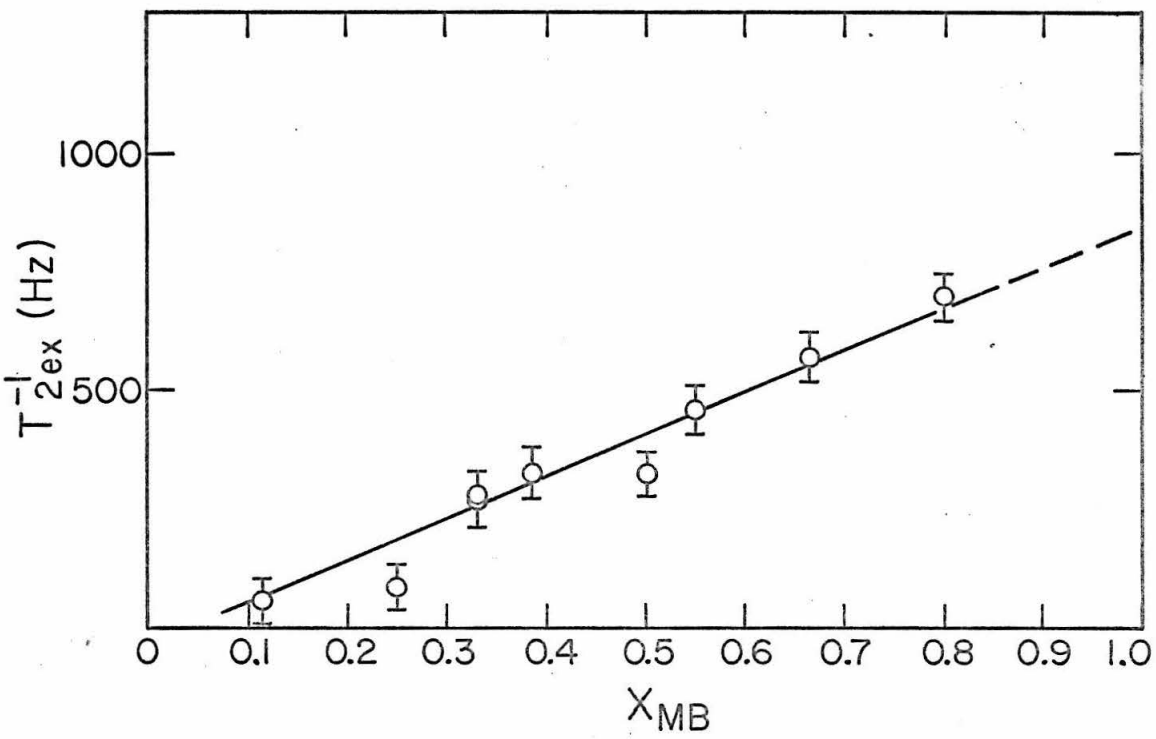
1000
500
T_{2ex}^{-1} (Hz)
0
0.1
0.2
0.3
0.4
0.5
0.6
0.7
0.8
0.9
1.0
X_{MB}

Several conclusions may be inferred from the foregoing experimental observations. The manganese concentration and viscosity changes as reflected through molecular reorientation or solvent fluctuations do not appear to influence the exchange linewidths within our experimental error and range. Obviously, in a sophisticated system of this sort, there are many possible dynamical events leading to field gradient fluctuations at the bromine nucleus. Just to mention a few potential candidates we have: (1) molecular reorientation as defined by the Debye model, (2) lifetime of bromide ion in the complex first coordination sphere, (3) lifetime of bromide ion in an activated complex of $MnBr_4^{-2}$, (4) solvent fluctuations including exchange with the solvent, (5) spin-state lifetime of the manganese (II) ion, (6) lifetime of bromide ion in a "dimerized" or clustered $MnBr_4^{-2}$ state, and (7) lifetime of the "dimerized" or clustered $MnBr_4^{-2}$ state itself. A "dimerized" or clustered state can also refer to a possible state resulting from the relatively slow passage of two or more bromine-bearing complexes. Unfortunately, several cooperative phenomena may act in parallel to attenuate the effect of macroscopic viscosity on linewidths and consequently obscure a quantitative description of the correlation time. However, in view of the electron spin resonance results, we know that as long as the state $MnBr_4^{-2}$, is guaranteed by the presence of excess bromide ion, the dominant electron spin relaxation is connected with $MnBr_4^{-2}$ concentration. This has been ascribed to dipolar interaction of spins between Mn^{+2} ions existing briefly in a clustered state of paramagnetic anions. Although quite speculative, we propose the possibility that the cluster state lifetime may determine the correlation time, τ_{cMB},

characterizing the persistence of interactions effecting the field gradient experienced by the bromine nuclei. Upon assuming this model, the cluster state lifetime can be related simply to the unimolecular rate constant k_1 characterizing the decomposition of the cluster, i. e.,

$$\tau_\ell = \frac{1}{k_1} \tag{49}$$

Another possible candidate, at least anticipated at the onset of this work, was the usual correlation time resulting from molecular reorientation of the paramagnetic anion. In the event that these two models are cooperative we may write

$$\tau_{cMB} = \frac{1}{k_1 + \frac{3kT}{4\pi a^3 \eta}} \tag{50}$$

and it follows that if $k_1 > 3kT/4\pi a^3\eta$, the effective correlation time, τ_{cMB}, can be dominated by a term constant with respect to viscosity and concentration. Still in the spirit of speculation, the most probable explanation for constant correlation time behavior is that τ_{cMB} is being partially controlled by spin-flipping of the Mn^{+2} $3d^5$ electrons. Of course, the lifetime of the electronic spin state is, in turn, dependent on the bromine concentration. If molecular reorientation and electronic spin state lifetime are coupled, the effective correlation time takes on the form

$$\tau_{cMB} = \frac{1}{k_2[Br^-] + \frac{3kT}{4\pi a^3 \eta}} \qquad (51)$$

with the terms bearing the same significance as previously defined. The denominator terms react diametrically to changes in Br^- concentration and if their relative magnitudes are of the same order, we can expect τ_{cMB} to remain approximately constant.

The constant correlation model at least appears to be feasible and is consistent with experimental results. Unfortunately, the complicated nature of this system precludes a definitive mechanism for the modulation of the field gradient.

Returning to the plots in Figures 4 through 9 relating exchange linewidths and mole fraction, X_B, we see that the lines extrapolate nearly through the origin at $X_{MB} = 0$ and extend through $X_{MB} = 1$ to provide linewidths for ^{81}Br and ^{79}Br in the $MnBr_4^{-2}$ complex. The linewidths deduced by extrapolation for both coupled and uncoupled cases are reported in Table XI.

Table XI. ^{79}Br and ^{81}Br Nuclear Magnetic Resonance Linewidths in $MnBr_4^{-2}$

System	Linewidth ΔH (Hz)		$\left(\frac{^{79}T_2^{-1}}{^{81}T_2^{-1}}\right)$	$\left(\frac{^{79}Q}{^{81}Q}\right)^*$
	^{79}Br	^{81}Br		
Coupled	1160	940	1.22	
Coupled (activity compensated)	1125	850	1.19	1.434
Uncoupled	1730	1305	1.35	

*Reference 44.

Appealing to the relation between T_2^{-1} and Q given in Eq. (12) we find

$$\frac{^{79}\Delta H}{^{81}\Delta H} = \frac{^{79}T_2^{-1}}{^{81}T_2^{-1}} = \left(\frac{^{79}Q}{^{81}Q}\right)^2 \tag{52}$$

Ratios computed from extrapolated experimental results shown in the above Table XI are in fair agreement with the squared quadrupole ratio (44) and therefore suggests that quadrupole interactions provide the dominant relaxation mechanism for bromine nuclei in the $MnBr_4^{-2}$ complex. Intensity measurements and the linear relationship between $(T_2^{-1})_{ex}$ and X_{MB} are clearly consistent with a process occurring in the rapid exchange limit. Furthermore, since the quadrupole interaction energy $|\langle E \rangle|$ depends on the manganese-bromine separation, r, as $r^{-\rho}$, $\rho \geq 3$, the quadrupole broadened linewidth then attenuates as $r^{-2\rho}$ and we note that the interaction is short-ranged and, in fact, suggests that the bromine exchanges into the first coordination sphere. Therefore, we may conclude that exchange is occurring between bromine in a "free" ionic state and bromine in the paramagnetic complex.

Finally, in the spirit of speculation, let us presume that the uncoupled model provides the correct molecular picture for the system. That is to say, we expect the paramagnetic anions to have a proprietary claim on their Bu_4N^+ counterions on the grounds of a weak electrostatic marriage. By the same token, the "free" solvated bromine ions demand the attention of their Bu_4N^+ counterions through a short range dynamical association making the respective counterions more or less unavailable as internuncios. Actually, it is impossible to determine the correct model from our experimental approach but, on the other

hand, it is almost irrelevant since the results are quite similar and lead to identical conclusions. Compensation for component activities had no bearing on the conclusions in any case.

3. Estimation of T_{2MB} and the Lower Limit of k_2

There are several important effects in this system that obscure the retrival of dynamical information: (1) rapid exchange of bromine nuclei between two mangetically non-equivalent sites, (2) quadrupole relaxation interactions leading to considerable line broadening and (3) lack of an observable chemical shift arising through scalar hyperfine coupling ($A\vec{S}\cdot\vec{I}$) between bromine nuclei and the electron spin system of the central manganese ion in the complex. Occasionally, it is possible, in such a situation, to attenuate the factors hiding desired information and at least get a glimpse of dynamical effects. For example, it may prove useful to "flood" a two-state system with the component having the larger relaxation time in order to uncover additional mechanisms contributing to the linewidth. At best only lower and upper limits of rate constants and relaxation times can be established. This approach has been employed with limited success by several investigators (17, 18, 21) on exchanging systems having quadrupole broadened linewidths.

The appropriate Bloch equations for a steady-state treatment of this problem has already been discussed in the theoretical section. As a matter of convenience we restate the relationship in a two-state framework for the express purpose of estimating the relaxation time, T_{2MB}, of bromine in $MnBr_4^{-2}$

$$(T_2^{-1})_{ex} = T_2^{-1} - T_{2A}^{-1} = \tau_A^{-1} \frac{\left(\frac{1}{T_{2MB}^2} + \frac{1}{T_{2MB}\tau_h} + \Delta\omega_{MB}^2\right)}{\left(\frac{1}{T_{2MB}} + \frac{1}{\tau_h}\right)^2 + \Delta\omega_{MB}^2} \qquad (53)$$

where $(T_2^{-1})_{ex}$ = residual or exchange linewidth compensated for broadening due to dynamical association of Bu_4NBr

τ_A = lifetime of bromine nuclei in "free" ionic state

τ_h = lifetime of bromine nuclei in paramagnetic anion

T_{2MB} = relaxation time of bromine nuclei in $MnBr_4^{-2}$

$\Delta\omega_B$ = frequency shift imposed by presence of $MnBr_4^{-2}$

We have already observed that $\Delta\omega_B = 0$ within experimental error. Let us now investigate the behavior of Eq. (53) in a limiting case where $X_B \rightarrow 0$. In effect we are "flooding" the system with the component having the larger relaxation time. Under these circumstances $[Br^-] \gg [MnBr_4^{-2}]$ and hence $\tau_A \gg \tau_h$ or equivalently $\tau_A^{-1} \ll \tau_h^{-1}$. If we make the further assumption that T_{2MB} and τ_h have the same order of magnitude, Eq. (53) may be expressed in the convenient form

$$(T_2^{-1})_{ex} = T_2^{-1} - T_{2A}^{-1} = \frac{\tau_h}{\tau_A}\left[\frac{1}{\tau_h + T_{2MB}}\right] \qquad (54)$$

Since τ_h/τ_A is equal to the ratio of probabilities in the two corresponding states, this expression becomes

$$(T_2^{-1})_{ex} = T_2^{-1} - T_{2A}^{-1} = \left[\frac{1}{\tau_h + T_{2MB}}\right] R \qquad (55)$$

where $$R \equiv \frac{4[MnBr_4^{-2}]}{[Br^-]}$$

To illustrate the nature of this relationship, we provide a plot of the exchange linewidth $(T_2^{-1})_{ex}$ as a function of the ratio R in Figure 10 from the data given in Table VII. The resulting plot is noticably curved with the steepest portion passing through the origin. From a previous examination of the experimental data, we inferred that $\tau_h > T_{2MB}$. As the ratio R approaches zero, it is reasonable to propose that the lifetime of bromine in $MnBr_4^{-2}$ becomes shorter and, in fact, smaller than T_{2MB}. In this case, the slope to the curve at R = 0 indicated by a broken line in Figure 10 provides an upper limit for the nuclear spin relaxation time of bromine nuclei in $MnBr_4^{-2}$: $T_{2MB} \approx 3 \times 10^{-7}$ sec compared to 1.2×10^{-7} sec calculated from the extrapolated data in Figure 9. On the other hand, if $\tau_h \geq T_{2MB}$ persists at R = 0 we can then establish a lower limit for τ_h^{-1} and the bimolecular rate constant, k_2, for the exchanging reaction under study. This follows from the often cited relationship

$$\frac{1}{\tau_h} = k_2[Br^-]$$

and gives $k_2 \approx 3 \times 10^7$ ℓ mole^{-1} sec^{-1}. Of course, this is tantamount to accepting the slow exchange model which has already been rejected on the grounds of intensity measurements. As a result, we believe that the slope at R = 0 provides only an estimate for T_{2MB} and, as expected, kinetic information cannot be derived from a system in a rapid exchange limit.

FIGURE 10

Exchange linewidth $(T_2^{-1})_{ex}$ plotted as a function of the probability ratio R defined as $4[MnBr_4^{-2}]/[Br^-]$.

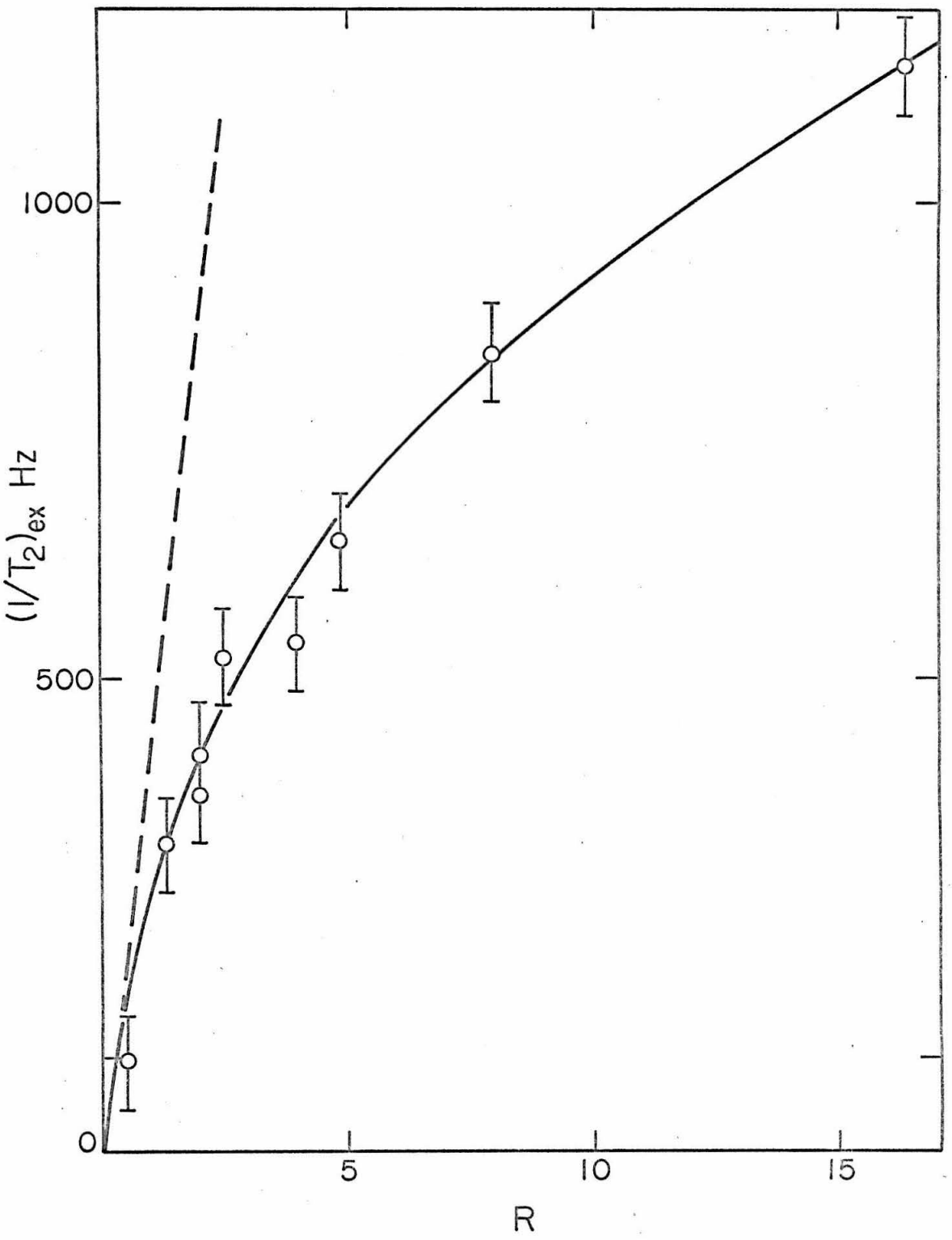
1000
500
0
$(1/T_2)_{ex}$ Hz
5
10
15
R

V. CONCLUSIONS

The interpretation of bromine linewidths in this system arising from nuclear magnetic relaxation was complicated by the presence of several exchanging components and elicited a two part study: (1) the linewidth behavior of Bu_4NBr in anhydrous CH_3CN in the absence of $MnBr_4^{-2}$ and (2) in the presence of $MnBr_4^{-2}$.

Tetra-n-butylammonium Bromide-Acetonitrile System

A single Lorentzian line was observed over the entire experimental range of concentration and strongly suggests that the system is in a rapid exchange limit with respect to the nuclear magnetic resonance time scale. The results are consistent with a bromine nucleus residing in a two-state framework: (1) a symmetrically solvated, "free", ionic state and (2) an associated state in which the bromine retains considerable ionic character. Dissociation and association of ionic compounds in solution is known to be very rapid (45). Typical second-order association rate constants are in the range of $k_2 = 10^{10}$ to 10^{11} ℓ mole^{-1} sec^{-1}. To our knowledge a wide-line nuclear magnetic resonance study of a rapidly associating system such as this has not been previously attempted. A surprising result in the present work was the apparent absence of viscosity effects on linewidths arising from the usual Debye limit correlation time for molecular reorientation. To explain this we proposed that the lifetime, τ_ℓ, of the bromide ion was very short, and, in fact, on the order of $4\pi a^3\eta/3kT$. Since the lifetime, τ_ℓ, and the rotational correlation time, τ_r, respond in opposite directions to changes in concentration, we believe that the "effective"

correlation time, τ_{cA}, consisting of two important components remains essentially constant within our range of observation. From the data it is evident that the linewidth is dominated by bromine in state B ($Bu_4N^+ \cdots Br^-$) and hence in Eq. (39) $q_B^2\tau_{cB} \gg q_A^2\tau_{cA}$. Therefore, we propose that the apparent constant correlation time arises mainly from τ_{cB} and is characterized by the unimolecular rate constant, k_1. The dynamical processes modulating the field gradients can either be coupled ($\tau_c^{-1} = \tau_h^{-1} + \tau_r^{-1}$) or uncoupled ($\tau_c = \tau_h + \tau_r$) and it is not really possible to distinguish between them from our results but it does not dilute our argument about the time-scale of interaction nor the constancy of the "effective" correlation time.

A comparison of the two isotopic bromine linewidth-mole fraction results led to the conclusion that quadrupole interactions provided the dominant relaxation mechanism. Thus, the stage was set for the more complicated $MnBr_4^{-2}$ system.

$MnBr_4^{-2}$-Bu_4NBr-CH_3CN

Preliminary work on the Bu_4NBr-CH_3CN system enabled us to determine the nature of nuclear spin relaxation and led us to the conclusion that dynamical association plays an important role in determining the bromine nuclear magnetic resonance linewidth. Thus, we were able to detect a "residual" linewidth in the complete system containing $MnBr_4^{-2}$ attributable to other relaxation mechanisms. Absence of a chemical shift and a simple calculation based on the intrinsic error in our linewidth measurements clearly eliminated isotropic hyperfine interactions as a relaxation mechanism. In addition, the "residual"

linewidth appears to be independent of both viscosity and bromide ion concentration and suggested that a Debye limit rotational correlation time was not a dominating factor in determining the interaction energy frequency spectrum and that dipolar interactions imposed a negligible influence on the linewidths within our experimental range. The dominant factor influencing "residual" linewidth was the $[MnBr_4^{-1}]/[Br^-]$ ratio. Intensity measurements and the observation of a single Lorentzian line throughout the entire concentration range indicated that an interaction process was in the rapid exchange limit, $\omega_i \gg |\omega_{MB} - \omega_A|$. A linear relation between the "residual" bromine linewidths and $MnBr_4^{-2}$ mole fraction, X_B, was observed and the linewidths for both ^{79}Br and ^{81}Br are clearly controlled by quadrupole interactions which appear to be modulated by very rapid dynamical processes other than molecular reorientation. We propose that this modulation may arise from spin-flipping of the Mn^{+2} $3d^5$ electrons. In this regard, the results bear a resemblance to the preliminary Bu_4NBr^- CH_3CN study where a rapid dynamical process also appears to attenuate the effects of macroscopic viscosity on linewidths.

We conclude that our "residual" linewidth has its origin in chemical exchange and that the bromine nuclei exchange rapidly between a "free" solvated ion and the paramagnetic complex, $MnBr_4^{-2}$. Although dynamical information is not directly forthcoming from components in a rapid exchange limit, we were able to estimate a lower limit for the bimolecular rate constant in a system "flooded" with bromide ion. The linewidth of bromine in the complex indicates that the field gradient imposed by the central Mn^{+2} ion is relatively small, although significant, and strongly suggests that the surrounding bromines are

essentially ionic. If bonding was more covalent, as in the case of $ZnBr_4^{-2}$ (17), line broadening effects would have been several orders of magnitude larger. Absence of a bromine chemical shift in the presence of $MnBr_4^{-2}$ provides additional testimony for an ionic model. Considering the rapid attenuation of field gradient intensities with distance, $\propto \langle r^{-3} \rangle$, it is quite reasonable to expect significant quadrupole relaxation effects only at very short range. Therefore on the basis of experimental evidence we propose that the exchanging bromide ion must enter the first coordination sphere of the paramagnetic anion. This was a primary objective of the nuclear magnetic resonance study and supports our claims drawn from the electron spin relaxation experiments described in Part I. A direct corroboration of the kinetic parameters should not be expected from magnetic resonance experiments conducted at such different frequencies. In fact measurable chemical exchange rates for experiments conducted at 6.5 megacycles would have destroyed our nanosecond exchange picture. So, by somewhat devious paths, we have supported our contention that chemical exchange provides a significant electron spin relaxation mechanism and that kinetic data occurring on the electron spin resonance time scale is directly available from information contained within a band envelope.

REFERENCES

1. F. Bloch, Phys. Rev. 70, 460 (1946).
2. H. S. Gutowsky, D. W. McCall, and C. P. Slichter, J. Chem. Phys. 21, 279 (1953).
3. H. M. McConnell, J. Chem. Phys. 28, 430 (1958).
4. R. K. Wangsness and F. Bloch, Phys. Rev. 89, 728 (1953).
5. F. Bloch, Phys. Rev. 102, 104 (1956).
6. U. Fano, Phys. Rev. 96, 869 (1954).
7. A. G. Redfield, IBM J. Res. and Devel. 1, 19 (1957).
8. Y. Saito, Can. J. Chem. 43, 2530 (1965).
9. J. E. Wertz, J. Phys. Chem. 61, 51 (1957).
10. J. E. Wertz and O. Jardetzsky, J. Chem. Phys. 25, 357 (1956).
11. O. Jardetzsky and J. E. Wertz, Arch. Biochem. Biophys. 65, 569 (1956).
12. O. Jardetzsky and J. E. Wertz, Am. J. Physiol. 187, 608 (1956).
13. O. Jardetzsky and J. E. Wertz, J. Am. Chem. Soc. 82, 318 (1960).
14. J. F. Hon, Mol. Phys. 15, 57 (1968).
15. T. R. Stengle and J. D. Baldeschwieler, Proc. Natl. Acad. Sci. U.S. 55, 1020 (1966).
16. R. G. Bryant, J. Am. Chem. Soc. 89, 2496 (1967).
17. H. G. Hertz, Z. Elektrochemie 65, 36 (1961).
18. T. J. Swift and R. E. Connick, J. Chem. Phys. 37, 307 (1962).
19. R. E. Connick and C. P. Coppel, J. Am. Chem. Soc. 81, 6389 (1959).
20. R. E. Connick and R. E. Poulson, J. Chem. Phys. 30, 759 (1959).

21. A. H. Zeltmann and L. O. Morgan, J. Phys. Chem. 70, 2807 (1966).

22. J. G. Powles and D. W. G. Smith, Phys. Letters 9, 239 (1964).

23. G. A. deWitt and M. Bloom, Can. J. Phys. 43, 986 (1965).

24. R. H. Cole, J. Chem. Phys. 42, 637 (1965).

25. R. E. Richards and B. A. Yorke, Mol. Phys. 6, 289 (1963).

26. C. Deverell, D. J. Frost, and R. E. Richards, Mol. Phys. 9, 565 (1965).

27. A. Abragam and R. V. Pound, Phys. Rev. 92, 943 (1953).

28. T. P. Das and E. L. Hahn, Nuclear Quadrupole Resonance Spectroscopy. Solid State Physics, Suppl. 1 (Academic Press, Inc., New York, 1958) p. 120.

29. F. Bloch, W. W. Hansen, and M. Packard, Phys. Rev. 70, 474 (1946).

30. N. Bloembergen, E. M. Purcell, and R. V. Pound, Phys. Rev. 73, 679 (1948).

31. I. Solomon, Phys. Rev. 99, 559 (1955).

32. N. Bloembergen, J. Chem. Phys. 27, 572, 595 (1957).

33. R. Hausser and G. Laukien, Z. Physik. 153, 394 (1959).

34. R. A. Bernheim, T. H. Brown, H. S. Gutowsky, and D. E. Woessner, J. Chem. Phys. 30, 950 (1959).

35. L. O. Morgan and A. W. Nolle, J. Chem. Phys. 31, 365 (1959).

36. N. Bloembergen and L. O. Morgan, J. Chem. Phys. 34, 842 (1961).

37. K. A. Valiev and B. M. Khabibullin, Russ. J. Phys. Chem. 35, 1118 (1961).

38. K. A. Valiev, Soviet Physics, J. E. T. P., 11, 883 (1960).

39. I. Itoh and Y. Yamagata, J. Phys. Soc. Japan, 13, 1182 (1959).

40. L. Lin, Ph. D. Thesis, California Institute of Technology, 1968.

41. C. Hall, R. E. Richards, G. N. Schulz, and R. R. Sharp, Mol. Phys. 16, 529 (1969).

42. R. I. Iwamasa, Ph. D. Thesis, California Institute of Technology, 1967.

43. L. D. Rollmann, private communication.

44. N. F. Ramsey, Molecular Beams, (Oxford Press, London, 1956) pp. 174.

45. E. F. Caldin, Fast Reactions in Solution, John Wiley and Sons Inc., New York, London, 1964.

PROPOSITIONS

PROPOSITION I

THE INFRARED SPECTRUM OF THE LOW FREQUENCY BENDING MODE, ν_4, of BCl_3. FORCE CONSTANTS OF BCl_3.

Abstract

The gas phase infrared spectrum of the low frequency bending mode, ν_4, of BCl_3 was observed under medium dispersion. The band located at 255.3 cm^{-1} was assigned to ν_4 of $^{11}B^{35}Cl_3$; the band at 252.8 cm^{-1} to overlapping A_1 and B_1 modes of $^{37}Cl^{11}B^{35}Cl_2$. These bands occur about 10 to 12 cm^{-1} higher than the reported value for ν_4. Potential constants calculated from the new data (disregarding anharmonicities) for $^{11}BCl_3$ are significantly different from previous results and are given as follows in M dynes/Å: $f_r = 3.738$, $f_{rr} = 0.415$, $f_\alpha = 0.169$, $f_{\alpha\alpha} = -0.084$, $f_{r\alpha} = -0.139$, $f_{r\alpha'} = 0.069$.

The gas phase infrared spectrum of ν_4 of normal BCl_3 and isotopically enriched $^{11}BCl_3$ were observed under medium dispersion. Bands were found at considerably higher frequencies than the often quoted value of 243-244 cm^{-1} obtained from combination bands.[1-4] Using the Green's function technique we were able to attribute the splitting in the Q branch to the presence of two permuted chlorine isotopes. From the new data and with the application of the Green's

function formalism in the internal coordinate representation,[5] the potential constants for $^{11}BCl_3$ were calculated.

Experimental

Normal BCl_3 (20% ^{10}B, 80% ^{11}B) was obtained from the Matheson Company and was purified by standard vacuum line techniques. The enriched $^{11}BCl_3$ was prepared directly from the elements followed by distillation and purification procedures. Enriched boron was obtained from Oak Ridge National Laboratory, and mass analysis indicated 98.6% ^{11}B.

A Beckman IR-7 with a CsI prism was used for the investigation. The spectral slit width was estimated to be 1 cm^{-1} in the region of operation and the scan time was 1.6 cm^{-1}/min. A 10 cm cell with CsI windows was used for gas samples. The instrument was carefully calibrated against pure rotational water bands[6] and checked with the calculated[7] and observed[8] rotational bands ($J = 11 \rightarrow 14$) of HCl in the region of operation. As a result, accuracy of the measurements are considered to be within ± 0.5 cm^{-1}.

Results

A spectrum of normal BCl_3 is shown in Fig. 1 and has the general appearance of a perpendicular band having PQR structure. However, the Q branch is distinctly split into two major parts with a shoulder on the low frequency side. Spectra of enriched $^{11}BCl_3$ were essentially the same except for a very slight line narrowing. Therefore, the splitting is not due to ^{10}B - ^{11}B shifts. This conclusion

FIGURE 1

Infrared spectrum of ν_4 of BCl_3.

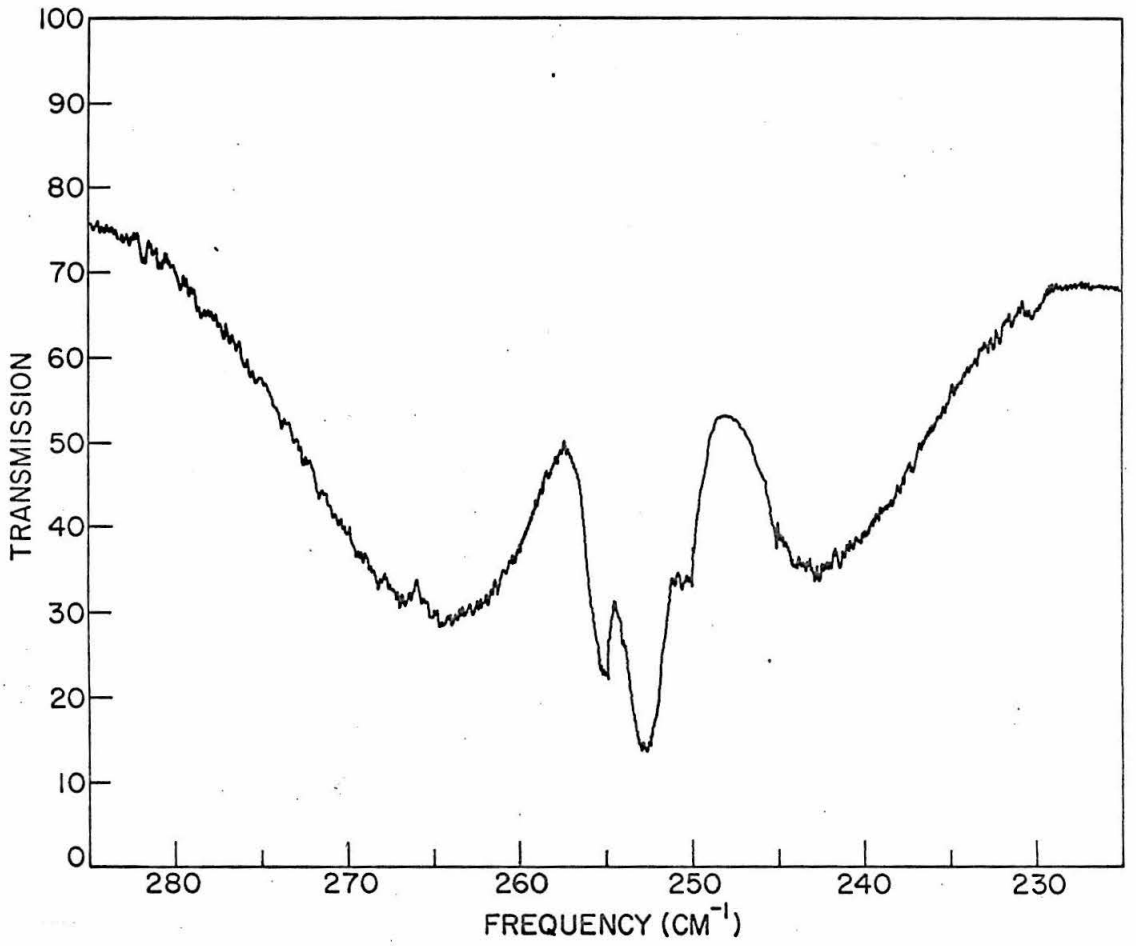
100
90
80
70
60
50
40
30
20
10
0
TRANSMISSION
280
270
260
250
240
230
FREQUENCY (CM^{-1})

is supported by Teller-Redlich product rule calculations which indicate a splitting (0.8 cm^{-1}) within the optical slit-width of our instrument.

Considering only the ^{11}B isotope, the various possible isotopic chlorine permutations are:

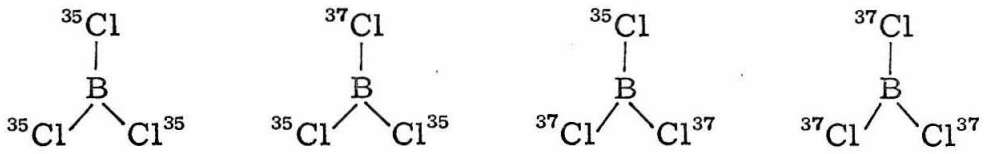

(1) (2) (3) (4)

From statistical considerations, the most probable distribution based on normal abundances (75.4% ^{35}Cl and 24.6% ^{37}Cl) would be:[9] (1) 42.87%, (2) 41.96%, (3) 13.69%, and (4) 1.49%. Consequently, components (1) and (2) are expected to dominate the spectrum. On this basis, the highest frequency Q branch was assigned to $^{11}B^{35}Cl_3$. In going from component (1) to (2) a degradation of symmetry occurs ($D_{3h} \rightarrow C_{2v}$) and both degenerate fundamentals are split into two levels belonging to symmetry types A_1 and B_1. The vibrational decomposition for (2) is $\Gamma_v = 3A_1 + 2B_1 + B_2$, all bands being infrared and Raman active.

Using techniques previously outlined,[10] all the dynamics of the perturbed molecule (2) were determined from the Green's function of the unperturbed molecules $^{11}BCl_3$ and $^{10}BCl_3$ using the new data included in Table I. In this case, changes in geometry and force fields were

Table I. Observed and Calculated Frequencies for the Fundamentals of BCl_3

	Observed frequencies (cm^{-1})			Calculated frequencies (cm^{-1})				
	$^{10}BCl_3$	$^{11}BCl_3$	Ref.	$^{37}Cl^{10}B^{35}Cl_2$	$^{37}Cl^{11}B^{35}Cl_2$	obs.	Symmetry	Assignment
ν_1	471(R)	471(R)	1, 12	466.8	466.8		A_1	B-^{35}Cl symmetric stretch (ν_1)
ν_2	473.3	454.9	12	472.9	454.5		B_2	Out-of-plane deformation (ν_6)
ν_3	993.7	954.2	12	993.7	954.2		B_1	B-^{35}Cl asymm. stretch (ν_4)
				991.3	951.6		A_1	^{37}Cl-B stretch (ν_2)
ν_4	256.1*	255.3	This work	254.2	253.4		A_1	B-^{35}Cl symm. deformation (ν_3)
						252.8		
				253.6	252.8		B_1	^{37}Cl-B in-plane deformation (ν_5)

$^{10}BCl_3$: a (mix. param) = -1.735

$^{11}BCl_3$: a (mix. param) = -1.638

(R) refers to Raman result

* Calculated from Teller-Redlich product rule

were assumed to be zero. If zero-order frequencies were available, the calculated spectrum would be exact. Results of the in-plane and out-of-plane calculations are also included in Table I. As expected, all fundamentals for (2) have been shifted to lower frequencies. Calculations indicate that the band centered at 252.8 cm^{-1} should consist of overlapped A_1 and B_1 modes associated with component (2). However, the low-frequency shoulder on this band occurring at 250 cm^{-1} is unexplained but may be due to component (3) which is present in much smaller quantities.

Force Constants

Using the Green's function formalism, the Cartesian force constants, F_{ij}^c, for BCl_3 were computed from the simple, explicit relationships:[5]

$$F_{36}^c = F_{34} = \frac{M_y}{2\sqrt{3A^2}\,D_1^2}\left[-(2ad_1 + 3r^2)\omega_2^2 + a(2d_1 - 3ar^2)\omega_3^2\right] \quad (1)$$

$$F_{33}^c = 2F_{44} = \frac{M_y}{3A^2 d_1^2 d_2^2}\left[(2ad_1 + 3r^2)^2\omega_2^2 + (2d_1 - 3ar^2)^2\omega_3^2\right] \quad (2)$$

$$F_{44}^c = \tfrac{1}{3}(F_{11} + 2F_{33}) = M_y\left[\frac{\omega_1^2}{3} + \left(\frac{d_2}{\sqrt{3}Ad_1}\right)^2\omega_2^2 + \left(\frac{ad_2}{\sqrt{3}Ad_1}\right)^2\omega_3^2\right] \quad (3)$$

$$F_{46}^c = \tfrac{1}{3}(F_{11} - F_{33}) = M_y\left[\frac{\omega_1^2}{3} - \frac{d_2}{6A^2 d_1^2}\omega_2^2 - \frac{a^2 d_2^2}{6A^2 d_1^2}\omega_3^2\right] \quad (4)$$

$$F_{33} = \frac{M_y d_2^2(\omega_2^2 + a^2 \omega_3^2)}{2A^2 d_1^2} \qquad (5)$$

$$F_{11} = M_y \omega_1^2.$$

Components of these equations are defined as follows:

$$r = [M_y/M_x]^{\frac{1}{2}} \qquad d_1 = [1 + 3r^2]^{\frac{1}{2}}$$

$$d_2 = [2 + 3r^2]^{\frac{1}{2}} \qquad A = [1 + a^2]^{\frac{1}{2}}$$

M_y = Mass of ^{35}Cl (34.969) $\qquad M_x$ = Mass of ^{11}B (11.009)

a, the mixing parameter for planar XY_3 molecules, completely defines the in-plane dynamics. The value of "a" depends critically on the in-plane frequencies and the expression from which it is determined has been previously published.[10] If M_y is in atomic mass units, the conversion factor $\omega_i^2 = 5.8894 \times 10^{-2} \nu_i^2$ (ν_i is observed frequency in wave numbers) produces F's in units of dynes/cm. ω_1 is the symmetric stretching frequency (ν_1), ω_2 is the asymmetric degenerate frequency (ν_3), ω_3 is the degenerate bending frequency (ν_4). The valence force constants were given by Ladd, Orville-Thomas, and Cox:

$$f_r = \tfrac{1}{3}(F_{11} + 2F_{33}), \qquad f_{r\alpha} - f'_{r\alpha} = F_{34}$$

$$f_{rr} = \tfrac{1}{3}(F_{11} - F_{33}), \qquad f_{\alpha} - f_{\alpha\alpha} = F_{44}$$

where f_r = bond stretching, f_α = bond bending, f_{rr} = bond-bond

interaction, $f_{\alpha\alpha}$ = angle-angle interaction, $f_{r\alpha}$ = bond-adjacent angle interaction. In order to obtain six unique force constants, the redundancy criteria described by Ladd, Orville-Thomas, and Cox[11] was applied to the above relationships. Finally,

$$f_{\alpha} = \tfrac{2}{3} F_{44} \qquad f_{\alpha\alpha} = -\tfrac{1}{3} F_{44}$$

$$f_{r\alpha} = \tfrac{2}{3} F_{34} \qquad f_{r\alpha} = -\tfrac{1}{3} F_{34}$$

Potential constants for $^{11}BCl_3$ and $^{10}BCl_3$ calculated from the new data are compared to other values in Table II.

Discussion

Assignments of the observed Q branches to components (1) and (2) are consistent with the calculations. According to the calculations, the other fundamentals also reflect an appreciable isotopic shift due to the presence of (2). Similar shifts may be expected in the various permutations of $^{10}BCl_3$. Obviously, these factors must be considered in order to determine accurate frequencies required in force field calculations. Our calculations suffer from the same limitations but were carried on to illustrate the magnitude of isotopic shift. It is probable that the reported frequencies for BCl_3 are "averages" from components (1) and (2). In this sense, the calculated potential constants will be slightly inaccurate. Using our data for ν_4 in collaboration with the data of Lindeman and Wilson[12] for ν_1 and ν_3, we calculated the potential constants for $^{11}BCl_3$ and $^{10}BCl_3$. The results are different from previously reported comparable values.[11, 12, 13]

Table II. Force Constants of BCl_3 ($M_{dynes}/Å$). Compared to Table IV of Reference 11.

Ref.	f_r	f_{rr}	f_α	$f_{\alpha\alpha}$	$f_{r\alpha}$	$f_{r\alpha'}$	$f_\alpha - f_{\alpha\alpha}$	$f_{r\alpha} - f_{r\alpha'}$
$^{10}BCl_3$*	3.729	0.420	0.169	-0.085	-0.136	0.068	0.254	-0.204
$^{11}BCl_3$*	3.738	0.415	0.169	-0.084	-0.139	0.069	0.253	-0.208
11	3.29	0.80	0.18	-0.09	0.02	-0.01	0.27	0.03
12	3.65	0.49						
13	3.30	0.67	0.28				0.24	-0.14

*This work.

This clearly reemphasizes the fact that the constants are highly frequency dependent and that it is pointless to attach much physical significance to the potential constants until all the frequencies have been accurately determined and corrected for anharmonicities. When this is done, the exact harmonic potential function may be determined from simple, explicit relationships given in the text (Eq. (1) through (6)).

References

1. T. F. Anderson, E. N. Lassettre, and D. M. Yost, J. Chem. Phys. 4, 703 (1936). It should be noted that the frequency (243 cm^{-1}) for ν_4 reported by these authors (Table II, pp. 705) was apparently deduced from combination bands (Table III, pp. 705) of gas-phase infrared data. However, this number has been quoted by some as a Raman result. Actually, the authors report 253 cm^{-1} (pp. 705) as the Raman result for liquid BCl_3 (ν_4).
2. S. Bhagavantam, Ind. J. Phys. 5, 73 (1930).
3. S. Venkateswaren, ibid. 6, 284 (1931).
4. A. B. D. Cassie, Proc. Roy. Soc. A148, 87 (1935).
5. T. Wolfram, C. D. Bass, R. E. DeWames, and L. Lynds, Chem. Soc. Japan Bull. 39, 201 (1966).
6. K. N. Rao, R. V. deVore, and E. K. Plyler, J. Res. Nat. Bur. Stand. 67A, 351 (1963).
7. I. M. Mills, H. W. Thompson, and R. L. Williams, Proc. Roy. Soc. A218, 29 (1953).
8. M. Czerny, Z. Phys. 34, 227 (1925).
9. J. H. Beynon, Mass Spectroscopy and Its Applications to Organic Chemistry, D. Van Nostrand Co., 1960, pp. 298.
10. C. D. Bass, L. Lynds, T. Wolfram, and R. E. DeWames, J. Chem. Phys. 40, 3611 (1964).
11. J. A. Ladd, W. J. Orville-Thomas, and B. C. Cox, Spectrochim. Acta 19, 1911 (1963).
12. P. Lindeman and M. Kent Wilson, J. Chem. Phys. 24, 242 (1956).
13. T. Wentink and V. H. Tiensuu, J. Chem. Phys. 28, 826 (1957).

PROPOSITION II

ELECTRON SPIN RESONANCE OF SMALL BORON RADICALS

This proposition relates to the formation and identification of small, paramagnetic radicals containing boron with electron spin resonance techniques. More specifically it is proposed that the molecular fragments $\cdot BH_2$ and $\cdot BX_2$ (where X = F, Cl, Br) can be formed under suitable conditions in quantities large enough to be detected and studied by electron spin resonance techniques.

It has been well established that many chemical reactions proceed through intermediate stages involving small, reactive molecular fragments possessing extremely short lifetimes. In the current and popular drive to understand chemical reactions at the atomic or molecular level and thus predict the course of a reaction under various external parameters, it is quite evident that these elusive intermediate species play the key role in directing chemical traffic. Hence, a deeper knowledge on the structural and dynamical behavior of these transitory fragments is immensely important to quantitatively understanding any system involving a chemical process. Frequently, the short-lived intermediate states are paramagnetic and their intrinsic reactivity usually limits isolation to exceedingly low concentration levels. Consequently, electron spin resonance techniques capable of detecting 10^{10} spins/gauss are particularly well suited in this application. Moreover, electron spin resonance provides direct information on (1) the distribution of unpaired spin density, or degree

of delocalization and (2) when hyperfine interactions are present, on the nature of the spin wave function at the various respective nuclei. In addition, many of the observed radicals are simple enough to warrant a rather complete theoretical treatment and, as a result, this lends considerable punch to the overall interpretation of a chemical reaction. These are a few of the reasons such work has been undertaken in the past and provides the rationable for suggesting an extension of these techniques to boron chemistry.

An extensive review of the literature to January, 1967, revealed only one rather nebulous publication dealing with boron radicals.[1] The authors claim to have identified the radical $B_{12}Cl_{11}$ with a $\langle g \rangle$ value of 2.011, however, the supporting evidence was glaringly absent.

It has long been established that diborane, under thermal promotion, condenses to form a large series of polynuclear boron hydrides possessing unusual valence relationships such as the three-center bond. Numerous polyborane components such as B_4H_{10}, B_5H_9, etc. have been silated and characterized. The mechanisms of the polymerization process has been the object of many studies although it is still not understood. Many of the proposed mechanisms have involved the condensation of the elusive monomer, BH_3, with diborane followed by subsequent addition to heavier species. Most of the conclusions were based on kinetic studies[2-9] of diborane pyrolysis and it is evident that the BH_3 model is inadequate in explaining the results. In view of the complexity of these systems, it is definitely possible that molecular fragments such as H· and $\cdot BH_2$ play a significant role in the

polymerization process. Recently, the electronic spectrum of BH_2 has been reported[10] and strongly supports the feasibility of preparation.

In a similar vein it has been known for some time that boron subhalides (i.e., B_2X_4, X = F, Cl, Br) are formed at low pressures when the corresponding boron trihalides (i.e., BX_3) are subjected to electrical discharges[11-14] from microwave radiation.[15] The overall reaction may be written

$$2\,BX_3 \xrightarrow[1\text{-}5\ mm]{h\nu} B_2X_4 + X_2\,. \qquad (1)$$

This strongly suggests the onset of a radical mechanism and a possible sequence of events is depicted below

$$BX_3 \xrightarrow{h\nu} \cdot BX_2 + \cdot X \qquad (2)$$

$$\cdot BX_2 + BX_3 \rightarrow \begin{matrix} X \\ X \end{matrix}\!\!\diagdown\!\!\diagup B-B \!\!\diagup\!\!\diagdown \begin{matrix} X \\ X \end{matrix} + \cdot X \qquad (3)$$

$$\cdot X + BX_3 \rightarrow \cdot BX_2 + X_2 \qquad (4)$$

$$\cdot BX_2 + \cdot BX_2 \rightarrow \begin{matrix} X \\ X \end{matrix}\!\!\diagdown\!\!\diagup B-B \!\!\diagup\!\!\diagdown \begin{matrix} X \\ X \end{matrix} \qquad (5)$$

$$\cdot X + \cdot X \rightarrow X_2$$

Other indirect evidence for the formation of free radicals during the preparation of B_2Cl_4 has been cited in the literature.[16-18]

It is known that BX_3 may be reduced with hydrogen in an electrical discharge conducted at low pressure[19] or in the presence of ^{60}Co γ radiation at atmospheric pressures.[19] The overall reaction is

$$H_2 + BX_3 \xrightarrow{h\nu} HBX_2 + HX. \qquad (7)$$

This observation also suggests the formation of $\cdot BX_2$. Part of the mechanism may include the following steps

$$BX_3 \xrightarrow{h\nu} \cdot BX_2 + \cdot X \qquad (8)$$

$$\cdot H + BX_3 \longrightarrow \cdot BX_2 + HX \qquad (9)$$

and, finally

$$\cdot H + \cdot BX_2 \longrightarrow HBX_2. \qquad (10)$$

It seems important that we should deliberately set forth to produce and trap these paramagnetic radicals and examine them by electron spin resonance techniques. The following rationale are given:

1. The EPR investigation of small boron radicals such as $\cdot BH_2$ and $\cdot BX_2$ has never been reported to the best of my knowledge and remains as an unexplored area of radical chemistry.
2. Since the quantum electronic state of boron is relatively simple, a correlation between theory and experiment is practical and should provide a particularly good understanding of the system.

3. Identification of radical species should help to provide a greater insight on the thermodynamics, kinetics, and reaction mechanisms postulated in boron chemistry.

These radicals should be well suited for an electron spin resonance study. It should be possible to unequivocally identify the species, estimate their geometry, obtain hyperfine splitting constants and the spin densities at the nuclei. Further it will provide a check against the hyperfine constants determined by the molecular beam measurements of Wessel,[20] Lew and Tittle.[21]

I propose that small boron radicals may be prepared by X-irradiating boron trihalides, diboron tetrahalides or diborane in a mixture with an inert gas maintained in solid state near 4°K. Molar ratios of the matrix media to radical producing precursor should be on the order of 100 to 500 to insure isolation of the paramagnetic intermediate. A high vacuum gas handling system is required and this should be tied directly into a microwave cavity suited for high vacuum, low temperature deposition and in-situ irradiation. Another technique which may be feasible in this connection is the molecular seive "quantum mechanical beaker" recently reported by Wood and Pietrzak.[22] The precursor is trapped in a seive cavity and is then subjected to an atomic beam generated by a microwave discharge. In this case, a radical may be produced by halogen abstraction according to Eq. (9).

From the large selection of boron compounds, the foregoing ideas will be specifically demonstrated with two examples. We consider

the molecular fragments $\cdot BF_2$ and $\cdot BH_2$ which may be formed from BF_3 and B_2H_6, respectively, by matrix isolation techniques at low temperatures. The isotopic distribution in naturally occurring boron is 20% ^{10}B (I = 3) and 80% ^{11}B (I = 3/2). If the nuclear spin density, $|\psi(0)|^2$, for boron is non-zero and hence if ^{11}B (I = 3/2) hyperfine splitting is large enough to be observed then a 12 line spectrum is anticipated with the F (I = 1/2) multiplets having a 1:2:1 intensity ratio. For the ^{10}B (I = 3) spectrum a 21 line spectrum is expected but should be attenuated owing to the lower natural abundance. In a strong magnetic field the Hamiltonian is

$$\mathcal{H} = \beta H \cdot \underset{\sim}{g} \cdot S + S \cdot \underset{\sim}{T} \cdot I - g_N \beta_N H \cdot I \qquad (11)$$

where $\underset{\sim}{g}$ is the g tensor (second rank) and $\underset{\sim}{T}$ is the hyperfine tensor (also second rank); the other terms bear their usual significance. The nuclear Zeeman term on the right of Eq. (11) is generally negligible; the second term on the right is the hyperfine term consisting of an isotropic and anisotropic part. For isotropic interactions the hyperfine Hamiltonian is

$$\mathcal{H}_{hyp} = A \vec{I} \cdot \vec{S} = -\frac{8\pi}{3} g_e \mu_o g_I \mu_N \sum_{n,i} \delta(r_n - r_i) \vec{I}_n \cdot \vec{S}_i \qquad (12)$$

$$A = \frac{-\frac{8\pi}{3} g_e \mu_o g_I \mu_N}{2S} |\psi(0)|^2. \qquad (13)$$

The magnitude of the hyperfine coupling arises from the spin density, $|\psi(0)|^2$, in Eq. (13) which is dependent on the sigma character of the molecular orbital. From experimental and theoretical considerations it may be possible to estimate angular parameters in these radicals. In the case of $\cdot BH_2$, the molecular orbitals are not complicated by interactions with d levels and are restricted to only s and p levels. The radical should be an excellent candidate for theoretical interpretation. Obviously these procedures can be extended to include many other permutations of compounds containing boron, hydrogen, deuterium and halogens.

From these investigations it should be possible to unequivocally identify a new class of radicals and determine their g-values, hyperfine constants, relaxation phenomena and spatial arrangements. However, one must apply discretion in the interpretation of such conclusions since the matrix may invoke considerable influence on spatial configuration. A study using various matrix media would be helpful in this connection.

If the concentrations of these radicals are sufficiently high, it would be interesting to look for the vibrational spectrum in the infrared. Such a coupling of studies could nicely supplement the electron spin resonance observations. Structural and vibrational assignments could lead to the determination of thermodynamic properties and eventually to an understanding of reaction mechanisms in a relatively new area of chemistry.

More important than just an identification of new radicals, which in itself is interesting, these compounds represent small molecules containing an element that is in the twilight zone between metal and non-metal. It is anticipated that a study of small boron radicals should contribute to an understanding of bonding concepts in inter-metallic compounds.

This proposition was submitted as a candidacy requirement in February, 1967. Recently, Nelson and Gordy (23) have observed the electron spin resonance spectrum of BF_2 radicals and have determined the structure. BF_2 was prepared by γ-irradiation of BF_3 in a Xe matrix maintained at 4.2°K. The hyperfine spectrum of both B and F were well resolved and the isotropic coupling constants were extracted: ^{10}B, 277.98 M Hz; ^{11}B, 826.24 M Hz; and ^{19}F, 532 M Hz. It was further concluded that the unpaired electron was in the σ system, that 93% of the electron spin density is in a nonbonding sp_2 hybrid on the B, and the remaining 7% is in hybridized bonding orbitals of the two F atoms. From the distribution of 2s (44%) and 2p (56%) character exhibited by the spin on the B nucleus for sp_2 hybridization it was concluded that the FBF angle was 112°.

References

1. G. Urry, E. P. Schram, and S. I. Weissman, J. Am. Chem. Soc., 84, 2654 (1962).

2. L. V. McCarty and P. A. DiGiorgio, J. Am. Chem. Soc., 73, 3138 (1951).

3. P. R. Clarke and R. N. Pease, J. Am. Chem. Soc., 73, 2132 (1951).

4. J. K. Bragg, L. V. McCarty and F. J. Norton, J. Am. Chem. Soc., 73, 2134 (1951).

5. A. B. Burg and H. I. Schlesinger, J. Am. Chem. Soc., 55, 4009 (1933).

6. S. H. Bauer, J. Am. Chem. Soc., 78, 5775 (1956).

7. P. C. Maybury and W. S. Koski, J. Chem. Phys., 21, 742 (1953).

8. R. A. Marcus, J. Chem. Phys., 23, 1107 (1955).

9. R. M. Adams, Boron, Metallo-Boron Compounds and Boranes, Interscience, 1964, pp. 572-580.

10. G. Herzberg and J. W. C. Johns, Proc. Roy. Soc. (London), A298, 145 (1967).

11. A. Stock, A. Brandt and H. Fischer, Ber., 58, 835 (1925).

12. T. Wartik, R. E. Moore and H. I. Schlesinger, J. Am. Chem. Soc., 71, 3265 (1949).

13. R. Adler and R. D. Stewart, J. Phys. Chem., 65, 172 (1961).

14. G. Urry, T. Wartik, R. E. Moore and H. I. Schlesinger, J. Am. Chem. Soc., 76, 5293 (1954).

15. J. W. Frazer and R. T. Holzmann, U.S. Patent 2,994,652, August 1, 1961.

16. J. F. Frazer and R. T. Holzmann, J. Am. Chem. Soc., 80, 2907 (1958).

17. A. K. Holliday and A. G. Massey, J. Am. Chem. Soc., 80, 4744 (1958).

18. R. T. Holzmann and W. F. Morris, J. Chem. Phys., 29, 677 (1958).

19. L. Lynds, unpublished report.

20. G. Wessel, Phys. Rev., 92, 1581 (1953).

21. H. Lew and R. S. Tittle, Can. J. Phys., 38, 868 (1960).

22. D. E. Wood and T. M. Pietrzak, Preprint, "Chemical Reactions in Molecular Sieves I. NO_3 Free Radical from Direct Reaction of NO_2 and Atomic Oxygen".

23. W. Nelson and W. Gordy, J. Chem. Phys., 51, 4710 (1969).

PROPOSITION III

APPLICATION OF THE MÖSSBAUER EFFECT AND INFRARED SPECTROSCOPY TO CHEMISORPTION

This proposition relates to the application of the Mössbauer effect and infrared techniques for studying surface adsorption phenomena.

One of the most critical aspects of chemical dynamics is the role played by a phase boundary (surface) in catalysis and chemical reactions. Unfortunately, the nature of the surface interface from a microscopic viewpoint is not well understood or appreciated. Conclusions regarding phenomena on the atomic level at a surface from thermodynamic observations are always speculative. The following discussion will be restricted to the phenomenon of chemisorption on metallic surfaces. As an example we shall consider the problem of carbon monoxide chemisorbed on metallic surfaces in some detail.

Several techniques have been used to investigate such surface phenomenon. Recently low energy electron diffraction (LEED) [1-3] and field emission microscopy (FEM) [4-6] utilizing sophisticated ultra-high vacuum techniques have been applied to this task in a number of elegant experiments to elucidate the nature of rather simple fragments chemisorbed on clean, oriented metal surfaces. Although quite limited, infrared techniques [7-10] have been successfully used to establish the presence of chemisorbed species on metallic surfaces. In the case of the latter technique, developed by Eischens, [7] typically,

a metal is deposited on a high surface area substrate such as Cab-O-Sil (SiO_2). After exposure to CO, bands appear in the infrared spectrum near the region attributed to the carbon-oxygen stretching motion. These bands cannot be removed by pumping on the sample and persist even at elevated temperatures. Under constant pumping and temperatures in excess of 200-300°C they are removed. This implies that substantial bonding occurs between metal and CO. The number of bands and band shapes appear to be dependent on the supporting metal and its preparation. A unanimous conclusion is that the band (or bands) result from CO chemisorbed on the surface. Deviation from the gas phase frequencies have been attributed to the influence invoked by the supporting surfaces. Since Eischens original work, numerous publications [11-15] have appeared on this subject under the permutations of different conditions and substrates. Conclusions regarding the nature of the chemisorbed specie and its disposition on the surface have been fluent. The casual reader may come to the conclusion that CO is oriented with the carbon against the metal. In the wake of all this speculation, it is still not known where on the surface the CO resides or, for that matter, it is not known "which end is up". A definitive experiment has not yet been conducted. It is the purpose of this proposition to suggest experiments which may contribute to our understanding of this problem.

In the following discussion the supported metals will consist of extremely small metallic particles where a substantial percentage of the metal occurs at the surface. Hollis and Selwood [16] demonstrated

in the case of H_2 chemisorbed on 15 Å nickel particles supported on silica that about 18% of the nickel atoms were at the surface or accessible to diffusing H_2. Formation of other small metallic particles exhibiting large surface areas on supporting substrates is well documented. We shall first consider application of infrared techniques to the stated problem.

Infrared Spectra of Chemisorbed CO

The vibrational bands associated with the carbon-oxygen stretching motion (~2100 cm^{-1}) have been observed for CO chemisorbed on numerous supported metals such as Fe,[11,12] Ni,[10,13,14] Pt,[7,8] Ir,[15] Ru,[15] Rh,[9,10] and Pd.[8] It is proposed that the infrared bands of the three isotopic molecules $^{12}C^{16}O$, $^{13}C^{16}O$ and $^{12}C^{18}O$ be examined. It would be particularly meaningful to locate the low frequency bands associated with the metal-carbon or metal-oxygen modes. From the characteristic frequencies for metal-carbon bands, the bands may be expected in the 200-500 cm^{-1} region. Characteristic metal-oxygen bands have been reported in the 400-600 cm^{-1} region. Since there is no a priori reason why the oxygen in CO cannot be oriented against the surface, an isotopic experiment is essential to decide the issue. Two cases have been reported for these low frequency modes[11,12] (assumed to be metal-carbon modes) but experimental conditions were undesirable and results were not conclusive. If both high and low frequency modes can be located, then the set of experiments illustrated in Fig. 1 should provide a definite

answer to our problem.

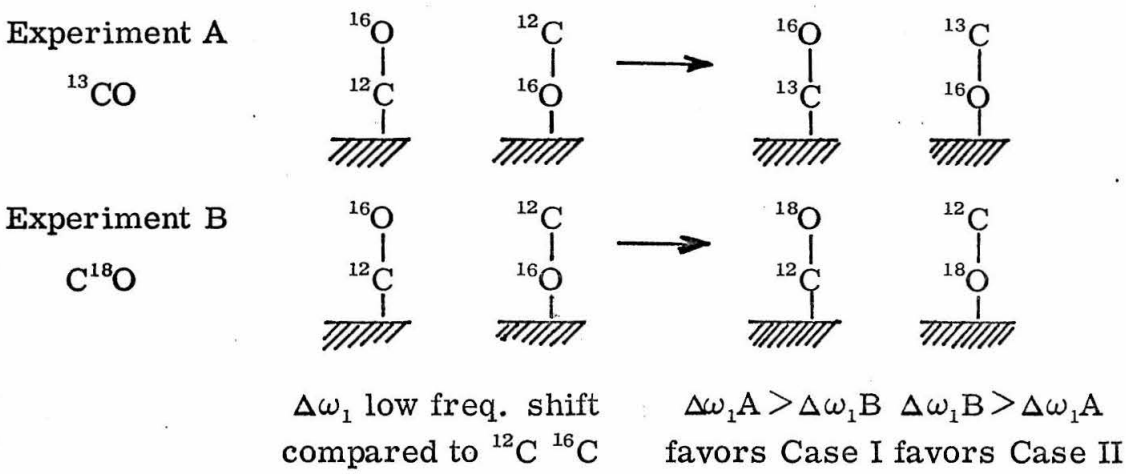

Figure 1

By comparing the results of $^{12}C^{16}O$ with $^{13}C^{16}O$ and $^{12}C^{18}O$ it should be possible to speculate about "which end is up" with more forceful arguments than previously available. It has been common practice to treat the chemisorbed molecule as a three body vibrational problem but this is naive and oversimplified. Since the metallic lattice is also vibrating, we must expect coupling between the modes of the lattice and chemisorbed specie. Strong coupling can be expected between the low frequency molecular mode and lattice mode; the smaller the difference between the molecular mode and the lattice band edge, the stronger the coupling. If the molecular frequency is below the band

edge, vibrational absorption will not be seen. The band edge of metals under consideration are in the 100-300 cm^{-1} region and it is anticipated that significant coupling will be observed. It will then be necessary to consider the "complete" treatment including the metal lattice. Fortunately this has been done in detail by T. B. Grimley.[17] If the molecular frequencies Ω_1 and Ω_2 lie far above the band edge, we may use an asymptotic form for the "corrected" frequencies which includes the effects imposed by the lattice. So stated by Grimley, the equations are

$$\omega_1^2 = \Omega_1^2 \left[1 + \frac{M_A + M_B}{M} \right] \tag{1}$$

$$\omega_2^2 = \Omega_2^2 \left[1 + M^{-1} \right] \tag{2}$$

Equation (2) is an approximation that is valid for the case $M_A + M_B \ll M$. Symbols are defined as follows:

ω_1 = corrected low frequency mode ← B ← AM (surface)
ω_2 = corrected high frequency mode ← BA ← M (surface)
Ω_1 = low frequency molecular mode ← B ← AM (surface)
Ω_2 = high frequency molecular mode ← BA ← M (surface)
M_A = mass of atom bonded directly to lattice atom
M_B = mass of atom away from surface
M = mass of lattice atom

To examine the order of isotopic shifts for molecular permutations denoted in Fig. 1, we consider the two metals Pt and Fe as supports for the chemisorbed specie. The band edges for these two metals are estimated from their Debye temperatures (Θ = 225°K and Θ = 467°K) and turn out to be 156 cm^{-1} and 331 cm^{-1}, respectively. Low frequency modes for CO chemisorbed on these two metals (as well as the high frequency modes) have been reported as stated earlier (Pt: ω_2 = 2000 cm^{-1}, ω_1 = 476 cm^{-1}; Fe: ω_2 = 1950 cm^{-1}, ω_1 = 580 cm^{-1}). Although the data was taken under rather bizarre experimental circumstances, it may serve in an "order of magnitude" calculation to predict several isotopic shifts and molecular frequencies generated by the molecular permutations depicted in Fig. 1. With the aid of Eqs. (1) and (2), results of these calculations are compiled in Table I. The calculations indicate that Pt and Fe are good candidates for these experiments. It may also be feasible to locate the bending modes which have never been observed. They are expected to lie at still lower frequencies. It should be pointed out that Grimleys' treatment did not include anharmonic effects. Further, there is a possibility that CO may be π-bonded to the surface and the question of "which end is up" may actually be one of "lying down". Nevertheless, location of low frequency modes and their isotopic shifts should help decide the issue. Finally, it appears that the orientation of CO with respect to the surface can be settled and the potential constants determined.

Table I. Calculated Results

	$\omega_2(cm^{-1})$	$\omega_1(cm^{-1})$	$\Omega_2(cm^{-1})$	$\Omega_1(cm^{-1})$
^{16}O-^{12}C-Pt	2000	476	2000	445
^{16}O-^{13}C-Pt	1955	469	1955	437
^{18}O-^{12}C-Pt	1952	462	1952	430
^{16}O-^{12}C-Fe	1950	580	1932	476
^{16}O-^{13}C-Fe	1905	573	1886	465
^{18}O-^{12}C-Fe	1902	564	1883	455

Mössbauer Effect

It is proposed that the Mössbauer effect may be used in studying surface phenomenon such as chemisorption. In similar fashion to the foregoing considerations it should be possible to chemisorb CO on small particles of ^{57}Fe supported on high surface area substrates such as Cab-O-Sil (SiO_2) or Linde B (Al_2O_3). Experimentally it would be possible to operate with long path lengths of CO chemisorbed on supported ^{57}Fe to guarantee adequate adsorption. Again it would be desirable to work with very small (~15 Å) metallic particles where a substantial percentage of the atoms occur at the surface. The supported and chemisorbed ^{57}Fe can act as the adsorber and ^{57}Fe in stainless steel as the source in a typical Mössbauer experiment.[19] It has already been demonstrated[18] that anomalous quadrupole

splittings were observed at 300°K for ^{57}Fe supported on Al_2O_3. At 77°K the effect vanishes and the authors attribute the asymmetries to the anistropy of the thermally driven vibrational amplitudes of the surface atoms. They also claim that upon determining the Debye-Waller factor it will be possible to uniquely determine the $\perp$ and $\parallel$ mean-square amplitudes and calculate the potential constants for the surface atoms.

At any rate it would be quite interesting to compare the Mössbauer spectra obtained from $^{12}C^{16}O$, $^{13}C^{16}O$ and $^{12}C^{17}O$ chemisorbed on ^{57}Fe. Since ^{13}C and ^{17}O have spins 1/2 and 5/2 respectively, it should be interesting to see the effect transmitted into the ^{57}Fe nucleus via Fermi contact, $|\psi(O)|^2$, in the absence and presence of additional quadrupole effects. Again it may be possible to decide on the molecular orientation by comparative means. Mass effects due to different isotopes should manifest themselves in the mean-square amplitudes of the surface atoms.

In practice, we can expect to see a six line (I = 5/2) spectrum for ^{57}Fe. A chemisorbed molecule should inflict drastic changes in the electronic structure around the ^{57}Fe atoms at the surface. The hyperfine energy levels will accordingly be altered and "chemical shifts" will occur. We may expect to see splitting of the ^{57}Fe spectrum because of a new surface-complex (^{57}Fe-CO or ^{57}Fe-OC, etc.). Intensity of new lines will be proportional to surface-bulk ratio (~10 - 18% in our hypothetical case). Low temperature experiments will minimize Doppler broadening generated by lattice vibrations.

Since attention is focused on the surface atom, whether or not direct contact is being made with the chemisorbed entity may be inferred from the Mössbauer spectrum. In this way, we may learn some of the more intimate details about the nature of the bond between surface and chemisorbed molecule.

The problem of chemisorbed CO, serving as an example in this proposition, remains as an important question in catalytic processes. Obviously these techniques, and particularly application of the Mössbauer effect, can be extended to many other important catalytic systems where chemisorbed states undoubtedly play a dominant role in catalytic phenomena.

References

1. H. E. Farnsworth, R. E. Schlier, T. H. George, and R. M. Burger, J. Appl. Phys. 29, 1150 (1958).

2. L. H. Germer and C. D. Hartman, J. Appl. Phys. 31, 2085 (1960).

3. H. E. Farnsworth, Advances in Catalysis 15, 31 (1964).

4. E. W. Muller, Ergeb. exakt. Natur. 27, 290 (1953).

5. R. H. Good and E. W. Muller, Handbuch der Physik edited by S. Flugge (Springer Verlag, Berlin, 1956), Vol. 21, p. 176.

6. R. Gomer, Field Emission and Field Ionization, Harvard University Press, Cambridge, Mass., 1961.

7. R. P. Eischens, W. A. Pliskin and S. A. Francis, J. Chem. Phys. 22, 1786 (1954).

8. R. P. Eischens, S. A. Francis and W. A. Pliskin, J. Phys. Chem. 60, 194 (1956).

9. A. C. Yang and C. W. Garland, J. Phys. Chem. 61, 1504 (1957).

10. H. L. Pickering and H. C. Eckstrom, J. Phys. Chem. 63, 512 (1959).

11. R. P. Eischens and W. A. Pliskin, Advances in Catalysis, Vol. X, 1958.

12. G. Blyholder, J. Chem. Phys. 36, 2036 (1962).

13. C. E. O'Neil and D. J. C. Yates, J. Phys. Chem. 65, 901 (1961).

14. R. A. Gardner and R. H. Petrucci, J. Am. Chem. Soc. 82, 5051 (1960).

15. L. Lynds, Spectrochim. Acta 20, 1369 (1964).

16. D. P. Hollis and P. W. Selwood, J. Chem. Phys. 35, 378 (1961).

17. T. B. Grimley, Proc. Phys. Soc. 79, 1203 (1962).

18. P. A. Flinn, S. L. Ruby, and W. L. Kehl, "The Mössbauer Effects of Surface Atoms", Westinghouse Research Laboratories Scientific Paper No. 63-128-117-P6.

19. G. K. Wertheim, Phys. Rev. Letters 4, 403 (1960).

PROPOSITION IV

TUNNEL DIODE MAGNETIC RESONANCE

This proposition relates to magnetic resonance induced by tunneling electrons.

Recently Jaklevic and Lambe [1] have reported an exciting and important discovery showing that tunneling electrons can react with vibrational states of molecules included at a metal-oxide interface in the form of a tunnel diode device. Conductance of the tunneling junction was observed to increase at certain characteristic bias voltages which were identified with vibrational transitions of molecules contained in the barrier. In this fashion, spectra of propionic and acetic acid were observed with a direct correspondence to the infrared spectrum in the 400-4000 cm^{-1} region. An amazing virtue of the experiment is that an infrared spectrum may be obtained by the simple measurement of potentials in the region of 0.05 to 0.5 volts. An important paper [2] on the generation of hot electrons in thin film devices preceded the Jaklevic and Lambe discovery. The authors demonstrated that hot electrons generated in an Al-SiO-Au junction are scattered coherently from the Au anode in a predictable manner within the framework of the Bragg relationship. Their conclusions are consistent with hot electrons rather than thermally excited electrons.

This proposition is an extension of Jaklevic and Lambe's discovery. It is proposed that magnetic resonance be conducted with

with a tunnel diode junction. To illustrate the idea we will consider a simple experiment. Trapped electrons can be produced in the insulator phase of an Al-AlO (or SiO)-Al junction by exposure to ^{60}Co γ radiation. The junction is placed in a homogeneous 3000 gauss magnetic field and the unpaired electrons will experience a splitting of their energy levels. To invoke transitions between spin states will require energies equivalent to those of X-band frequencies ($\sim$10 Gc). A simple calculation indicates that a junction bias voltage around 0.1-0.2 millivolts will accomplish the same thing. These potentials can easily be scanned and measured with high accuracy and precision. Resonance will be accompanied by a sharp increase in conductance upon sweeping from lower to higher energies. In contrast to standard EPR experiments it will be possible to sweep the exciting energies (potential) at constant field strengths. The reverse procedure can be done as well. Obviously the absence of bulky microwave paraphernalia and the small size of the junction would permit the use of larger and more homogeneous fields. Excluding the magnet and its power supply, the spectrometer would constitute only a tunnel junction, a low voltage D. C. supply and a potentiometer. It should be possible to perform a tunnel diode magnetic resonance (TDMR) experiment over a much wider range of exciting energies and fields than normally possible with available EPR equipment.

The simple experiment will now be considered in greater detail. In the Jaklevic and Lambe experiment,[1] a 30 Å Al-oxide layer was formed on a 2000 Å Al film. Then, the freshly formed Al-oxide film

was briefly exposed to the sample vapor (propionic and acetic acid). After brief pumping the junction was completed by high vacuum deposition of the anodic metal (~1 μ thickness). For the present we will exclude a foreign vapor and proceed with a pure diode junction, i.e., 2000 Å Al - 30 Å Al-O (or Si-O) - 1 μ Al. An energy diagram of this arrangement is presented in Fig. 1.

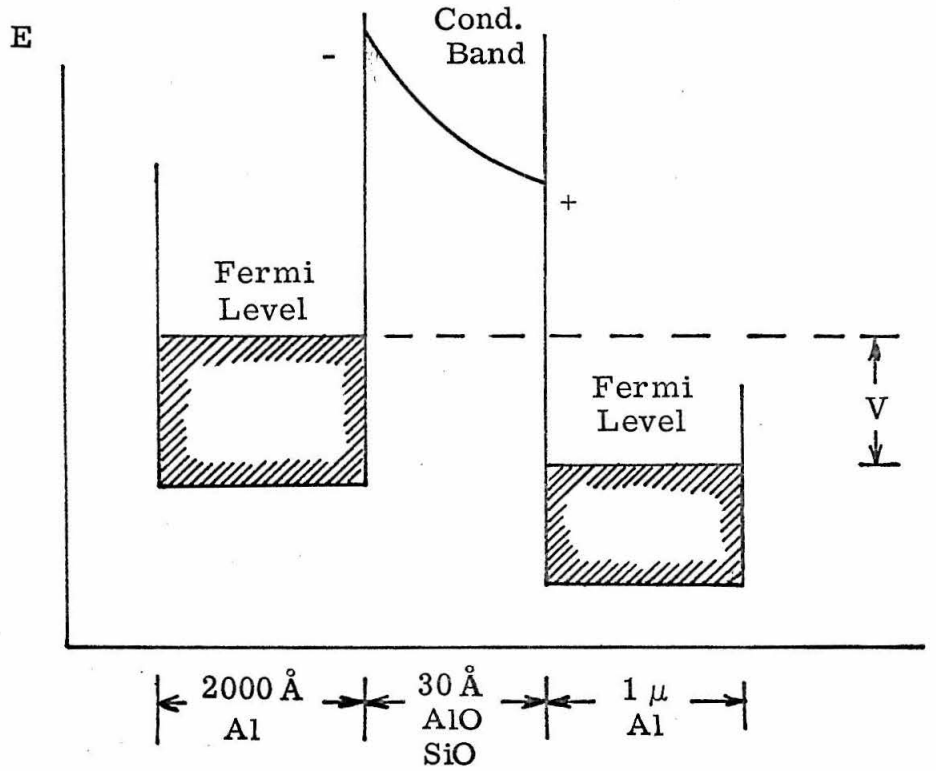

Figure 1

Actually, shapes of the potential surfaces are not exact and do not include influences exerted by the surface interface states. A current of hot electrons through the junction will occur when a bias voltage is applied to the device. The hot electrons will have potential V. As mentioned previously, unpaired electrons are introduced into the insulator phase Al-O (or Si-O) by exposure to ^{60}Co γ radiation. Resolution of TDMR will be limited by the distribution of the density of electronic states in the metal electrodes. Density of states is given by[3]

$$g(E) = \frac{1}{2\pi^2}\left(\frac{2m}{\hbar^2}\right)^{3/2} E^{1/2} \tag{1}$$

and at absolute zero, density of states as a function of energy is shown in Fig. 2(a). As the temperature is increased from absolute zero, the Fermi level is spread out by the probability of electrons being excited into unoccupied states lying above the Fermi level. This situation is depicted in Fig. 2(b). Therefore, it will probably be necessary to conduct these experiments at or below 80°K. This is consistent with the observations of Jaklevic and Lambe.[1] The junction should be oriented in the magnetic field so that the tunneling electrons and field are parallel to minimize interaction. This condition is given by

$$\begin{aligned} \vec{v} \times \vec{B} &= 0 \\ \vec{F} &= q\vec{E} \end{aligned} \tag{2}$$

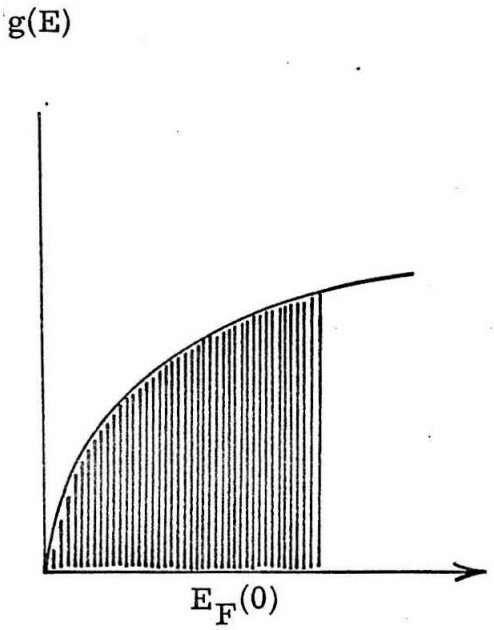

Figure 2(a)

$E_F(0)$ is Fermi energy at 0°K

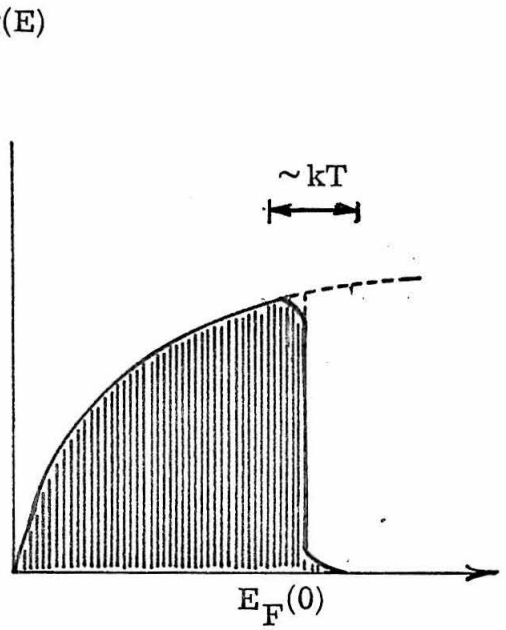

Figure 2(b)

$T > 0; \quad T \ll \frac{E_F}{k}$

In 3000 gauss fields resonance should occur with junction bias voltages around 0.1 - 0.2 millivolts as stated before.

Success in loading junction interfaces with common organic compounds suggests the feasibility of performing all sorts of magnetic and radical experiments in the solid state. As an example, mixtures of CH_3Cl and an inert gas could be loaded on the barrier junction. High energy radiation will then produce matrix isolated CH_3 radicals. In addition to TDMR experiments on trapped radicals of this sort, their vibrational frequencies could be investigated, in-situ, by merely operating at higher potentials. Furthermore,

an electron scattering process will not suffer from the usual unallowed transitions invoked by molecular symmetry.

In summary, it was proposed that magnetic resonance can be induced by hot electrons generated in a tunnel diode merely by scanning potentials in the appropriate range. The small physical dimensions of tunnel junctions and the simplicity of supporting equipment are appealing from an experimental viewpoint. TDMR may permit investigations over much wider energy ranges and experimental conditions. Strong interactions at the interfaces are also expected to influence the spin states and should provide additional information on the "magical" nature of the boundary layer.

References

1. R. C. Jaklevic and J. Lambe, Phys. Rev. Letters 17, 1139 (1966).

2. J. G. Simmons, R. R . Verderber, J. Lytollis, and R. Lomax, Phys. Rev. Letters 17, 675 (1966).

3. C. Kittel, Introduction to Solid State Physics, John Wiley and Sons, Inc., 2nd Ed., 1957, pp. 250.

PROPOSITION V
TRANSFER OF TRANSLATIONAL ENERGY INTO INTERNAL EXCITATION OF REACTION PRODUCTS

This proposition suggests a class of experiments in which the internal excitation of reaction products can be studied as a function of reactant translational energy.

In a gaseous non-reactive collisions there are at least ten different kinds of energy transfer which can occur. It is clear that these processes play an important role in understanding the fundamental nature of hydrodynamics, reaction kinetics, electrical discharges and gas lasers. When a chemical reaction takes place the mechanisms of energy transfer are further obscured by the onset of a transient "activated complex" and the subsequent formation of products. Accordingly the microscopic details of the energy distribution among the reaction partners becomes increasingly difficult to unravel. As pointed out by Herschbach (1), the molecular dynamics of chemical reactions can be studied most directly in reactive crossed-beam experiments in which it is possible to determine the distribution of velocity vectors of product molecules immediately after a single reactive collision. An analysis of product angular distribution and kinetic energy provides a basis for understanding the intimate details of chemical reaction during the instant of time when reactive components come together. Most of the crossed beam experiments to date have involved reactions between alkali metals and halogen compounds.

Several typical experiments leading to anisotropic product distributions are tabulated below with references:

Reaction	Mechanism	Reference
(1) $K + CH_3I \rightarrow KI + CH_3$	rebound	2, 3
(2) $K + Br_2 \rightarrow KBr + Br$	stripping	
(3) $M + I_2 \rightarrow MI + I$	"	4, 5

where M = Na, K, Rb, Cs

Certainly the scope of these studies has been limited for practical reasons to relatively simple systems but the insight provided into molecular dynamics has, indeed, been very rewarding. For example, from the thermochemistry of these reactions cited above and a kinematic analysis of angular distributions it is concluded that a large fraction of reaction energy appears as internal excitation of the products. In the above reactions proceeding via a "stripping" mechanism indirect arguments indicate that vibrational excitation of newly formed product bonds is dominant. Amazingly, for these reactions the cross section, σ_r, varies from $\lesssim 10$ Å to >100 Å which is exceptionally large. These enormous cross sections have inspired much further experimental and theoretical work. As σ_r increases, the favored recoil direction for the alkali halide products gradually shifts from a "rebound" mechanism to a forward or "stripping" mechanism. Correspondingly the angular distribution of alkali metal atoms scattered non-reactively shows a marked narrowing at wide angles. It is now evident that careful measurements augmented by theoretical

considerations can lead to a much deeper understanding about the paths of reaction. Unfortunately, the partitioning of energy in the rotational and vibrational quantum states of the reaction products cannot be directly determined by crossed beam methods.

The classic diffusion flame experiments conducted by Polanyi (6-9) brought a new dimension into the study of molecular dynamics. By observing the infrared emission it was possible to determine the distribution of energy in the vibrational and rotational quantum states of the molecular products. Many studies of this nature have now been performed and clearly corroborate the crossed beam experiments in that the reaction products are almost always borne in excited rotational and vibrational states. The discovery that population inversions were sometimes attained, of course, led to the development of the chemical laser demonstrated in practice by Pimentel and co-workers (10-12). Using a high power flash photolyzed chemical laser Pimentel and co-workers were able to estimate the bimolecular rate constant ratios for reactions leading to vibrationally and rotationally excited states:

$$\begin{aligned} F + H_2 &\xrightarrow{k_V} HF_V^* + H && k_2/k_1 \sim 5.5 \\ F + D_2 &\xrightarrow{k_V} DF_V^* + D && k_3/k_2 \sim 1.6 \qquad (13) \\ Cl + HD &\xrightarrow{k_H} HCl + D \\ Cl + HD &\xrightarrow{k_D} DCl + H \end{aligned} \Bigg\} \quad k_H/k_D = 1.9 \qquad (12)$$

Results are not as yet very accurate since laser emission occurs within the 30 μS flash pulse width initiation. Nevertheless, these techniques are truly imaginative and point the way to many potentially fascinating experiments that should provide new insight into molecular dynamics.

There are four general types of reactions that involve separation of chemical bonds and lead to excited state products (14). These are

I	$X + Y + M \rightarrow XY^* + M$ $X + Y + M \rightarrow XY + M^*$	Recombination Excitation
II	$XY + M^* \rightarrow A^* + B + M$	Associative Energy Transfer
III	$X + YZ \rightarrow XY^* + Z$ $X + YZ \rightarrow XY + Z^*$	Exothermic Chemical Exchange Reactions
IV	$XYZ \xrightarrow{h\nu} XY^* + Z$ $XY \xrightarrow{h\nu} X^* + Y$	Photodissociation

It is suggested in this proposition that an exothermic exchange reaction (III) be conducted with one reactant having an adjustable translational energy. More specifically, it is proposed that translationally "hot" hydrogen atoms provide one of the reaction partners. The availability of this component is both practical and well documented (15-17). Hot H atoms are readily formed by the photodissociation of HI

$$HI \xrightarrow[h\nu]{\lambda = 1849\,\text{Å}} H(2.7\ \text{eV}) + I(^2P_{1/2})$$

resulting from a transition to a repulsive state

$$^3\Pi_0^+ \longleftarrow {}^1\Sigma^+ .$$

Conservation of momentum requires that all energy from the primary process in excess of the bond energy ($D_0 = 3.02$ eV) and electronic excitation winds up as translational energy of the H atom. If a ground state I is formed

$$HI \xrightarrow[h\nu]{\lambda = 1849\,\text{Å}} H(3.6\ \text{eV}) + I(^2P_{3/2})$$

and the corresponding transition is

$$^3\Pi_1 \longleftarrow {}^1\Sigma^+.$$

Thus it is practical to generate hot H atoms with specific energies up to ~3.6 eV. Several interesting reactions can then be studied by low pressure flames or chemical lasers:

1. $H^T + Cl_2 \rightarrow HCl^* + Cl$
2. $H^T + Br_2 \rightarrow HBr^* + Br$
3. $H^T + HI \rightarrow HI^* + H$
4. $D^T + HI \rightarrow DI^* + D$
5. $H^T + O_2 \rightarrow HO^* + O$
6. $H^T + O_3 \rightarrow HO^* + O_2$

7. $H^T + NO \rightarrow HNO^*$

Since one can essentially control the H translational energy by the photodissociation source energy, the reaction dynamics can be studied as a function of H energy (0.3 → 3.6 eV) in a range not easily accessible by other means. We can then obtain the internal partitioning of vibrational and rotational energy as a function of H energy. Moreover, if the systems can be made to lase, the bimolecular rate constant ratios (k_V/k_{V-1}) and reactive cross sections can be determined as a function of H energy. From the known thermodynamic data for these reactions, it should be possible to deduce new and interesting information about "activated" intermediates and their properties during the "moment of truth" when reaction partners are close enough to perform chemistry.

References

1. D. R. Herschbach, Appl. Opt. Suppl. 2, 128 (1965).
2. D. R. Herschbach, Disc. Faraday Soc. 33, 149 (1962).
3. D. R. Herschbach, G. H. Kwei and J. A. Norris, J. Chem. Phys. 34, 1842 (1961); Bull. Am. Phys. Soc. 5, 503 (1960).
4. S. Datz and R. E. Minturn, J. Chem. Phys. 41, 1153 (1964).
5. K. R. Wilson, G. H. Kwei, J. A. Norris, R. R. Herm, J. H. Birely, and D. R. Herschbach, J. Chem. Phys. 41, 1154 (1964).
6. J. K. Cashion and J. C. Polanyi, J. Chem. Phys. 29, 455 (1958).
7. J. K. Cashion and J. C. Polanyi, Proc. Roy. Soc. A258, 570 (1960).
8. P. E. Charters and J. C. Polanyi, Disc. Faraday Soc. 33, 107 (1962).
9. K. G. Anlauf, P. J. Kuntz, D. H. Maylotte, P. D. Pacey and J. C. Polanyi, Disc. Faraday Soc. 44, 183 (1967).
10. K. L. Kompa and G. C. Pimentel, J. Chem. Phys. 47, 857 (1967).
11. J. V. V. Kasper and G. C. Pimentel, Phys. Rev. Letters 14, 352 (1965).
12. P. H. Corneil and G. C. Pimentel, J. Chem. Phys. 49, 1379 (1968).
13. J. H. Parker and G. C. Pimentel, J. Chem. Phys. 51, 91 (1969).
14. K. E. Shuler, T. Carrington and J. C. Light, Appl. Opt. Suppl. 2, 81 (1965).
15. R. A. Ogg, Jr. and R. R. Williams, Jr., J. Chem. Phys. 13, 586 (1945).
16. R. M. Martin and J. E. Willard, J. Chem. Phys. 40, 2999 (1964).
17. H. A. Schwarz, R. R. Williams, Jr. and W. H. Hamill, J. Am. Chem. Soc. 74, 6007 (1952).